

# THE DEVELOPMENT OF AN INORGANIC DIRECT METHANOL FUEL CELL

*by*

*Touhami Mokrani*



A dissertation submitted in partial fulfillment of the  
requirements for the degree of  
Doctor of Philosophy  
in the Department of Chemistry,  
University of the Western Cape,  
Cape Town, Western Cape, South Africa

**Supervisor:** Prof. V.M. Linkov

**November, 2004**

## DEDICATION

**I dedicate this thesis to my mother, my wife and to my daughter “Samia”**



## DECLARATION

I declare that “The development of an inorganic direct methanol fuel cell” is my own work, that it has not been submitted for any degree or examination in any other university, and that all the sources I have used or quoted have been indicated and acknowledged by complete references.



---

**Touhami Mokrani**

## ABSTRACT

A fuel cell is an energy device that converts chemical energy to electrical energy. Low temperature fuel cells, namely the hydrogen fuel cell and the direct methanol fuel cell are preferred amongst other fuel cell types for stationary and vehicular applications, due to their small size and their low operating temperature.

The direct methanol fuel cell (DMFC) has several advantages over the hydrogen fuel cell including ease of transport and storage since methanol is a liquid. Since methanol is used directly in the cell there is no need for a reforming process, which results in a less complicated system. However, direct methanol fuel cells are in their infancy and many problems need to be overcome before reaching commercialization.

The direct methanol fuel cell has several disadvantages, namely, the sluggish methanol oxidation reaction, the high cost of state-of-the-art proton exchange membranes (e.g. Nafion<sup>®</sup> membrane a trade mark of DuPont), the high methanol permeability from anode to cathode (known as methanol crossover) and the dependence of the conductivity on membrane water content, which limits their use to temperatures below the boiling point of water - typically at 80°C - while the need is to work at high temperatures (120°C-150°C) to avoid CO absorption on the catalyst surface.

Attempts to overcome the disadvantages of the state-of-the-art membrane were made in this study, including the development of novel proton exchange membranes

and also the modification of existing state-of-the-art membranes (e.g. Nafion<sup>®</sup> membranes).

Flexible inorganic materials purchased from Creavis Technology and Innovation under the trade name CREAMFILTER<sup>®</sup> were used as a matrix for composite membranes. CREAMFILTER<sup>®</sup>s matrices were impregnated with proton conductive materials, namely, zirconium bis (monohydrogen phosphate) mono-hydrate,  $Zr(HPO_4)_2 \cdot H_2O$  (denoted as ZrP) and Nafion<sup>®</sup> solution.

Four types of CREAMFILTER<sup>®</sup> were investigated: Z100G, Z240G, S450P and Z450P. It was found that these matrices are chemically and thermally stable, and furthermore, mechanically stable down to 30  $\mu m$  thickness.

CREAMFILTER<sup>®</sup> impregnated with ZrP shows good characteristics for DMFC applications including high conductivity, reduced methanol permeability and high water content.

The selectivity factor ( $\beta$ ) which is the ratio between conductivity and methanol permeability, was adopted as a way of comparing membranes with a standard membrane (Nafion<sup>®</sup> 117 in this case).

The composite inorganic CREAMFILTER<sup>®</sup> Z240G impregnated with ZrP shows a selectivity factor ( $\beta$ ) of 4.9 which is higher than that of Nafion<sup>®</sup> 117 ( $\beta = 4.5$ ). CREAMFILTER<sup>®</sup> Z240G/ZrP composite membrane will perform better than Nafion<sup>®</sup> 117 in the direct methanol fuel cell mode. Inorganic CREAMFILTER<sup>®</sup> matrices Z100G and S450P impregnated with ZrP show similar selectivity factors to Nafion<sup>®</sup> 117, showing the potential of these membranes for application in fuel cells.

The inorganic CREAMFILTER<sup>®</sup> matrices were also impregnated with Nafion<sup>®</sup> solution. These composite membranes show high conductivity ( $\sim 10^{-2}$  S/cm) and low methanol permeability. Furthermore, this type of composite has an advantage over similar composite membranes (e.g. Gore Select<sup>®</sup> a trade mark from Gore and Associates) due to its higher water content since CREAMFILTER<sup>®</sup>s are fabricated from metal oxides (SiO<sub>2</sub>, ZrO<sub>2</sub> and Al<sub>2</sub>O<sub>3</sub>) which are well known for their high water content.

Recast Nafion<sup>®</sup> is brittle, cracks easily and is soluble in solvents. A recast film annealed at high temperatures (around 160°C) produced a mechanically stable film. Recast Nafion<sup>®</sup> / inorganic fillers were prepared and investigated. The inorganic fillers used were ZrO<sub>2</sub> and two different ZrP: firstly ZrP powder prepared by phosphorization of ZrO<sub>2</sub> powder, and secondly by using the ion exchange capacity of Nafion<sup>®</sup>, where H<sup>+</sup> ions are exchanged with Zr<sup>+4</sup> by soaking Nafion<sup>®</sup> membrane in ZrOCl<sub>2</sub> solution. ZrP was precipitated *in situ* by soaking the membrane in H<sub>3</sub>PO<sub>4</sub>. Introducing inorganic fillers in recast Nafion<sup>®</sup> enhanced the desired characteristics, namely, increased mechanical stability, reduced methanol permeability and increased water content.

The CREAMFILTER<sup>®</sup> matrix impregnated with ZrP was improved further by coating the composite membrane with Nafion<sup>®</sup> film. The Nafion<sup>®</sup> coating serves as a barrier to ZrP leaching and also to methanol permeability. Furthermore, the Nafion<sup>®</sup> coating will play an important role in membrane electrode assembly fabrication.

CREAMFILTER<sup>®</sup>s impregnated with Nafion<sup>®</sup> were prepared with high conductivity and reduced methanol permeability. On the other hand, ZrP was found to

be the best inorganic additive to proton conductive polymers, since ZrP it is itself a proton conductor and has a high water content. A composite membrane was successfully prepared by impregnating CREAMFILTER<sup>®</sup> with Nafion<sup>®</sup> solution, followed by the introduction of ZrP via an ion exchange of H<sup>+</sup> in the Nafion<sup>®</sup> with Zr<sup>+4</sup>, followed by precipitation of ZrP.

Preliminary results in a single fuel cells show the potential of the prepared membrane for direct methanol fuel cell application. However, an appropriate membrane electrode assembly fabrication protocol needs to be developed.



## TABLE OF CONTENTS

<b>DECLARATION</b> .....	i
<b>ACKNOWLEDGMENTS</b> .....	ii
<b>ABSTRACT</b> .....	iii
<b>TABLE OF CONTENTS</b> .....	vii
<b>LIST OF FIGURES</b> .....	x
<b>LIST OF TABLES</b> .....	xiii
<b>LIST OF ABBREVIATIONS</b> .....	xiv
<b>CHAPTER 1</b>	
<b>INTRODUCTION</b> .....	1
1.1 FUEL CELLS.....	1
1.2 PROTON CONDUCTOR MEMBRANES .....	2
1.3 OBJECTIVES .....	3
1.4 REALIZING OBJECTIVES .....	3
1.4.1 A New Type of Proton Conductor Membrane.....	4
1.4.2 Modification of the State-of-the-art Membranes .....	4
1.5 THESIS SCOPE.....	5
<b>CHAPTER 2</b>	
<b>LITERATURE REVIEW</b> .....	6
2.1 INTRODUCTION.....	6
2.1.1 Background .....	6
2.1.2 Low Temperature Fuel Cells .....	8
2.1.3 Advantages and Disadvantages of H <sub>2</sub> -PEMFCs .....	12
2.1.4 Advantages and Disadvantages of DMFCs .....	13
2.1.5 Hydrogen versus Methanol as a Fuel.....	14
2.1.6 Other Fuels for Low Temperature Fuel Cells.....	17
2.2 PROTON CONDUCTOR MEMBRANES .....	21
2.2.1 First Proton Conductor Membranes.....	21
2.2.2 Perfluorinated Membranes .....	22
2.2.3 Partially Fluorinated Ionomer Membranes .....	32
2.2.4 Non Perfluorinated Membranes.....	33
2.2.5 Organic / Inorganic Composite Membranes.....	40
2.2.6 Other Polymeric Proton Conductor Membranes .....	46
2.2.7 Inorganic Proton Conductor Membranes.....	48
2.3 DMFC COMPONENTS.....	53
2.3.1 Anode Catalyst - Methanol Oxidation .....	53
2.3.2 Cathod Catalyst - Oxygen Reduction .....	57
2.3.3 Backing Layers.....	57
2.3.4 Electrodes for Low Temperature Fuel Cells.....	60
2.4 METHANOL CROSSOVER IN FUEL CELL MEMBRANES .....	70
<b>CHAPTER 3</b>	
<b>CHEMICALS, INSTRUMENTS AND METHODS</b> .....	75
3.1 CHEMICALS.....	75
3.2 INSTRUMENTS.....	76
3.2.1 X-Ray Diffraction (XRD).....	76
3.2.2 Fourier-Transform Infrared (FTIR).....	76
3.2.3 Scanning Electron Microscopy (SEM).....	77



## Table of Contents

---

3.2.4	Transmission Electron Microscopy (TEM).....	77
3.2.5	Brunauer-Emmett-Teller (BET) Analysis .....	77
3.2.6	Thermogravimetric Analysis (TGA) and Differential Scanning Calorimetry (DSC).....	78
3.3	METHODS.....	78
3.3.1	Conductivity Measurement.....	78
3.3.2	Water Uptake of Membranes.....	82
3.3.3	Methanol Permeability - Diffusion Cell .....	82
3.3.4	DMFC Test Rig.....	84

## CHAPTER 4

<b>MEMBRANE PREPARATION AND CHARACTERIZATION .....</b>	<b>87</b>
4.1 INTRODUCTION.....	87
4.2 INORGANIC MATRIX DESCRIPTION AND STABILITY TESTS .....	88
4.2.1 Matrix Descriptions.....	88
4.2.2 Matrix Stability Test.....	92
4.2.3 Methanol Permeability in Bare CREAMFILTER <sup>®</sup> s .....	93
4.3 INORGANIC CREAMFILTER <sup>®</sup> MATRIX IMPREGNATED WITH ZIRCONIUM PHOSPHATE.....	96
4.3.1 Introduction .....	96
4.3.2 Membrane Preparation .....	96
4.3.3 ZrO <sub>2</sub> Sources Characterization .....	97
4.3.4 Zirconium Phosphate Powder Characterization .....	104
4.3.5 Composite Membrane Characterization .....	112
4.3.6 Discussion and Conclusions .....	121
4.4 INORGANIC CREAMFILTER <sup>®</sup> MATRIX IMPREGNATED WITH NAFION <sup>®</sup> SOLUTION.....	123
4.4.1 Introduction .....	123
4.4.2 Membrane Preparation .....	123
4.4.3 Recast Nafion <sup>®</sup> Characterization.....	124
4.4.4 Composite CREAMFILTER <sup>®</sup> Matrix Impregnated with Nafion <sup>®</sup> Solution Membrane Characterization.....	127
4.4.5 Discussion and Conclusions.....	132
4.5 RECAST NAFION <sup>®</sup> / ZrO <sub>2</sub> POWDER COMPOSITE MEMBRANES .....	133
4.5.1 Introduction .....	133
4.5.2 Membrane Preparation .....	134
4.5.3 Membrane Characterization .....	135
4.5.4 Discussion and Conclusions.....	141
4.6 RECAST NAFION <sup>®</sup> / ZrP POWDER COMPOSITE MEMBRANES .....	142
4.6.1 Introduction .....	142
4.6.2 Membrane Preparation .....	142
4.6.3 Membrane Characterization .....	143
4.6.4 Discussion and Conclusions.....	149
4.7 NAFION <sup>®</sup> 117 / ZrP (VIA ION EXCHANGE OF Zr <sup>+4</sup> ) COMPOSITE MEMBRANES .....	150
4.7.1 Introduction .....	150
4.7.2 Membrane Preparation .....	150
4.7.3 Membrane Characterization .....	151
4.7.4 Discussion and Conclusions.....	158
4.8 COMPOSITE INORGANIC CREAMFILTER <sup>®</sup> MATRIX / ZrP / NAFION <sup>®</sup> SOLUTION MEMBRANES.....	158
4.8.1 Composite Inorganic CREAMFILTER <sup>®</sup> Matrix / ZrP / Nafion <sup>®</sup> Solution Membranes .....	158
4.8.2 Composite Inorganic CREAMFILTER <sup>®</sup> Matrix / Nafion <sup>®</sup> Solution / ZrP Membranes .....	161

<b>CHAPTER 5</b>	
<b>DMFC PARAMETER OPTIMIZATION.....</b>	<b>165</b>
5.1 INTRODUCTION.....	165
5.2 INK COMPOSITION.....	165
5.3 BACKING LAYERS.....	169
5.4 INFLUENCE OF OPERATING PARAMETERS ON CELL PERFORMANCE.....	174
5.5 DISCUSSION AND CONCLUSIONS.....	183
<b>CHAPTER 6</b>	
<b>DEVELOPED MEMBRANE PERFORMANCE.....</b>	<b>185</b>
6.1 INTRODUCTION.....	185
6.2 MEA FABRICATION.....	185
6.3 SINGLE CELL PERFORMANCE.....	187
6.4 DISCUSSION AND CONCLUSIONS.....	190
<b>CHAPTER 7</b>	
<b>OVERALL CONCLUSION AND RECOMONDATIONS FOR FUTUR WORK.....</b>	<b>191</b>
7.1 OVERAL CONCLUSION.....	191
7.2 RECOMONDATIONS FOR FUTURE WORK.....	197
<b>REFERENCES.....</b>	<b>199</b>
<b>APPENDIX A.....</b>	<b>236</b>



---

**LIST OF FIGURES**

<b>Figure 2.1:</b> Low temperature fuel cells components.....	11
<b>Figure 2.2:</b> Principle of H <sub>2</sub> -PEMFC .....	11
<b>Figure 2.3:</b> Principle of DMFC.....	11
<b>Figure 2.4:</b> $\alpha$ -zirconium phosphate structure.....	53
<b>Figure 2.5:</b> Schematic representation of the influence of Nafion <sup>®</sup> loading in the catalyst layer .....	68
<b>Figure 2.6:</b> Voltametric method to measure methanol crossover .....	73
<b>Figure 3.1:</b> Cole-Cole plot of ZrP composite membrane.....	80
<b>Figure 3.2:</b> Bode plot of ZrP composite membrane .....	80
<b>Figure 3.3:</b> Conductivity measurement cell.....	81
<b>Figure 3.4:</b> Methanol permeability measurement cell (diffusion cell) .....	83
<b>Figure 3.5:</b> Lynntech Methanol Test Kit .....	85
<b>Figure 3.6:</b> Lynntech endplates.....	85
<b>Figure 3.7:</b> DMFC test rig.....	86
<b>Figure 4.1:</b> SEM micrographs of the surface and cross-section of Z240G.....	90
<b>Figure 4.2:</b> SEM micrographs of surface of S450P and Z450P.....	90
<b>Figure 4.3:</b> XRD analysis of Z100G and Z240G.....	91
<b>Figure 4.4:</b> XRD analysis of S450P.....	92
<b>Figure 4.5:</b> Methanol concentration in the receiving compartment as function of time in Z100G, Z240G, Z450P and Nafion <sup>®</sup> 117 .....	94
<b>Figure 4.6:</b> Methanol concentration in the receiving compartment as function of time in Z240G, S450P and Nafion <sup>®</sup> 117.....	95
<b>Figure 4.7:</b> SEM micrographs of ZrO <sub>2</sub> -D, ZrO <sub>2</sub> -L and ZrO <sub>2</sub> -C.....	98
<b>Figure 4.8:</b> TEM micrograph of ZrO <sub>2</sub> -D as received.....	98
<b>Figure 4.9:</b> TEM micrograph of ZrO <sub>2</sub> -D suspension in acetic acid.....	99
<b>Figure 4.10:</b> TEM micrograph of ZrO <sub>2</sub> -L.....	99
<b>Figure 4.11:</b> XRD analysis of ZrO <sub>2</sub> -D.....	100
<b>Figure 4.12:</b> XRD analysis of ZrO <sub>2</sub> -L .....	101
<b>Figure 4.13:</b> Pore size distribution of ZrO <sub>2</sub> -D .....	103
<b>Figure 4.14:</b> Pore size distribution of ZrO <sub>2</sub> -L.....	103
<b>Figure 4.15:</b> TGA analysis of ZrO <sub>2</sub> -D and ZrO <sub>2</sub> -L.....	104
<b>Figure 4.16:</b> TEM micrograph of ZrP prepared from ZrO <sub>2</sub> -D.....	107
<b>Figure 4.17:</b> TEM micrograph of ZrP prepared from ZrO <sub>2</sub> -L .....	107
<b>Figure 4.18:</b> SEM micrographs of ZrO <sub>2</sub> and ZrP.....	108
<b>Figure 4.19:</b> XRD analysis of ZrP powder .....	109
<b>Figure 4.20:</b> FTIR analysis of ZrP powder .....	110
<b>Figure 4.21:</b> TGA analysis of ZrP powder prepared from ZrO <sub>2</sub> -D and ZrO <sub>2</sub> -L.....	111
<b>Figure 4.22:</b> DSC analysis of ZrP powder prepared from ZrO <sub>2</sub> -D and ZrO <sub>2</sub> -L .....	112
<b>Figure 4.23:</b> ZrP uptake in CREAMFILTER <sup>®</sup> Z240G.....	113
<b>Figure 4.24:</b> Conductivity as a function of No of impregnations in Z240G.....	113
<b>Figure 4.25:</b> XRD analysis of CREAMFILTER <sup>®</sup> Z240G/ZrP.....	114

---

---

<b>Figure 4.26:</b> SEM micrographs of Z100G/ZrP prepared from ZrO <sub>2</sub> -D.....	117
<b>Figure 4.27:</b> SEM micrographs of Z240G/ZrP prepared from ZrO <sub>2</sub> -D.....	117
<b>Figure 4.28:</b> SEM micrographs of Z450P/ZrP prepared from ZrO <sub>2</sub> -D.....	117
<b>Figure 4.29:</b> SEM micrographs of Z100G/ZrP prepared from ZrO <sub>2</sub> -L.....	118
<b>Figure 4.30:</b> SEM micrographs of Z240G/ZrP prepared from ZrO <sub>2</sub> -L.....	118
<b>Figure 4.31:</b> SEM micrographs of Z450P/ZrP prepared from ZrO <sub>2</sub> -L.....	118
<b>Figure 4.32:</b> Methanol concentration in the receiving compartment as function of time in Z100G/ZrP, Z240G/ZrP, Z450P/ZrP and Nafion <sup>®</sup> 117.....	119
<b>Figure 4.33:</b> TGA analysis of Z450P/ZrP, S450P/ZrP and Nafion <sup>®</sup> 117.....	121
<b>Figure 4.34:</b> XRD analysis of Nafion <sup>®</sup> 117 and recast Nafion <sup>®</sup> .....	125
<b>Figure 4.35:</b> Recast Nafion <sup>®</sup> solubility.....	127
<b>Figure 4.36:</b> SEM micrograph of Z100G impregnated with Nafion <sup>®</sup> solution.....	128
<b>Figure 4.37:</b> SEM micrograph of Z240G impregnated with Nafion <sup>®</sup> solution.....	128
<b>Figure 4.38:</b> SEM micrograph of S450P impregnated with Nafion <sup>®</sup> solution.....	129
<b>Figure 4.39:</b> Methanol concentration in the receiving compartment as function of time in Z100G/ Nafion <sup>®</sup> , Z240G/ Nafion <sup>®</sup> and Nafion <sup>®</sup> 117.....	129
<b>Figure 4.40:</b> TGA analysis of Z100G/ Nafion <sup>®</sup> , S450P/ Nafion <sup>®</sup> and Nafion <sup>®</sup> 117.....	132
<b>Figure 4.41:</b> SEM micrographs of cross-sections of recast Nafion <sup>®</sup> / ZrO <sub>2</sub> .....	136
<b>Figure 4.42:</b> TEM micrograph of cross-sections of recast Nafion <sup>®</sup> / ZrO <sub>2</sub> (5%).....	137
<b>Figure 4.43:</b> TEM micrograph of cross-sections of bare recast Nafion <sup>®</sup> .....	137
<b>Figure 4.44:</b> XRD analysis of recast Nafion <sup>®</sup> / ZrO <sub>2</sub> (12%).....	138
<b>Figure 4.45:</b> Methanol concentration in the receiving compartment as function of time in bare recast Nafion <sup>®</sup> and recast Nafion <sup>®</sup> / ZrO <sub>2</sub> .....	139
<b>Figure 4.46:</b> TGA analysis of bare recast Nafion <sup>®</sup> and recast Nafion <sup>®</sup> / ZrO <sub>2</sub> .....	140
<b>Figure 4.47:</b> Water uptake in Nafion <sup>®</sup> 117, recast Nafion <sup>®</sup> and recast Nafion <sup>®</sup> / ZrO <sub>2</sub> .....	140
<b>Figure 4.48:</b> SEM micrographs of cross-sections of recast Nafion <sup>®</sup> / ZrP.....	144
<b>Figure 4.49:</b> TEM micrograph of cross-sections of recast Nafion <sup>®</sup> / ZrP.....	145
<b>Figure 4.50:</b> XRD analysis of recast Nafion <sup>®</sup> / ZrP.....	146
<b>Figure 4.51:</b> Methanol concentration in the receiving compartment as function of time in bare recast Nafion <sup>®</sup> and recast Nafion <sup>®</sup> / ZrP.....	147
<b>Figure 4.52:</b> TGA analysis of bare recast Nafion <sup>®</sup> and recast Nafion <sup>®</sup> / ZrP.....	148
<b>Figure 4.53:</b> Water uptake in Nafion <sup>®</sup> 117, recast Nafion <sup>®</sup> and recast Nafion <sup>®</sup> / ZrP.....	148
<b>Figure 4.54:</b> SEM micrographs of cross-sections of Nafion <sup>®</sup> 117 / ZrP via Zr <sup>+4</sup> .....	152
<b>Figure 4.55:</b> TEM micrograph of cross-sections of Nafion <sup>®</sup> 117 / ZrP via Zr <sup>+4</sup> .....	153
<b>Figure 4.56:</b> XRD analysis of Nafion <sup>®</sup> 117 / ZrP via Zr <sup>+4</sup> .....	154
<b>Figure 4.57:</b> FTIR scan of bare Nafion <sup>®</sup> film.....	155
<b>Figure 4.58:</b> FTIR scan of Nafion <sup>®</sup> film / ZrP via Zr <sup>+4</sup> (24%).....	155
<b>Figure 4.59:</b> Methanol concentration in the receiving compartment as function of time in bare recast Nafion <sup>®</sup> 117 and Nafion <sup>®</sup> 117 / ZrP via Zr <sup>+4</sup> .....	156
<b>Figure 4.60:</b> TGA analysis of bare Nafion <sup>®</sup> 117 and Nafion <sup>®</sup> 117 / ZrP via Zr <sup>+4</sup> .....	157
<b>Figure 4.61:</b> Water uptake in Nafion <sup>®</sup> 117, recast Nafion <sup>®</sup> and Nafion <sup>®</sup> 117 / ZrP.....	157
<b>Figure 4.62:</b> Methanol concentration in the receiving compartment as function of time in Nafion <sup>®</sup> 117, Z240G/ ZrP and Z240G/ ZrP/ Nafion <sup>®</sup> film.....	160
<b>Figure 4.63:</b> XRD analysis of recast Nafion <sup>®</sup> / ZrP via Zr <sup>+4</sup> .....	162

---

<b>Figure 4.64:</b> XRD analysis of Z240G / Nafion <sup>®</sup> / ZrP via Zr <sup>+4</sup> .....	163
<b>Figure 5.1:</b> Cyclic voltammograms of methanol oxidation for catalytic inks with different Nafion <sup>®</sup> content .....	167
<b>Figure 5.2:</b> Cell performance with different Nafion <sup>®</sup> content in the catalyst layer .....	168
<b>Figure 5.3:</b> I-V curve at 80°C for different solvents.....	169
<b>Figure 5.4:</b> Surface morphology of different backing layers.....	170
<b>Figure 5.5:</b> Influence of PTFE content on Toray paper backing layers structures .....	171
<b>Figure 5.6:</b> Influence of PTFE content on cell performance .....	172
<b>Figure 5.7:</b> Cell performance using two backing layers .....	173
<b>Figure 5.8:</b> DMFC polarization curve: influence of moisturizing on cell performance	175
<b>Figure 5.9:</b> Polarization curve of a DMFC with different moisturizing methods.....	176
<b>Figure 5.10:</b> Effect of anode catalyst loading on cell performance at 80°C .....	176
<b>Figure 5.11:</b> SEM micrograph of anode electrode, 1 mg/cm <sup>2</sup> catalyst loading .....	177
<b>Figure 5.12:</b> SEM micrograph of anode electrode, 2.3 mg/cm <sup>2</sup> catalyst loading .....	177
<b>Figure 5.13:</b> Influence of temperature on cell performance, E-TEK cloth .....	179
<b>Figure 5.14:</b> Influence of temperature on cell performance, Toray paper.....	180
<b>Figure 5.15:</b> DMFC performance with different air cathode flow rate .....	181
<b>Figure 5.16:</b> Influence of air cathode pressure on cell performance at 80°C .....	182
<b>Figure 5.17:</b> DMFC performance using air and oxygen at the cathode.....	183
<b>Figure 6.1:</b> SEM cross-section of an MEA with Nafion <sup>®</sup> 117 as the membrane .....	186
<b>Figure 6.2:</b> SEM cross-section of an MEA with CREAMFILTER <sup>®</sup> Z240G / ZrP / Nafion <sup>®</sup> solution as the membrane.....	186
<b>Figure 6.3:</b> DMFC performance of CREAMFILTER <sup>®</sup> Z240G impregnated with ZrP and Nafion <sup>®</sup> 117 .....	189
<b>Figure 6.4:</b> DMFC performance of CREAMFILTER <sup>®</sup> S450P impregnated with Nafion <sup>®</sup> solution and Nafion <sup>®</sup> 117.....	189

---


**LIST OF TABLES**

<b>Table 2.1:</b> Fuel cells systems .....	7
<b>Table 2.2:</b> Specific gravimetric and volumetric energy densities of selected fuels and comparison with batteries .....	16
<b>Table 2.3:</b> Physical properties of hydrogen, methanol and petrol relevant to accident safety .....	17
<b>Table 2.4:</b> Perfluorinated membranes .....	23
<b>Table 2.5:</b> Reported Nafion <sup>®</sup> 117 proton conductivities .....	27
<b>Table 2.6:</b> Inorganic proton conductors in the temperature range 25-200°C .....	48
<b>Table 2.7:</b> Backing layers for low temperature fuel cells .....	59
<b>Table 3.1:</b> Chemicals .....	75
<b>Table 3.2:</b> XRD operating parameters .....	76
<b>Table 4.1:</b> Inorganic CREAMFILTER <sup>®</sup> matrix characteristics .....	89
<b>Table 4.2:</b> Inorganic CREAMFILTER <sup>®</sup> matrix stability test .....	93
<b>Table 4.3:</b> BET surface area for ZrO <sub>2</sub> sources .....	102
<b>Table 4.4:</b> Conductivities of ZrP powders .....	105
<b>Table 4.5:</b> Composite CREAMFILTER <sup>®</sup> / ZrP membranes specifications .....	115
<b>Table 4.6:</b> Composite CREAMFILTER <sup>®</sup> / Nafion <sup>®</sup> membranes specifications .....	130
<b>Table 4.7:</b> Composite CREAMFILTER <sup>®</sup> / ZrP / Nafion <sup>®</sup> membrane specifications .....	161
<b>Table 6.1:</b> DMFC performance in 5 cm <sup>2</sup> three layers stack .....	188
<b>Table A.1:</b> Calculated methanol permeability in bare CREAMFILTER <sup>®</sup> s and Nafion <sup>®</sup> 117 .....	238
<b>Table A.2:</b> Calculated methanol permeability in CREAMFILTER <sup>®</sup> s impregnated with zirconium phosphate .....	239
<b>Table A.3:</b> Calculated methanol permeability in CREAMFILTER <sup>®</sup> s impregnated with Nafion <sup>®</sup> solution .....	239
<b>Table A.4:</b> Calculated methanol permeability in bare recast Nafion <sup>®</sup> (RN), recast Nafion <sup>®</sup> / ZrO <sub>2</sub> and recast Nafion <sup>®</sup> / ZrP powder .....	240

## LIST OF ABBREVIATIONS

DMFC	Direct Methanol Fuel Cell
FC	Fuel Cell
GDL	Gas Diffusion Layer
MEA	Membrane Electrode Assembly
PEMFC	Proton Exchange Membrane Fuel Cell
PBI	Polybenzimidazole
S-PEEK	Sulfonated Polyetheretherketone
S-PSU	Sulfonated Polysulfone
SEM	Scanning Electron Microscopy
TEM	Transition Electron Microscopy
XRD	X-ray Diffraction
ZrP	zirconium biz (monohydrogen phosphate) mono-hydrate (Zr (HPO <sub>4</sub> ) <sub>2</sub> .H <sub>2</sub> O)

## LIST OF SYMBOLS



$\beta$	Selectivity factor ( $\beta$ is the ratio between proton conductivity ( $\sigma$ ) and methanol permeability ( $P$ ))
$\sigma$	Proton conductivity [S/cm]
$P$	Methanol permeability [cm <sup>2</sup> /s]
$R$	Resistance [ $\Omega$ ]
$l$	Membrane thickness [cm]
$S$	Surface area [cm <sup>2</sup> ]
$I$	Current density [A/cm <sup>2</sup> ]
$V$	Cell voltage [V]

# CHAPTER 1

## INTRODUCTION

### 1.1 FUEL CELLS

Fuel cells are the new energy devices for stationary and vehicular applications. A fuel cell is an electrochemical system which converts chemical energy to electrical energy. Low temperature fuel cells, namely hydrogen fuel cells (referred to as H<sub>2</sub>-PEMFC: proton exchange membrane fuel cell) and methanol fuel cells (referred to as DMFC: direct methanol fuel cell), are preferred to other fuel cell types, due to their small size and low operating temperature, typically below 200°C.

The hydrogen fuel cell is well developed. However, hydrogen storage and transportation are strong impediments to commercialization. Hydrogen can be produced by reforming any hydrocarbon (e.g. gasoline, methanol, ethanol), but formed CO will absorb on the catalyst surface, thereby reducing the efficiency of the cell.

Fuel cells which use methanol directly have several advantages. Methanol is a liquid, and therefore easy to store and transport. Furthermore, there is no need for reforming, thus complicating the system less. However, DMFCs have several disadvantages to overcome before reaching commercialization. The sluggish methanol oxidation reaction needs to be improved, mainly by introducing a promoter (e.g. Ru or Mo)-to-platinum catalyst. Methanol permeability through the membrane, known as methanol crossover, needs to be reduced by developing a new type of proton conductor membrane or by modifying state-of-the-art membranes. Methanol oxidation



at high temperature, typically around 130-150°C, shows no formation of intermediate components (e.g. CO); thus a membrane that can retain the conductivity at high temperature needs to be developed. Methanol needs to flow to the membrane/catalyst interface, and CO<sub>2</sub>, a product of methanol oxidation, needs to flow counter-currently to methanol. For a better efficiency a two-phase flow needs to be avoided and thus an appropriate flow channel and gas diffusion layer needs to be optimized.

## 1.2 PROTON CONDUCTOR MEMBRANES

The proton conductor membranes are the heart of the fuel cell; they are the key components that achieve high performance. The state-of-the-art proton conductor membranes are the perfluorinated polymeric type, e.g. the Nafion<sup>®</sup> series from DuPont and the Flemion<sup>®</sup> series from Asahi Glass Co. These types of membranes have several advantages, namely:

- High mechanical strength;
- High chemical stability; and
- High conductivity up to 80°C.

However, perfluorinated membranes have several disadvantages in direct methanol fuel cell applications, including:

- High cost, due to the complicated manufacturing process;
- Low conductivity above 100°C, since the proton conductivity depends on water; and

- High methanol permeability (including Nafion<sup>®</sup> 117 (175  $\mu\text{m}$  thick)), the thicker the membrane used in the fuel cell.

### 1.3 OBJECTIVES

The objective of this thesis is to develop a proton conductive membrane, which can overcome at least one of the disadvantages of state-of-the-art membranes, namely:

- Low cost membranes and easy manufacturing process;
- Low methanol permeability;
- High conductivity at high temperature (above 100°C), by developing a proton conductive membrane where the conductivity does not depend on water or by modifying the existing state-of-the-art membranes; and
- Enhancing methanol oxidation by increasing the fuel cell working temperature up to 130-150°C.

### 1.4 REALIZING OBJECTIVES

Two directions are followed to satisfy the objectives of this thesis

- Development of a new type of proton conductor membrane
- Modification of the state-of-the-art membrane to reach the desired characteristics

### 1.4.1 A New Type of Proton Conductor Membrane

The development of new membranes includes the use of a non-conductive matrix as support, and an impregnation technique with a proton conductive material which was adopted in membrane preparation.

The matrix chosen in this study is an inorganic flexible ceramic with high chemical and thermal stability, reduced thickness (30-200  $\mu\text{m}$ ) and high mechanical stability. Furthermore, the inorganic matrix metal oxide content ( $\text{ZrO}_2$ ,  $\text{SiO}_2$  and  $\text{Al}_2\text{O}_3$ ) are well known for their high water content.

Two proton conductor materials were chosen for the impregnation technique, namely, zirconium phosphate (an inorganic proton conductor) and a polymeric proton conductor (Nafion<sup>®</sup> solution). Since zirconium phosphate is well known as a surface conductor, a high surface area (small particle size) material needs to be developed. Recast Nafion<sup>®</sup> is brittle, easily cracks and is soluble in solvents. An appropriate method to recast Nafion<sup>®</sup>, with characteristics similar to the received polymer, needs to be found.

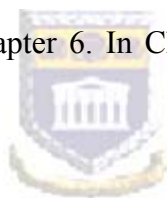
### 1.4.2 Modification of the State-of-the-art Membranes

The polymeric state-of-the-art proton conductive membranes can be modified to achieve the desired characteristics. The modification method adopted in this study, is to develop an organic / inorganic composite membrane. The organic proton conductor chosen is Nafion<sup>®</sup>. As inorganic materials zirconium oxide and zirconium

phosphate were chosen. The composite membranes prepared were investigated mainly for their water content and methanol permeability.

### **1.5 THESIS SCOPE**

The thesis is structured as follows: Chapter 2 summarizes the literature review. Chapter 3 deals with the methods used in the measurement, namely, conductivity measurement, methanol permeability (Diffusion Cell) and single cell testing. Membrane preparations and characterizations are reported in Chapter 4. Chapter 5 reports on the optimization of DMFC parameters in a single cell and using a standard membrane (e.g. Nafion<sup>®</sup> 117). The cell performances with the newly developed membranes are summarized in Chapter 6. In Chapter 7, the overall conclusions are discussed.



## CHAPTER 2

# LITERATURE REVIEW

### 2.1 INTRODUCTION

#### 2.1.1 Background

The criteria that are going to influence the evolution of the world energy system in the present century are complex. The most important new factor is the need to preserve the environment, both locally and globally, through the use of new technologies and sustainable use of existing resources.


The Kyoto protocol, which put a limit on greenhouse gas emissions (mainly CO<sub>2</sub>) from the industrialized countries, is a turning point in the global energy chain. On the other hand, the 2005 fuel specifications to control automotive exhaust gas emission obligate fuel producers to look for different ways of making clean fuel. Automakers are also obligated to look for alternative technology to internal combustion engines. The interest in studies on energy sources alternative to fossil fuels is linked both to the reduction of their availability and the increasing environmental impact caused by their use [1]. In the energy field, an important cause of pollutant emissions is linked to ground transportation. In the last 40 years, some economic, social and cultural changes have encouraged a wide proliferation of vehicles. For example, in Europe, private cars have increased from 232 to 435 per 1000 inhabitants in the period 1971-1995 [2].

Fuel cells are alternative power sources that can meet global emission regulations, and clean production. Although fuel cells have been used since the 1960's for aerospace and military applications, cost was a strong impediment to terrestrial applications.

Five major types of fuel cells are available and are defined by their electrolyte. These include alkaline (AFC), phosphoric acid (PAFC), molten carbonate (MCFC), solid oxide (SOFC) and proton exchange membrane fuel cells (PEMFC). Table 2.1 summarizes some characteristics of these fuel cells. Proton exchange membrane fuel cells are the most attractive candidate for alternative automotive and stationary power sources due to their smaller size and much lower operating temperature compared to other fuel cell systems.

In this dissertation, we only consider low temperature fuel cells namely the H<sub>2</sub>-proton exchange membrane fuel cell (H<sub>2</sub>-PEMFC) and the direct methanol fuel cell (DMFC), with emphasis on DMFC.

**Table 2.1:** Fuel cells systems [3, 4]



Type	Electrolyte	Charge carrier in the electrolyte	Temperature (°C)	Likely applications
Alkaline fuel cells (AFC)	aqueous KOH solution	OH <sup>-</sup>	<100	Transportation, Space, Military Energy storage systems
Proton exchange membrane fuel cells (PEMFC)	proton exchange membrane	H <sup>+</sup>	60-120	Transportation, Space, Military Energy storage systems
Phosphoric acid fuel cells (PAFC)	concentrated phosphoric acid	H <sup>+</sup>	160-220	Combined heat and power for decentralised stationary power systems
Molten carbonate fuel cells (MCFC)	mixture of molten carbonates (Li <sub>2</sub> CO <sub>3</sub> /K <sub>2</sub> CO <sub>3</sub> )	CO <sub>3</sub> <sup>2-</sup>	600-650	Combined heat and power for decentralised stationary power systems and for transportation (trains, boats)
Solid oxide fuel cells (SOFC)	ceramic solid ZrO <sub>2</sub> (Y <sub>2</sub> O <sub>3</sub> )	O <sub>2</sub> <sup>-</sup>	800-1000	Combined heat and power for decentralised stationary power systems and for transportation (trains, boats)

### 2.1.2 Low Temperature Fuel Cells

A fuel cell is an electrochemical system which converts chemical energy to electrical energy. A fuel cell differs from a battery in that fuels are continuously supplied and the products are continuously removed. There are two distinct fuels for low temperature fuel cells: hydrogen as used in a H<sub>2</sub>-PEMFC, and methanol as used in a DMFC. These fuel cells consist of six major parts: end plates, current collectors, flow channel blocks, gaskets, gas diffusion layers, and a membrane electrode assembly (MEA). Figure 2.1 shows the components of a low temperature fuel cell. The fuel cell principle enables a separation between power and energy. The maximum power required determines the size of the fuel cell; the energy required determines the amount of fuel to be carried. The specific power (W kg<sup>-1</sup>) of the H<sub>2</sub>-PEMFC is roughly twice that of the DMFC [5]. Because no mobile electrolyte is employed, corrosion problems in low temperature fuel cells are reduced and cell construction is simplified with few moving parts [6]. Also, fuel cells operate very quietly, therefore, reducing noise pollution [4]

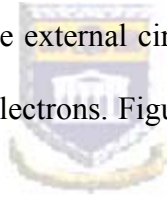
Since the proton exchange membrane used for the electrolyte is a solid phase, it does not penetrate deeply into the electrode as does a liquid one; therefore the reaction area is limited to the contact surface between the electrode and membrane [7]. The advantage of using solid electrolyte is that no electrolyte leakage will occur [8-9].

To meet the requirements of practical application a large number of single cells are assembled together to form a stack. The performance of a stack is different from

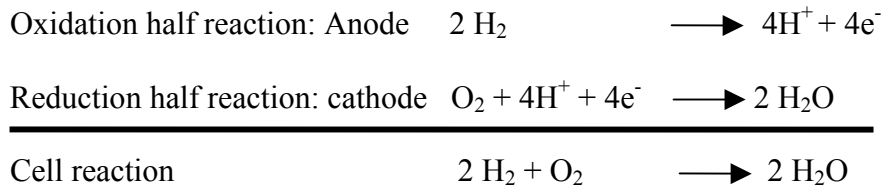
that of a single cell. The stack has a much higher operating voltage, a greater power and better fuel-energy efficiency [10].

### 2.1.2.1 Principle of the H<sub>2</sub>-PEMFC

H<sub>2</sub>-proton exchange membrane fuel cells have existed since the 1960's; in fact they were used in the Gemini aerospace program of the National Aeronautics and Space Administration (NASA) of the United States. The MEA for H<sub>2</sub>-PEMFCs consists of five components namely: a porous backing layer, an anode catalyst layer, a proton exchange membrane, a cathode catalyst layer, and a porous backing layer. Hydrogen is oxidized at the anode. The proton formed migrates through the membrane while the electrons flow through the external circuit. In the cathode reaction water is formed from oxygen, protons and electrons. Figure 2.2 shows the principle of the H<sub>2</sub>-PEMFC.



The two half reactions for the H<sub>2</sub>-PEMFC are as follows:



### 2.1.2.2 Principle of the DMFC

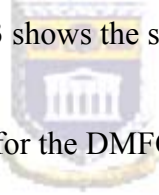
DMFC technology is relatively new compared to the H<sub>2</sub>-PEMFC. However, the direct oxidation of methanol in a DMFC has been investigated over many years and some prototypes were built in the 1960's and early 1970's by the Shell Research



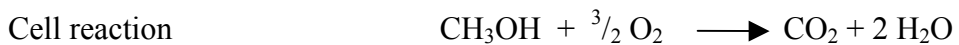
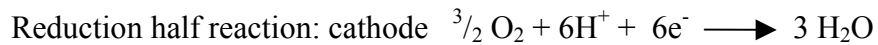
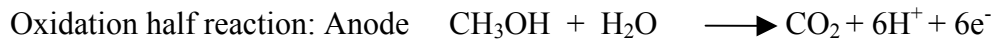
Center in England [11, 12] and by Hitachi Research Laboratories in Japan [13, 14]. These studies were abandoned in the mid-1980's due to the low performance (25 mW cm<sup>-2</sup> at best) resulting from the use of a liquid acid electrolyte [11,15,16]. An alkaline electrolyte was also used, but evolved CO<sub>2</sub> caused carbonation of the electrolyte resulting in decreased efficiency by reducing the electrolyte conductivity and depolarizing the cathode [17,18].

Currently all the research in DMFCs focuses on using solid proton exchange membranes as electrolyte, largely due to its proliferation in H<sub>2</sub>-PEMFCs.

The structure of the DMFC is similar to the H<sub>2</sub>-PEMFC. At the anode methanol is directly oxidized to carbon dioxide, and the reaction at the cathode is similar to the H<sub>2</sub>-PEMFC. Figure 2.3 shows the structure of a DMFC.



The two main half reactions for the DMFC can be summarized as follows:



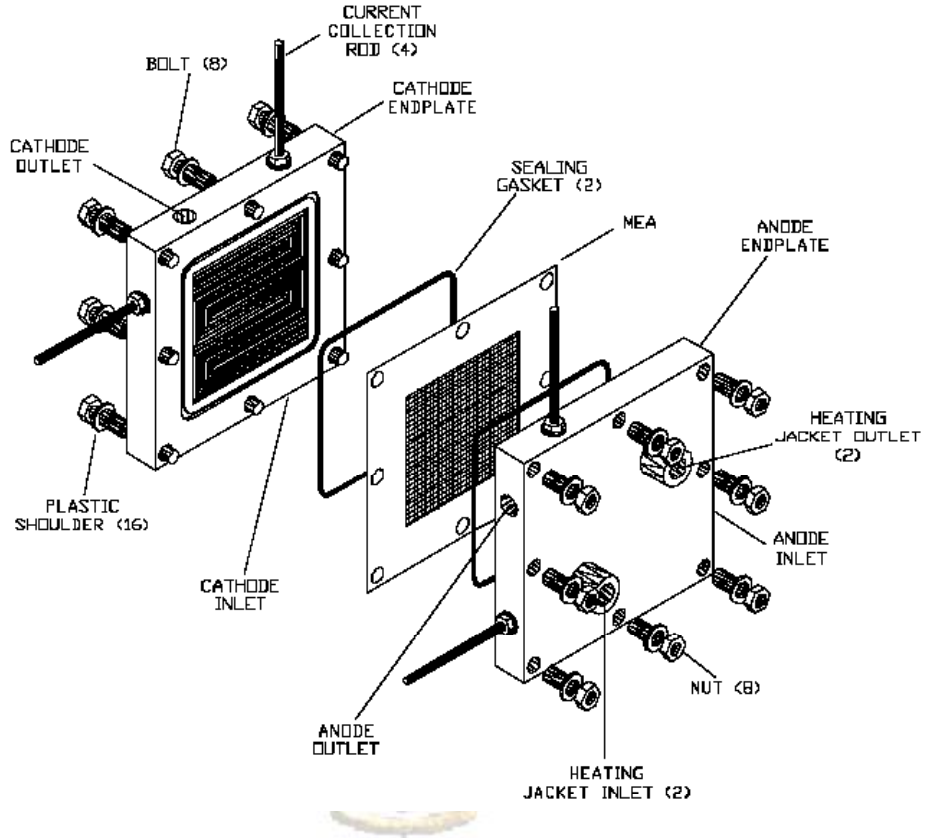


Figure 2.1: Low temperature fuel cell components [19].

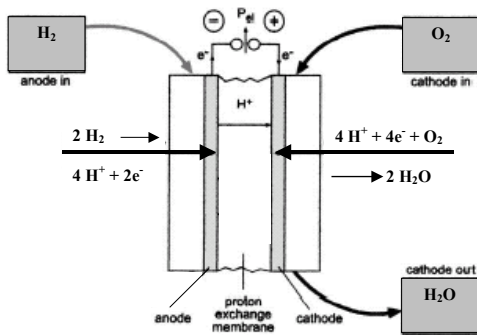


Figure 2.2: Principal of H<sub>2</sub>-PEMFC.

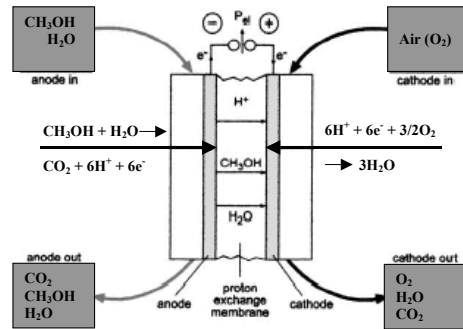


Figure 2.3: Principal of DMFC.

### 2.1.3 Advantages and Disadvantages of H<sub>2</sub>-PEMFCs

H<sub>2</sub>-PEMFCs have attracted the most attention due to their high electrochemical reactivity [20-23] and very low noble catalyst loading since the development of a method at Los Alamos National Laboratory (LANL) to reduce the platinum loading to ca. 0.1 mg/cm<sup>2</sup> [24-27] compared to 35 mg/cm<sup>2</sup> and 4 mg/cm<sup>2</sup> used respectively in the Gemini program and at General Electric in the 1970s [28-29]. The efficiency achievable is higher than in power plants and internal combustion engines [30] and there is practically zero pollution. However, the H<sub>2</sub>-PEMFC has several disadvantages including hydrogen storage and transportation and the public acceptance of hydrogen as fuel. It is well known that hydrogen and air mixtures are explosive (e.g. the Challenger disaster). Hydrogen safety measures are still one of the major implications when it comes to the commercialization of H<sub>2</sub>-PEMFCs. Adequate water content of the membranes is essential to maintain the conductivity of the polymeric proton exchange membrane [31-35]. During fuel cell operation, water molecules migrate through the membrane under electro-osmotic drag, fluid convection, and molecular diffusion, making it difficult to retain a high water content within the membrane. Generally, humidification is applied to the inlets of the anode and/or cathode in order to supply water to the membrane. However, excessive amounts of liquid water could impede mass transport within the electrode structure [33]. A thinner membrane is preferred in H<sub>2</sub>-PEMFCs because it can provide an improvement in water management due to the enhanced back-diffusion of production water from the cathode to the anode side [36]. The oxygen reduction reaction (ORR) is very slow compared to the

hydrogen reaction; typically hydrogen electro-oxidation on Pt is shown by an exchange current density of  $10^{-3}$  A cm<sup>-2</sup> Pt at ambient temperature. This is some  $10^7$  to  $10^9$  times more facile than the oxygen reduction at the cathode [37]. Thus, oxygen reduction is a rate limiting factor in H<sub>2</sub>-PEMFCs [38,39].

#### **2.1.4 Advantages and Disadvantages of DMFCs**

The thermodynamic reversible potential for a DMFC is 1.21V at 25°C [40]. This value is comparable to that for a H<sub>2</sub>-PEMFC, which is 1.23V [41-44]. In practice, a DMFC has a much lower open circuit voltage (OCV) [42] and electrochemical losses at both electrodes lead to a significant reduction in overall performance from the theoretical thermodynamic maximum [45].

Since methanol is used directly at the anode, and as a consequence, a DMFC requires less auxiliary equipment and is therefore a more simplified system compared to a H<sub>2</sub>-PEMFC. Methanol is a liquid made from natural gas or renewable biomass sources, which is relatively cheap. Methanol is also easy to store, transport, and distribute, where advantage can be taken of the existing gasoline infrastructure. The anodic reaction is exothermic for both the H<sub>2</sub>-PEMFC and the DMFC; heat management is a problem in H<sub>2</sub>-PEMFC stacks. In contrast, aqueous methanol acts as a coolant in DMFCs [46-49].

However, as the DMFC is still in its infancy, many problems need to be overcome to reach the commercialization stage. This includes the very sluggish methanol oxidation reaction, methanol crossover through the polymeric proton

exchange membrane, CO<sub>2</sub> evolution at the anode [43,45,50,51], and cathode flooding [19, 52-54].

The methanol crossover through the polymer electrolyte leads to a mixed potential at the cathode, which results from the ORR and the methanol oxidation occurring simultaneously. This effect causes a negative potential shift at the cathode and a significant decrease of performance in the DMFC. Methanol crossover also causes fuel losses; it had been found that over 40% of methanol can be wasted in a DMFC across Nafion<sup>®</sup> membranes [55].

In a DMFC, cathode flooding, which typically occurs unless high cathode stoichiometries are used, can determine to a great extent overall cell performance [19, 52-54]. Water management in the DMFC is especially critical because anode water activity is near unity due to contact with liquid methanol solution [56]. Thus, unlike a H<sub>2</sub>-PEMFC, no back-diffusive flux of water from cathode to anode will occur, and as a result, vapourization into dry cathode flow is the only pathway for removal of excess cathode-side water accumulation from electro-osmotic drag, ORR, and diffusion [56].

### **2.1.5 Hydrogen versus Methanol as a Fuel**

There are many production processes possible for hydrogen. The current main industrial processes include Steam Methane Reforming (SMR) of natural gas, coal gasification and water electrolysis. These processes are well known and understood.

A major issue in the advancement of the H<sub>2</sub>-PEMFC is that of hydrogen storage. Hydrogen storage can occur in one of the following forms: pressurized gas,

cryogenic liquid, in absorbed form as metal hydrides, in absorbed form in carbon nanotubes, and as chemical storage in the form of a liquid fuel.

Hydrogen compressed into a steel or reinforced plastic composite gas cylinder [57], can be achieved, but with considerable resultant size and weight penalty. Liquid hydrogen can be obtained by cooling hydrogen gas down to  $-253^{\circ}\text{C}$ . The storage facility for liquid hydrogen must be very well insulated. Liquid hydrogen storage is an energy intensive process due to the high amount of energy needed to convert hydrogen to a liquid. Thus, liquid hydrogen is an inefficient choice [3]. It takes up to two hours to refuel tanks of three buses [58]. Hydrogen storage can also be in carbon nanotubes [59-63] and metal hydrides [57, 64-66]. A metal alloy exposed to hydrogen can form a metal hydride depending on the type of alloy. The release of hydrogen usually involves the heating up of the metal hydride [3]. There have been a number of companies that have offered commercial hydride storage containers for many years, e.g. Ergenics Inc., Hydrogen Components, Inc., Gesellschaft fur Electrometallurgie, Japan Metals and Chemicals, Texaco Ovonic Hydrogen Systems L.L.C., HERA Hydrogen Storage Systems, etc. Chemical storage in liquid fuel form has the advantage of being able to utilize an already available infrastructure for fuel distribution to end-users [67]. On the other hand, an on-board fuel processor is necessary to convert liquid fuel to hydrogen [68]. A comparison of the specific energy densities of selected fuels and batteries is presented in Table 2.2.

**Table 2.2:** Specific gravimetric and volumetric energy densities of selected fuels and comparison with batteries [69]

	<b>kW/kg</b>	<b>kWh/l</b>
Diesel fuel	10.0	8.3
Gasoline	10.2	7.0
Ethanol	6.9	5.8
Methanol	5.0	4.2
Liquid H <sub>2</sub>	5.0	1.8
Compressed natural gas (CNG) (300 bar)	3.0	1.8
Pressurized hydrogen (300 bar)	1.1	0.4
Ti-Fe-hydride	0.4	1.2
Na/S batteries	0.12	0.13
Pb/PbO batteries	0.025	0.070

Methanol is produced from steam reformed natural gas and carbon dioxide using copper-based catalyst, and also from renewable biomass sources. Methanol is a leading candidate to provide the hydrogen necessary to power a fuel cell, especially in vehicular applications [68]. Methanol is currently used as a feed stock for a variety of widely used organic chemicals, including formaldehyde, acetic acid, chloromethane, and methyl tert-butyl ether (MTBE).

Since 1965, methanol has been used in the United States as a fuel in certain vehicles (e.g. racing cars), either as pure methanol (M100) or as a gasoline-methanol mixture which consists of 15% gasoline and 85% methanol (M85). Nearly 15,000 methanol vehicles have been operating for nearly a decade now in California, New York and elsewhere in the United States. These methanol vehicles are supported by a fueling infrastructure of 100 methanol fueling stations in California alone and many more across the United States. A recent study by EA Engineering, Science, and

Technology, Inc., shows that the capital cost of increasing the throughput of an existing gasoline station by adding a methanol storage and methanol compatible piping and dispenser was about US\$ 62,400 [70]. Table 2.3 outlines a number of important properties of hydrogen, methanol and petrol relevant to the assessment of safety in case of an accident [71].

**Table 2.3:** Physical properties of hydrogen, methanol and petrol relevant to accident safety [71]

	<b>Hydrogen</b>	<b>Methanol</b>	<b>Petrol</b>
Molecular weight	2.016	32.04	107
Liquid density (gml <sup>-1</sup> )	71 (LH <sub>2</sub> ) 0.0013 (GH <sub>2</sub> )	791	
Vapour density relative to air (=1)	14 × lighter	1.1 × heavier	2-5 × heavier
Volatility (RVP-psi)		4.6 – 5.3	9 - 15
Boiling point (K)	20.27	338	
Minimum ignition energy (mJ)	0.14	0.02	0.024
Diffusion coefficient (cm <sup>2</sup> s <sup>-1</sup> )	0.61	0.0042	0.05
Flammability limits (vol.%)	4 – 75	6 – 36.5	1 – 7.6
Explosive limits (vol.%)	18.3 – 59.0	6 – 36	1.1 – 3.3
Fraction of heat in radiative form	17 – 25	17	30 – 42
Flame temperature in air (K)	2318		2470

### 2.1.6 Other Fuel for Low Temperature Fuel Cells

The question of whether customers will be fuelling their vehicles directly with hydrogen or via the hydrogen-rich carrier (e.g. methanol, ethanol, gasoline, diesel, etc.) still seems to be unanswered. This is a very important issue not just from a refueling infrastructure perspective but also from the public perception and from the gearing up of production, and developing guidelines for dealing with safety issues that will need to put in place for the new fuel [71].



In principle, any type of liquid fuel may be employed as a hydrogen source, e.g. gasoline, diesel, methanol, ethanol, etc. Hydrogen is produced on-board by a reforming process.

It was shown in Section 2.1.5 that methanol is a desired fuel to produce hydrogen on-board. Methanol can be reformed to hydrogen by different processes including steam reforming [72-79,], partial oxidation [80-82] and autothermal reforming [83-86].

Steam reforming of methanol occurs by two different pathways [76-77]. The first one involves the decomposition of methanol into CO and H<sub>2</sub> through the following reaction:



followed by a water gas shift reaction:



The second mechanism for methanol steam reforming consists of the reaction of water and methanol to CO<sub>2</sub> and hydrogen:



which can be followed by a reverse shift reaction to establish the thermodynamic equilibrium:



Methanol steam reforming is endothermic and therefore requires that external heat, typically 300°C, is supplied. Steam reforming of methanol is usually catalyzed over Cu/ZnO type catalyst and can be performed in fixed-bed reactors [78].

Methanol powered cars would consume less energy than diesel or gasoline powered cars. Furthermore, the overall emissions from the system are 90% less than from conventional vehicles [87].

Among other candidate liquid fuels, ethanol is a particular case, since it can be easily produced in great quantity by the fermentation of sugar-containing raw materials. In addition, in some countries (e.g. Brazil) ethanol is already distributed in gas stations for use in conventional cars with internal combustion engines.

Hydrogen is produced from ethanol in a process unit consisting of either a steam reformer (SR) or a partial oxidation (POX) reactor in series with a water-gas shift (WGS) reactor and a reactor for selective oxidation (SOX) of CO. Product gas from the reformer or the POX reactor, which operates at an exit temperature higher than 677°C, contains a mixture of H<sub>2</sub>, CO, CO<sub>2</sub>, CH<sub>4</sub> and H<sub>2</sub>O. After cooling, this stream enters the WGS reactor, where a large fraction of CO reacts with H<sub>2</sub>O towards CO<sub>2</sub> and H<sub>2</sub> at a temperature of 200°C. The product gas of the WGS reactor contains 0.1-1.5% of residual CO and enters the SOX reactor, where CO is totally oxidized - with the addition of a small amount of air - to CO<sub>2</sub> with residual CO being less than 10 ppm. The CO free, hydrogen rich stream is then fed to the H<sub>2</sub>-PEMFC [88].

Hydrogen can also be obtained from diesel fuel by a reforming process with an efficient overall cell design. A diesel fuel infrastructure is already in place; therefore the associated start-up cost of fueling with diesel would be significantly less than for methanol-fueled systems. Diesel also has a much higher potential energy density than

methanol. However, diesel fuel reforming is more complicated and requires much higher temperatures [89].

The tailpipe emission of hydrogen-fuelled fuel cell vehicles, in terms of the normally monitored pollutants, is zero, since the cell produces only water and heat. However, when a reformat hydrogen is used, the reforming process produces some pollutants; therefore, the principle of zero pollution is compromised.

Direct fuel utilization will be of interest. Besides methanol, other alcohols, particularly those coming from biomass resources, are being considered as alternative fuels. Ethanol as an attractive fuel for electrical vehicles was investigated in direct-ethanol fuel cells [15,90-92]. However, multimetallic catalysts are necessary to orientate the oxidation reaction selectively in the direction of complete combustion to carbon dioxide [15]. The reaction mechanisms of anodic oxidation of ethanol are more difficult to elucidate than methanol oxidation, since the number of electrons exchanged greatly increases (12 electrons per ethanol molecule versus 6 electrons for methanol), thus many adsorbed intermediates and products are involved [15]. However, a direct ethanol fuel cell was investigated by Aricò *et al.* [93] using a high temperature membrane (Nafion<sup>®</sup>/Silica), and also by Wang *et al.* [94] using a phosphoric acid doped polybenzimidazol (PBI) membrane.

Other fuels that were investigated for direct fuel cells included ethylene glycol [95-97], glycerol [98], propanol [15,94,99-103], propane [104-105], trimethoxy methane, [106], and dimethyl ether (DME) [107].

## 2.2 PROTON CONDUCTOR MEMBRANES

Proton exchange membranes or proton conductor membranes are the most important component of low temperature fuel cells. Since the development of a solid polymer electrolyte, all the researchs on fuel cells focus on the use of these types of electrolyte.

### 2.2.1 First Proton Conductor Membranes

The first proton conductor ionomer membranes based on hydrocarbon polymers have been developed by General Electric; phenol-formaldehyde sulfonic acid was developed in 1935 by Adams and Holmes [108,109] followed by the development of the polystyrene sulfonic acid membrane by D'Alelio [110-112].

Polystyrene sulfonic acid membrane, cross-linked with divinyl-benzene, found application between 1962 and 1964 - in fact they were used for the Gemini Fuel Cell Programme. These membranes represented considerable progress as compared to phenol-formaldehyde sulfonic acid, both in efficiency and lifetime. Power densities of approximately 50 mW/cm<sup>2</sup> versus a few mW/cm<sup>2</sup> were obtained. Long-term stability at 50-60° C could be obtained for several thousands of hours versus a lifetime of only about 100 hours for phenol-formaldehyde sulfonic acid. However, the stability rapidly decreased above 70°C [113].

It was found that these membranes show insufficient chemical stability, especially since tertiary C-H bonds and benzylic bonds are easily attacked by oxygen, forming hydroperoxide radicals [114].

The development of perfluorinated membranes by DuPont in the 1960's has played a vital role in electrochemical system applications (chlor/alkali electrolysis, fuel cells, etc.). The perfluorinated membranes are particularly suitable for fuel cells.

### **2.2.2 Perfluorinated Membranes**

The first commercially available perfluorinated membrane material from DuPont was Nafion<sup>®</sup> 120 (1200 equivalent weight (EW), 250  $\mu\text{m}$  thick) followed by Nafion<sup>®</sup> 117 (1100 EW, 175  $\mu\text{m}$  thick). These high equivalent weight materials were found to have limited use in fuel cells. In 1988, The Dow Chemical Company developed their own perfluorinated polymer membrane with low equivalent weight, typically in the range of 800-850. Nafion<sup>®</sup> of DuPont and Dow<sup>®</sup> membranes have identical backbones and are structurally and morphologically similar, but the side chain is shorter in the Dow polymer.

Since the success of Dow Chemical, where it was found that the Dow<sup>®</sup> membrane performed better than the DuPont membrane in  $\text{H}_2/\text{O}_2$  fuel cells, DuPont has been active in further developing their membranes with respect to durability and continuous improvement. They increased power densities by further decreasing the equivalent weight from 1100 to 1000 EW and membrane thickness from 175 to 25  $\mu\text{m}$ . Table 2.4 shows the latest DuPont membranes with some characteristics. Nafion<sup>®</sup> 117 is the preferred membrane for DMFCs.

In the 1990's, Aciplex<sup>®</sup> perfluorinated ion exchange membranes were introduced by the Asahi Chemical Industry, and the Flemion<sup>®</sup> series were introduced

by Asahi Glass Co. [115]. In general these membranes are in the category of long chain perfluorinated membranes, like Nafion<sup>®</sup>. Some characteristics of these perfluorinated membranes are summarized in Table 2.4.

**Table 2.4:** Perfluorinated membranes

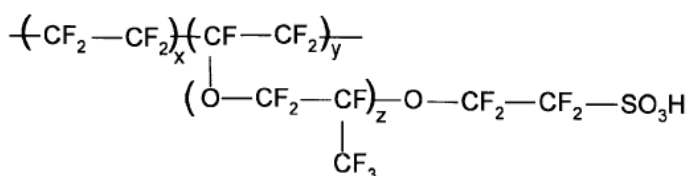
<b>Membrane</b>	<b>Thickness (<math>\mu\text{m}</math>)</b>	<b>Equivalent Weight</b>
<b>Nafion<sup>®</sup> series (DuPont)</b>		
Nafion <sup>®</sup> 117	175	1100
Nafion <sup>®</sup> 115	125	1100
Nafion <sup>®</sup> 112	50	1100
Nafion <sup>®</sup> 111	25	1100
Nafion <sup>®</sup> 1135	87	1100
Nafion <sup>®</sup> 1035	87	960
Nafion <sup>®</sup> 105	125	960
<b>Dow Chemicals Co.</b>		
Dow <sup>®</sup> XUS 13204.10	127	800-850
<b>Flemion<sup>®</sup> series (Asahi Glass Co.)</b>		
Flemion <sup>®</sup> R	50	900
Flemion <sup>®</sup> S	80	900
Flemion <sup>®</sup> T	120	900
<b>Aciplex<sup>®</sup> series (Asahi Chemicals Industry)</b>		
Aciplex <sup>®</sup> 1004	100	1000

Nafion<sup>®</sup> membranes are chemically synthesized in four steps according to the DuPont de Nemours process [116]: 1) The reaction of tetrafluoroethylene with  $\text{SO}_3$  to form the sulfone cycle; 2) The condensation of these products with sodium carbonate followed by co-polymerization with tetrafluoroethylene to form an insoluble resin; 3) The hydrolysis of this resin to form a perfluorosulfonic polymer and 4) The chemical exchange of the counter ion  $\text{Na}^+$  with the proton in an appropriate electrolyte.

The Dow<sup>®</sup> membrane is prepared by the co-polymerisation of tetrafluoroethylene with vinyl ether monomer. The polymer can be described as having a Teflon-like backbone structure with a side chain attached via an ether group. This side chain is characterized by a terminal sulfonate functional group [117].

### 2.2.2.1 Nafion<sup>®</sup> Structure

The perfluorinated sulfonic acid membrane consists of a hydrophobic polytetrafluoroethylene (PTFE or Teflon) backbone which terminates with a hydrophilic polar headgroup SO<sub>3</sub>H [118,119]. Since Nafion<sup>®</sup> is similar in structure to PTFE, it has excellent mechanical strength, water insoluble, and chemical and thermal stability.



Nafion<sup>®</sup> chemical structure

The emerging structure in the hydrated state possesses hydrophilic ionic clusters which contain the solvated SO<sub>3</sub><sup>-</sup>-heads, water, and counter-ions (predominantly H<sup>+</sup>). These cluster regions are connected by short and narrow channels. The water-containing cluster network is “embedded” in the surrounding, sponge-like medium of the hydrophobic PTFE-backbones [120-122]. The exact structure of Nafion<sup>®</sup> is not known but there have been several models proposed to describe the way in which ionic groups aggregate within the Nafion<sup>®</sup> membrane

[120,122-126]. Yeager and Steck [124] describe Nafion<sup>®</sup> as consisting of three regions: a fluorocarbon region, an interfacial zone and an ionic cluster region. The fluorocarbon region consists of the fluorocarbon backbone and is quite hydrophobic. The ionic cluster region consists of clusters of pendant sulfonate groups. This region is quite hydrophilic - most absorbed water and counter-ions exist in this region. The interfacial zone contains the pendant side chain material and sulfonate groups that are not clustered. Hence, only part of the absorbed water and counter-ions exist in this region.

#### **2.2.2.2 Proton Conductivity Mechanisms**

Proton transfer phenomena follow two principle mechanisms, namely the vehicle mechanism [127] and the Grotthuss mechanism [128]. In the vehicle mechanism, the proton diffuses through the medium together with a “vehicle”, for example, with H<sub>2</sub>O as H<sub>3</sub>O<sup>+</sup>. The counter-diffusion of unprotonated vehicles (H<sub>2</sub>O) allows the net transport of protons. The observed conductivity, therefore, is directly dependant on the rate of vehicle diffusion. In the Grotthuss mechanism, the vehicles show pronounced local dynamics but reside on their sites. The protons are transferred from one vehicle to the other by hydrogen bonds (proton hopping). Simultaneous reorganization of the proton environment, consisting of reorientation of individual species or an even more extended ensemble, then leads to the formation of an uninterrupted path for proton migration. These two principle mechanisms essentially reflect the difference in nature of the hydrogen bonds formed between the protonated



species and their environment. In media which supports strong hydrogen bonding, the Grotthuss mechanism is preferred; the vehicle mechanism is characteristic of species with weaker bonding. Consequently, Grotthuss-type mechanisms are progressively dominated by vehicle-type mechanisms with increasing temperature.

Due to its importance in several electrochemical processes (e.g. chlor/alkali electrolysis, fuel cells, etc.), the Nafion<sup>®</sup> conductivity mechanism was studied extensively [120,122,129,130]. Kreuer [129] described the proton conductivity of Nafion<sup>®</sup> as follows: “in the presence of water only the hydrophilic part of the micro-structure is hydrated. The water of hydration then acts as a plasticizer mobilizing the polymer backbone which leads to a further phase separation. Eventually, a stationary micro-structure is formed which absorbs and desorbs water almost reversibly at moderate temperatures. The hydrated hydrophilic domains provide the very high proton conductivity. The latter depends very much on the presence of water”. It is well known that dry Nafion<sup>®</sup> is a poor proton conductor, but the proton conductivity increases sharply with water content [31-34].

### **2.2.2.3 Proton Conductivity Measurements**

Accurate measurements of the specific conductivity of proton exchange membranes pose a significant experimental challenge. Many groups have studied the conductivity of Nafion<sup>®</sup> membranes, predominantly using ac impedance spectroscopy [31,33-35,115,131-143] although dc techniques have also been adopted [133,144-147]. Kolde *et al.* [133] used both techniques in one technical paper. A few groups

have looked at the performance of the membrane *in situ* in the PEMFC using ac impedance [139] and a current pulse technique [148]. A variety of environments have been employed including 1M H<sub>2</sub>SO<sub>4</sub> [115,133,144,145,147], water [33,34,131-134], water vapour [31,33,34,131,132,135-137,149,150], and humidified gases [139,148] at temperatures from 20 to 95°C. The impact of such a wide range of factors on the conductivity of the Nafion<sup>®</sup> membranes has resulted in a wide range of proton conductivities being published. Some of the reported Nafion<sup>®</sup>117 proton conductivities are summarized in Table 2.5. The technique and the environment in which the conductivity was measured are also reported.

**Table 2.5:** Reported Nafion<sup>®</sup> 117 proton conductivities

Membrane Thickness (μm)	Conductivity (S/cm)	Technique	Electrolyte	Temperature (°C)	Ref.
231	0.088	dc current pulse	immersed in 1M H <sub>2</sub> SO <sub>4</sub>	20	144,145
231	0.231	dc current pulse	immersed in 1M H <sub>2</sub> SO <sub>4</sub>	80	144,145
175	0.100	ac impedance	immersed in water	30	33,34
175	0.190	ac impedance	immersed in water	90	33,34
175	0.060	ac impedance	water vapour @ 100%RH	30	33,34
200	0.066	dc method	immersed in 2M HCl	25	146
200	0.140	“Kelvin” four-point probe	immersed in 1M H <sub>2</sub> SO <sub>4</sub>	25	133
200	0.100	ac impedance	immersed in water	25	133
175	0.090	ac impedance	immersed in water	20	134
210	0.140	ac impedance	water vapour @ 100%RH	65	135
175	0.076	ac impedance	immersed in 1M H <sub>2</sub> SO <sub>4</sub>	25	115
200	0.068	ac impedance	water vapour @ 100%RH	30	31
200	0.078	ac impedance	water vapour @ 100%RH	20	136
175	0.050	ac impedance	water vapour @ 100%RH	20	137
170	0.080	ac impedance	immersed in water	20	138
203	0.105	current-pulse	<i>in situ</i> , humidified gases	60	148
175	0.070	ac impedance	water vapour @ 100%RH	25	149
	0.052	ac impedance	water vapour @ 100%RH	20	150
210	0.087	ac impedance	water vapour @ 100%RH	25	151
210	0.074	ac impedance	water vapour @ 100%RH	80	151

#### 2.2.2.4 Disadvantages of Perfluorinated Membranes

The perfluorinated membranes, including Nafion<sup>®</sup>, Dow<sup>®</sup> membrane, Aciplex<sup>®</sup> and Flemion<sup>®</sup> are expensive, because of the complication and the longevity of the manufacturing process [117], which includes strongly toxic and environment-unfriendly intermediates [114] and also fluorine chemistry [150]. The high methanol permeability in these membranes from anode to cathode - known as methanol crossover - which affects severely the DMFC performance is another disadvantage of this category of proton conductor membranes. Since the very high proton conductivity of perfluorinated membranes relies on the presence of liquid water, the maximum operation temperature in fuel cells is approximately given by the boiling point of water (100°C at  $P = 10^5$  Pa), while it is desired to work at 150°C.

#### 2.2.2.5 Modified Nafion<sup>®</sup> Membranes

Since Nafion<sup>®</sup> has several disadvantages, e.g. the high methanol crossover and working at a temperature of less than 100°C, attempts to overcome these problems have been made. One approach is to introduce a palladium film to reduce the crossover or by creating a barrier by plasma polymerization.

##### *a) Palladium film*

This approach was suggested first by Pu *et al.* [152] where they used a palladium foil 25  $\mu\text{m}$  thick sandwiched between two Nafion<sup>®</sup> 115 sheets. They proved that with this approach methanol crossover can be reduced, but the cell performance will be lower due to the increase in membrane thickness. Choi *et al.* [153] used the

same approach by sputtering metallic palladium on the surface of Nafion<sup>®</sup> 117. The palladium film was found to be 20 nm thick. Methanol permeability was reduced from  $2.392 \times 10^{-6}$  cm<sup>2</sup>/s in unmodified Nafion<sup>®</sup> 117 to  $1.7 \times 10^{-6}$  cm<sup>2</sup>/s in Pd-sputtered membrane. Ma *et al.* [154] used the same approach as Pu *et al.*, but using palladium alloy (Pd-Ag film of 1 μm thickness). The membrane fabricated was of the form of Nafion<sup>®</sup> 117/{Pt/Pd-Ag/Pt/ Nafion<sup>®</sup> (recast)}, and in contrast to Pu *et al.* they used recast Nafion<sup>®</sup> film (4-5 μm thick) instead of Nafion<sup>®</sup> polymer on one side of the membrane. Unfortunately, no methanol permeability was reported.

#### ***b) Plasma polymerization***

Thin plasma polymerized barrier films can be deposited on Nafion<sup>®</sup> 117 membrane. A plasma polymer layer with a thickness of approximately 0.27 μm on Nafion<sup>®</sup> 117 reduces the permeability to methanol by a factor of approximately 20 [155,156]. Hobson *et al.* [157] reported on the modification of Nafion<sup>®</sup> 117 by low dose electron beam (EB) exposure. The membrane obtained reduced methanol crossover to about 7% of that of Nafion<sup>®</sup> 117 and DMFC performance improved by up to 51%. Choi *et al.* [153] also reported on plasma etching on Nafion<sup>®</sup> 117, where the methanol crossover was reduced to  $2.106 \times 10^{-6}$  cm<sup>2</sup>/s. Finsterwalder and Hambitzer [36] achieved the plasma deposition of a ca. 300 nm thin layer of a polymer onto Nafion<sup>®</sup>. Methanol crossover was suppressed without reducing dramatically the conductivity. Modification of Nafion<sup>®</sup> membranes by plasma polymerization was also reported by Zeng *et al.* [158].

***c) Phosphoric acid doped Nafion<sup>®</sup>***

Savinell and co-workers [159-163] investigated the possibility of equilibrating Nafion<sup>®</sup> membranes with phosphoric acid. They showed that at elevated temperatures reasonably high conductivity ( $>0.05$  S/cm) can be obtained with Nafion<sup>®</sup>/H<sub>3</sub>PO<sub>4</sub> membranes. The phosphoric acid acts as a Bronsted base, ionizing the strong sulfonic acid groups and solvating the proton in the same manner as water. However, due to the low vapour pressure of phosphoric acid, ionization and solvation are not lost at temperatures above 100°C. Incorporating phosphoric acid within Nafion<sup>®</sup> is not equivalent to the use of phosphoric acid in an inert matrix [159]. The disadvantage of these membranes is that H<sub>3</sub>PO<sub>4</sub> or its dissociation products are strongly absorbed on Pt-based catalyst [159].

***d) Micro-reinforced Nafion<sup>®</sup> composite membranes***

Since the development of Nafion<sup>®</sup> solution [164,165], attempts to recast Nafion<sup>®</sup> from the polymer solution were made. Recast Nafion<sup>®</sup> at low temperature is brittle, easily cracked, and soluble in organic solvents, and especially water [165-167]. In order to improve the properties of the casting film, either high-boiling solvent is added into the Nafion<sup>®</sup> solution [165,166] or the recast film is annealed at high temperature in air or under vacuum [167].

A composite membrane has many advantages: reduced cost of the membrane, since it uses less polymer, reduced methanol crossover by suppressing the swelling, and the availability of thin membranes with high mechanical strength.

Nafion<sup>®</sup> composite membranes were studied in the literature, mainly by impregnating a non-woven polytetrafluoroethylene (PTFE) matrix with Nafion<sup>®</sup> ionomer [168-171]. Martin and co-workers [168-170] investigated the transport properties of the composite membranes, while Verbrugge *et al.* [171] investigated the transport characteristics of the composite membrane. In 1995, as a consequence, W.L. Gore and Associates made the first commercial composite membrane under the trade name Gore Select<sup>®</sup>, with reduced thickness down to 5  $\mu\text{m}$ , leading to a proton conductivity which is a factor of 10 higher than the proton conductivity of Nafion<sup>®</sup> [133,172]. The Gore Select<sup>®</sup> membranes have a translucent appearance with no visible evidence of any micro-reinforcement [117]. The success of Gore Select<sup>®</sup> membranes led to a series of investigations [135,173-177]. All these composite membranes used PTFE as matrix. In contrast, Haufe and Stimming [177] used a glass fiber fleece from Hollingsworth & Voss Co. Ltd. Also a PTFE-fibrils reinforced Flemion<sup>®</sup> series was developed by Asahi Glass Company Ltd. by dispersing PTFE-fibrils (<1  $\mu\text{m}$  in diameter) in ion-exchange membranes [178].

Others modifications to Nafion<sup>®</sup> were made. Tricoli [179] exchanged  $\text{H}^+$  in Nafion<sup>®</sup> 117 membranes with  $\text{Cs}^+$  to several degrees of doping. He found that methanol permeability at room temperature in Nafion<sup>®</sup> membranes can be drastically reduced by appropriate doping with cesium ions. Methanol permeability was reduced by over one order of magnitude, while the doped membranes retained good proton conductivity. Watanabe and co-workers [180] developed a new approach for self-

humidification of the membrane. This approach includes the dispersion of Pt particles (1-2 nm in diameter) in Nafion<sup>®</sup> 112 or a recast Nafion<sup>®</sup>. H<sub>2</sub> and O<sub>2</sub> crossover were recombined on Pt particles inside the membrane to form water. The advantages of this type of membrane are: the self humidification and also the suppression of crossover of reactant gases.

### **2.2.3 Partially Fluorinated Ionomer Membranes**

#### **2.2.3.1 Sulfonated Copolymer based on the $\alpha,\beta,\beta$ -trifluorostyrene Monomer**

The Canadian Ballard company developed proton conductor membranes based on trifluorostyrene monomer, under the trade name BAM1G and BAM2G (Ballard Advanced Materials first and second generation, respectively). The longevity of these polymers was limited to approximately 500 hours under practical fuel cell operating conditions [117]. Based on the above work, Ballard developed third generation membranes under the trade name BAM3G [119,181-183]. The BAM3G membranes consist of sulfonated copolymers incorporating  $\alpha,\beta,\beta$ -trifluorostyrene and a series of substituted  $\alpha,\beta,\beta$ -trifluorostyrene co-monomers. These membranes have an equivalent weight ranging between 375 and 920. The water content of the sulfonated BAM3G is much higher than that of Nafion<sup>®</sup> and Dow membranes. BAM3G membranes demonstrated a lifetime approaching 15,000 hours when tested in a Ballard MK5 single cell and also exhibited performances superior to Nafion<sup>®</sup> and Dow<sup>®</sup> membranes in a H<sub>2</sub>/O<sub>2</sub> fuel cell. Disadvantages of these membranes include the complicated

production process for the monomer  $\alpha,\beta,\beta$ -trifluorostyrene [184] and the difficult sulfonation procedure [114,183].

### **2.2.3.2 Grafted Ionomer Membranes**

Partially fluorinated membranes can be obtained by using a simultaneous and pre-radiation grafting of monomers onto a base polymer film, and subsequent sulfonation of the grafted component [113,150,185-194]. These membranes were prepared by pre-irradiation of fluoropolymer films, such as poly(tetrafluoroethylene-*co*-hexafluoropropylene (FEP) or poly(ethylene-*alt*-tetrafluoroethylene) (ETFE), using an electron beam or gamma irradiation source. The pre-irradiated films were grafted by exposing them to solutions of styrene and other radically polymerizable monomers. The grafted films are sulfonated using chlorosulfonic acid. The grafting mixture was crosslinked with divinylbenzene (DVB) and tri-allyl cyamirate (TAC) [189,195,196] or poly(vinylidene fluoride) [197]. A disadvantage of membranes using styrene and divinylbenzene monomers is that their oxidation stability is limited, due to the tertiary C-H bonds which are sensitive to O<sub>2</sub> and hydrogen peroxide attack [114].

## **2.2.4 Non-Perfluorinated Membranes**

### **2.2.4.1 Polybenzimidazole (PBI)**

PBI is synthesized from aromatic bis-*o*-diamines and dicarboxylates (acids, esters, amides), either in the molten state or in solution [198]. PBI is relatively low cost and is a commercially available polymer known to have excellent oxidation and



thermal stability. The commercially available polybenzimidazole is poly-[2,2'-(*m*-phenylene)-5,5'-bibenzimidazole], which is synthesized from diphenyl-iso-phthalate and tetra-aminobiphenyl.

Hoel and Grunwald [199] reported on proton conductivity values of PBI in the range of  $2 \times 10^{-4} - 8 \times 10^{-4}$  S/cm at relative humidities (RH) between 0 and 100%. Other authors observed proton conductivity some two to three orders of magnitude lower [200-202].

PBI is a suitable basic polymer which can readily be complexed with strong acids [104,198,200,201,203-209]. The immersion of PBI film in aqueous phosphoric acid leads to an increase in both its conductivity and thermal stability [201].

Savinell and co-workers [203] prepared PBI/H<sub>3</sub>PO<sub>4</sub> via two different routes: a) directly casting a film of PBI from a solution containing phosphoric acid; b) preparation by immersion of a preformed PBI membrane in 11M phosphoric acid for several days [203,206]. The typical thickness for different films was 75 μm. The conductivity depends on the quantity of phosphoric acid in the membrane. Conductivity in the range  $5 \times 10^{-3}$  to  $2 \times 10^{-2}$  S/cm at 130°C and  $5 \times 10^{-2}$  S/cm at 190°C have been reported [204]. The conductivity for type “a” membranes is higher than those of type “b” membranes. At a temperature above 150°C, the conductivity of type “a” membranes is similar to that of Nafion<sup>®</sup> at 80 °C and 100% RH.

It was shown that the methanol crossover through doped PBI type “a” membrane, was at least ten times less than that observed with Nafion<sup>®</sup>. The disadvantage of these membranes is that the H<sub>3</sub>PO<sub>4</sub> molecules can diffuse out of the

membrane towards basic polymer sites because they are in excess. PBI/H<sub>3</sub>PO<sub>4</sub> membranes are suitable for direct methanol fuel cell application at a temperature >100°C. However, they can only be used with a feed of vapourized methanol, because when a liquid contacts the membrane, the phosphoric acid leaches out of the membrane and the proton conductivity drops considerably [114].

#### 2.2.4.2 Sulfonated Polyimide Membranes

The sulfonated polyimide (SPI) membranes were obtained by casting on a glass plate the polymer solution and evaporating the solvent [210-219]. The polymer solution synthesis was achieved in different ways: The first way was based on the phthalimide-five member imide (4,4'-diamino-biphenyl 2,2' disulfonic acid (BDSA), 4,4' oxy-diphthalic dianhydride (ODPA) and 4,4'-oxydianiline (ODA)) at 200°C. The second way was based on the naphthalimide-six member imide ring (BDSA, 1,4, 5,8-naphthalene tetracarboxylic dianhydride (NTDA) and ODA) at 160°C [210-212]. The third way was based on the 3,3',4,4'-benzophenone-tetracarboxylic dianhydride (BTDA), BDSA and ODA [112]. The fourth way was based on BDSA/NTDA/mAPI (bis-[3-(Aminophenoxy)-4-phenyl]isopropylidene) [217]. The water content of membranes at 25°C for the phthalic and naphthalenic sulfonated polyimide membranes is 26% and 30%, respectively. The water content obtained for Nafion<sup>®</sup> membranes under the same conditions was 20% [210,212]. It was also claimed that the sulfonated polyimide membranes were 3 times less permeable to hydrogen gas than Nafion<sup>®</sup> membranes. The lifetime measurements were performed on a 175 µm

phthalic polyimide and a 70  $\mu\text{m}$  naphthalenic sulfonated polyimide film at 60°C, 3 bar pressure for  $\text{H}_2$  and  $\text{O}_2$  and under a constant current density. It was found that the membrane based on the phthalic structure broke after 70 hours whereas the membrane based on the naphthalic polyimide was stable over 3000 hours [212]. The proton conductivity of SPI was found to be half of Nafion<sup>®</sup> 117, typically  $4.1 \times 10^{-2}$  S/cm, and methanol permeability was found to be  $7.34 \times 10^{-8}$  compared to  $2.38 \times 10^{-6}$   $\text{cm}^2/\text{s}$  for Nafion<sup>®</sup> 117 [214].

#### **2.2.4.3 Phosphazene-based Cation-Exchange Membranes**

It was shown that polyphosphazene-based cation-exchange membranes have a low methanol permeability, low water swelling ratios, satisfactory mechanical properties, and a conductivity comparable to that of Nafion<sup>®</sup> 117 [220-226]. Polyphosphazene-based membranes have been fabricated from poly[bis(3-methylphenoxy)phosphazene] by first sulfonating the base polymer with  $\text{SO}_3$  and then solution-casting a thin film [220,222,226]. Polymer crosslinking was carried out by dissolving benzophenone photoinitiator in the membrane casting solution and then exposing the resulting films after solvent evaporation to UV light [221]. The conductivity of the polyphosphazene membranes were either similar to or lower than that of Nafion<sup>®</sup> 117 membranes [221,226]. However, methanol permeability of a sulfonated membrane was about 8 times lower than that of the Nafion<sup>®</sup> 117 membrane [226]. Sulfonated/crosslinked polyphosphazene films showed no signs of mechanical failure (softening) up to 173°C and a pressure of 800 kPa [221].

#### 2.2.4.4 Sulfonated Poly(arylethersulfone) Membranes

Polysulfone (PSU) is a low cost, commercially available polymer (e.g. PSU Udel™ from Amoco) which has very good chemical stability. The synthesis and characterization of sulfonated polysulfone (S-PSU) has been achieved by Johnson *et al.* [227] and Nolte *et al.* [228]. It was found that membranes cast from S-PSU (Udel™ P-1700) solutions were completely water soluble [228] and become very brittle when drying out which can happen in the fuel cell application under intermittent conditions [229].

There are two new but different procedures for the sulfonation of polysulfone. In one procedure, the sodium-sulfonated group was introduced in the base polysulfone via the metalation-sulfination-oxidation process [230,231]. In the other procedure, trimethylsilyl chlorosulfonate was used as the sulfonating agent [232].

Lufrano *et al.* [233,234] prepared S-PSU via trimethylsilyl chlorosulfonate with different degrees of sulfonation. Different membranes with sulfonation degree from 23% to 53% [233] on the one hand and 49%, 61% and 77% [234] on the other hand were prepared. With a 61% sulfonation degree a proton conductivity for S-PSU of  $2.7 \times 10^{-2}$  S/cm at 25°C was reported [234]. This conductivity was 3.5 times lower than Nafion® 117, but was compensated by the lower thickness, 90 μm vs. 210 μm for Nafion® 117. The cell performance obtained by Lufrano *et al.* [234] was almost the same for S-PSU and Nafion® in a H<sub>2</sub>/O<sub>2</sub> fuel cell. This is higher than that reported previously by Kerres *et al.* [231] and Baradie *et al.* [232]. Kim *et al.* [235] prepared sulfonated poly(arylether sulfone) membranes.

Promising alternatives suggested by Kerres and co-workers, include composite membranes made from blends of acidic and basic polymers [229,236-240] or modified PSU via the metalation-sulfochlorination and the metalation-amination routes [241] or crosslinked S-PSU [242-244]. These alternatives are made by blending acidic polymers such as S-PSU with basic polymers such as poly(4-vinylpyridine) (P4VP), polybenzimidazole (PBI) or a basically substituted polysulfone. Crosslinked S-PSU blend membranes have been produced via a new crosslinking process. The blends have been obtained by mixing PSU Udel™ Na-sulfonate and PSU Udel™ Li-sulfinate in *N*-methyl pyrrolidone. The membranes have been crosslinked by S-alkylation of PSU sulfinate groups with di-halogenoalkanes. These membranes show very good performance in H<sub>2</sub>/O<sub>2</sub> fuel cells and DMFCs [114,238-239]. These membranes also show a markedly reduced methanol permeability [114,237,245].

#### **2.2.4.5 Sulfonated Poly(aryletherketone) Membranes**

The poly(arylether ketones) are a class of non-fluorinated polymers consisting of sequences of ether and carbonyl linkages between phenyl rings, that can either “ether-rich” like PEEK and PEEKK, or “ketone-rich” like PEK and PEKEKK. The most common material is polyetheretherketone (PEEK) which is commercially available under the name Victrex™ PEEK from ICI Advanced Materials. A number of groups are developing proton conducting polymer materials based on this classification of materials including ICI Victrex, Fuma-Tech and Axiva/Aventis/Hoechst.

Sulfonated-PEEK (S-PEEK) membranes were prepared as proton conductors in PEMFCs by Schneller *et al.* [246]. Sulfonation of polyetherketones can be carried out directly in concentrated sulfonic acid or oleum - the extent of sulfonation being controlled by the reaction time and temperature [247-250]. Direct sulfonation of PEEK can give materials with a wide range of equivalent weights to form S-PEEK. However, the complete sulfonation of the polymer results in a fully water-soluble product. A sulfonation level of around 60% was found to be a good compromise between the conductivity and mechanical properties of membranes. The backbone of S-PEEK is less hydrophobic than the backbone of Nafion<sup>®</sup>, and the sulfonic acid functional group is less acidic [251].

Various studies have been made on the conductivity of S-PEEK [129,251,252-258]. The conductivity increases as a function of the degree of sulfonation, the ambient relative humidity, temperature and thermal history. The conductivity of these materials was found to be high at room temperature [259]. In S-PEEK with 65% sites sulfonated, the conductivity was higher than that of Nafion<sup>®</sup> 117 measured under the same conditions - the conductivity reaching  $4 \times 10^{-2}$  S/cm at 100°C and 100% RH [253]. S-PEEK membranes exhibit at 160°C and 75% RH, sufficiently high values of protonic conductivity - typically  $5 \times 10^{-2} - 6 \times 10^{-2}$  S/cm - for possible applications in low temperature fuel cells [255]. The dependence of the conductivity on RH is more marked for S-PEEK than for Nafion<sup>®</sup> under the same conditions [256].

Sulfonated polyaryls have been demonstrated to suffer from hydroxyl radical initiated degradation [260]. In contrast, S-PEEK was found to be durable under fuel

cell conditions over several thousand hours by Kreuer [251]. The brittleness of S-PEEK makes their handling difficult and may lead to mechanical membrane failure during operation. These types of membranes become very brittle when drying out.

S-PEEK can also be chemically cross-linked to reduce membrane swelling and increase its mechanical strength. Materials prepared by cross-linking are comparable to commercial Nafion<sup>®</sup> in terms of their mechanical strength and proton conductivity [261]. Kerres and co-workers prepared novel acid-base polymer blend membranes composed of S-PEEK as the acidic compound, and of P4VP or PBI as the basic compounds [229,240].

### **2.2.5 Organic / Inorganic Composite Membranes**

The organic / inorganic composite proton conductors are developed to overcome the disadvantages of the actual state-of-the-art membranes which require increasing the operating temperature above 100°C and /or reducing methanol permeability (methanol crossover).

The method of inclusion of inorganic particles involves a bulk powder dispersed in a polymer solution, leading specifically to particles of highly dispersed inorganic proton conductors of particle size in the sub-micronic range. These methods make use of mild chemistry techniques, including intercalation/exfoliation, sol-gel chemistry, and ion-exchange [198,262]. Such approaches generally avoid any sedimentation of the inorganic component, enhance the intimacy of contact between the inorganic and organic components at the molecular level which assures the

greatest possible interface and, at such small particle sizes, the mechanical properties can be improved when compared to those of a polymer-only membrane [198]. In addition, as in many proton conductors with conductivity suitable for electrochemical applications, the proton transfer process takes place on the surface of the particles; an increase in surface area (small particle size) will increase the conductivity [198].

### **2.2.5.1 Nafion<sup>®</sup>/ Inorganic Composite Membranes**

One of the main drawbacks of DMFCs is the slow methanol oxidation kinetics. An increase in the operating temperature of the DMFC from 90 to about 150°C is highly desirable. Also operation at high temperature will enhance CO toleration when a reformat hydrogen is used in a H<sub>2</sub>-PEMFC. One approach to achieve water retention at high temperature is to fabricate a composite membrane constituted of Nafion<sup>®</sup> and inorganic materials. Silica as an additive to Nafion<sup>®</sup> was widely studied [93,151,263-271]. Both recast Nafion<sup>®</sup> [264,266-269] and Nafion<sup>®</sup> polymer [151,267,270] are used in the fabrication of the composite membrane. Silica can be added to Nafion<sup>®</sup> in two ways; the first using silicon dioxide particles (e.g. Aerosil A380 from Degussa) [93,264,266,268,269], the other is to introduce silica oxide incorporated via an *in situ* sol-gel reaction with tetraethoxysilane (TEOS) [151,267,270-273].

Staiti *et al.* [274] prepared recast Nafion<sup>®</sup>-silica composite membranes doped with phosphotungstic (PWA) and silicotungstic (SiWA) acids for application in DMFCs at high temperature (145°C). The PWA-based membrane showed better



electrochemical characteristics at high current densities with respect to both SiWA-modified membrane and recast Nafion<sup>®</sup>-silica membrane. A similar membrane was prepared by Shao *et al.* [275] and Aricò *et al.* [276,277].

Zirconium bis(monohydrogen phosphate) mono-hydrate,  $\alpha$ -Zr(HPO<sub>4</sub>)<sub>2</sub>.H<sub>2</sub>O (denoted as ZrP) can be added to Nafion<sup>®</sup> to increase the working temperature [278-281]. Yang *et al.* [279-281] introduced ZrP into Nafion<sup>®</sup> through ion exchange of Zr<sup>4+</sup> followed by precipitation of ZrP by treatment with phosphoric acid as described by Grot and Rajendran [278].

Dimitrova *et al.* [269] prepared a recast Nafion<sup>®</sup>-based composite membrane containing molybdophosphoric acid. This composite membrane exhibits significantly higher conductivity in comparison to Nafion<sup>®</sup> 117 and pure recast Nafion<sup>®</sup>. An enhancement in the conductivity by a factor 3 at 90°C was observed.

Tazi and Savadogo [282,283] fabricated Nafion<sup>®</sup> membranes containing SiWA and thiophene. They reported an increase of up to 60% in water uptake and a considerable improvement in the fuel cell current density, when compared to the plain Nafion<sup>®</sup> membrane. Apichatachutapan *et al.* [284] prepared Nafion<sup>®</sup>/(zirconium oxide) hybrid membranes via *in situ* sol-gel techniques.

Nafion<sup>®</sup> has been impregnated with poly(1-methylpyrrole) by *in situ* polymerization by Jia *et al.* [285]. It was found that the ionic resistance increased dramatically with high loading, which, methanol permeability can be reduced up to 90%. The high resistance prevents the use of this membrane in fuel cells. However, at

lower poly(1-methylpyrrole) loading, a decrease in methanol permeability by as much as 50% can be realized without significant increase in ionic resistance [285].

### 2.2.5.2 Polymers / Inorganic Composite Membranes

Since the very high proton conductivity of hydrated polymers relies on the presence of liquid water, the maximum operating temperature is approximately given by the boiling point of water. It has been shown that substitution of water by heterocyclic compounds such as imidazole, pyrazole, or benzimidazole, leads to proton conductivities which are comparable to the conductivities of hydrated polymers between 150 and 250°C [251,286,287].

Dispersion of submicronic particles of phosphoantimonic acid fillers in a solution of S-PSU gives a viscous suspension allowing the material to be shaped in thin films. Conductivity values close to those of the Nafion<sup>®</sup>117 have been determined under the same experimental conditions. Furthermore, the inorganic filler improves both mechanical strength and the gas permeability of the filled membrane when compared to an unfilled PSU membrane [232,288].

Organic/inorganic composite membranes based on sulfonated polyetherketone (S-PEK) and S-PEEK for application in DMFCs were synthesized by Nunes and co-workers [289-291]. The inorganic fillers were introduced via *in situ* generation of SiO<sub>2</sub>, TiO<sub>2</sub> or ZrO<sub>2</sub>. The modification with ZrO<sub>2</sub> led to a 60-fold reduction of the methanol flux. However, a 13-fold reduction of conductivity was also observed [289]. A good balance of high conductivity, and low water and methanol permeability was

obtained with a mixture of  $ZrO_2$  and zirconium phosphate (ZrP) [289], since ZrP includes phosphate particles which are able to contribute to proton conduction in the membrane. ZrP was prepared using procedures analogous to that described by Belyakov and Linkov [292]. Ponce *et al.* [290] developed a composite membrane by using S-PEK as an organic polymer matrix and different heteropolyacids with an inorganic network of  $ZrO_2$  or  $RSiO_{3/2}$ . The inorganic oxide network had the function of decreasing the methanol and water permeability across the membrane, as well as decreasing the bleeding out of the heteropolyacid. Different heteropolyacids were investigated, including commercial tungstophosphoric acid (TPA) and molybdophosphoric acid (MoPA), and two heteropolyacids synthesized in the laboratory. The highest conductivity values - typically 86-110 mS/cm were found for the hybrid membranes with S-PEK and  $ZrO_2$ -TPA.

Zaidi *et al.* [254] prepared a series of composite membranes using S-PEEK as polymer matrix and TPA, with the sodium salt of TPA and MoPA as inorganic fillers. The conductivity of the composite membranes exceeded  $10^{-2}$  S/cm at room temperature and reached values of about  $10^{-1}$  S/cm above  $100^\circ\text{C}$  [254]. Jones and Rozière [198] prepared a composite membrane by using S-PEEK as polymer matrix and incorporating metal (IV) phosphates (zirconium phosphate (ZrP) or tin phosphate (SnP)) as the inorganic fillers. The conductivity of S-PEEK membranes incorporating ZrP particles is higher than either that of the polymer-only membrane recorded under the same conditions, or that of bulk ZrP [262]. When the membrane S-PEEK/ZrP was tested in a  $H_2/O_2$  fuel cell, improvement in performance was observed as the

temperature was increased from 85 to 100°C. Alberti *et al.* [255] suggested the fabrication of organic/inorganic composite membranes based on S-PEEK as polymer matrix and zirconium sulfophenyl phosphonates, since acceptable electrical conductivity is obtained with the latter [293].

Staiti *et al.* [294,295] prepared a composite membrane based on PWA absorbed on silica (SiO<sub>2</sub>) as inorganic materials and PBI as binding polymer. The SiO<sub>2</sub> has the double function of entrapping the heteropolyacid preventing its dissolution in water and retaining water, thus improving the proton conduction. The composite membrane prepared with 50 wt.% of inorganic material was mechanically stable and gave a proton conductivity of  $1.2 \times 10^{-3}$  S/cm at 160°C and 100% RH.

Park and Nagai [296] prepared composite membranes constituted of 3-glycidoxypropyltrimethoxysilane (GPTS), SiWA and ZrP. The polymer matrix obtained through hydrolysis and the condensation reaction of GPTS showed apparent proton conduction at high relative humidity with conductivity ranging from  $1.0 \times 10^{-7}$  to  $3.6 \times 10^{-6}$  S/cm. By addition of SiWA, the conductivity increased up to  $1.9 \times 10^{-2}$  S/cm. By incorporating ZrP into the GPTS-SiWA polymer matrix, the composite membrane showed increased conductivity at temperatures around 80°C, indicating weak dependence on humidity by molecular water in ZrP.

Honma *et al.* [297-299] investigated organic/inorganic hybrid polymer membranes of SiO<sub>2</sub>/ polymer (polyethylene oxides (PEO); polypropylene oxide (PPO); and polytetramethylene oxide (PTMO)). These membranes have been synthesized through sol-gel processes in flexible, ductile free-standing thin form.

However, the process is very complex and the composites showed low chemical stability [296].

### **2.2.5.3 Organic / Inorganic Hybrid Polymers**

Another class of proton conductor membranes are organic-inorganic protonic polymers such as “ormolyte-organically modified silane electrolyte” [300,301] or “ORMOCER” [302,303]. Poinsignon and co-workers [300,301] developed an organic-inorganic proton conductor using grafted arylsulfonic anions, for example, poly(benzylsulfonic acid siloxane), in contrast to Popall and co-workers [302,303] who used grafted alkylsulfonic anions.

These proton conductors are produced by a sol-gel process, and can be cross-linked via hydrosilylation [301] or via UV-initiated and/or thermal polymerization [302]. In these materials the conductivity results from the mobility of the acidic proton solvated by water molecules, which shows an ionic conductivity of  $10^{-2}$  S/cm at ambient temperature [301,303]. Further development of this type of material was carried out with methacryl and epoxy alkoxy silanes [304], which lately were replaced by styrene derivative functionalized alkoxy silanes [305] to improve the electrochemical stability of the materials for applications in DMFCs.

### **2.2.6 Other Polymeric Proton Conductor Membranes**

The styrene/ethylene-butadiene/styrene triblock copolymer is a commercially available product, such as Kraton<sup>®</sup> G1650, containing a saturated carbon block. This

membrane has been developed by the DAIS Company in the USA [306-308]. A sulfonation level of 60% was found to provide a good balance of electrical and mechanical properties. It was also found that the conductivities at sulfonation levels above 50 mole% of styrene units, exceed that of Nafion<sup>®</sup> under similar measurement conditions. The predicted lifetimes of DAIS-membrane-based fuel cells were 2,500 hours at 60°C and 4,000 hours at room temperature.

Carretta *et al.* [309] have partially sulfonated a commercial non-crosslinked poly(styrene) to various extents. They found a proton conductivity of  $5 \times 10^{-2}$  S/cm at room temperature at sulfonate concentrations of 20 mol%, which is very close to the conductivity of Nafion<sup>®</sup>. This membrane exhibits a conductivity to permeability ratio about 70% higher than Nafion<sup>®</sup>, which makes it very attractive for DMFC applications.

Yamaguchi *et al.* [310] developed a membrane consisting of a poly (vinyl-sulfonic acid/acrylic acid) crosslinked gel in a porous PTFE substrate. This had high proton conductivity with reduced membrane methanol permeability, and was thermally stable to 130°C.

Another class of proton conductor membranes are the so-called “hydrogels”, which showed high conductivity at ambient and sub-ambient temperatures. Such proton conductive polymer blends with for example, poly(vinylalcohol)/H<sub>3</sub>PO<sub>4</sub> have conductivities exceeding  $10^{-3}$  S/cm at ambient temperature [311], similarly poly(ethylenoxide)/poly(methylmethacrylate)/H<sub>3</sub>PO<sub>4</sub> [312] and poly(acrylamide)/poly(ethylenoxide)/ H<sub>3</sub>PO<sub>4</sub> blends [313]. It has been shown that the conductivity of

such membranes can be increased by at least one order of magnitude after humidification with moist gases, but they exhibit poor mechanical and chemical stability after humidification [117]. Their suitability for fuel cell application is questionable due to the presence of easily oxidizable tertiary C-H bonds in the polymers forming the hydrogels [114].

### 2.2.7 Inorganic Proton Conductor Membranes

Very few inorganic materials which have high proton conductivity in the temperature range 25-200°C have been adopted as membranes for fuel cells. Alberti and Casciola [314] summarized them as shown in Table 2.6.

**Table 2.6:** Inorganic proton conductors in the temperature range 25-200°C

Proton conductor	Conductivity (S/cm)	T°C	%RH	Ref.
$\alpha$ -Zr(HPO <sub>4</sub> ) <sub>2</sub> · nH <sub>2</sub> O	$1 \times 10^{-4}$	25		315
$\alpha$ -Zr(HPO <sub>4</sub> ) <sub>2</sub> · H <sub>2</sub> O	$1.5 \times 10^{-4}$	100	97	316
$\gamma$ - Zr(PO <sub>4</sub> )(H <sub>2</sub> PO <sub>4</sub> ).2H <sub>2</sub> O	$3 \times 10^{-4}$	25		317
$\gamma$ - Zr(PO <sub>4</sub> )(H <sub>2</sub> PO <sub>4</sub> ).2H <sub>2</sub> O	$3 \times 10^{-4}$	100	95	318
$\alpha$ -Zr sulfophenylphosphonate	$1.6 \times 10^{-2}$	25		319
$\alpha$ -Zr sulfophenylphosphonate	$1 \times 10^{-2}$	100	60	320
$\alpha$ -Zr sulfophenylphosphonate	$1 \times 10^{-5}$	180	0	320
$\gamma$ -Zr sulfophenylphosphonate	$1 \times 10^{-2}$	25		293
$\gamma$ -Zr sulfophenylphosphonate	$5 \times 10^{-2}$	100	95	293
$\gamma$ -Zr sulfophenylphosphonate	$1.3 \times 10^{-2}$	150	80	321
SiO <sub>2</sub> · 0.33 $\alpha$ -ZrP	$3 \times 10^{-3}$	100	97	316
H <sub>4</sub> SiW <sub>12</sub> O <sub>40</sub> · 28H <sub>2</sub> O	$2 \times 10^{-2}$	25		322,323
H <sub>3</sub> PW <sub>12</sub> O <sub>40</sub> · 29H <sub>2</sub> O	$8 \times 10^{-2}$	25		322,323
CsHSO <sub>4</sub>	$5 \times 10^{-3}$	142		324

The proton conductivity of a tin mordenite/SnO<sub>2</sub> composite has been found to be around  $1 \times 10^{-3}$  S/cm at 25°C, which increases to  $6 \times 10^{-2}$  S/cm at 120°C and 100% RH [325]. The introduction of highly hydrated aluminium ions, such as  $[\text{Al}_{13}\text{O}_4(\text{OH})_{24}(\text{H}_2\text{O})_{12}]^{7+}$ , into the interlayer space of tin hydrogenophosphates shows a conductivity of  $10^{-2}$  S/cm at 80°C and 100% RH [326].

The most promising inorganic proton conductors, heteropolyacids and layered acidic phosphates and phosphonates, are difficult to utilize in fuel cells. Heteropolyacids were found to dissolve in product water in H<sub>2</sub>-PEMFCs and in aqueous methanol. Furthermore, there are few alternatives to the sintered and compacted ceramic concept of making inorganic membranes. The most important alternative is the formation of composite membranes by the introduction of the inorganic electrolyte in an organic polymer matrix - the latter acting as a binder.

In spite of the difficulties of fabricating an inorganic proton conductor membrane for fuel cell applications, a few attempts have been made. Poltarzewski *et al.* [327] synthesized a composite membrane with zeolites (Zeolon 100H) dispersed in PTFE suspension. After drying the mixture (Zeolon 100H, PTFE suspension, water and iso-propanol), the conductivity of the composite membrane was found to vary with zeolite content. Conductivities of  $10^{-2}$  S/cm and  $4 \times 10^{-4}$  S/cm were reported with 90 wt.% and 40 wt.% zeolite content, respectively. The cell performance with methanol and oxygen at 70°C and using 90 wt.% zeolite composite membrane was very low - reaching a maximum of 4 mW/cm<sup>2</sup>. Kenjo and Ogawa [328] and Cappadonia *et al.* [329] prepared a membrane based on ammonium polyphosphate.



Conductivities of  $5 \times 10^{-3}$  S/cm [328] and 0.1 S/cm [329] at 300°C were reported. But no fuel cell performance with this type of membrane was reported. Boysen *et al.* [330] prepared a composite membrane constituted of CsHSO<sub>4</sub> as proton conductor and PVDF as a binder. The conductivity of the composite membrane exhibits a sharp increase with temperature at 140°C. The OCV (open circuit voltage) was high, typically around 0.97 V. However, due to the thickness of the membrane used (1 mm), attempts to draw current leads to a sharp drop in voltage.

The most studied inorganic proton conductor membrane for fuel cell applications, is ZrP due to its greater ability to withstand fuel cell oxidizing conditions, and its ability to retain water at high temperature. Furthermore, ZrP is not soluble in water.

The original pioneering effort on the use of ZrP as cation exchange material was performed by Kraus [331,332], Amphlett *et al.* [333-335], Larsen and Vissers [336] and was extensively study by Clearfield [337-343] and Alberti [344-346].

Alberti [347] described a glass fibre membrane impregnated with ZrP, but the conductivity and the temperature stability of the membranes were not sufficient for fuel cell application. Hamlen [348] and Dravnieks and Bregman [349-351] were the first to employ ZrP membranes in hydrogen-oxygen fuel cells. The performances were marginal and the membrane weak, and it was done at ambient temperature. Hamlen and Szymalak [352] have used a specially prepared ZrP-PTFE matrix and applied in a hydrogen fuel cell over the range 125-175°C. Berger and Strier [353] prepared a membrane consisting of ZrP and the zeolite material “Zeolon H”, and obtained stable

fuel cell performance over the temperature range 25-151°C. Abe *et al.* [354] prepared ZrP gel-glasses using sol-gel processing techniques, which gave room temperature conductivities of approximately  $10^{-2}$  S/cm. They claim that these materials are stable and can be used in H<sub>2</sub>/O<sub>2</sub> fuel cells, but unfortunately, no results on fuel cell performance were reported. Park *et al.* [355] prepared a highly conductive ZrP / PTFE composite membrane by using partially polymerized PTFE particles as a fixing matrix, and commercially available ZrP powder from Daiichi Kigenso Kagaku Kogyo Co. as a proton conductor. Proton conductivity above  $10^{-3}$  S/cm was reported with ZrP particles sizes of 0.5 -1  $\mu\text{m}$  and 5-15  $\mu\text{m}$  for  $\alpha$ -ZrP and  $\gamma$ -ZrP, respectively. Tamura *et al.* [356] prepared a composite membrane for DMFC constituted of ZrP and 5P<sub>2</sub>O<sub>5</sub>-95SiO<sub>2</sub> glass. The conductivity of this composite membrane was about  $10^{-3}$  -  $10^{-4}$  S/cm at 100°C. No fuel cell performance was reported.

$\alpha$ -ZrP can be prepared by two methods giving rise to either a crystalline [357] or amorphous form [337]. The  $\alpha$ -ZrP used as fuel cell electrolyte was of the amorphous-type prepared with excess H<sub>3</sub>PO<sub>4</sub>. Hamlen and Szymalak [352] showed that most of the conductivity of these electrolytes was caused by excess acid. Clearfield and Stynes [337] report loss of phosphate from amorphous  $\alpha$ -ZrP in contrast to crystalline  $\alpha$ -ZrP by prolonged washing with water. Ahrland *et al.* [358] investigated the hydrolysis of ZrP gels in detail and found no loss of phosphate at pHs below 7-8. They also found that H<sub>3</sub>PO<sub>4</sub> which adheres to the surface of the crystallites can only be removed by very extensive washing.

The crystal structure of ZrP was determined by Clearfield and coworkers [339,340,342]. The structure is formed by zirconium phosphate layers with adjacent layers forming cavities in which the water molecules are located. Each layer consists of  $Zr^{+4}$  ions arranged pseudo-hexagonally in a plane which is lined on each side by sheets constructed of  $HPO_4^{2-}$  tetrahedra. The three oxygens at the basis of each tetrahedron are bound to three  $Zr^{+4}$  ions, whereas the fourth carrying an acidic proton is directed towards a neighbouring layer. Thus each zirconium ion is surrounded by a slightly distorted octahedron of phosphate oxygen atoms belonging to six different  $HPO_4^{2-}$  tetrahedrals. The water molecule is held in the cavity by three intralayer H-bonds involving two phosphate acidic protons and one water proton. The other hydrogen atom of the water molecule forms no hydrogen bond. There are no interlayer H-bonds and the layers are held together by van der Waals forces only. Figure 2.4 shows the structure of  $\alpha$ -ZrP.

Alberti and co-workers [346] found that the mobility of surface ions in  $\alpha$ -ZrP is  $10^4$  times higher than those of interlayer ions, and that the low activation energy (11-13 kJ/mol) for ionic conduction was due to the transport of surface ions. Therefore, the surface ions of layer-structured  $\alpha$ -ZrP compound significantly contributes to the total conduction. Krogh Andersen *et al.* [359] found that the conductivity of  $\alpha$ -ZrP decreases with increasing particle size, whereas the activation energy is independent of the particle size, showing  $\alpha$ -ZrP to be a surface conductor.

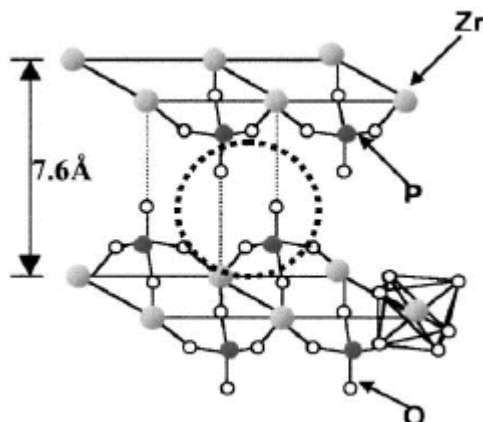


**Figure 2.4:**  $\alpha$ -zirconium phosphate structure (denoted  $\alpha$ -ZrP) [355].

## 2.3 DMFC COMPONENTS

The MEA is the heart of the DMFC. As discussed in Section 2.1.2, the MEA is constituted of: anode backing layer, anode catalytic layer, proton exchange membrane, cathode catalytic layer and cathode backing layer.

### 2.3.1 Anode Catalyst - Methanol Oxidation

Methanol oxidation has been extensively studied for the last 3 decades. Very few electrode materials are capable of methanol oxidation - only platinum and platinum-based catalysts have been found to display the necessary reactivity and stability in the acidic environment of the DMFC, and almost all mechanistic studies have concentrated on these materials [49,360].

Methanol oxidation and its mechanisms on different catalyst systems under well-characterized conditions have been reviewed [16,41,49,360-373]. Methanol

oxidation can be summarized in terms of two basic functionalities: (a) Electrosorption of methanol onto the substrate and (b) Addition of oxygen to adsorbed carbon-containing intermediates to generate CO<sub>2</sub> [360].

Morphology appears to play a major role in the electroactivity of platinum [374], with roughened platinum showing much higher activity [375]. Methanol adsorption is inhibited in general by the adsorption of anions: chloride ions strongly inhibit methanol oxidation at platinum, while bromide and iodide ions entirely arrest the process [376]. Adsorbed phosphate also inhibits the rate of methanol oxidation [377].

The influence of particle size on methanol oxidation has been investigated by numerous authors [378-386]. However, there is considerable controversy over whether there exists a “size effect” in methanol oxidation. Some authors have observed a decrease in activity with decreasing particle size for particles with diameter less than 5 nm [378-385]. Earlier data from Shell suggested that there was a pronounced size effect, with an optimal Pt cluster diameter of ca. 3 nm [381,382] and the Oxford group suggested an optimal diameter of ca. 2 nm [383-385]. However, Watanabe *et al.* [386] do not find any evidence for size effects, even for particles as small as 1.4 nm. The methods of electrocatalyst preparation and their subsequent treatment in reducing atmospheres differ considerably in the various studies relating to the particle size effect [387,388].

It was first shown by Electrochemically Modulated Infrared Reflectance Spectroscopy (EMIRS) that the main poisoning species formed during the

chemisorption and oxidation of methanol on a platinum electrode is CO, either linearly bonded or bridge bonded to the surface [389]. The coverage by linearly bonded CO can reach 90% on a pure platinum electrode, so that most of the active sites are blocked [15]. Such results were widely confirmed [96,361,390-399].

Platinum itself, though widely studied as an electrocatalyst for methanol oxidation, is not sufficiently active, and there has been an intensive search for other active materials - in particular, materials that might be able to combine with platinum as promoter by facilitating the oxidation of the chemisorbed CO [360].

Pt promotion can be obtained by using surface ad-atoms deposited on the platinum surface, such as Au [400], Sn [401-405], Ru [405-407], Pb [405,408] and Bi [403,405,409]. Also Pt promotion can be effected by alloying platinum with different metals, where the second metal forms a surface oxide in the potential range for methanol oxidation [360,410]. Such alloys are Pt-Sn [401,405,411-413], Pt-Os and Pt-Ir [414], Pt-Pd [415] and Pt-Ru [402,412,414,416-427]. WO<sub>3</sub> as a promoter for Pt was also investigated [428-436]. Electrodeposited Mo on Pt has also been reported [437-438]. The combination of Pt with a base-metal oxide as promoter (e.g. Nb, Zr and Ta) has been reported by Hamnett *et al.* [428].

The methanol electro-oxidation activity of the Pt-Ru was found to be the highest of the binary Pt-based alloys [46,49,439-442]. Studies on Pt-Ru suggested that the reaction occurs by the dissociative adsorption of methanol on platinum sites to form a strongly adsorbed intermediate, CO. In parallel at higher levels of polarization, water adsorbs and dissociates on Ru sites to provide a hydroxylic species that

subsequently oxidizes the CO. The dissociation of water on Ru occurs at lower potentials than on Pt, resulting in the enhanced activity for Pt-Ru over pure Pt [443-446].

Given the effectiveness of binary alloy formation, particularly with Pt-Ru, attention has turned to ternary alloys. The Pt-Ru-Sn system was explored [447,448], but it was found that alloying Pt-Ru with tin tends to expel the Ru, leading to no advantage [447]. Other ternary systems reported were Pt-Ru-Os [449-451], Pt-Ru-W [452,453]. Quaternary systems were also explored, including Pt-Ru-Os-Ir [450], Pt-Ru-Mo-W [454] and Pt-Ru-Sn-W [455-457].

Various chemical routes are available for the synthesis of Pt-Ru catalyst. A common method is the reduction of metal chloride salts, but this preparation technique leads to significant amounts of chloride poisoning. The widely used chemical preparation technique is based on the oxidation and subsequent reduction of metal sulphite salts, which can be prepared from chloride metal salts [414,458]. Recently, the Bönemann method was used to synthesize colloidal precursors for carbon supported and unsupported Pt-Ru catalysts by the Bönemann group [459-463] and subsequently by other groups [453,464]. Furthermore, metal-oxide modified Pt-Ru catalyst was recently prepared [465]. A new method was also proposed by Dickinson *et al.* [466], where the catalyst is produced from carbonyl metal complexes by deposition of the precursors on carbon in high boiling-point solvent.

### 2.3.2 Cathode Catalyst – Oxygen Reduction

The ORR occurs as the cathodic process in numerous energy conversion processes, including low temperature fuel cells. Therefore, the ORR has been studied in detail [467-489]. Pt is the best known electrocatalyst for oxygen reduction and is widely used for electrochemical energy conversion [490].

It is considered that the Damjanovic mechanism is the most realistic for the ORR on platinum. The mechanism considers that the main reaction is the direct reduction of  $O_2$  to  $H_2O$  - the rate determining step being  $O_2$  protonation which takes place on bare platinum atoms. The secondary reaction is a parallel reduction to  $H_2O$  with an intermediate species:  $H_2O_2$  in acidic media [491-495].

A particle size effect on ORR kinetics has been demonstrated [496-499]. The high activity was found to be associated with a catalyst size between 3-4 nm [379].

In the  $H_2$ -PEMFC, ORR is much slower than hydrogen oxidation (see Section 2.1.3). In the DMFC, though, the anode reaction (methanol oxidation) is even slower. The cathodic oxygen reaction cannot be assumed to be a rate determining step under most operating conditions [500].

### 2.3.3 Backing Layers

The backing layer, usually carbon cloth or carbon paper, is the layer which sandwiches the MEA. Little attention was devoted to these types of materials in the 1990's [27,478,501,502]. However, some interest has emerged recently [503-510]. Up to now, finding the optimal backing layer is still a matter of trial and error. An ill-



chosen backing layer can easily render the most advanced flow field designs and electrocatalytic layers virtually ineffective. The requirements of an ideal backing layer are several, including the following:

- i) good reactant diffusion properties in both thickness and across the surface to distribute the reactants evenly onto the electrode surface;
- ii) water permeable to a certain degree to assist in water management by allowing passage of water into or out of the electrode without flooding;
- iii) low contact and bulk resistance to conduct electrons between the electrode and the flow plate; and
- iv) physical durability and chemical stability.

In the open literature, the backing layers used differ according to different authors. Table 2.7 summarizes these backing layers with some characteristics. In general, E-TEK carbon cloth is considered a standard backing layer for low temperature fuel cells. However, it was found that single sided ELAT performed better than the standard ELAT (carbon black microporous coatings on both sides of the web) in H<sub>2</sub>-PEMFCs [502]. On the other hand, Wilson *et al.* [27] found that E-TEK carbon cloth performed better than Kureha carbon paper, due to the cathode flooding in the latter in H<sub>2</sub>-PEMFCs. By structuring carbon paper electrodes, similar cell performance to carbon cloth can be achieved [511-518]. Furthermore, Gamburzev and Appleby [508] achieved better H<sub>2</sub>-PEMFC performance with carbon paper than carbon cloth.

In DMFCs, CO<sub>2</sub> is a reaction product that should be removed from the electrode structure and cell as efficiently as possible to maintain effective reaction [43,45,50,519-522]. The anode of a DMFC is a complex porous electrode system due to the three dimensional structure of the electrocatalyst region, the porous diffusion layer and the generation of carbon dioxide gas [520].

**Table 2.7:** Backing layers for low temperature fuel cells

Backing Layer	Company	Type	Thickness (mm)	Porosity (%)
Type "A"	E-TEK	Cloth	0.36	85
Standard ELAT	E-TEK	Cloth		
TGP H 120	Toray	Paper	0.36	77
TGP H 090	Toray	Paper	0.26	
E-715	Kureha	Paper	0.3 - 0.35	90
PWB-3	Stakepole	Cloth		
SIGRACET	SGL Carbon	Paper	0.28 - 0.42	
CARBEL	Gore & Associates			

In the most common DMFC operation mode, the anode is fed with liquid water-methanol mixture, which has a fairly low capacity for dissolved CO<sub>2</sub>. Therefore, CO<sub>2</sub> is evolved as a gas in the cell [50,519,522,523]. The CO<sub>2</sub> and aqueous methanol solution move counter-currently in the catalyst layer, in the gas diffusion layer and in the porous backing layer. Using high liquid methanol inlet flow rates and high pressures are effective in removing CO<sub>2</sub> bubbles [50,522].

Ideally, the gas and liquid flows should be insulated such that discrete paths for gas flow and for liquid flow exist, rather than a two-phase flow with gas bubbles

moving against a liquid flow. To avoid the two-phase flow a hydrophobic carbon surface is required, thereby creating regions for free gas movements [43,45,50]. PTFE can be added to the carbon backing layer or gas diffusion layer. Scott *et al.* [43] found that the best cell performance (efficient CO<sub>2</sub> removal) was achieved with a PTFE content between 13 to 20 % in the backing layer.

### 2.3.4 Electrodes for Low Temperature Fuel Cells

Since DMFCs use H<sub>2</sub>-PEMFC MEA fabrication technology, the electrode structures are discussed for both of them.

The electrodes are a complex structure and the fabrication techniques are mainly undisclosed. It has been shown that altering the composition of the electrodes can lead to substantial improvements in the performance of the cell [40,47,511,515,524-526]. For example, Hogarth *et al.* [47] prepared three types of electrodes for DMFCs. The three layer electrodes were prepared from the same catalyst, with the same Pt loading. The catalyst layer was constituted of the catalyst, water, iso-propanol, PTFE and Nafion<sup>®</sup> solution. Only by structuring the electrode, was the peak power density increased from 8 mW/cm<sup>2</sup> for the first electrode to 53 mW/cm<sup>2</sup> for the second electrode and to 79 mW/cm<sup>2</sup> for the third electrode.

The performance of the electrodes depend upon many parameters

- i) Type of support (carbon paper or carbon cloth) and its characteristics (porosity and thickness);

- ii) Type of catalyst (Pt only, Pt with other metals), Pt amount, Pt particle size, type of carbon support;
- iii) PTFE amount;
- iv) Nafion<sup>®</sup> amount;
- v) Thermal treatment;
- vi) Thickness of diffusion and catalyst layer; and
- vii) Fabrication process.

Most of the structural requirements of the electrode for its efficient operation are mutually self-exclusive and hence the optimization of electrode fabrication parameters is a difficult task [527]. On the other hand, it is also difficult to evaluate the influence of one parameter separately with other properties being constant [528,529]. For example, a change in the ionomer content affects reactant permeability, catalyst activity, and ionic resistance simultaneously.

The first descriptions of low catalyst loading carbon supported gas diffusion electrodes for H<sub>2</sub>-PEMFCs were made in the late 1980s, where it involved a ten fold diminution of the catalyst loading from 4 mg/cm<sup>2</sup> to 0.4 mg/cm<sup>2</sup> by impregnating the standard gas diffusion electrodes for a phosphoric acid fuel cell with solubilized Nafion<sup>®</sup> ionomer [24,530-533]. Nevertheless, this impregnation technique results in a catalyst utilization of only about 10 to 20% [27]. These electrodes are also prone to delaminate from the membrane, especially when the cells are shut down and then turned on again.

Further improvements were made by Gottesfeld and coworkers [25,27,534] who prepared the catalyst layer by mixing the solubilized ionomer with Pt/C catalyst. The catalyst layer is applied to the membrane, rather than to the backing layer. This electrode preparation produced a very thin film catalyst layer, typically less than 10  $\mu\text{m}$ .

To bind the thin-film structure together, special treatments of the recast films are necessary during fabrication. Initially, the durability of the recast composite film was improved by heat treating the catalyst layer [534]. Later, higher ionic conductivities and a moderate degree of robustness were achieved with an electrode fabrication process based on a high temperature casting technique that utilizes the ionomer in the  $\text{Na}^+$  form [25]. Further improvements were by using a thermoplastic form of the ionomer in the  $\text{TBA}^+$  (tetrabutylammonium) form [27].

Further advances in the attainment of high power densities have been made with a better localization of platinum near the front of the surface. The electrodes have been fabricated with a higher percentage of Pt on carbon and by sputter-deposition of a thin film of platinum (0.05 mg) on the front surface corresponding to a thickness of 50 nm and maintaining the final Pt content at 0.4  $\text{mg}/\text{cm}^2$  [474,535,536].

There are two distinguishable electrode structures: a dual electrode and a three layer electrode. The dual layer consists of a backing layer and a catalyst layer, while the three layer electrode consists of a backing layer, a gas diffusion layer and a catalyst layer. The gas diffusion layer is fabricated from a mixture of carbon black and PTFE suspension, called carbon ink, which is spread onto the backing layer. Zhang *et*

*al.* [537] developed a gas diffusion layer which is fabricated only by spreading a layer of ionomer solution onto the backing layer. In the absence of this diffusion layer, the catalyst ink absorbs into the macroporous backing layer, where it is not effective for catalytic reactions in the fuel cell [511,512]. The three layer electrodes were investigated mainly when a carbon paper was used as a backing layer [48,511-518,538-540].

The fabrication of both diffusion and catalyst layers can be carried out by different techniques such as screen-printing, rolling, brushing, filtering and spraying.

The incorporation of PTFE into the diffusion layer or catalyst layer serves two functions: binding the high surface area carbon particles into a cohesive layer, and imparting some hydrophobic character to the layer; thus allowing reactants transport to and from the catalyst layer.

Paganin *et al.* [525] investigated the performance of H<sub>2</sub>-PEMFCs with varying PTFE content in the gas diffusion layer, where it was found that the PTFE content has a small effect on cell performance. The best performance was found with 15 wt.% PTFE content. However, the thickness of the diffusion layer was found to play an important role.

Nordlund *et al.* [51] applied PTFE in the thin film catalyst layer developed at Los Alamos National Laboratory [27]. It was found that PTFE did not improve DMFC performance and the best performance was found without the addition of PTFE. However, adding PTFE may make the morphology more favorable for CO<sub>2</sub> to evolve as a gas by creating the necessary pores. These results are in agreement with the

finding of Passalacqua *et al.* [512], where it was demonstrated that eliminating PTFE in the catalyst layer for H<sub>2</sub>-PEMFCs, increases the free sites for proton access and available catalyst sites for the electrochemical reaction. However, this is in contradiction to the finding of Wei *et al.* [541], where, using the same electrode structure and thin film technique [25], they found that adding PTFE to the catalyst layer influences the DMFC performance, with the best results being achieved with 20 wt.% PTFE content.

#### **2.3.4.1 Ink Composition**

In a low temperature fuel cell, the electrode incorporates the catalyst powder, a proton transporting polymer and an electronically conductive additive [16]. In the electrode a three-phase zone is needed, where the electrode must have an electron conductive path, a proton conductive path and some porosity for reactants to freely move to and from the catalyst sites. Before electrode fabrication, the components of the electrode are mixed together to form an ink. Not much information has been reported about the preparation of the catalytic inks, and the composition varies with authors. The inks in general are constituted of the catalyst powder (supported or unsupported), proton conductive polymer, mainly Nafion<sup>®</sup> solution and a solvent. The state of the ink depends on the type of solvent. Uchida *et al.* [8] classified the inks in three categories: i) solution, ii) colloid, and iii) precipitation, depending on the dielectric constant ( $\epsilon$ ) of the organic solvent. A solution can be formed with a solvent

with  $\epsilon > 10$ ; for a solvent with  $\epsilon$  between 3 to 10, a colloidal solution can be formed; and in solvents with  $\epsilon < 3$ , a precipitate occurred [8].

In the solution method, it is considered possible for an ionomer to block the conduction of electrons as a result of covering the surface of carbon by ionomers thereby decreasing platinum utilization when electron insulating ionomers cover the surface of carbon excessively [7]. In the colloidal method, ionomer colloids adsorb the catalyst powders and the size of the agglomerates of catalyst powder increases. Then the porosity of the electrode will increase and, accordingly, the mass transfer resistance will be diminished. The continuous network of ionomers throughout the catalytic layer will be also increased, which will improve proton movement from the electrode to the membrane [7,8].

In the open literature, three types of organic solvent are used: glycerol ( $\epsilon = 42.50$ ) [27,512,513,516,517,543-545], iso-propanol ( $\epsilon = 18.30$ ) [51,511,518,525, 541,546-548], and butyl acetate ( $\epsilon = 5.01$ ) [7,8,456,457,542,549]. Glycerol and iso-propanol formed a solution, while butyl acetate formed a colloid. Glycerol can improve the paintability of the ink [543]. However, due to the high boiling point (290°C), molecules of glycerol can remain in the pores even after MEA heat treatment [550,551]. Glycerol can also react with Nafion<sup>®</sup> in sulfuric acid. The esters formed are hardly soluble in water [551]. Iso-propanol is widely adopted as solvent. However, according to Uchida *et al.* [8] butyl acetate performs better than iso-propanol due to its capability to distribute the ionomer over the whole catalyst layer with high density, thus increasing the continuity of the ionomer network for proton conductivity.



At the DLR (German Aerospace Center), a new technique for electrode preparation was developed that completely avoids the use of solvents [552,553]. The fundamental idea of this technique is to spray a dry mixture of electrode materials either on the membrane or on the backing layer. An electrode with a thickness between 5 and 50  $\mu\text{m}$  can be reproducibly produced [552]. At Johnson Matthey, the electrode is fabricated from an aqueous Nafion<sup>®</sup> solution [554,555]. The aqueous Nafion<sup>®</sup> solution was used to reduce the possibility of reaction between the Pt-based electrocatalyst and organic solvents in the original Nafion<sup>®</sup> solution [554].

#### **2.3.4.2 Nafion<sup>®</sup> Content in the Electrodes**

The loading of the polymer electrolyte and its distribution in the catalyst layer play an important role in determining the electrochemical activity. In fact, optimizing these parameters results in not only a high catalyst utilization due to a large active area in the electrode (extended reaction zone), but also easier migration of protons through the electrolyte retained in the pores of the catalyst layer [8,456,556-558].

The ionic conductivity of the catalyst layer can be measured directly [559] and indirectly [560]. Boyer *et al.* [560] demonstrated that the specific protonic conductivity of a catalyst layer prepared with recast Nafion<sup>®</sup> is proportional to the volume fraction of Nafion<sup>®</sup> in the catalyst layer.

Nafion<sup>®</sup> content in the electrodes and its effect on catalyst utilization were studied [513,528,529,558,561-569]. Poltarzewski *et al.* [561] studied the influence of Nafion<sup>®</sup> loading in dual electrode systems. The catalyst layer was impregnated with

Nafion<sup>®</sup> solution by floating the electrode on a 5 wt.% Nafion<sup>®</sup> solution. They found, at low Nafion<sup>®</sup> loading, that the polymeric electrolyte uniformly fills the micro and macropores of the electrode structure and increases its ionic conductivity. Further addition of the polymer results in the formation of a film on the external surface of the electrode. This film causes an additional resistance in the active layer [529,561,562]. It was suggested that the cast film must have a higher conductivity than the bulk polymer since it is much thinner [133]. But for recast Nafion<sup>®</sup> film at low temperature, the conductivity is much lower as was demonstrated by Siroma *et al.* [563-565]. The conductivity of the cast film (70 nm) and Nafion<sup>®</sup> 117 were found to be respectively 0.06 S/cm and 0.21 S/cm at 80°C, when measured under the same conditions. Furthermore, when the Nafion<sup>®</sup> loading is too low, the connection of the ionic pathway is insufficient, and the effective interface is limited to just near the membrane electrolyte. When the optimal amount is exceeded, it inhibits reactant access [564]. Figure 2.5 shows the structure of the electrode with different Nafion<sup>®</sup> content.

A very thin recast film was investigated using Scanning Electron Microscopy (SEM) analysis where it was found that Nafion<sup>®</sup> micelles tend to agglomerate to form an inverted micellar structure and different shapes as well as significant voids inside agglomerates [566]. Dynamic Light Scattering measurements were made in order to determine the average dimension of Nafion<sup>®</sup> micelles in a water-alcohol solution. It was observed that the average size of the Nafion<sup>®</sup> micelles strongly depended on the degree of dilution of the solution. An average size of 200 nm was determined for a solution (1:1 Nafion<sup>®</sup> 5 wt.%-water) [566].

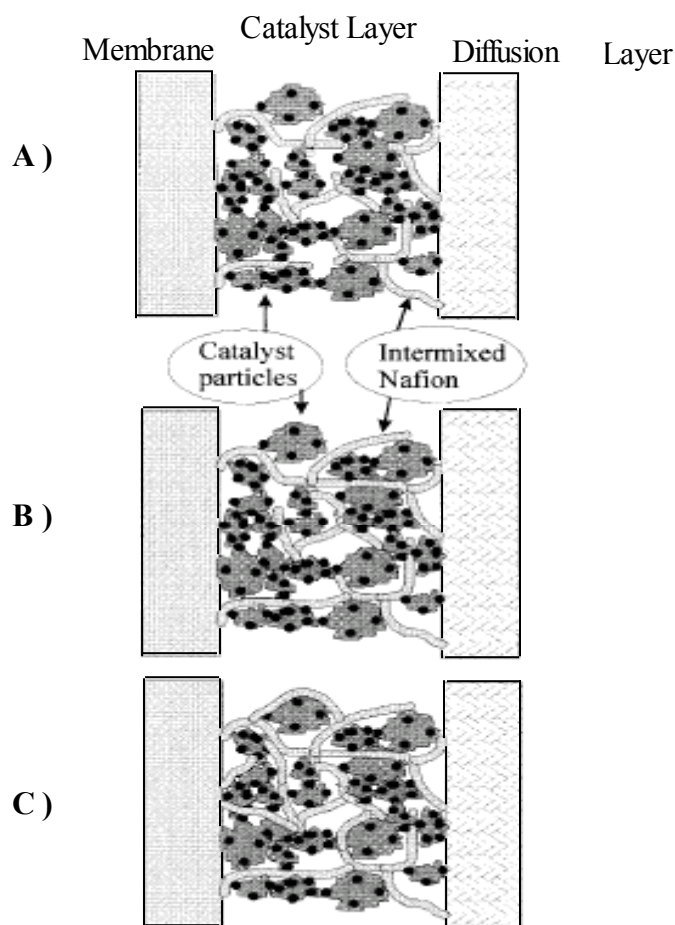


**Figure 2.5:** Schematic representation of the influence of Nafion<sup>®</sup> loading in the catalyst layer [528]. A) low Nafion<sup>®</sup> content, B) optimal Nafion<sup>®</sup> content, C) too much Nafion<sup>®</sup> content.

Transmission Electron Microscopy (TEM) analysis of the catalyst layer (Pt-Ru on carbon, Nafion<sup>®</sup> solution in water and low alcohols) showed that the size of Nafion<sup>®</sup> micelles was about 200 nm, and that the pores formed by carbon agglomerates are not accessible to the big Nafion<sup>®</sup> micelles. Nafion<sup>®</sup> particle agglomeration in the catalyst layer is quite less significant than observed in the recast

ionomer. The absence of a significant interconnected network of Nafion<sup>®</sup> particles inside the catalyst layer, in contrast to recast ionomer film, suggests that some limitation for ionic transport could occur in composite electrodes [566]. The absence of a continuous network of Nafion<sup>®</sup> particles inside the catalyst layer seems to be related to the preparation procedure and the use of water as dispersing agent. The high dielectric constant of water appears to limit the formation of the inverted micelle structure [8,566].

Gottesfeld and coworkers [558] studied the influence of Nafion<sup>®</sup> content in the catalyst layer using two unsupported Pt-Ru catalysts, RV3030 and HiSPEC 6000 supplied by E-TEK and Johnson Matthey, respectively. Their half cell and DMFC results with E-TEK RV3030 were unexpected, where the current increased with decreasing amount of Nafion<sup>®</sup> in the catalyst layer. The best performances were found to be with no addition of Nafion<sup>®</sup> solution. Johnson Matthey catalyst followed the normal known trend, i.e. increasing the Nafion<sup>®</sup> content increased the cell performance. X-Ray Diffraction (XRD) analysis suggested that E-TEK RV3030 contains some form of ruthenium oxide (RuO<sub>x</sub>) [558]. The amount of RuO<sub>x</sub> could be sufficient to provide protonic conductivity. It was found by Rolison *et al.* [570,571] that hydrous RuO<sub>x</sub> can have a proton conductivity of 10<sup>-3</sup> to 10<sup>-2</sup> S/cm, depending of the hydration level. However, Aricò *et al.* [566] studied the structure of 40% Pt-20% Ru supported on Vulcan XC-72 from E-TEK, and they found no evidence of the presence of RuO<sub>x</sub>.

### 2.3.4.3 Pore Forming Additives

Recently, a new approach was adopted to increase the porosity of the active layer by introducing a pore forming additive. Optimal amounts of pore forming additives increase the volume porosity of the active layer. The increased volume porosity resulted in a significant reduction in the mass transport resistance in the active layer, and therefore an improvement in electrode performance [508,572].

Gamburzev *et al.* [508,572] used unspecified pore forming material, while Fischer *et al.* [544] used  $\text{Li}_2\text{CO}_3$ , ammonium carbonate and ammonium oxalate ( $(\text{NH}_4)_2\text{C}_2\text{O}_4$ ). Wei *et al.* [541] introduced  $(\text{NH}_4)_2\text{C}_2\text{O}_4$  as pore forming additive in a thin film catalyst layer. Passalacqua *et al.* [550] used ammonium carbonate as pore former. The addition of pore forming additives in all the experiments showed satisfactory results due to the decrease in mass transport limitation into the electrodes [541].

## 2.4 METHANOL CROSSOVER IN FUEL CELL MEMBRANES

Methanol crossover is a critical factor in a DMFC. Perfluorosulfonic acid membranes have high methanol diffusivity [573,574]. It has been found that over 40% of the methanol can be wasted across perfluorosulfonic acid membranes, and also a mixed potential occurs at the cathode (see Section 2.1.4). It was also found that methanol crossover is controlled by cell temperature; a higher temperature increases methanol crossover [55,574-576].

Methanol crossover has been studied from its influence on the performance of the fuel cell [152,577-581]. Methanol crossover has been widely studied by monitoring the CO<sub>2</sub> at the cathode exhaust outlet using a CO<sub>2</sub> sensor [30,157,582-587], gas chromatography [580,588-590], and Multipurpose Electrochemical Mass Spectroscopy (MPEMS) [591,592]. Measurement by precipitation as BaCO<sub>3</sub> has also been reported [586,593]. This method is based on the assumption that methanol permeating through the membrane is completely oxidized to CO<sub>2</sub>, which is unlikely. It was found that the products of methanol oxidation included formaldehyde, formic acid, methylformate, carbon monoxide and carbon dioxide [588,592,594,595]. Fan *et al.* [594,595] used *in situ* Fourier Transform Infrared-Diffuse Reflection Spectroscopy (FTIR-DRS) on an operating DMFC at room temperature. While, Lin *et al.* [372] used FTIR online in a DMFC operated at 150°C and 185°C, where it was found that complete oxidation of methanol to CO<sub>2</sub> was achieved.

Nevertheless, these methods require lengthy and careful calibration of both the exhaust flow rate and CO<sub>2</sub> sensor. Furthermore, it was found that at high cell current density the CO<sub>2</sub> generated from the anode may permeate through the membrane to reach the cell cathode, contributing to an overestimation of the methanol crossover rate using CO<sub>2</sub> sensors [586,596]. Thus, the measurement of methanol crossover by monitoring CO<sub>2</sub> at the cathode exhaust is likely to be inaccurate.

Ren *et al.* [596,597] developed a method to measure methanol crossover rate under cell operating conditions at open circuit. The set-up used a voltametric method and accounting for electro-osmotic drag effects. In the voltametric method, the anode

and cathode were reversed when compared to a DMFC as shown in Figure 2.6. Methanol solution was fed to the anode electrode as in a DMFC. Methanol then permeated through the anode backing layer, anode catalyst layer and the proton exchange membrane to reach the cathode side. The cathode side differs from a DMFC in that an inert atmosphere is used, such as well-humidified nitrogen or pure water. The reaction occurring at the anode was proton reduction to form hydrogen gas and the reaction occurring at the cathode is the oxidation of methanol that crosses through the membrane. When the applied voltage is high enough to quickly oxidize the entire methanol diffusing to the cathode side, a limiting current is achieved. This limiting current represents approximately the rate of methanol crossover at open circuit. This method was adopted by different researchers [194,598,599].

The methods mentioned above depend on a working fuel cell, which is a difficult task for a newly developed membrane, especially in the case of MEA fabrication. For a fast screening of newly developed membranes, alternative methods to measure methanol crossover without a fuel cell is needed. Three types of experiment were used in the open literature, namely pervaporation, pressure change in the two compartment arrangement, and the diaphragm diffusion cell. In the pervaporation arrangement, a membrane is clamped between two compartments. Methanol solution is pumped through one compartment while the other one is purged with a continuous flow of an inert gas, such as nitrogen [155,156,268,269], a vacuum [289,290] or water [36]. Methanol concentration is measured at the permeate by means of gas chromatography [155,156,268,269,289,290] or Differential Electroche-

mical Mass Spectroscopy (DEMS) [36,600]. Savinell and co-workers [159,601] used the two compartment arrangement, but instead of measuring methanol concentration, the pressure in the small compartment was monitored.

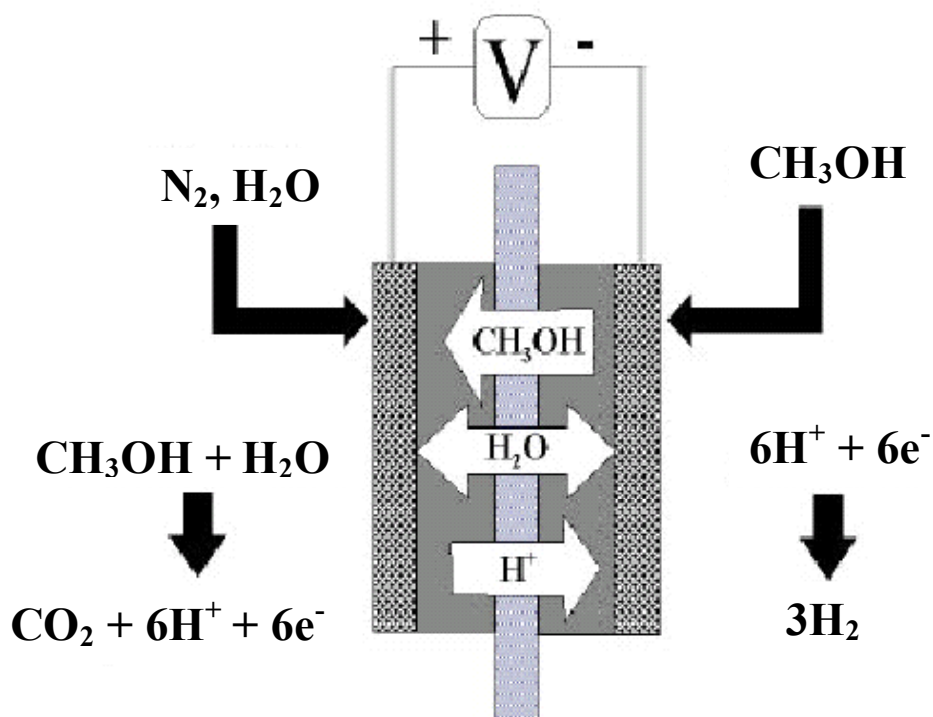


**Figure 2.6:** Voltametric method to measure methanol crossover.

In the diaphragm diffusion cell, a two compartment arrangement was utilized for a methanol permeability test. One compartment was filled with an aqueous solution of methanol while the other compartment was filled with pure deionized water. The membrane was clamped between the two compartments, and the two compartments were kept under stirring conditions during the experiment. A methanol



flux is established across the membrane owing to the concentration gradient between the two compartments. The flux of methanol across the membrane was constant, and its concentration in the receiving compartment was measured several times during the experiment.

Methanol permeability is calculated from the slope of the straight line of the curve of methanol concentration in the receiving compartment vs time [602,603]. Appendix A shows the derivation of the methanol permeability equation. The diaphragm diffusion cell was widely adopted to measure methanol permeability in newly developed membranes [153,157,175,179, 226, 270, 309,604-609].

## CHAPTER 3

# CHEMICALS, INSTRUMENTS AND METHODS

### 3.1 CHEMICALS

Chemicals used in this study are summarized in Table 3.1 with suppliers names and some specifications.

**Table 3.1:** Chemicals

Chemicals	Supplier	Specifications
ZrO <sub>2</sub> powder ZrO <sub>2</sub> Sol	Degussa Alfa Aesar	20% in H <sub>2</sub> O, colloidal dispersion, 0.005-0.01 micro particle in liquid
Zirconium oxychloride (ZrOCl <sub>2</sub> )	Shanghai Reagent Company, China	
Dimethyl sulfoxide (DMSO)	Aldrich	99.6%
Dimethylacetamide (DMAc)	Aldrich	99%
N-methylpyrrolidone (NMP)	Aldrich	99%
Butyl Acetate (BAc)	Alfa Aesar	99%
20%Pt - 10%Ru on Carbon black	Alfa Aesar; Johnson Matthey	Pt 19.20 wt.%, Ru 10.30 wt., 2.1 nm size
30%Pt - 15%Ru on Carbon black	Alfa Aesar; Johnson Matthey	Pt 29.1 wt.%, Ru 14.84 wt., 2.3 nm size
40%Pt on Carbon black	Alfa Aesar; Johnson Matthey	Pt 38.530 wt.%, 3.8 nm size
Nafion <sup>®</sup> solution	Ion Power	5 wt.%, 1100 EW
Nafion <sup>®</sup> solution	Aldrich	5 wt.% in a mixture of lower aliphatic alcohols and water
Iso-propanol (IPA)	Sigma- Aldrich	99.5%

### 3.2 INSTRUMENTS

#### 3.2.1 X-Ray Diffraction (XRD) Analysis

XRD measurements are carried out with D8 Advance, Bruker AXS equipment using  $\text{CuK}_\alpha$  source.

Instrument	D8 Advanced
X-Ray Detector	Copper source
Detector	Scintillation
Slits	Divergence V20
Antiscattering	V20
Generator	V20 40 kV
Generator current	40 mA

**Table 3.2:** XRD operating parameters

<b>XRD operating parameters</b>	
Range ( $2\theta$ )	5-70
Step size	0.02
Scan speed	7s/step
Scan type	Locked couple
Scan time	7 hours
Scan mode	Continuous
Synchronous rotation	On

#### 3.2.2 Fourier Transform Infrared (FTIR) Analysis

FTIR spectra were obtained with a Perkin-Elmer Paragon 1000 FTIR instrument over the range of  $4000\text{-}400\text{ cm}^{-1}$  and a resolution of  $4\text{ cm}^{-1}$ . For the powder analysis, appropriate mixtures of the samples and KBr were used. The IR spectra of the membranes were obtained on  $100\text{ }\mu\text{m}$  thick films.

### 3.2.3 Membrane Morphology Analysis by Scanning Electron Microscopy (SEM)

The matrix surface and the surface and cross-section of the composite membranes morphology were investigated by means of SEM. SEM images were obtained on a Hitachi x650. The cross-sections of the composite membrane were obtained by breaking the membrane into small pieces under liquid nitrogen.

Hitachi	x650
Accelerating voltage	25kV
Aperture	0.4 mm
Tilt angle	0°
Resolution	6 nm
Working distance	15 mm

### 3.2.4 Transmission Electron Microscopy (TEM) Analysis

Powders and membranes cross section were observed by TEM in a Leo 912 electron microscope. The powders were suspended in methanol in an ultrasonic bath, followed by dropping some suspension onto a copper grid. For membrane sectioning, a Reichert Ultracut S (Leica) ultramicrotome was used. The sample was embedded in resin. Then, a cross section was cut off using the ultramicrotome with a glass knife fitted with a water boat. After sectioning, the copper grids were dipped in the boat to capture the samples.

### 3.2.5 Brunauer-Emmett-Teller (BET) Analysis

The surface area of the samples was determined by the BET technique using a Micromeritics Accelerated SA and Porisimetry (ASAP) 2010 system.

### 3.2.6 Thermogravimetric Analysis (TGA) and Differential Scanning Calorimetry (DSC)

TGA and DSC data were obtained with model STA (Simultaneous Thermal Analyzer) 1500 (supplied by Rheometric Scientific Ltd, UK), over nitrogen and at a heating rate of 10°C/min.

## 3.3 METHODS

### 3.3.1 Conductivity Measurement

#### 3.3.1.1 Definitions

The membrane resistance ( $R$ ) is defined as the potential drop ( $\Delta\phi$ ) over a membrane at given current ( $I$ ).

$$R = \frac{\Delta\phi}{I} \quad [\Omega]$$



The area resistance is defined as:

$$R_A = RA_M \quad [\Omega \text{ cm}^2]$$

where  $A_M$  is the membrane area

If different membrane materials shall be compared with one another the specific resistance  $R_M$  independent of membrane thickness has to be used:

$$R_M = \frac{R_A}{l} \quad [\Omega \text{ cm}]$$

alternatively, the specific conductivity ( $\sigma$ ) of a membrane is employed:

$$\sigma = \frac{1}{R_M} = \frac{l}{R_A} = \frac{1}{R} \times \frac{l}{A_M} \quad [\text{S/cm}]$$

### 3.3.1.2 Membrane Resistance Measurements

The membrane resistance can be measured with several techniques. The most popular methods used to measure proton conductivity in membranes are: direct current [133,144-147] and ac impedance spectroscopy [31,33-35,115,131-143]. In this dissertation, ac impedance spectroscopy technique was adopted.

#### *Principle of Impedance Spectroscopy*

The impedance ( $Z$ ), which is the complex of the ac resistance, is determined as a function of the frequency ( $f$ ). The impedance is defined in analogy to Ohm's law:

$$Z(t) = \frac{U(t)}{I(t)}$$

Where the voltage  $U(t)$  is:

$$U(t) = U_0 \sin(2\pi ft)$$

and the current  $I(t)$  is:

$$I(t) = I_0 \sin(2\pi ft + \varphi)$$

$U_0$  and  $I_0$  are the amplitudes of the oscillations  $U(t)$  and  $I(t)$ .

$\varphi$  is the phase angle of the current response shifted with respect to a voltage signal.

An impedance spectrum can be displayed as a Cole-Cole plot or Bode plot. In the Cole-Cole plot, the real impedance  $|Z''|$  is plotted as a function of the imaginary impedance  $|Z'|$  as shown in Figure 3.1. In the Bode plot the absolute value of the impedance  $|Z|$  and the absolute phase angle  $|\varphi|$  are plotted versus the frequency  $f$  as shown in Figure 3.2.



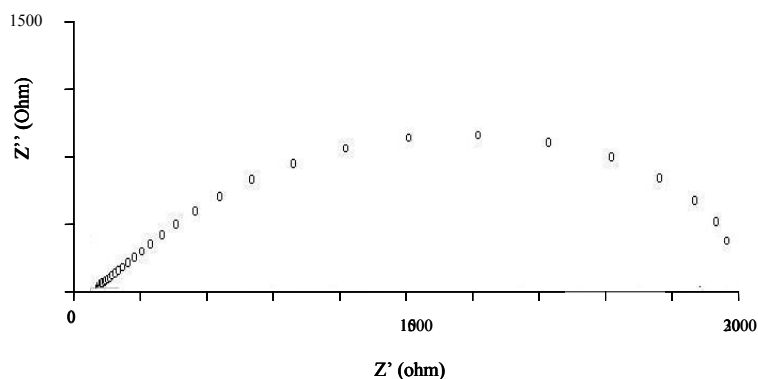


**Figure 3.1:** Cole-Cole plots of ZrP composite membrane ( $Z''$  is the real resistance and  $Z'$  is the imaginary resistance).

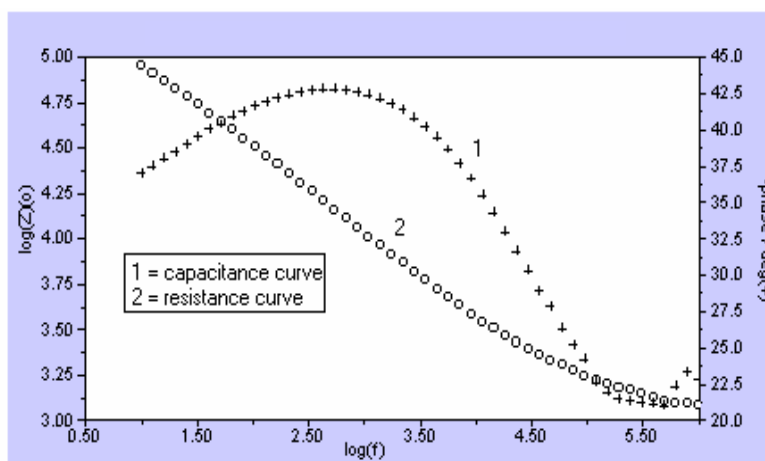


**Figure 3.2:** Bode plot of ZrP composite membrane.

The conductivity measurement cell is depicted in Figure 3.3. The cell consists of an upper and a lower chamber, each of them containing a gold plated copper electrode ( $0.28 \text{ cm}^2$  surface area). Good centering is important for the homogeneity of the electrical field. The electrodes serve as a working and reference electrode.

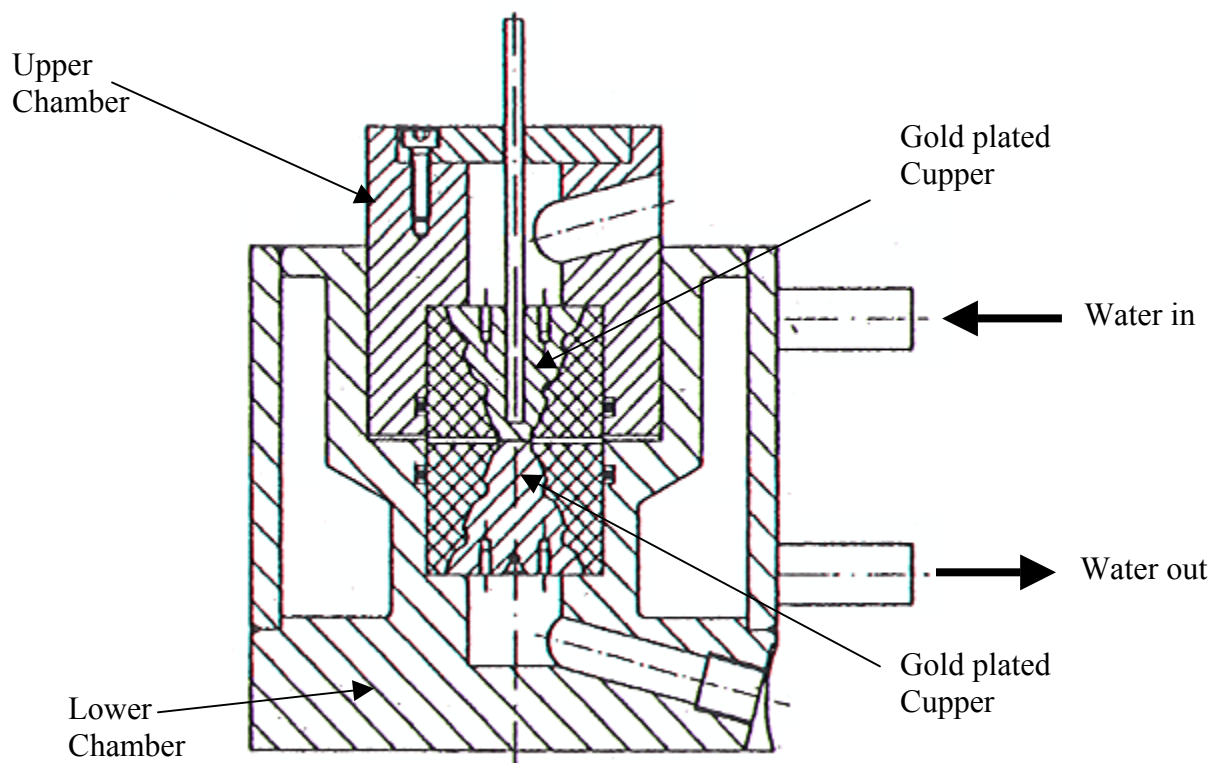


**Figure 3.3:** Conductivity measurement cell [610].

Impedance measurements were conducted using an Autolab potentiostat/galvanostat PGSTAT30 (Eco Chemie, the Netherlands) in combination with the computer controlled frequency response analyzer over the frequency ranges 0.1 Hz to 100 kHz. For measurement, the membrane was placed between two Nafion<sup>®</sup> 117 membranes. After measurement of the three-membrane stack, the ohmic resistance of the two Nafion<sup>®</sup> membranes was measured via the same way, and the resistance of the membrane was finally calculated by subtraction of the ohmic resistance value of the three-membrane stack. Before impedance measurements the membranes were soaked in water at least for 2 hours.



### 3.3.2 Water Uptake of Membranes

Samples of the membranes were weighed ( $W_1$ ) after drying in a vacuum oven at 100°C for 8 hours. Next, the samples were weighed ( $W_2$ ) after immersion in deionized water for three days at room temperature. Water uptake ( $\Delta W$ ) was calculated with the following equation:

$$\Delta W \text{ (wt.\%)} = \frac{W_2 - W_1}{W_1} \times 100$$

### 3.3.3 Methanol Permeability Measurement

Diffusion cell was adopted to measure methanol permeability in membranes. This method was chosen based on the literature review for methanol crossover measurement (see Section 2.4). The diffusion cell is the most suitable method to measure methanol permeability in newly developed membranes. The method used however, does not provide an accurate measure of permeability, but it is the only means of comparison of new membranes to a standard membrane (which is Nafion<sup>®</sup> 117 for DMFC application).

A two-compartment glass cell was utilized to investigate the methanol permeability of the membrane as depicted in Figure 3.4. One compartment (A) was filled with an aqueous solution of 1M methanol, the second compartment (B) was filled with pure water. The membrane was clamped between the two compartments. A methanol flux was established across the membrane owing to the concentration gradient between the two compartments. Samples of solution were withdrawn from the receiving compartment (B) by means of a microsyringe (1 $\mu$ l) and analyzed by a gas chromatograph (HP 5890 Series II) fitted with a flame ionization detector (FID)

and Porapak Q column. The concentration in the receiving compartment was measured several times during an experiment, and methanol permeability was calculated from the slope of the straight line [603]. The following equation was used to calculate methanol permeability ( $P$ ) [226, 603]:

$$P = DH = \frac{IV_B}{At} \ln \frac{C_{1,B}^0 - C_{1,A}}{C_{1,B} - C_{1,A}} \quad [\text{equation 3.1}]$$

where  $D$  is the diffusion coefficient,  $H$  the partition coefficient,  $C_{1,B}^0$  is the methanol concentration in the receiving compartment at the beginning of the experiment ( $t = 0$ ),  $C_{1,B}$  is the methanol concentration at a given time ( $t = t_{\text{exp}}$ ),  $C_{1,A}$  is the methanol concentration in the aqueous methanol compartment (A) which is constant (1M),  $A$  and  $l$  are the exposed area and membrane thickness respectively, and  $V_{\text{sample}}$  is the volume of the receiving compartment (B).

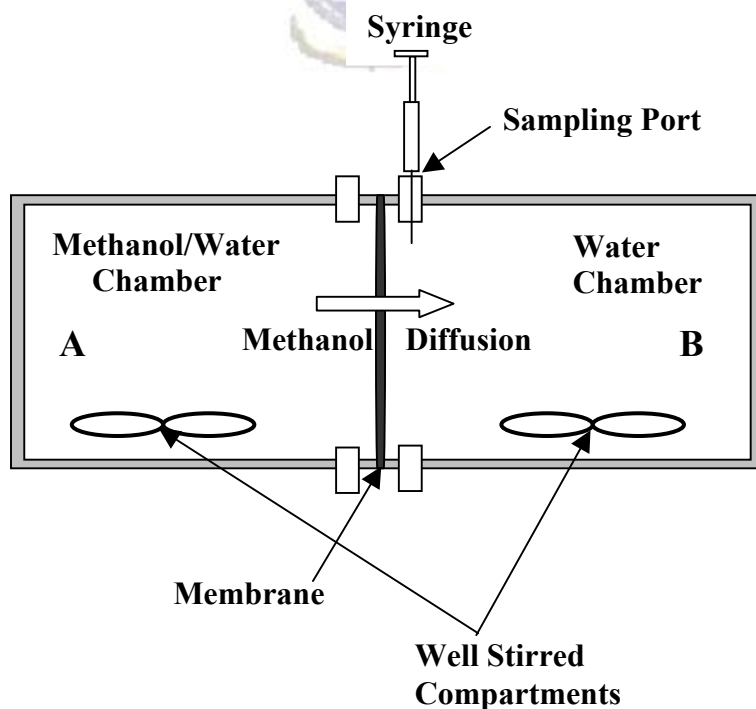


**Figure 3.4:** Methanol permeability measurement cell (diffusion cell).

### 3.3.4 DMFC Test Rig

The test rig is constituted of a methanol reservoir (1 liter) connected to the Methanol Test Kit (MTK) purchased from Lynntech. The MTK is equipped with a heater to heat methanol to the desired temperature, typically 80°C. The temperature is controlled by a temperature probe at the entrance of the reservoir. The reservoir is also fitted with a level control connected to the MTK. Figure 3.5 shows the Methanol Test Kit (MTK). The connections between the MTK and the methanol reservoir are made of PTFE.

The single fuel cell is constituted of endplates and an MEA. The endplates used are also purchased from Lynntech, with an area of 5 cm<sup>2</sup> (Figure 3.6). The flow fields for the reactants were of serpentine configuration with three serpentes connected in parallel. The endplates are also fitted with holes to accommodate a heating cartridge and a thermocouple for the temperature controller. The cell temperature is also controlled by the MTK.

Methanol is fed to the anode from the reservoir by means of peristaltic pump (HPLC pump, Millipore Waters, Model 510). The connection between the methanol reservoir and the cell are also made of PTFE and a heating tape was used to keep the temperature of methanol similar to the cell temperature. A circulating mode was adopted, where the unreacted solution was fed back to the reservoir.



**Figure 3.5:** Lynntech Methanol Test Kit. **Figure 3.6:** Lynntech endplates.

The cathode is fed with air or oxygen from a gas cylinder. The flow rate of the gas is controlled by a mass flow controller for accurate flow rate delivery - a flow rate between 500 ml/min to 5 l/min can be chosen. The cylinder is connected to the MTK, and to the cathode cell, as shown in Figure 3.7. A back pressure can be applied, if desired, by fitting a needle valve at the cell cathode exhaust. Air or oxygen is supplied to the cell without prior humidification and heating. PTFE connections are also used between the gas cylinder and the cell.

The gold coated endplates are also used as current collectors. The anode and cathode sides are fitted with connections to a potentiostat/galvanostat Auto Lab (Echo Chemi, The Netherlands). The polarization curve - which is the current as a function of voltage - can be obtained by applying a voltage and recording the current or vice-versa. In this study a voltage was applied and the produced current is recorded. The Autolab allows one to measure the current as function of time.

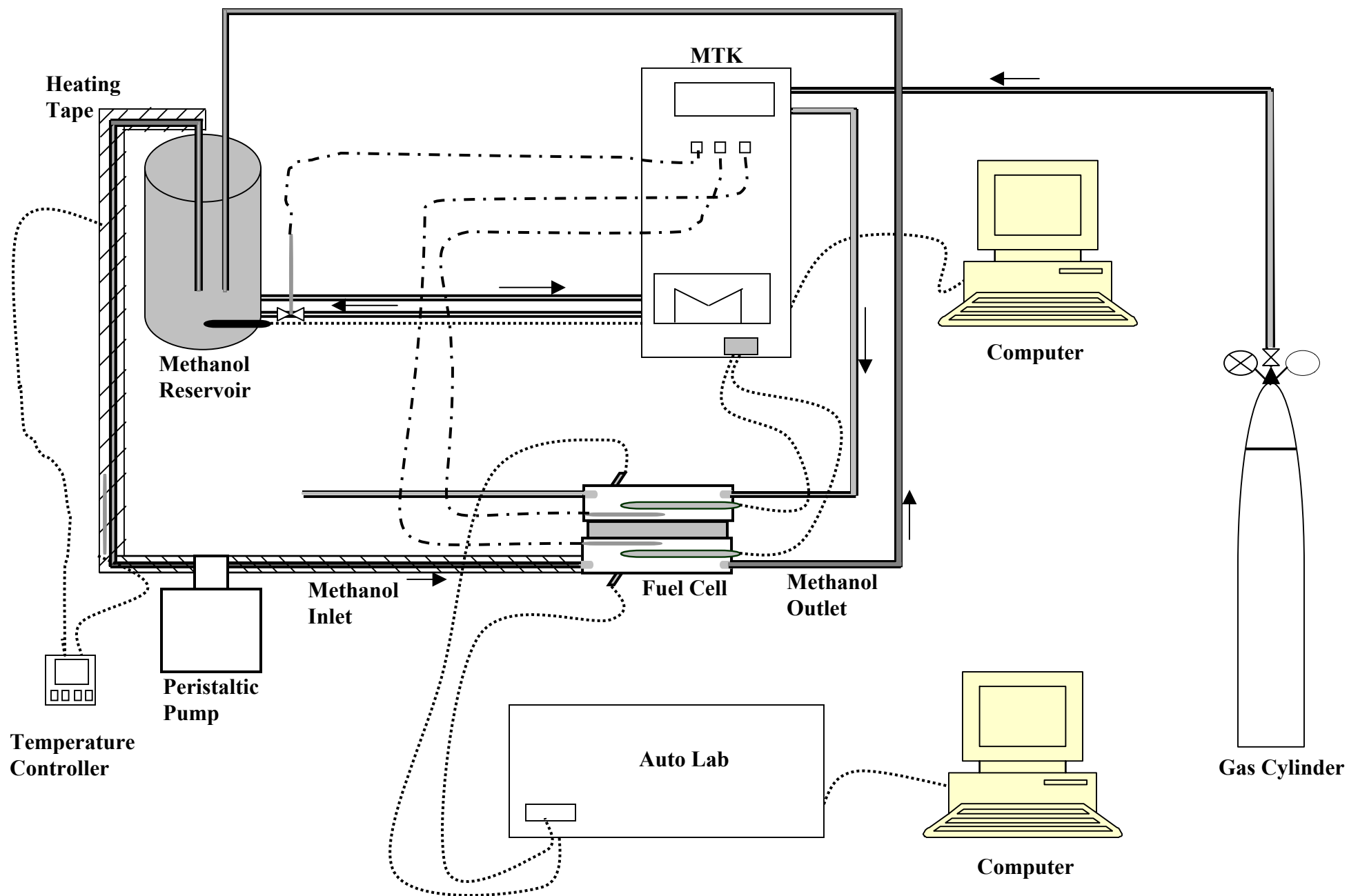


Figure 3.7: Direct methanol fuel cell test rig.

## CHAPTER 4

# MEMBRANE PREPARATION AND CHARACTERIZATION

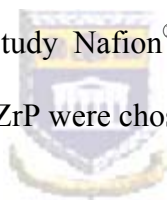
### 4.1. INTRODUCTION

The proton conductive membranes are the key components of the DMFC. The actual state-of-the-art membranes (e.g. Nafion<sup>®</sup>) have several disadvantages including:

- High cost, because of the complexity and duration of the manufacturing process [117] which includes strongly toxic and environment-unfriendly intermediates [114];
- High methanol permeability in these membranes from anode to cathode - known as methanol crossover - which severely affects DMFC performance;
- Working temperature at around 80°C, since the conductivity depends on water. High temperatures (around 150°C) are desirable to avoid CO absorption on the catalyst surface.

The aim of this study is to develop a proton conductive membrane, which can at least overcome one of the disadvantages listed above. Different approaches were undertaken to develop proton conductive membranes. ZrP can be mixed with a non-conductive polymer as a binder, but with this type of composite membrane, the inorganic proton conductive material must form at least 60% of the composite, otherwise the mechanical stability of the membrane is questionable. The approach

followed in this study is to use a highly mechanical stable inorganic material as a matrix, followed by impregnation with a proton conductive material. The inorganic material support chosen is CREAMFILTER<sup>®</sup> and the proton conductive materials are ZrP and Nafion<sup>®</sup> ionomer. Organic / inorganic composite membranes are also new types of proton conductive materials. The organic material provides the necessary conductivity, while the inorganic material enhances the characteristics of the membrane, namely mechanical stability, reduced methanol permeability and provides high water content above the boiling point of water (100°C). The inorganic materials usually added in the literature, are metal oxide (e.g. SiO<sub>2</sub> and ZrO<sub>2</sub>) and ZrP. ZrP is the inorganic material of choice to be added to organic proton conductors, since it is also a proton conductor. In this study Nafion<sup>®</sup> was chosen as the organic proton conductor material while ZrO<sub>2</sub> and ZrP were chosen as the inorganic materials.



## **4.2 INORGANIC MATRIX DESCRIPTION AND STABILITY TESTS**

### **4.2.1 Matrix Descriptions**

The matrices used were a non-conducting glass support or polymer coated with ceramic developed by Creavis Technology and Innovation, Germany, under the trade name CREAMFILTER<sup>®</sup> [611, 612]. CREAMFILTER<sup>®</sup> combines the advantages of both polymeric and ceramic membranes. They are flexible and have good chemical and thermal stability [611]. Four types of CREAMFILTER<sup>®</sup> were tested as matrix for composite membrane preparation, namely Z100G, Z240G, S450P and Z450P. The characteristics of the matrix are summarized in Table 4.1. Two of the

CREAFILTER<sup>®</sup>s used glass supports (Z100G, Z240G), while the other two used polymer supports (S450P, Z450P). The pore size varied according to the type and size of the ceramic coating - from 100 nm for Z100G to 450 nm for Z450P; also the thickness of the matrix varied from 30  $\mu\text{m}$  for S450P to 200  $\mu\text{m}$  for Z450P. The thickness of the composite proton conductive membranes is an important factor for high conductivity, since the conductivity is inversely proportional to the thickness.

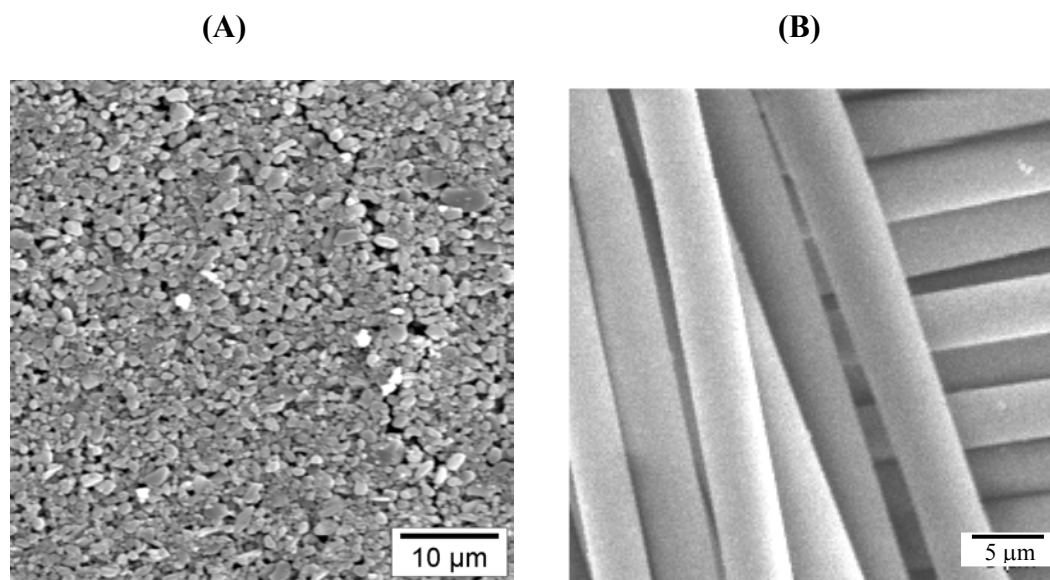
**Table 4.1:** Inorganic CREAMFILTER<sup>®</sup> matrix characteristics

CREAFILTER <sup>®</sup>	Composition	Thickness ( $\mu\text{m}$ )	Pore size (nm)	Methanol permeability ( $\text{cm}^2/\text{s}$ )
Z100G	ZrO <sub>2</sub> and Al <sub>2</sub> O <sub>3</sub>	100	100	$9 \times 10^{-7}$
Z240G	ZrO <sub>2</sub> and Al <sub>2</sub> O <sub>3</sub>	90	240	$11 \times 10^{-7}$
S450P	SiO <sub>2</sub> and Al <sub>2</sub> O <sub>3</sub>	30	450	$21 \times 10^{-7}$
Z450P	ZrO <sub>2</sub> and Al <sub>2</sub> O <sub>3</sub>	200	450	$18 \times 10^{-7}$

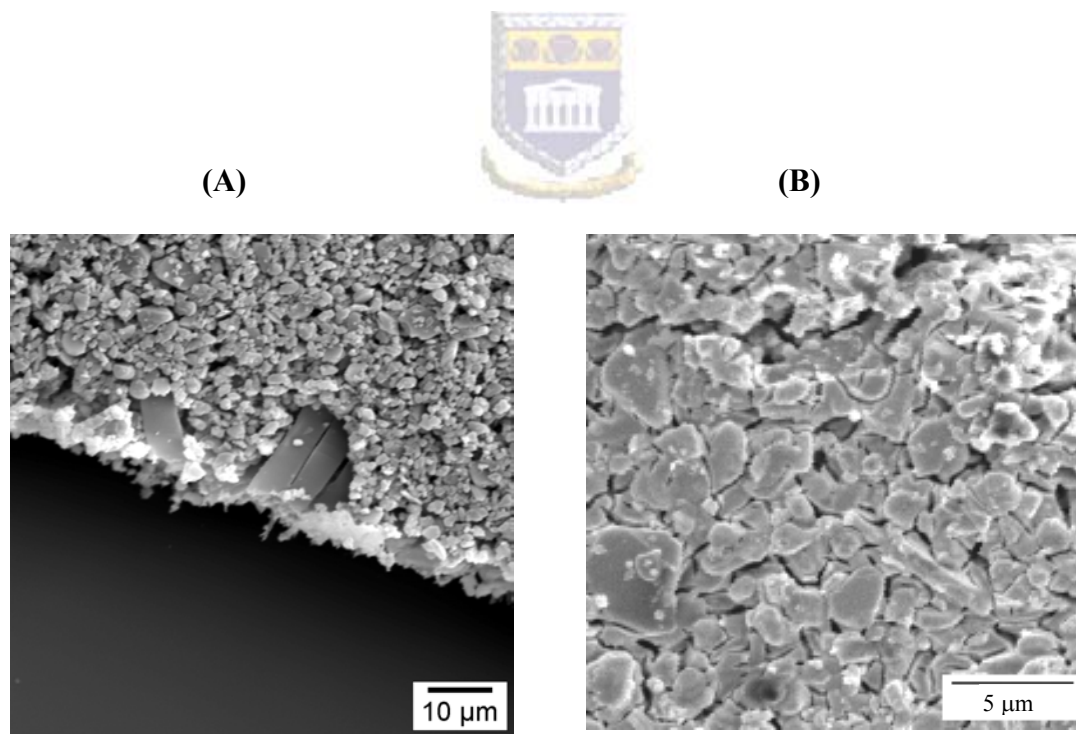
Table 4.1 shows some characteristics of the inorganic CREAMFILTER<sup>®</sup> matrix, including the type of ceramic used to coat the support. Metal oxides are used as ceramic coatings - a mixture of ZrO<sub>2</sub> and Al<sub>2</sub>O<sub>3</sub> are used for the Z type, whereas SiO<sub>2</sub> and Al<sub>2</sub>O<sub>3</sub> are used for S type.

Figure 4.1 shows the structure of CREAMFILTER<sup>®</sup> Z240G, which is constituted of ceramic (ZrO<sub>2</sub> and Al<sub>2</sub>O<sub>3</sub>) and glass fiber support. Figure 4.1 (A) shows the surface while (B) shows a cross-section.





**Figure 4.1:** SEM micrograph of the surface (A) and cross-section (B) of CREAMFILTER® Z240G.



**Figure 4.2:** SEM micrograph of the surface of (A) CREAMFILTER® S450P and (B) CREAMFILTER® Z450P.

The SEM micrographs of the surface of CREAMFILTER<sup>®</sup> (Figure 4.1 (A), Figure 4.2 (A) and Figure 4.2 (B)) revealed the presence of two different sized inorganic materials on the surface of the support. Figure 4.1 (B) shows the glass fiber support used to prepare Z type CREAMFILTER<sup>®</sup>, and Figure 4.2 (A) shows the polymer used as a support for CREAMFILTER<sup>®</sup> S450P. According to Creavis Technology and Innovation (the supplier), the polymer used in S450P is polyethylene tetrathalate (PET).

Figure 4.3 shows the X-ray diffraction pattern of CREAMFILTER<sup>®</sup> Z100G and Z240G, while Figure 4.4 shows the X-ray diffraction pattern of S450P. The X-ray diffraction patterns of Z100G and Z240G are the same since they are using the same materials (see Table 4.1). The X-ray analyses were done on CREAMFILTER<sup>®</sup> for comparison studies, when the composite membranes will be prepared.

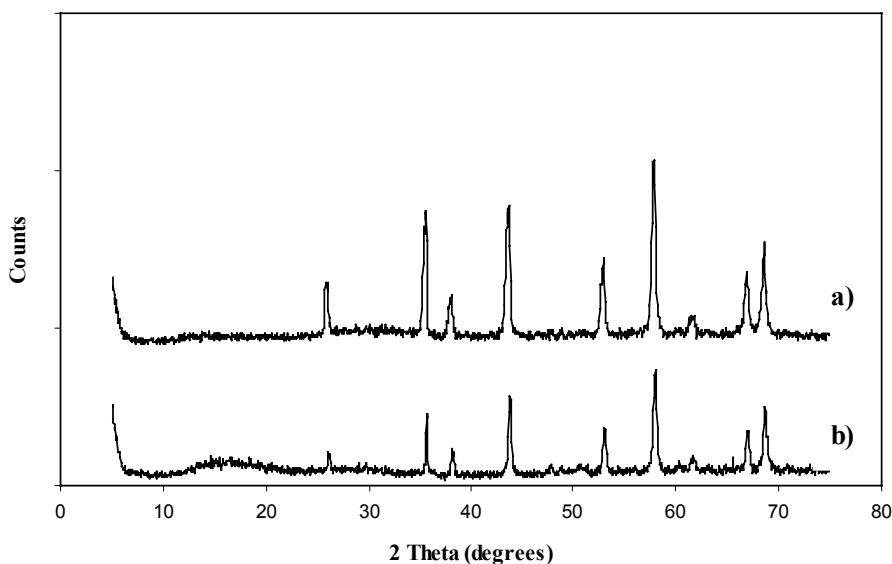


**Figure 4.3:** XRD analysis of bare CREAMFILTER<sup>®</sup> Z240G (a) and bare CREAMFILTER<sup>®</sup> Z100G (b).

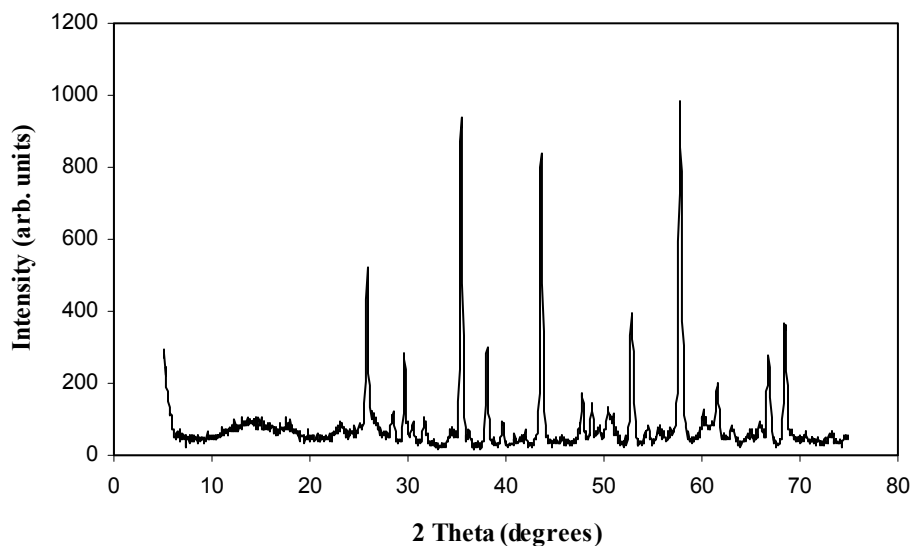


**Figure 4.4:** XRD analysis of bare CREAMFILTER® S450P.

#### 4.2.2 Matrix Stability Test

The stability of the matrix materials was tested by soaking them in different solvents over three months at room temperature. The stability tests were performed with H<sub>2</sub>SO<sub>4</sub>, H<sub>3</sub>PO<sub>4</sub>, methanol and organic solvents such as DMSO (Sigma-Aldrich), DMAc (Aldrich) and NMP (Aldrich).

Table 4.2 shows the changes that occur on CREAMFILTER® during soaking in different solvents. It can be clearly seen that CREAMFILTER®s are chemically stable in organic solvents. However, CREAMFILTER® Z450P dissolved in concentrated H<sub>2</sub>SO<sub>4</sub> and H<sub>3</sub>PO<sub>4</sub>, and cracks with neat NMP, DMSO and DMAc, but is stable with

methanol. CREAMFILTER<sup>®</sup> Z100G, Z240G and S450P are suitable for matrix use for proton conductive materials (e.g. ZrP).

**Table 4.2:** Inorganic CREAMFILTER<sup>®</sup> matrix stability test

	v. %	Z100G	Z240G	S450P	Z450P
H <sub>2</sub> SO <sub>4</sub>	10%	None	None	None	None
	50%	None	None	None	Yellow color
	100%	None	None	Crack	Dissolved
H <sub>3</sub> PO <sub>4</sub>	10%	None	None	None	None
	50%	None	None	None	Dissolved
	100%	None	None	None	Dissolved
Methanol	10%	None	None	None	None
	50%	None	None	None	None
	100%	None	None	None	None
NMP	10%	None	None	None	None
	50%	None	None	None	None
	100%	None	None	None	Crack
DMSO	10%	None	None	None	None
	50%	None	None	None	None
	100%	None	None	None	Crack
DMAc	10%	None	None	None	None
	50%	None	None	None	None
	100%	None	None	None	Crack

#### 4.2.3 Methanol Permeability in Bare CREAMFILTER<sup>®</sup>s

A diffusion cell was used to measure methanol permeability as discussed in Section 3.3.3. Methanol permeability in bare CREAMFILTER<sup>®</sup>s is reported in Figure 4.5 and Figure 4.6.

Figure 4.5 shows the measured methanol concentration in the receiving compartment (B) as function of the exposed time in different inorganic CREAMFILTER<sup>®</sup> matrixes namely Z100G, Z240G, Z450P and Nafion<sup>®</sup> 117. Nafion<sup>®</sup> 117 was studied as a reference, since it is the membrane of choice for DMFC.

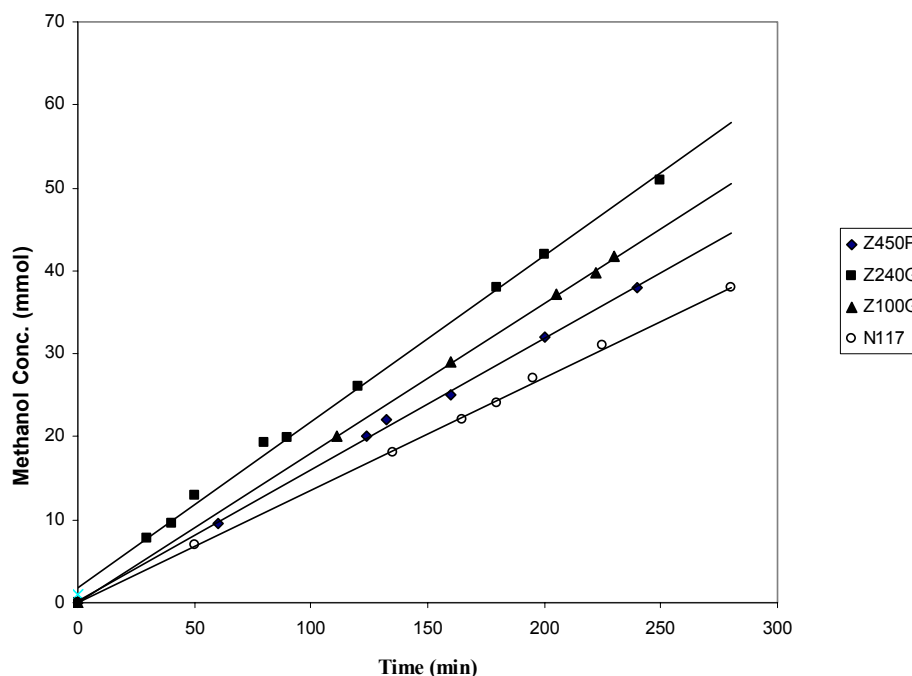


**Figure 4.5:** Methanol concentration in the receiving compartment (B) as function of the exposed time in bare CREAMFILTER<sup>®</sup> Z100G, Z240G, Z450P and Nafion<sup>®</sup> 117.

As can be seen from Figure 4.5, methanol permeability in CREAMFILTER<sup>®</sup>s is higher than in Nafion<sup>®</sup> 117, and can be attributed to particular diffusion phenomenon: in Nafion<sup>®</sup> polymer, by diffusion and solubility in the polymer, and in CREAMFILTER<sup>®</sup> solely by molecular sieve action. Methanol permeability in CREAMFILTER<sup>®</sup> is

expected to increase with the increase in pore size or a decrease in thickness. In comparison, the methanol permeability in Z450P is the least of all CREAMFILTER<sup>®</sup>s since it is the thicker one - 200  $\mu\text{m}$  compared to 90  $\mu\text{m}$  and 100  $\mu\text{m}$  for Z240G and Z100G, respectively. The pore size effect is more obvious for Z100G and Z240G, where they have nearly the same thickness, but a large difference in pore size - 240 nm for Z240G versus 100 nm for Z100G - thus the permeability in Z100G is less than Z240G. Figure 4.6 shows methanol permeability in CREAMFILTER<sup>®</sup>Z240G and S450P. For S450P the thickness effect is dominant - 30  $\mu\text{m}$  versus 90  $\mu\text{m}$  for Z240G. The calculated methanol permeability coefficient ( $P$ ) for CREAMFILTER<sup>®</sup>s and Nafion<sup>®</sup> 117 are reported in Table 4.1. Equation 3.1 was used for the calculation, and the detailed calculations appear in Appendix A.

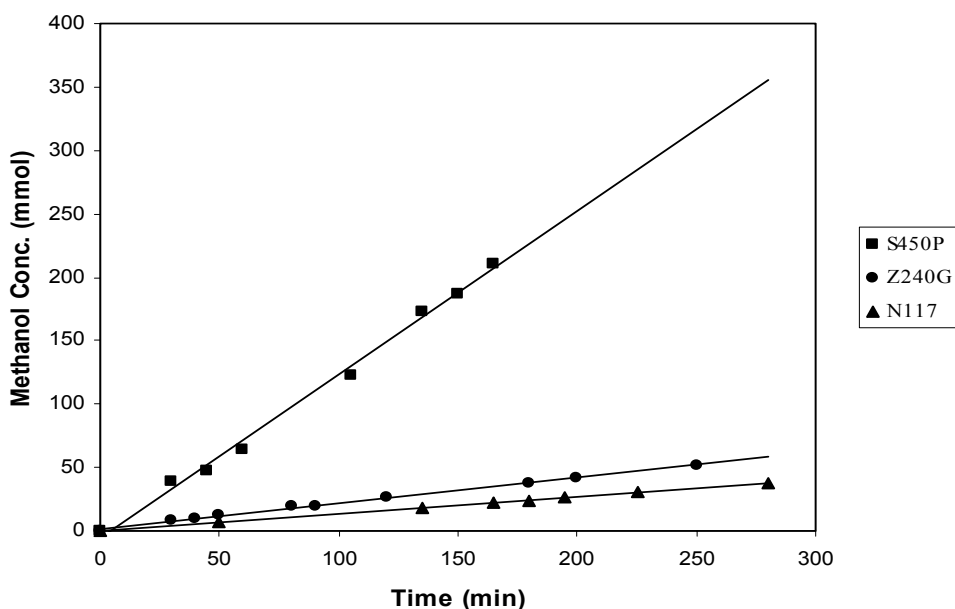


**Figure 4.6:** Methanol concentration in the receiving compartment (B) as function of the exposed time in bare CREAMFILTER<sup>®</sup> S450P, Z240G and Nafion<sup>®</sup> 117.

### 4.3 INORGANIC CREAMFILTER<sup>®</sup> MATRIX IMPREGNATED WITH ZIRCONIUM PHOSPHATE

#### 4.3.1 Introduction

ZrP was chosen as a proton conductor. It is well known that ZrP has high water content above 100°C. It is also well known that ZrP is a surface conductor with a conductivity varying from  $10^{-5}$  to  $10^{-2}$  S/cm, depending on the state of the produced material. To obtain highly conductive materials, ZrP must be produced with the highest possible amorphous content, or reduced particle size (high surface area). The problem found with ZrP membrane in previous attempts in the literature, is to make a mechanically stable membrane. In this study a novel approach was followed: the use of an impregnation technique as described by Belyakov and Linkov [292].



#### 4.3.2 Membrane Preparation

CREAFILTER<sup>®</sup> was impregnated with ZrP in two steps following the Belyakov and Linkov method [292]. For the first step the CREAMFILTER<sup>®</sup> was soaked in ZrO<sub>2</sub> sol (laboratory made or commercial ZrO<sub>2</sub> sol). ZrO<sub>2</sub> powder (supply from Degussa) was also used - a suspension of ZrO<sub>2</sub> in acetic acid was prepared to facilitate the first impregnation step. Then the membrane was dried at 80°C in an air oven. The second step - referred to as phosphorization - is where the membrane was soaked in concentrated H<sub>3</sub>PO<sub>4</sub> at 80°C to form ZrP *in situ*. To reach the desired characteristics (conductivity and methanol permeability) the two step impregnation process was repeated several times (in this case typically 5 times).

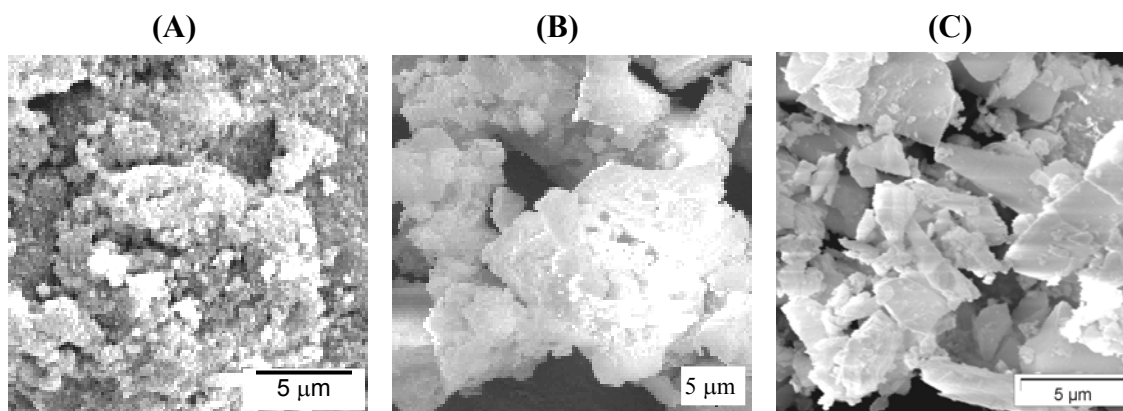
Laboratory made  $\text{ZrO}_2$  sol was prepared as follows: 1M recrystallized  $\text{ZrOCl}_2 \cdot 9\text{H}_2\text{O}$  (Shanghai Reagent Company, China) was prepared and heated in a beaker under vigorous stirring. 25%  $\text{NH}_4\text{OH}$  was added drop by drop to the  $\text{ZrOCl}_2$  solution, to the stage where crystals begin to form. The solution was vigorously stirred for few minutes to redissolve the crystals. At the end a clear sol was obtained. The sol obtained was cooled down to room temperature prior use. Commercial  $\text{ZrO}_2$  sol was purchased from Alfa Aesar (20%  $\text{ZrO}_2$  in aqueous solution) with particle sizes in the range 5 nm to 0.01  $\mu\text{m}$ .

### 4.3.3 $\text{ZrO}_2$ Sources Characterization

Different types of zirconium oxide ( $\text{ZrO}_2$ ) starting materials were investigated, with attempts to establish the optimal  $\text{ZrO}_2$  to be used in composite membrane preparation, and the most suitable for the impregnation of the inorganic CREAMFILTER<sup>®</sup> matrix. Three sources of  $\text{ZrO}_2$  were used in the 1<sup>st</sup> step in membrane preparation, namely,  $\text{ZrO}_2$  powder (Degussa), laboratory made  $\text{ZrO}_2$  sol and commercial  $\text{ZrO}_2$  sol (Alfa Aesar), and are referred to hereafter as  $\text{ZrO}_2$ -D,  $\text{ZrO}_2$ -L and  $\text{ZrO}_2$ -C, respectively.

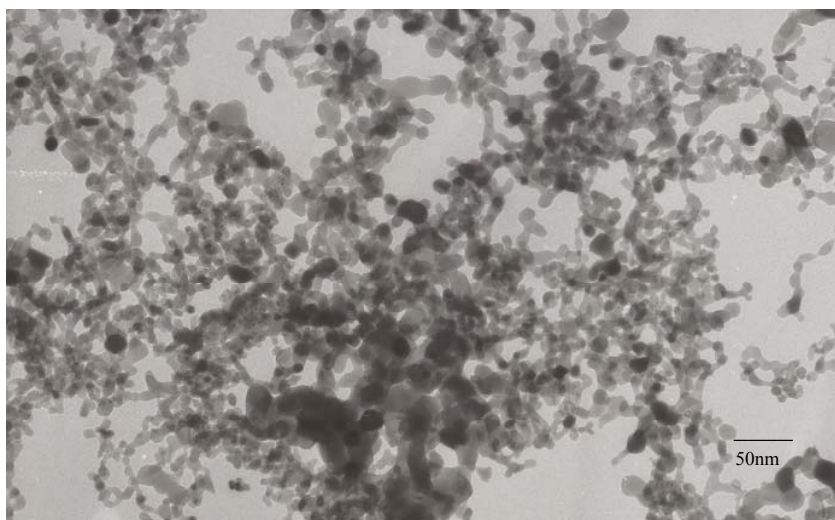
Figure 4.7 shows the structure of  $\text{ZrO}_2$  from the three sources used in this study.  $\text{ZrO}_2$ -D has a non-uniform rough surface morphology, while  $\text{ZrO}_2$ -L and  $\text{ZrO}_2$ -C form well defined crystals with  $\text{ZrO}_2$ -C forming sharp crystals.



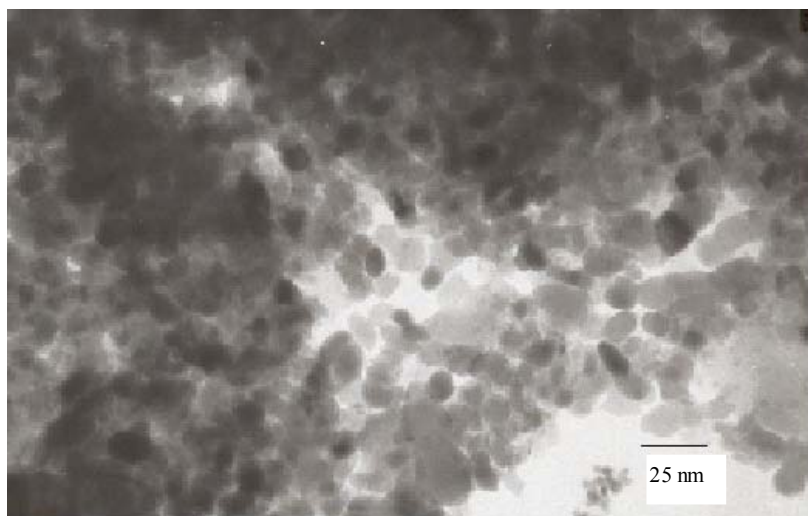


**Figure 4.7:** SEM micrographs of the three different  $\text{ZrO}_2$  sources: (A)  $\text{ZrO}_2\text{-D}$ , (B)  $\text{ZrO}_2\text{-L}$  and (C)  $\text{ZrO}_2\text{-C}$ .

Figure 4.8 and Figure 4.9 show TEM micrographs of  $\text{ZrO}_2\text{-D}$  as received and  $\text{ZrO}_2\text{-D}$  suspension in acetic acid, respectively. Particle sizes of the range 12 to 14 nm were observed for  $\text{ZrO}_2\text{-D}$ , while the micrograph of  $\text{ZrO}_2\text{-D}$  suspension in acetic acid does not show significant agglomeration.

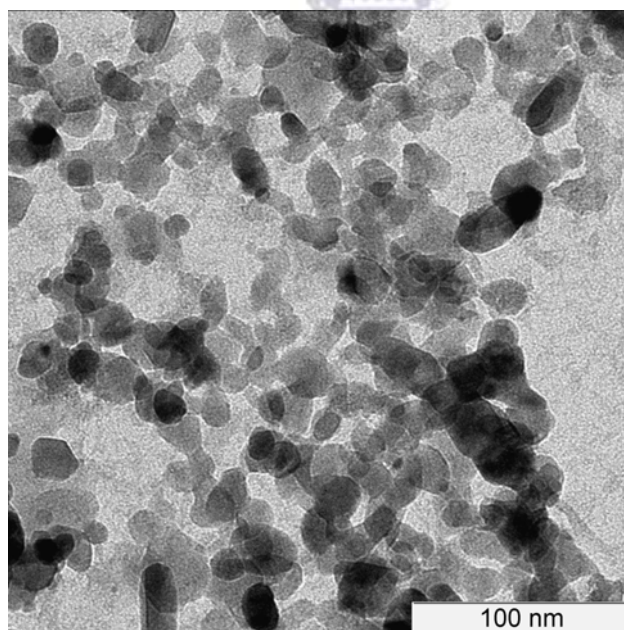


**Figure 4.8:** TEM micrograph of  $\text{ZrO}_2\text{-D}$  as received.



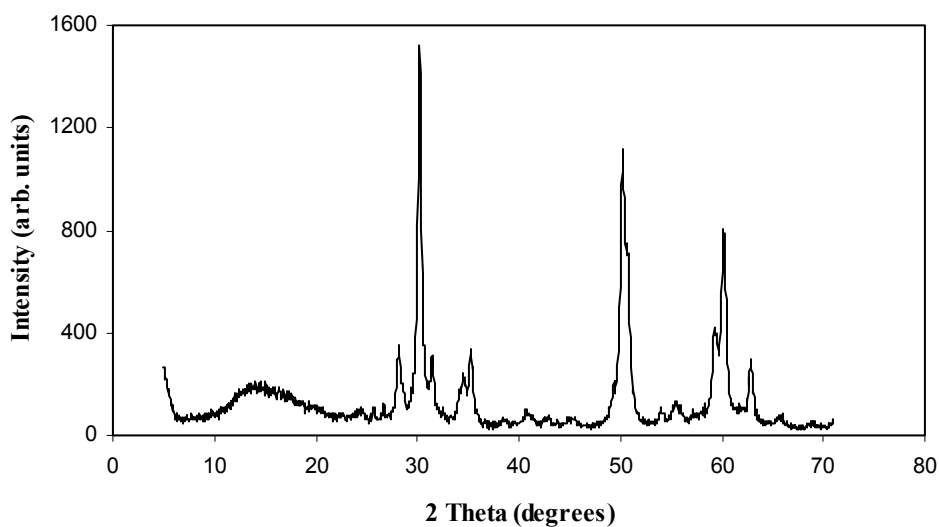
**Figure 4.9:** TEM micrograph of  $\text{ZrO}_2\text{-D}$  suspension in acetic acid.

Figure 4.10 shows the TEM micrograph of  $\text{ZrO}_2\text{-L}$ . An average particle size of 14 nm was observed, showing the nanostructure of  $\text{ZrO}_2$ .



**Figure 4.10:** TEM micrograph of  $\text{ZrO}_2\text{-L}$ .

Figure 4.11 and Figure 4.12 show the X-ray diffraction analysis of  $ZrO_2$ -D and  $ZrO_2$ -L, respectively. The X-ray diffraction analysis of  $ZrO_2$ -D (Fig. 4.11) revealed the presence of both monoclinic and tetragonal structures. The Bragg angles ( $2\theta$ ) of the monoclinic structure appears at  $24.4^\circ$ ,  $28.2^\circ$ ,  $31.5^\circ$ ,  $34.5^\circ$  and  $62.3^\circ$ , whereas the angles for the tetragonal structure are  $30.2^\circ$ ,  $50.2^\circ$ ,  $50.7^\circ$ ,  $59.3^\circ$  and  $60.2^\circ$  [613]. X-ray diffraction analysis of  $ZrO_2$ -L (Fig. 4.12) is completely different - an orthorhombic structure was found. Bragg angles ( $2\theta$ ) of the orthorhombic structure appear at  $32.6^\circ$ ,  $54^\circ$  and  $58.5^\circ$  [614]. Furthermore, the X-ray analysis of  $ZrO_2$ -L revealed the presence of unknown peaks at  $2\theta = 22.9^\circ$ ,  $40.4^\circ$  and  $47^\circ$ . These are due to the impurities in the  $ZrOCl_2$  starting material used in the preparation of  $ZrO_2$ -L.



**Figure 4.11:** XRD analysis of  $ZrO_2$ -D.

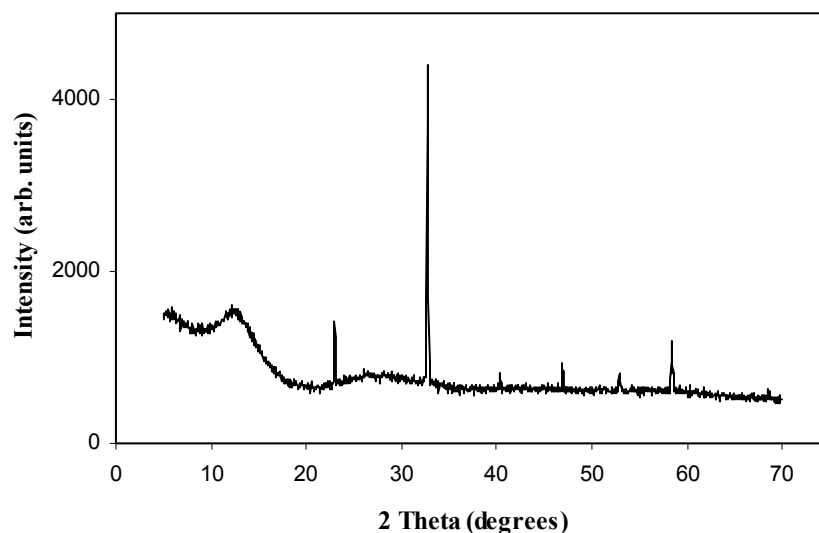


**Figure 4.12:** XRD analysis of ZrO<sub>2</sub>-L.

The particle size was calculated from the X-ray diffraction analysis of ZrO<sub>2</sub>-D by using the Scherrer formula:

$$D = \frac{0.9\lambda}{\beta} \cos \theta$$

where:  $D$  is the particle size,  $\lambda$  is the wave length of the X-ray ( $\lambda_{CuK\alpha} = 1.5418 \text{ \AA}$ ),  $\beta$  is the width of the most intense peak,  $\theta$  is the intersection with the x axis.

The calculated particle size was found to be 10 nm. This is in agreement with the TEM analysis, where particle sizes of 12 to 14 nm were found.

The BET surface areas for the different ZrO<sub>2</sub> sources are summarized in Table 4.3. ZrO<sub>2</sub>-D shows the higher surface area compared to ZrO<sub>2</sub>-L and ZrO<sub>2</sub>-C. ZrO<sub>2</sub>-D also has a surface area double that reported by Bedilo and Klabunde [615], where a value of 565 m<sup>2</sup>/g was found. Since ZrP is a surface conductor and ZrO<sub>2</sub>-D has the

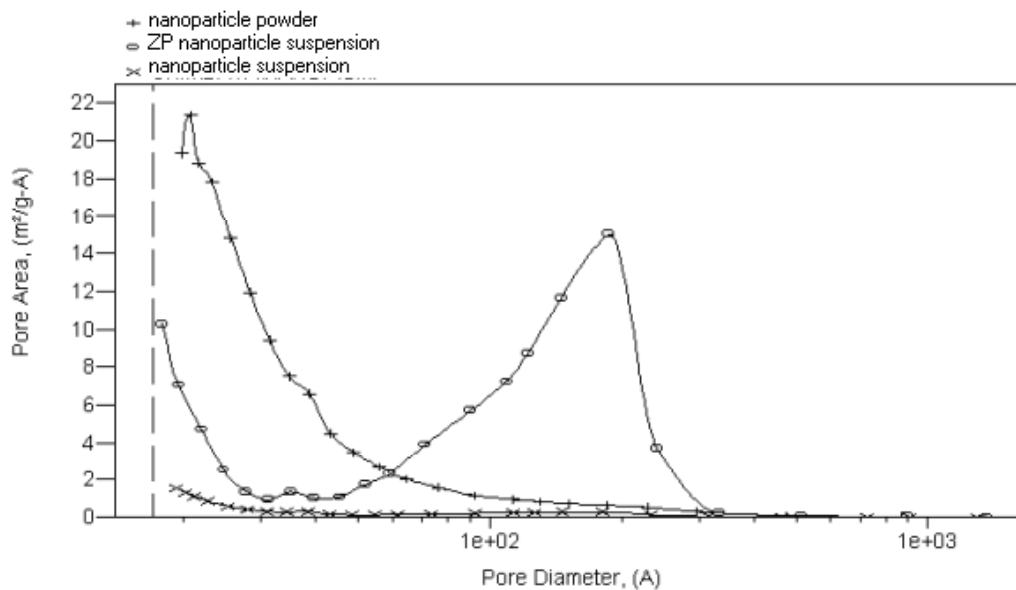
highest surface area, it can be expected that ZrP prepared from ZrO<sub>2</sub>-D will produce the highest conductivity.

**Table 4.3:** BET surface area for ZrO<sub>2</sub> sources

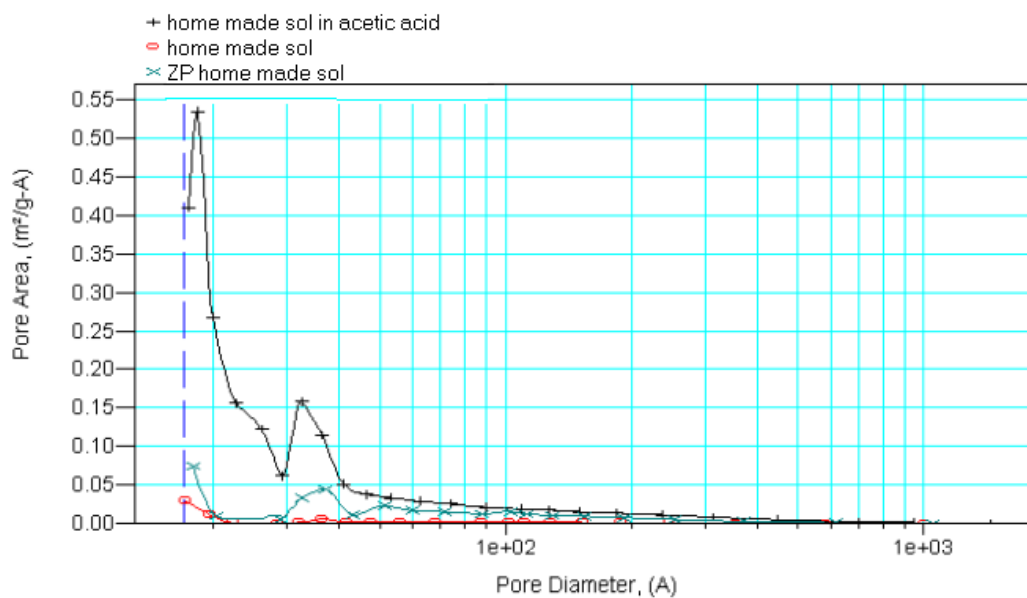
ZrO <sub>2</sub> sources	Single point surface area (m <sup>2</sup> /g)	BET surface area (m <sup>2</sup> /g)
ZrO <sub>2</sub> -L	0.5	0.6
ZrO <sub>2</sub> -C	5.1	5.4
ZrO <sub>2</sub> -D	> 1000	>1000
ZrO <sub>2</sub> (ref. 615)	542	565
ZrO <sub>2</sub> -D suspension in acetic acid	64.1	66

Figure 4.13 reports the results of the pore size distribution as a function of pore area for ZrO<sub>2</sub>-D, ZrO<sub>2</sub>-D suspension in acetic acid, and ZrP prepared from ZrO<sub>2</sub>-D. From Figure 4.13, it can be seen that ZrO<sub>2</sub>-D has a high surface area with a small pore diameter and showed the presence of a peak at ~50 Å. This peak disappeared when dispersed in acetic acid. After treatment of ZrO<sub>2</sub>-D with phosphoric acid a high intensity peak beyond 100 Å was observed - this peak being due to the presence of ZrP.

The pore size distribution as a function of pore area for ZrO<sub>2</sub>-L, ZrO<sub>2</sub>-L suspension in acetic acid, and ZrP prepared from ZrO<sub>2</sub>-L are shown in Figure 4.14. ZrO<sub>2</sub>-L has a low surface area with high pore diameter. The peak at ~50 Å as showed earlier was also observed here. In contrast to ZrO<sub>2</sub>-D, the intensity of the peak increased when dispersed in acetic acid. ZrP prepared from ZrO<sub>2</sub>-L did not show significant peaks.



**Figure 4.13:** Pore size distribution of  $ZrO_2$ -D.



**Figure 4.14:** Pore size distribution of  $ZrO_2$ -L.

Figure 4.15 shows the Thermogravimetric analysis of  $ZrO_2$ -D and  $ZrO_2$ -L. At temperatures under  $200^\circ\text{C}$ ,  $ZrO_2$ -L has a higher water retention than  $ZrO_2$ -D. This was expected from the high surface area of  $ZrO_2$ -D.

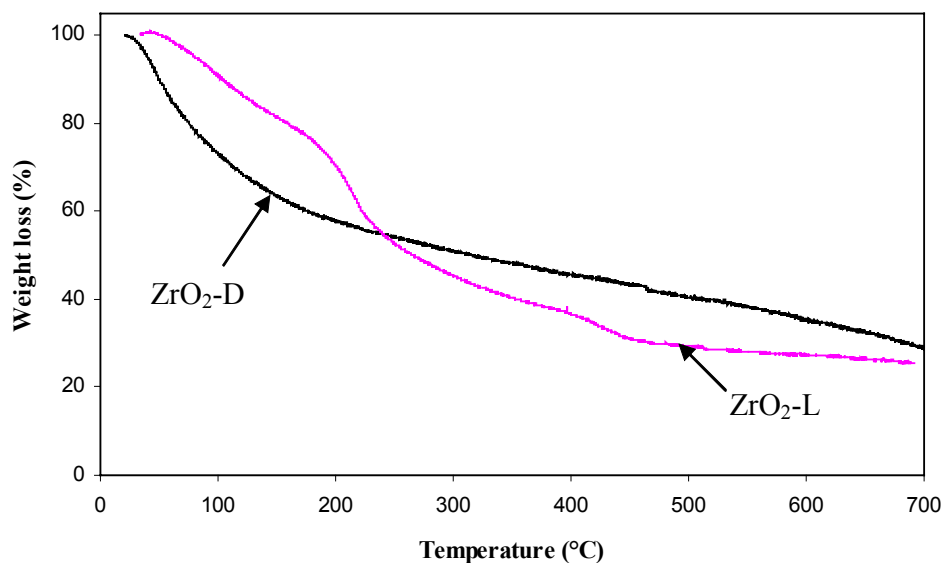


**Figure 4.15:** TGA analysis of ZrO<sub>2</sub>-D and ZrO<sub>2</sub>-L.

#### 4.3.4 Zirconium Phosphate Powder Characterization

ZrP powders were prepared from different ZrO<sub>2</sub> sources (see Section 4.3.3). The powders were prepared by mixing ZrO<sub>2</sub> and phosphoric acid. For conductivity measurement, a pellet of ZrP was prepared by adding Teflon<sup>®</sup> (PTFE) fine powder (DuPont product and purchased from Spurlock Specialty Tools) to the prepared ZrP. Teflon<sup>®</sup> was added to the ZrP to act as a binder. The conductivity was measured using the cell in Figure 3.3 and using ac impedance spectroscopy as described in section 3.3.1.2. The conductivity results are summarized in Table 4.4.

The measured conductivities of the ZrP powders were not expected, since ZrO<sub>2</sub>-D was found to be the most appropriate for high conductivity. The conductivity results show that ZrP prepared from ZrO<sub>2</sub>-L is the most conductive ( $10^{-2}$  S/cm), while ZrP prepared from ZrO<sub>2</sub>-D and ZrO<sub>2</sub>-C has a conductivity of the order of  $10^{-3}$  S/cm.

The conductivity of  $10^{-3}$  S/cm was the highest found in the literature for amorphous ZrP prepared from zirconium nitrate [345,346]. The type of PTFE added to the powder will influence the conductivity, since  $ZrO_2$  powder will behave differently (as can be seen below) and the interaction between the polymer and the powder also will differ. PTFE is a hydrophobic polymer, while ZrP is highly hydrophilic. This mixed hydrophobic-hydrophilic character will produce materials with different water content, and thus different conductivities.

**Table 4.4:** Conductivities of ZrP powders

Zirconium phosphate types	Conductivity (S/cm)
ZrP-D (made from $ZrO_2$ -D)	$3.8 \times 10^{-3}$
ZrP-L (made from $ZrO_2$ -L)	$1.0 \times 10^{-2}$
ZrP-C (made from $ZrO_2$ -C)	$9.6 \times 10^{-3}$

It would appear from Table 4.4 that ZrP prepared from  $ZrO_2$ -L is the highly moisturized one, while ZrP prepared from  $ZrO_2$ -D is not sufficiently moisturized, thereby exhibiting the lowest conductivity. According to previous research on composite proton conductive membranes (polymer and zirconium phosphate) [262], the conductivity of ZrP powder will not reflect the conductivity of the composite membrane. In general, the conductivity between the conductivity of the polymer and the conductivity of ZrP powder was reported as being dependent on the interaction between the polymer and ZrP powder. It was found that the smaller the size of the ZrP particles the better the interaction is between the polymer and the powder, leading to higher conductivity. Furthermore, in this study, the preparation procedure for ZrP

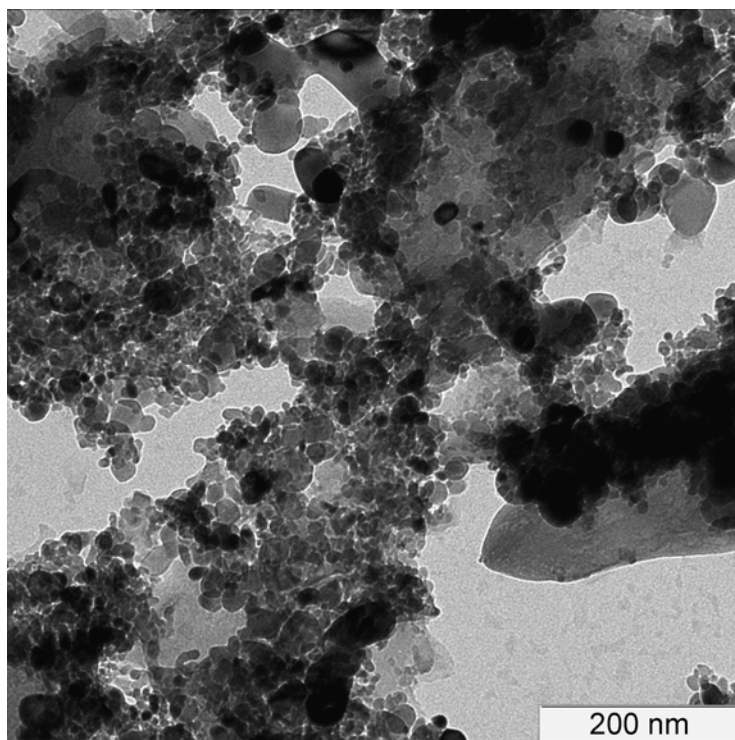


powder and the preparation of the composite membrane are different. The conductivities of the powder will not reflect the conductivities of the composite membranes, as will be seen in the next Section (Section 3.3.5).

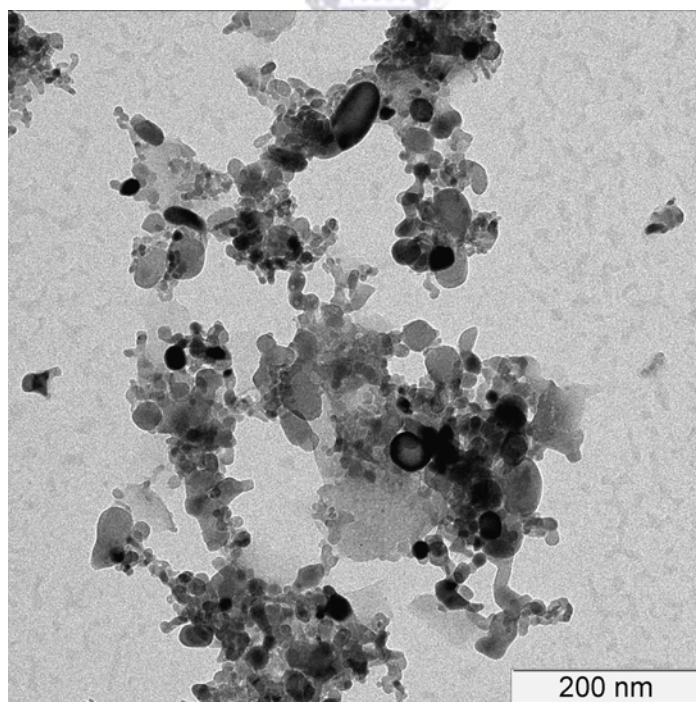
Figure 4.16 and Figure 4.17 show TEM micrographs of ZrP prepared from ZrO<sub>2</sub>-D and ZrO<sub>2</sub>-L, respectively. The particle sizes revealed by TEM analysis are in the range 30 to 40 nm.

Figure 4.18 shows SEM micrographs of different ZrO<sub>2</sub> and ZrP prepared from respective ZrO<sub>2</sub> sources. As can be seen, the morphology of the ZrO<sub>2</sub> and phosphorized ZrO<sub>2</sub> (ZrP) are different, and furthermore, the separate ZrP morphology are different. The morphology of sample A.2 is dense with a homogeneous distribution of ZrP particles and crack free. The morphology of sample B.2 is amorphous with uniformly dispersed ZrP, but with some cracks. Sample C.2 is the most different, where a crystalline structure can be seen with sharp edges. From micrographs A.2, B.2 and C.2, it can be concluded that membranes impregnated with ZrP prepared from ZrO<sub>2</sub>-D and ZrO<sub>2</sub>-L will be much better than membranes prepared from ZrO<sub>2</sub>-C, especially with respect to conductivity (size effects).

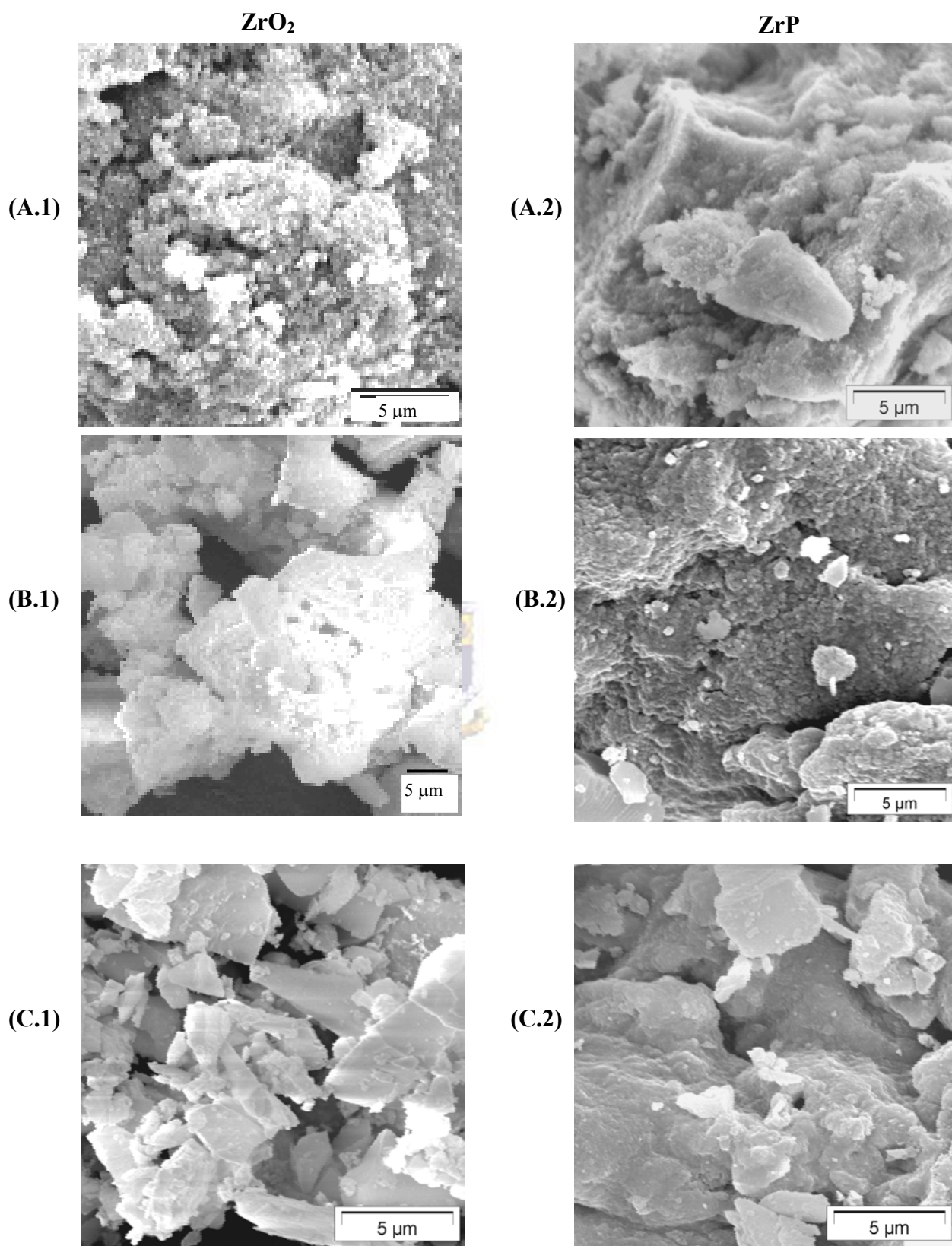
The presence of cracks in the structure of ZrP cannot indicate if this is in favor of the membrane or not. A crack free membrane will produce a less methanol permeable membrane, while a membrane with cracks will provide the membrane with a higher moisturizing effect, and thus a higher conductivity. Furthermore, since an impregnation technique is used, sample A.2 and B.2 will be the ideal materials to fill the pores of the CREAMFILTER<sup>®</sup> matrix.



**Figure 4.16:** TEM micrograph of ZrP prepared from  $ZrO_2$ -D.

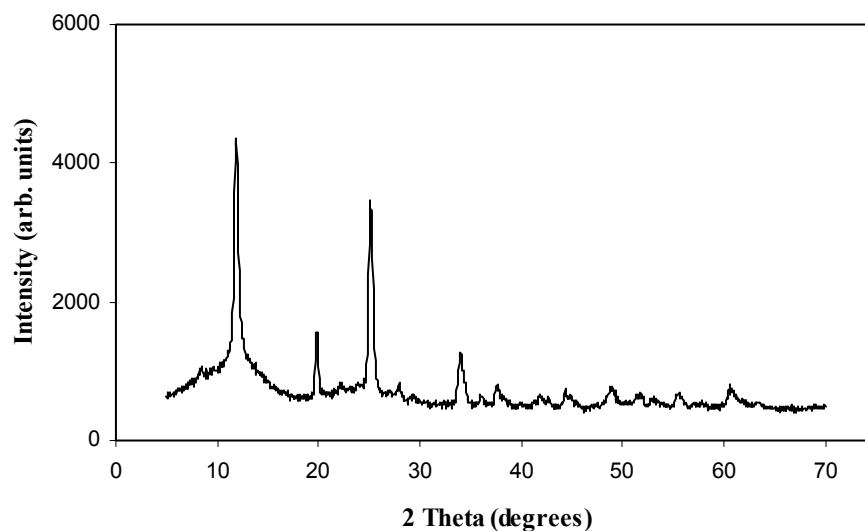


**Figure 4.17:** TEM micrograph of ZrP prepared from  $ZrO_2$ -L.



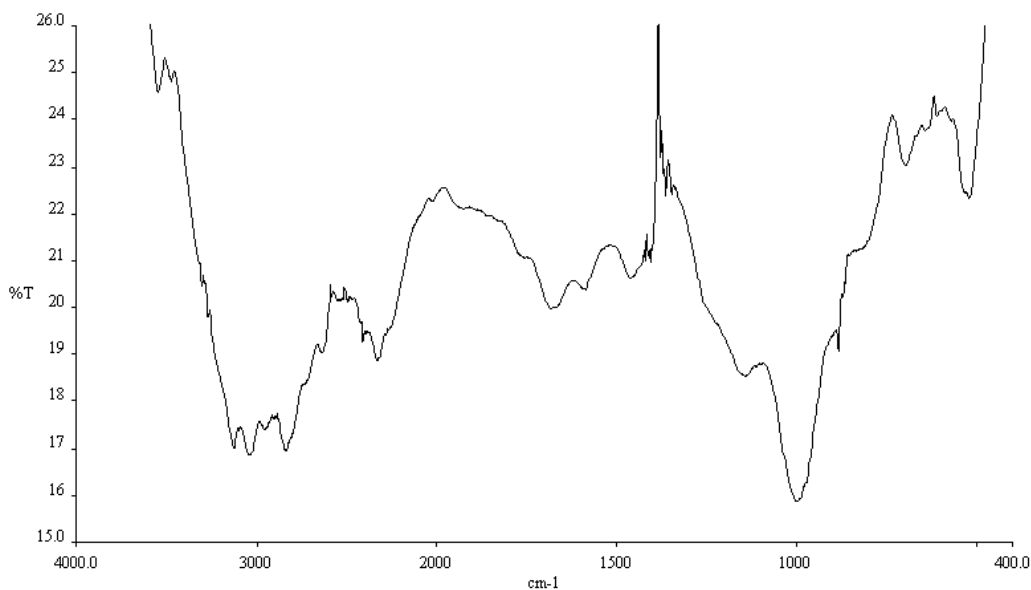
**Figure 4.18:** SEM micrographs of  $ZrO_2$  and  $ZrP$ : (A.1)  $ZrO_2$ -D, (A.2)  $ZrP$  prepared from  $ZrO_2$ -D, (B.1)  $ZrO_2$ -L, (B.2)  $ZrP$  prepared from  $ZrO_2$ -L, (C.1)  $ZrO_2$ -C, (C.2)  $ZrP$  prepared from  $ZrO_2$ -C.

Figure 4.19 shows the X-ray diffraction pattern of ZrP powder prepared from ZrO<sub>2</sub>-D. The four distinguishing peaks of ZrP can be clearly seen at Bragg angles ( $2\theta$ ) 11.7°, 20°, 25° and 34.1° [339].



**Figure 4.19:** XRD analysis of ZrP powder prepared from ZrO<sub>2</sub>-D.

Figure 4.20 shows the FTIR of ZrP powder prepared from ZrO<sub>2</sub>-D. According to Colomban and Novak [616] and Horsley *et al.* [617], the FTIR spectra of ZrP exhibited weak bands at 3550 and 3120 cm<sup>-1</sup> representing OH stretching vibrations of water and a second weak band at 1670 cm<sup>-1</sup> representing water. The bands at 1250 and 1000 cm<sup>-1</sup> were assigned to phosphate groups.



**Figure 4.20:** FTIR analysis of ZrP powder prepared from ZrO<sub>2</sub>-D.

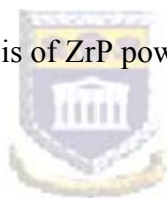
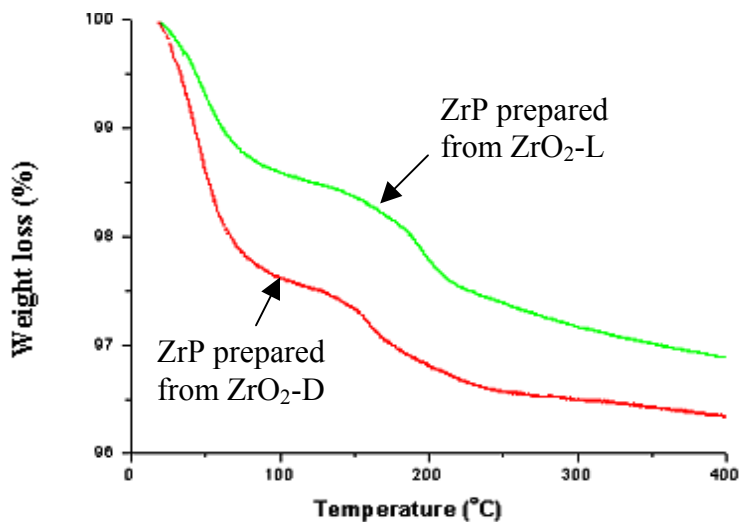


Figure 4.21 shows the TGA analysis of ZrP powder prepared from ZrO<sub>2</sub>-D and ZrO<sub>2</sub>-L. It can be seen that ZrP prepared from ZrO<sub>2</sub>-D has higher water content than ZrP prepared from ZrO<sub>2</sub>-L. Thus, this supports the high conductivity found in ZrP from ZrO<sub>2</sub>-D composite membranes. Figure 4.21 also shows that ZrP prepared in this study is different to the crystalline ZrP prepared by the refluxing method. TGA of crystalline ZrP shows a sharp weight loss at 100°C and another one at around 440°C. Between 100-440°C only a small amount of water is released [618].



**Figure 4.21:** TGA analysis of ZrP powder prepared from ZrO<sub>2</sub>-D and ZrO<sub>2</sub>-L.



Figure 4.22 shows the DSC analysis of ZrP powder prepared from ZrO<sub>2</sub>-D and ZrO<sub>2</sub>-L. Both results show two endothermic peaks. The first endothermic peak at 50°C, is related to the absorbed water. The second endothermic peak is at 160°C and 200°C for ZrP obtained from ZrO<sub>2</sub>-D and ZrO<sub>2</sub>-L, respectively.

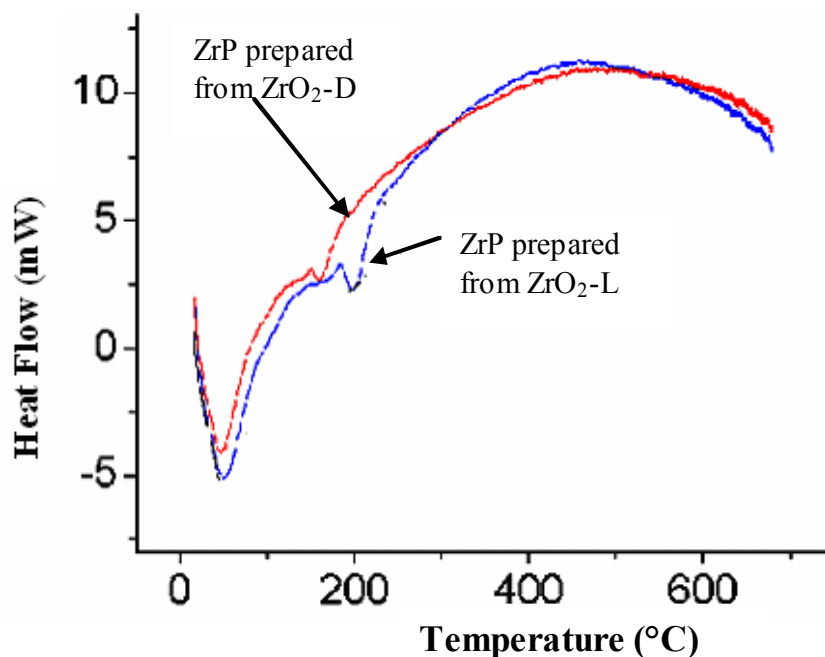


**Figure 4.22:** DSC analysis of ZrP powder prepared from ZrO<sub>2</sub>-D and ZrO<sub>2</sub>-L.

### 4.3.5 Composite Membrane Characterization

CREAFILTER<sup>®</sup>s are impregnated with ZrP as described in Section 4.3.2. Since CREAMFILTER<sup>®</sup> Z450P is not stable in concentrated H<sub>3</sub>PO<sub>4</sub>, a concentration of 1M was used to prepare the composite membrane.

Figure 4.23 shows the ZrP uptake in Z240G with the number of impregnations. As can be seen, ZrP uptake increases with each of the five impregnations. This increase in uptake would increase the conductivity of the composite membrane. The weight increase (%) was calculated from the dried bare CREAMFILTER<sup>®</sup> and the weight of the dried CREAMFILTER<sup>®</sup> after each impregnation using the following

$$\text{formula: Weight increase (\%)} = \frac{M_2 - M_1}{M_1} \times 100$$

where:  $M_2$  is the final weight (g);  $M_1$  is the initial weight (g)

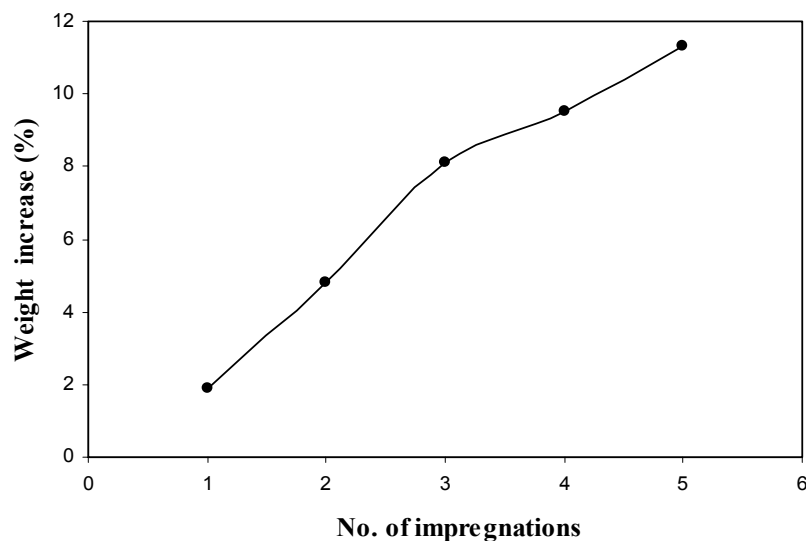


**Figure 4.23:** ZrP uptake in CREAMFILTER® Z240G.

Figure 4.24 shows how the conductivity changes with the number of impregnations in CREAMFILTER® Z240G. The conductivity increases as the number of impregnations increases, as was expected - from  $3.89 \times 10^{-3}$  S/cm for the first impregnation to  $3.02 \times 10^{-2}$  S/cm for the fifth impregnation.

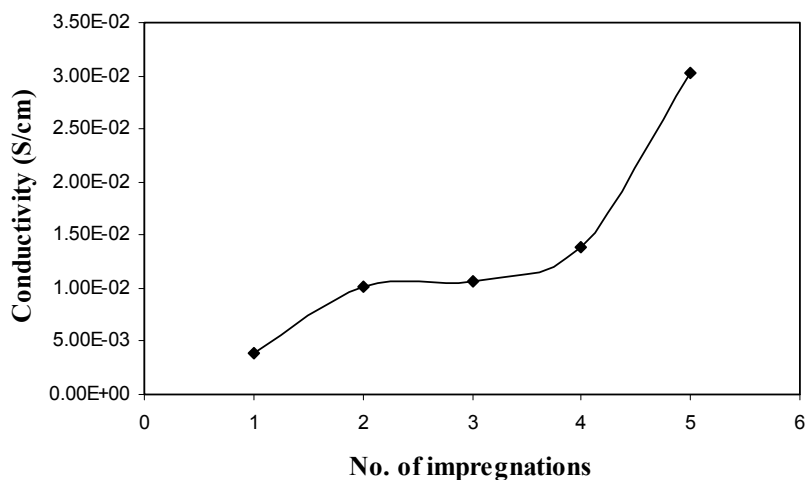


**Figure 4.24:** Conductivity as function of the number of impregnations in CREAMFILTER® Z240G.



Figure 4.25 shows the X-ray diffraction pattern of CREAMFILTER<sup>®</sup> Z240G impregnated with ZrP, from which can be clearly seen that both the peaks of the bare CREAMFILTER<sup>®</sup> and the peaks of ZrP are present in the composite membrane.

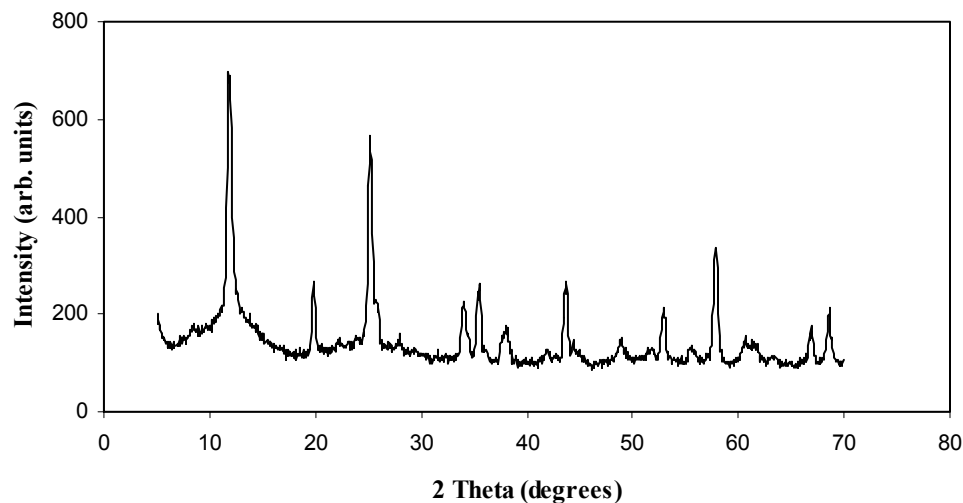


**Figure 4.25:** XRD analysis of CREAMFILTER<sup>®</sup> Z240G / ZrP.

Table 4.5 summarizes the characteristics of CREAMFILTER<sup>®</sup>s impregnated with ZrP prepared from ZrO<sub>2</sub>-D. ZrP prepared from ZrO<sub>2</sub>-D was chosen, since the conductivity of the composite membranes prepared with ZrP from ZrO<sub>2</sub>-L and ZrO<sub>2</sub>-C was very low compared to ZrO<sub>2</sub>-D as was expected from the size effect and since ZrP is a surface conductor. The maximum conductivities obtained were 10<sup>-3</sup> S/cm and 10<sup>-4</sup> S/cm for ZrP prepared from ZrO<sub>2</sub>-L and ZrO<sub>2</sub>-C, respectively.

**Table 4.5:** Composite CREAMFILTER<sup>®</sup> / ZrP membranes specifications

Membranes	Thickness dry ( $\mu\text{m}$ )	Conductivity ( $\sigma$ ) (S/cm)	Methanol permeability ( $P$ ) ( $\text{cm}^2/\text{s}$ )	Selectivity factor ( $\beta = \log(\sigma/P)$ )
Z100G	120	$6 \times 10^{-3}$	$7 \times 10^{-7}$	3.9
Z240G	120	$3 \times 10^{-2}$	$3.5 \times 10^{-7}$	4.9
S450P	50	$4 \times 10^{-2}$	$17 \times 10^{-7}$	3.4
Z450P	220	$3 \times 10^{-3}$	$17 \times 10^{-7}$	3.3
Nafion <sup>®</sup> 117	175	$5 \times 10^{-2}$	$14 \times 10^{-7}$	4.5

From Table 4.5 it can be seen that after the fifth impregnation, Z240G and S450P reach a conductivity similar to that of Nafion<sup>®</sup> ( $\sim 10^{-2}$  S/cm) measured under the same conditions. For comparison with the measured value, the conductivity of Nafion<sup>®</sup> 117 reported in the literature and measured under similar conditions is equal to  $8 \times 10^{-2}$  S/cm [138]. The conductivity of CREAMFILTER<sup>®</sup> Z100G is very low compared to CREAMFILTER<sup>®</sup> Z240G. This can be explained from the high loading of ZrP in Z240G compared to Z100G (see Figure 4.26 (C) and Figure 4.27 (C)). Since Z450P is not stable with concentrated  $\text{H}_3\text{PO}_4$ , a concentration of 1M was used to prepare the composite membrane. The conductivity found after the fifth impregnation was around  $3 \times 10^{-3}$  S/cm. Thus, this composite membrane is not suited for fuel cell application.

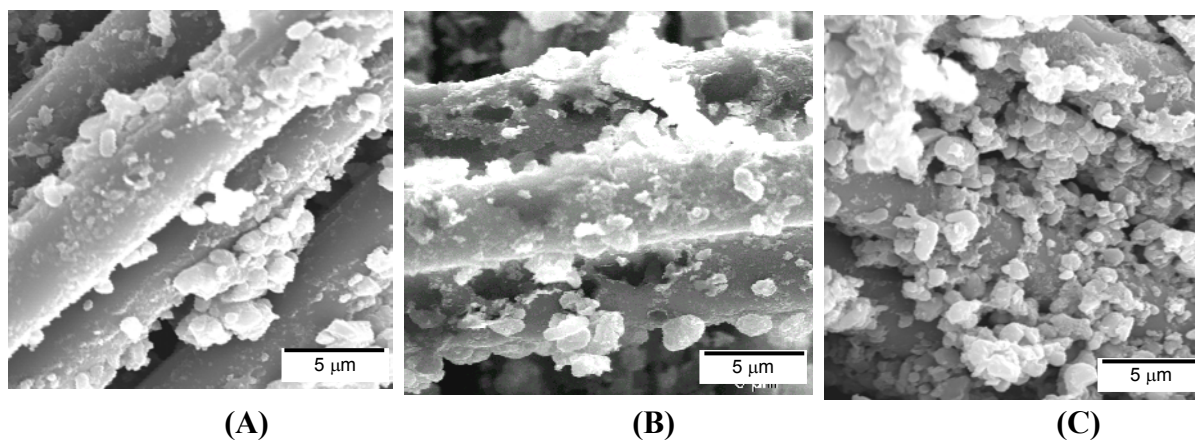
Figure 4.26 shows CREAMFILTER<sup>®</sup> Z100G impregnated with ZrP prepared from  $\text{ZrO}_2\text{-D}$ . Figure 4.26 (A) impregnated once, (B) impregnated three times and (C) impregnated five times. The results show that after only one impregnation, the membrane fibers are not fully covered by ZrP particles. Subsequent impregnation led

to the fibers being fully enveloped by ZrP particles after typically five impregnations. However, the structure is not very uniform.

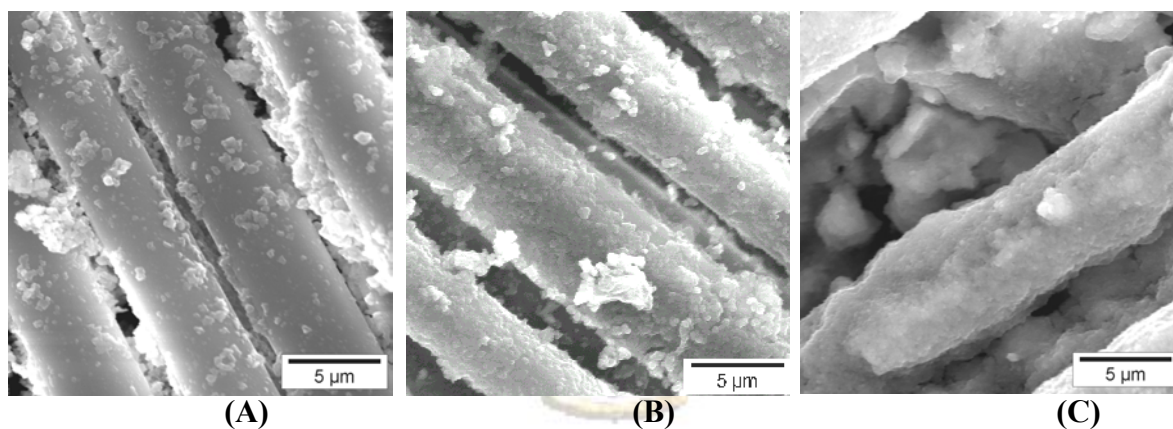
Figure 4.27 shows CREAMFILTER<sup>®</sup> Z240G impregnated with ZrP prepared from ZrO<sub>2</sub>-D. Figure 4.27 (A) impregnated once, (B) impregnated three times and (C) impregnated five times. The results show that ZrP uptake is much higher than in CREAMFILTER<sup>®</sup> Z100G. Increasing the number of impregnations led to an increase in ZrP loading. After the fifth impregnation (Figure 4.27 (C)), the fibers are covered with ZrP particles, leading to a uniform distribution of ZrP particles between the fibers and also the coverage of the fibers. This uniformity and high loading is expected to lead to an increase in its conductivity.

Figure 4.28 shows CREAMFILTER<sup>®</sup> Z450P impregnated with ZrP prepared from ZrO<sub>2</sub>-D. Figure 4.28 (A) impregnated once, (B) impregnated three times and (C) impregnated five times. Since the structure of CREAMFILTER<sup>®</sup> Z450P is different to the previous ones, the ZrP produced after the fifth impregnation is of a crystalline structure.

Figure 4.29, Figure 4.30 and Figure 4.31 show CREAMFILTER<sup>®</sup> Z100G, Z240G and Z450P impregnated with ZrP prepared from ZrO<sub>2</sub>-L, respectively. Figure (A) shows the first impregnation, (B) the third impregnation and (C) the fifth impregnation. The same trend is observed for the impregnation of CREAMFILTER<sup>®</sup>s as before, where ZrP loading increases with the number of impregnations. However, ZrP produced by impregnating CREAMFILTER<sup>®</sup>s from ZrO<sub>2</sub>-L is different to ZrP produced in Figures 4.26, 4.27 and 4.28.



**Figure 4.26:** SEM micrographs of CREAMFILTER<sup>®</sup> Z100G/ ZrP prepared from ZrO<sub>2</sub>-D: (A) first impregnation, (B) third impregnation and (C) fifth impregnation.



**Figure 4.27:** SEM micrographs of CREAMFILTER<sup>®</sup> Z240G/ ZrP prepared from ZrO<sub>2</sub>-D: (A) first impregnation, (B) third impregnation and (C) fifth impregnation.

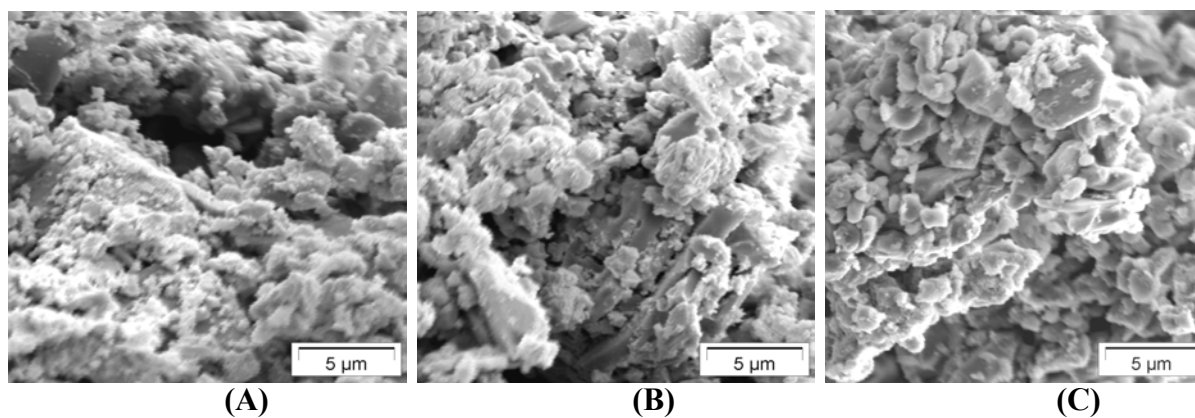


**Figure 4.28:** SEM micrographs of CREAMFILTER<sup>®</sup> Z450P/ ZrP prepared from ZrO<sub>2</sub>-D: (A) first impregnation, (B) third impregnation and (C) fifth impregnation.

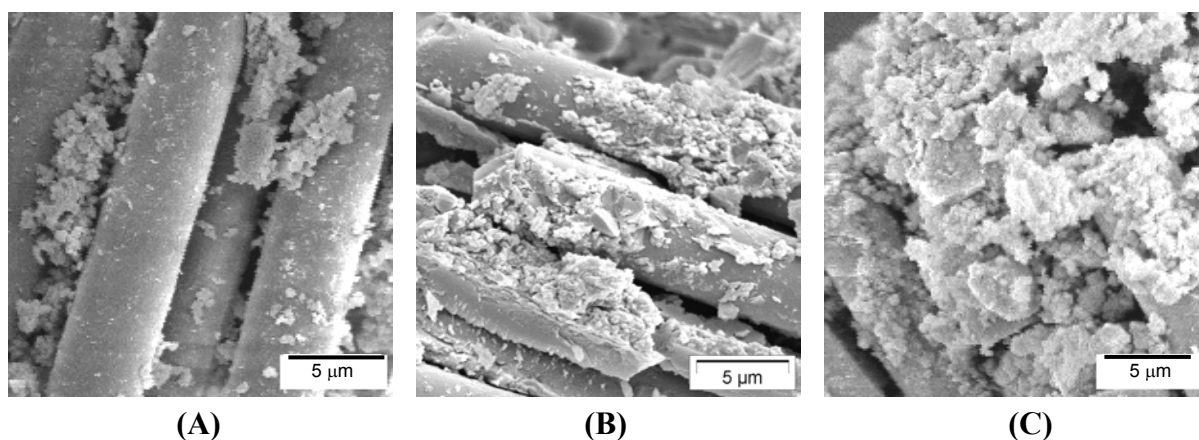


**Figure 4.29:** SEM micrographs of CREAMFILTER<sup>®</sup> Z100G/ ZrP prepared from ZrO<sub>2</sub>-L: (A) first impregnation, (B) third impregnation and (C) fifth impregnation.

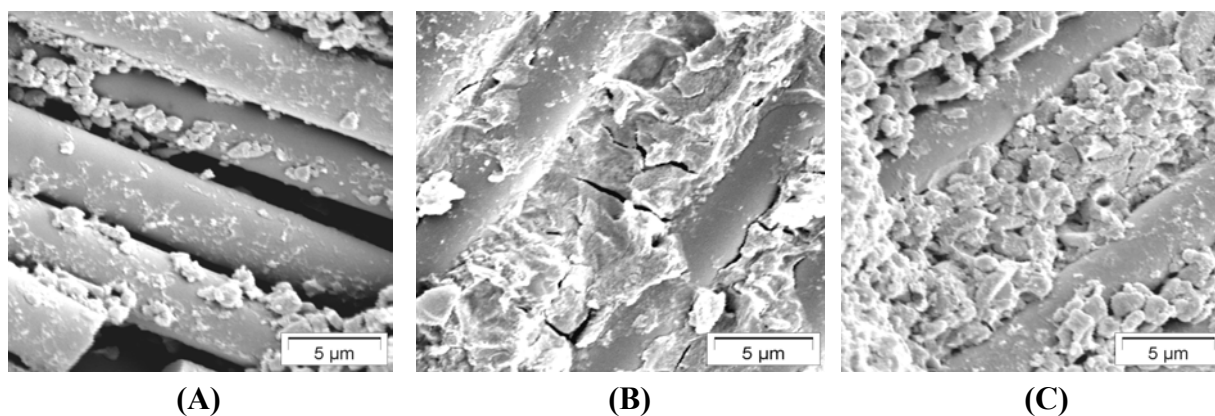


**Figure 4.30:** SEM micrographs of CREAMFILTER<sup>®</sup> Z240G/ ZrP prepared from ZrO<sub>2</sub>-L: (A) first impregnation, (B) third impregnation and (C) fifth impregnation.

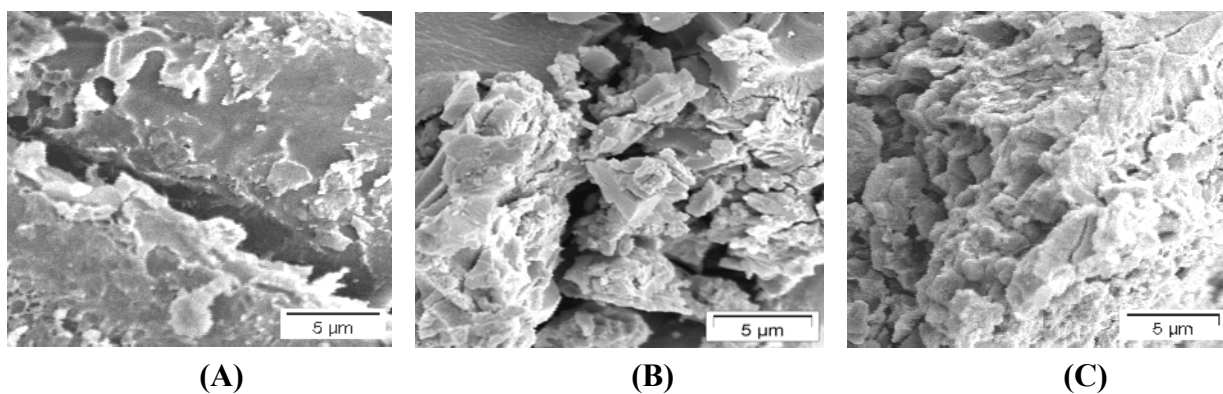


**Figure 4.31:** SEM micrographs of CREAMFILTER<sup>®</sup> Z450P/ ZrP prepared from ZrO<sub>2</sub>-L: (A) first impregnation, (B) third impregnation and (C) fifth impregnation.

Figure 4.32 shows the measured methanol concentration in the receiving compartment (B) as a function of the exposed time in different inorganic CREAMFILTER<sup>®</sup> matrixes, namely Z100G, Z240G, Z450P impregnated with ZrP and Nafion<sup>®</sup> 117. Nafion<sup>®</sup> 117 was studied as a reference, since it is the membrane of choice for DMFCs.

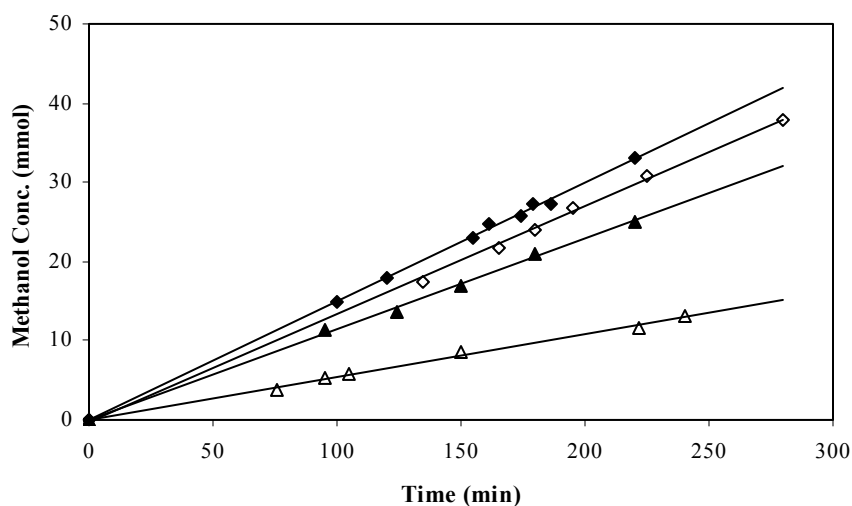


**Figure 4.32:** Concentration of methanol in compartment B as a function of time: composite Z450P/ZrP (◆); Nafion<sup>®</sup> 117 (◇); composite Z100G/ZrP (▲) and composite Z240G/ZrP (△).

The calculated methanol permeability coefficient ( $P$ ) for CREAMFILTER<sup>®</sup>s impregnated with ZrP and Nafion<sup>®</sup> 117 are reported in Table 4.5. Equation 3.1 was used for the calculation, and the detailed calculations appear in Appendix A. The methanol permeability coefficient ( $P$ ) for Nafion<sup>®</sup> 117 was found to be  $14 \times 10^{-7}$  cm<sup>2</sup>/s, which is in agreement with the value reported in the literature [179,604].

It can be seen that the composite membrane had a lower methanol permeability than Nafion<sup>®</sup> 117 - being reduced from  $9 \times 10^{-7}$  to  $7 \times 10^{-7}$  cm<sup>2</sup>/s for Z100G and from  $11 \times 10^{-7}$  to  $3.5 \times 10^{-7}$  for Z240G. Further impregnation with ZrP decreases methanol permeability by approximately 4 times for Z240G. CREAMFILTER<sup>®</sup> Z450P and S450P impregnated with ZrP had higher methanol permeability than Nafion<sup>®</sup> 117. This is due to the high pore sizes of these CREAMFILTER<sup>®</sup>s - typically 450 nm. Thus these composite membranes are not fully covered with ZrP.

Figure 4.33 shows TGA analyses for CREAMFILTER<sup>®</sup> Z450P and S450P impregnated with ZrP obtained from ZrO<sub>2</sub>-D and compared to Nafion<sup>®</sup> 117. Both composite membranes have higher water content than Nafion<sup>®</sup> 117, since they are constituted of metal oxide (Table 4.1). SiO<sub>2</sub> and ZrO<sub>2</sub> are widely used as additives for Nafion<sup>®</sup> to increase water content at high temperature. Figure 4.33 also shows that S450P has higher water content than Z450P, since this is directly related to the type of metal oxide on CREAMFILTER<sup>®</sup>. S450P is constituted of SiO<sub>2</sub> and Al<sub>2</sub>O<sub>3</sub>, while Z450P is constituted of ZrO<sub>2</sub> and Al<sub>2</sub>O<sub>3</sub>. The water content of the metal oxide differs with the type of metal used - SiO<sub>2</sub> has the highest water content, followed by ZrO<sub>2</sub> and thereafter Al<sub>2</sub>O<sub>3</sub> [277]. This trend is also observed in CREAMFILTER<sup>®</sup> membranes impregnated with ZrP.

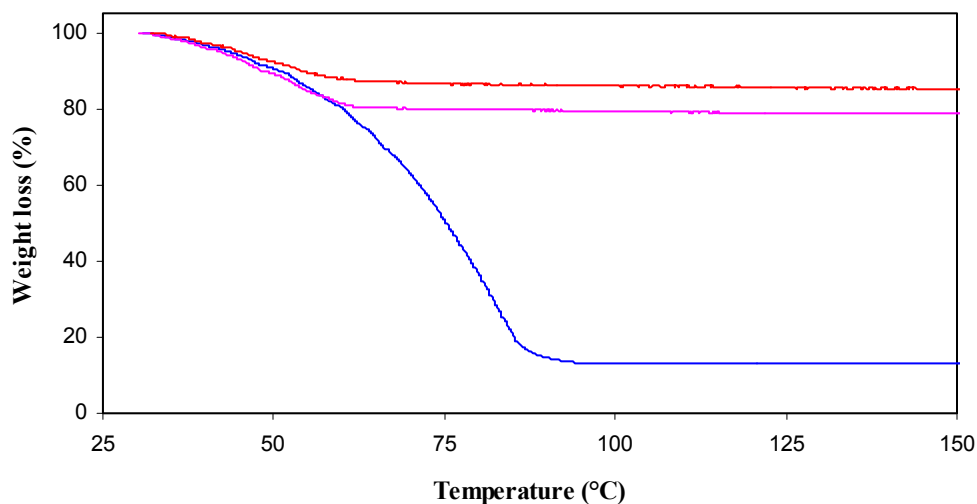


**Figure 4.33:** TGA analysis of Nafion<sup>®</sup> 117 (—), composite CREAMFILTER<sup>®</sup> Z450P / ZrP (—) and composite CREAMFILTER<sup>®</sup> S450P / ZrP (—).

#### 4.3.6 Discussion and Conclusions

The principle of using a flexible ceramic CREAMFILTER<sup>®</sup> matrix impregnated with ZrP was proved to be a successful approach to prepare a novel proton conductor membrane. CREAMFILTER<sup>®</sup> provides the mechanical strength to the composite membrane. Furthermore, CREAMFILTER<sup>®</sup> provides high water content, since it is prepared from metal oxides. Repeating the impregnation process proved to be necessary to reach the desired characteristics, namely, the proton conductivity and methanol permeability. Increasing the number of impregnations increased the loading, thus increasing the conductivity, and at the same time, an increasing ZrP loading covered the pores of the inorganic CREAMFILTER<sup>®</sup> matrix, thereby decreasing methanol permeability. After the fifth impregnation with ZrP, CREAMFILTER<sup>®</sup> Z240G



and S450P reach conductivities similar to that of Nafion<sup>®</sup> 117, measured under the same conditions.

Methanol permeability was reduced in composite membranes by further impregnation with ZrP from  $9 \times 10^{-7} \text{ cm}^2/\text{s}$  and  $11 \times 10^{-7} \text{ cm}^2/\text{s}$  to  $7 \times 10^{-7} \text{ cm}^2/\text{s}$  and  $3.5 \times 10^{-7} \text{ cm}^2/\text{s}$  for Z100G and Z240G, respectively. These results represent a methanol reduction of 2 and 4 times for Z100G and Z240G, respectively.

The selectivity factor ( $\beta$ ), which is the ratio between the conductivity ( $\sigma$ ) and permeability ( $P$ ), was used to compare the prepared composite membranes with Nafion<sup>®</sup> 117 (Table 4.5). CREAMFILTER<sup>®</sup> Z240G impregnated with ZrP has a selectivity factor higher than that of Nafion<sup>®</sup> 117 - 4.9 compared to 4.5. Therefore, CREAMFILTER<sup>®</sup> Z240G impregnated with ZrP has the potential to perform similarly to Nafion<sup>®</sup> 117. The selectivity factor for Z100G and S450P were found to be very close to that of Nafion<sup>®</sup> 117, showing the potential of these composite membranes for DMFCs. However, CREAMFILTER<sup>®</sup> Z450P impregnated with ZrP has the lowest selectivity factor ( $\beta$ ), and is therefore, not suited for fuel cell application.

Furthermore, the composite inorganic CREAMFILTER<sup>®</sup> matrix impregnated with ZrP shows higher water content than Nafion<sup>®</sup> 117, thus these types of composite can be used at high temperature without moisturizing.

During methanol permeability measurement, it was observed that there is some bleeding of ZrP from the membrane. However, this leaching can be avoided by further coating the composite membrane with a polymer or palladium film. The coating

process can be done by soaking the composite membrane in a proton conductive polymer (e.g. Nafion<sup>®</sup> solution or S-PEEK), as will be seen in Section 4.8.

## **4.4 INORGANIC CREAMFILTER<sup>®</sup> MATRIX IMPREGNATED WITH NAFION<sup>®</sup> SOLUTION**

### **4.4.1 Introduction**

Nafion<sup>®</sup> solution, in general, is added to the electrodes in fuel cells to extend the three-phase zone. Nafion<sup>®</sup> solution acts as a binder for the catalyst but also provides the necessary proton conductivity. As was discussed in Section 2.2.2.5, several researchers investigated the possibility of using PTFE impregnated with Nafion<sup>®</sup> solution as proton conductor membranes. The conductivity found for this type of composite is similar and, in some cases (e.g. Gore Select<sup>®</sup> membranes), is much higher than Nafion<sup>®</sup> polymer conductivity. In all previous research, the developed composite membranes are tested for use in a H<sub>2</sub>/O<sub>2</sub> fuel cell. Furthermore, these membranes are developed for use at temperatures around 80°C. In this study, attempts to develop a composite membrane constituted of inorganic CREAMFILTER<sup>®</sup> matrix impregnated with Nafion<sup>®</sup> solution were developed for DMFC application.

### **4.4.2 Membrane Preparation**

Nafion<sup>®</sup> in ethanol solution was prepared according to the Moore and Martin method [165]. The original solvents of the commercial 5 wt.% Nafion<sup>®</sup> solution (EW 1100, Ion Power) were evaporated at 80°C in an air oven. After the Nafion<sup>®</sup> ionomer was obtained, it was dissolved in neat ethanol to obtain an 18% Nafion<sup>®</sup> in ethanol

solution. The CREAMFILTER<sup>®</sup> matrices were soaked in ethanol for 30 minutes and dried at 50-60°C for 30 minutes. The matrices were soaked in Nafion<sup>®</sup>/ethanol solution for 1 hour and dried in an air oven for 1 hour at 50-60°C. The soaking procedure was repeated at least 5 times [135]. Finally, the composite membranes were dried at 60°C for 24 hours and annealed at high temperature (typically 160°C) for 30 minutes.

The composite membranes and Nafion<sup>®</sup> 117 were treated with the standard procedure, viz boiling the membranes in 3 vol.% H<sub>2</sub>O<sub>2</sub> for 1 hour, washing in boiling water (Modulab Water System, 18 MΩ/cm), followed by soaking the membranes in 1M H<sub>2</sub>SO<sub>4</sub> for 1 hour, and washing several times with boiling water.

#### 4.4.3 Recast Nafion<sup>®</sup> Characterization

Since the principle of preparing this type of composite is similar to making recast Nafion<sup>®</sup>, some of its characteristics were investigated, namely, its structure and solubility. The recast Nafion<sup>®</sup> was prepared with a similar procedure to making the composite membrane. Nafion<sup>®</sup> solution in ethanol (18%) was stirred in an ultrasonic water bath for 30 minutes. When the solution is poured into a glass Petri dish, the amount of Nafion<sup>®</sup> solution will determine the thickness of the recast Nafion<sup>®</sup> membrane. The Petri dish with Nafion<sup>®</sup> solution was dried for 24 hours at 60°C, followed by a treatment at 160°C for 30 minutes - the last step being necessary to increase the crystallinity of the film and thus increase its mechanical stability. The film is pulled off from the Petri dish by adding a small amount of water.

Figure 4.34 shows the X-ray diffraction pattern of Nafion<sup>®</sup> 117 and recast Nafion<sup>®</sup>. The pattern displays a broad diffraction feature at  $2\theta = 12-22^\circ$ , which can be deconvoluted into two peaks - one assigned to the amorphous form ( $2\theta = 16^\circ$ ) and the other to the crystalline form ( $2\theta = 17.5^\circ$ ) [126,166]. The others peaks present with recast Nafion<sup>®</sup> are due to the impurities in the sample, since no further treatment was done after recasting. The standard method to treat Nafion<sup>®</sup> includes hydrogen peroxide to remove organic impurities and sulfuric acid to remove inorganic impurities, and also to complete Nafion<sup>®</sup> protonation. The treated recast Nafion<sup>®</sup> with the standard method has the same peaks as Nafion<sup>®</sup> 117. In general, the structure of Nafion<sup>®</sup> 117 and recast Nafion<sup>®</sup> are the same. However, the crystallinity of the recast Nafion<sup>®</sup> is higher in this case. The crystallinity depends largely on the thermal treatment.

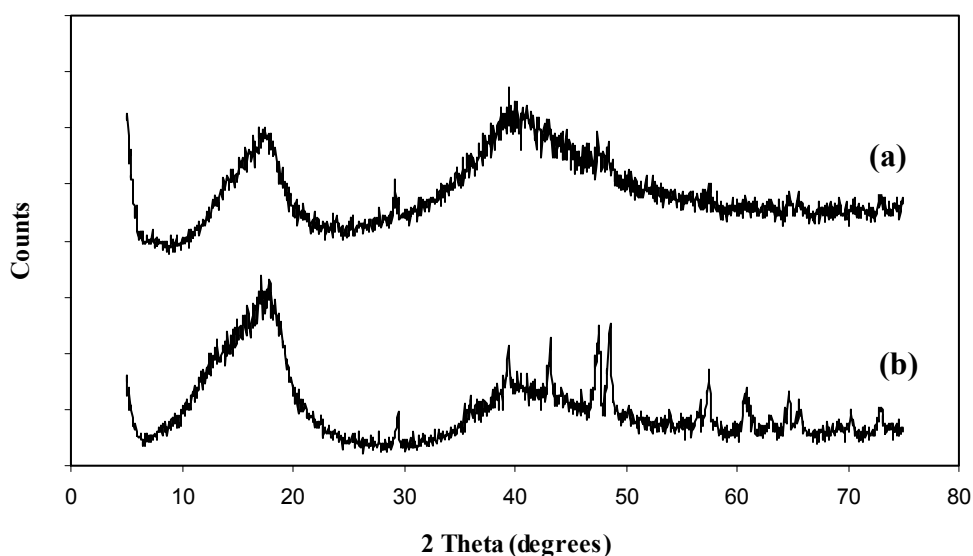


**Figure 4.34:** XRD analysis of (a) Nafion<sup>®</sup> 117 and (b) recast Nafion<sup>®</sup>.

Recast Nafion<sup>®</sup> at low temperature is brittle, easily cracked, and soluble in organic solvents, and especially water [165-167]. The solubility of the recast Nafion<sup>®</sup> was assessed by the Moore and Martin method [166]. The composite membrane was soaked in a 50:50 ethanol-water solution, and agitated in an ultrasonic bath for 1 hour. The ethanol-water solution was then filtered through a filter paper, and evaporated to dryness. The solid residue was weighed. The percentage of Nafion<sup>®</sup> that had dissolved was calculated by the following formula:

$$\% \text{ soluble} = \frac{\text{wt. of residue}}{\text{wt. of recast film}} \times 100$$

According to Gebel *et al.* [167] a mechanically stable Nafion<sup>®</sup> film can be obtained if the recast film is processed at temperatures typically around 200°C. Different temperatures were used to thermally treat the recast Nafion<sup>®</sup> film, and the solubility studies were performed on these films. Figure 4.35 represents the results. Increasing casting temperature will decrease the film solubility. It is well known that high temperatures increase the crystallinity of Nafion<sup>®</sup> film, thereby increasing its mechanical stability. The film treated at 120°C has a solubility of around 4%, which value is very low, but the recast film was partially disintegrating during the solubility test- the other films disintegrated completely below 120°C. Only the film treated at 160°C, which has a solubility of 2.3%, did not disintegrate and was mechanically stable. Thus, 160°C was chosen as the temperature for preparing the composite membranes.

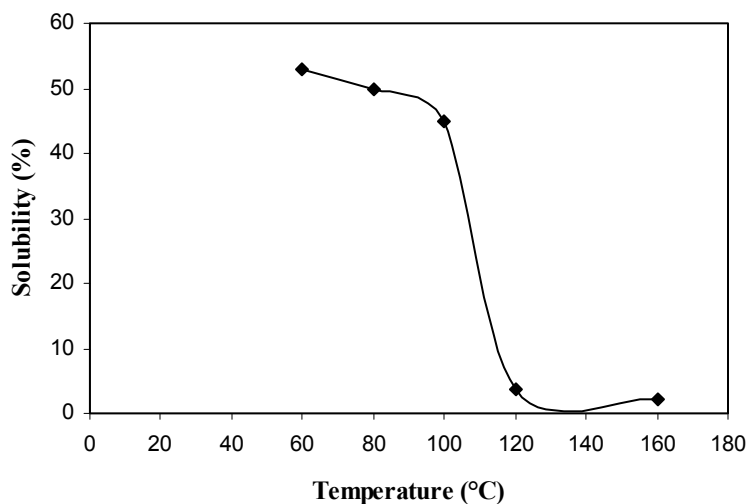


**Figure 4.35:** Recast Nafion<sup>®</sup> solubility.

#### 4.4.4 Composite CREAMFILTER<sup>®</sup> Matrix Impregnated with Nafion<sup>®</sup> Solution

##### Membrane Characterization

Figure 4.36 shows CREAMFILTER<sup>®</sup> Z100G impregnated with Nafion<sup>®</sup> solution. As can be seen, the surface is coated with Nafion<sup>®</sup>, but very little Nafion<sup>®</sup> is present in the pores. Figure 4.37 shows a cross-section of CREAMFILTER<sup>®</sup> Z240G impregnated with Nafion<sup>®</sup> solution, where the pores are filled with Nafion<sup>®</sup>. The SEM images support the high conductivity of CREAMFILTER<sup>®</sup> Z240G impregnated with Nafion<sup>®</sup> solution. The Nafion<sup>®</sup> uptake in Z240G is much higher than in Z100G - this will influence the conductivity as will be seen below. Figure 4.38 shows CREAMFILTER<sup>®</sup> S450P impregnated with Nafion<sup>®</sup> solution, where the surface is completely covered with Nafion<sup>®</sup>.

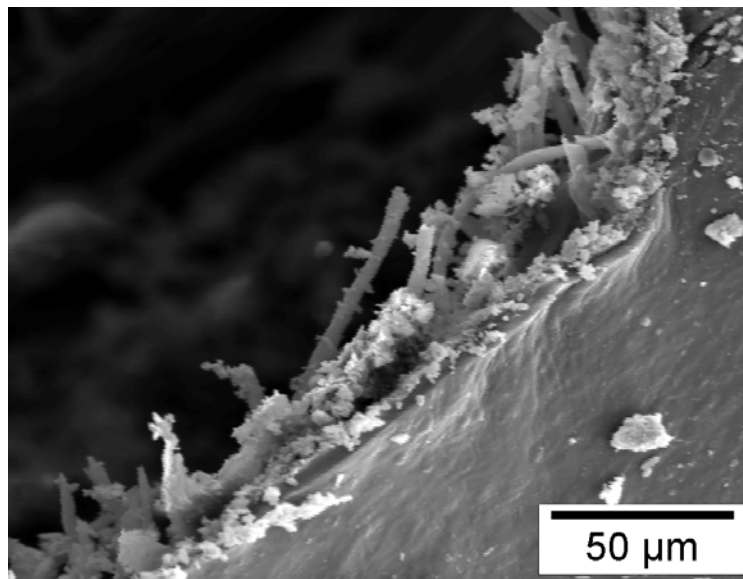


**Figure 4.36:** SEM micrograph of a cross-section of CREAMFILTER<sup>®</sup> Z100G impregnated with Nafion<sup>®</sup> solution.

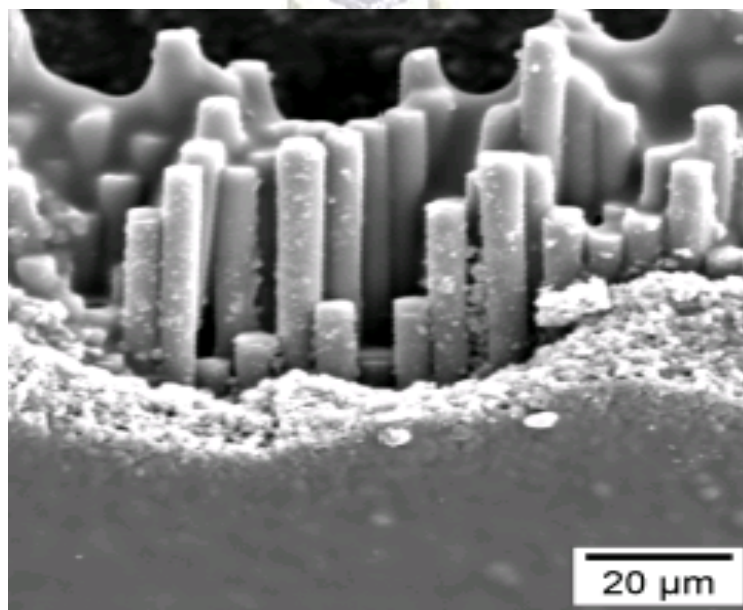


**Figure 4.37:** SEM micrograph of a cross-section of CREAMFILTER<sup>®</sup> Z240G impregnated with Nafion<sup>®</sup> solution.



**Figure 4.38:** SEM micrograph of the surface of CREAFILTER<sup>®</sup> S450P impregnated with Nafion<sup>®</sup> solution.

Figure 4.39 shows the measured methanol concentration in the receiving compartment (B) as a function of the exposed time in different composite membranes.

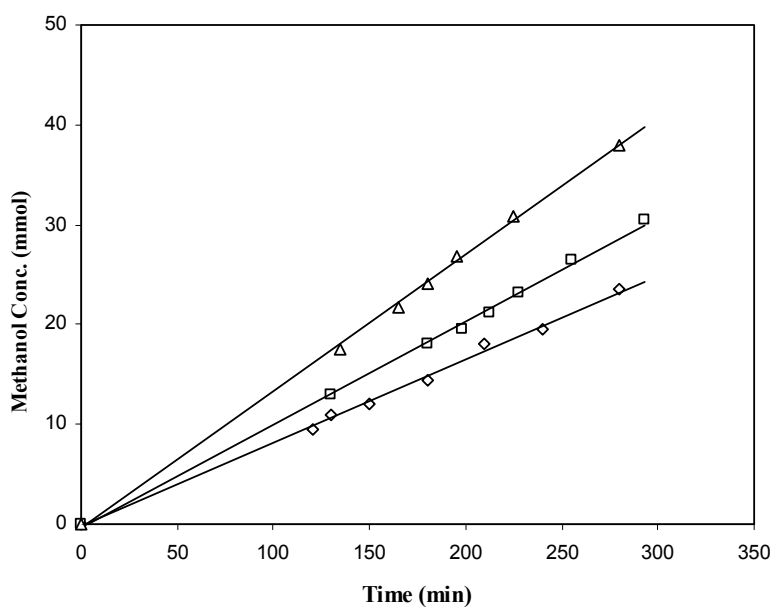


**Figure 4.39:** Concentration of methanol in compartment B as a function of time: Nafion<sup>®</sup> 117 ( $\Delta$ ), composite Z100G/Nafion<sup>®</sup> ( $\square$ ), and composite Z240G/Nafion<sup>®</sup> ( $\diamond$ ).



Methanol permeability is reported in Table 4.6. It can be seen from Figure 4.39 and Table 4.6 that the composite membranes had a lower methanol permeability than Nafion<sup>®</sup> 117 - being reduced from  $9 \times 10^{-7}$  to  $6 \times 10^{-7}$  cm<sup>2</sup>/s for Z100G and from  $11 \times 10^{-7}$  to  $5.5 \times 10^{-7}$  cm<sup>2</sup>/s for Z240G. As the bare CREAMFILTER<sup>®</sup> Z100G and Z240G have lower methanol permeability than Nafion<sup>®</sup> 117, further impregnation with Nafion<sup>®</sup> solution decreases methanol permeability to approximately 2.5 and 3 times, respectively.

Table 4.6 summarizes the characteristics of the composite membranes. Membrane conductivity was calculated from the measured resistance as described in Section 3.3.1 and using the following formula:

$$\sigma = \frac{1}{R} \times \frac{l}{A}$$

where  $\sigma$  is the conductivity,  $l$  and  $A$  (0.28 cm<sup>2</sup>) are the membrane thickness and the electrode area, respectively.

**Table 4.6:** Composite CREAMFILTER<sup>®</sup> / Nafion<sup>®</sup> membranes specifications

Membranes	Thickness wet (μm)	Nafion <sup>®</sup> uptake (%)	Water uptake (%)	Conductivity (S/cm)	Methanol permeability (cm <sup>2</sup> /s)
Z100G	130	61	17	$8 \times 10^{-3}$	$6 \times 10^{-7}$
Z240G	120	70	18	$2.5 \times 10^{-2}$	$5.5 \times 10^{-7}$
S450P	60	87	21	$4.5 \times 10^{-2}$	$13 \times 10^{-7}$
Nafion <sup>®</sup> 117	210	100	16	$5 \times 10^{-2}$	$14 \times 10^{-7}$

Table 4.6 shows conductivities obtained for CREAMFILTER<sup>®</sup> impregnated with Nafion<sup>®</sup>. After the fifth impregnation Z240G and S450P reach a conductivity similar to that of Nafion<sup>®</sup> ( $\sim 10^{-2}$  S/cm) measured under the same conditions. The conductivity of Nafion<sup>®</sup> 117 reported in the literature under similar conditions is equal to  $8 \times 10^{-2}$  S/cm [138]. Z240G and S450P have a Nafion<sup>®</sup> uptake of 70% and 87%, respectively. Nafion<sup>®</sup> uptake was calculated from the weight of the bare CREAMFILTER<sup>®</sup> and the weight after impregnation (dry state). However, Z100G has a lower conductivity than Z240G. The structure of these two materials is the same, and nearly the same thickness - 100  $\mu\text{m}$  and 90  $\mu\text{m}$  for bare Z100G and Z240G, respectively, but Nafion<sup>®</sup> uptake in Z240 is higher than Z100G. According to Aricò *et al.* [566], Nafion<sup>®</sup> micelles have a size of approximately 200 nm, which is slightly smaller than the pore size of Z240G and much bigger than the pores of Z100G - thus, the pores of Z100G are not completely filled with Nafion<sup>®</sup>. S450P has a pore size of 450 nm, leading to a Nafion<sup>®</sup> uptake of 87%. Furthermore, the composite membrane was very thin compared to Nafion<sup>®</sup> 117 with a thickness of 50  $\mu\text{m}$ , and as a consequence, the highest conductivity was obtained.

Figure 4.40 shows the thermogravimetric analysis of CREAMFILTER<sup>®</sup>s impregnated with Nafion<sup>®</sup> and Nafion<sup>®</sup> 117. CREAMFILTER<sup>®</sup>s have much higher water content than Nafion<sup>®</sup> 117, since they are constituted of metal oxide (Table 4.1). SiO<sub>2</sub> and ZrO<sub>2</sub> are widely used as additives for Nafion<sup>®</sup> to increase the water content at high temperature. Figure 4.40 also shows that S450P has higher water content than Z100G

which is directly related to the type of metal oxide on CREAMFILTER<sup>®</sup>. S450P is constituted of SiO<sub>2</sub> and Al<sub>2</sub>O<sub>3</sub>, while Z100G is constituted of ZrO<sub>2</sub> and Al<sub>2</sub>O<sub>3</sub>. The water content of the metal oxide depends on the type of metal used - SiO<sub>2</sub> has the highest water content, followed by ZrO<sub>2</sub> and thereafter Al<sub>2</sub>O<sub>3</sub> [277]. This trend is also observed in CREAMFILTER<sup>®</sup> membranes.

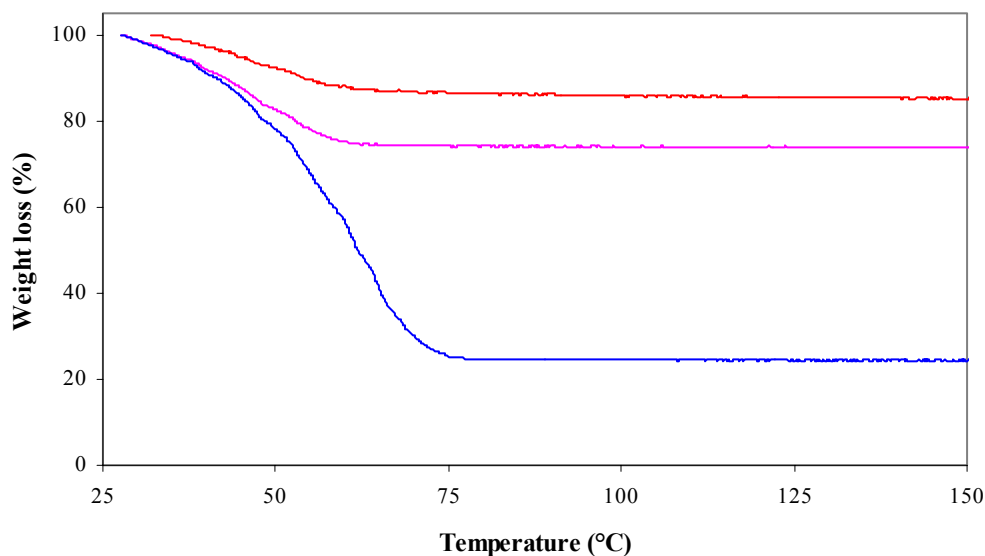


**Figure 4.40:** TGA analysis of Nafion<sup>®</sup> 117 (—), composite Z100G/Nafion<sup>®</sup> (—) and composite S450P/Nafion<sup>®</sup> (—).

#### 4.4.5 Discussion and Conclusions

The inorganic CREAMFILTER<sup>®</sup> matrix was found to be a suitable support for Nafion<sup>®</sup> solution to form a composite proton conductor membrane. The solvent plays a role in Nafion<sup>®</sup> micelle formation - in this study Nafion<sup>®</sup> ionomer dissolved in ethanol (18%) was used. Nafion<sup>®</sup> film in the composite membrane is not soluble, since the composite membrane was annealed at high temperature, typically 160°C. The

composite membrane formed shows the potential to be an alternative to Nafion<sup>®</sup> polymer. The prepared membranes exhibit similar conductivity to Nafion<sup>®</sup> 117, measured under the same conditions. Conductivities of  $2.5 \times 10^{-2}$ ,  $4.5 \times 10^{-2}$  and  $5 \times 10^{-2}$  S/cm were found for Z240G, S450P and Nafion<sup>®</sup> 117, respectively. Furthermore, methanol permeability was found to be lower in composite membranes - reduction by a factor of approximately 3 was found for composite CREAMFILTER<sup>®</sup> Z240G. The selectivity factor ( $\beta$ ), which is the ratio between the conductivity ( $\sigma$ ) and permeability ( $P$ ), is adopted to compare the composite membranes and Nafion<sup>®</sup> 117. Selectivity values of 4.1, 4.6, 4.5 and 4.5 were found for Z100G, Z240G, S450P and Nafion<sup>®</sup> 117, respectively. It can be concluded that these composite membranes have the potential to be an alternative to Nafion<sup>®</sup>. The composite membranes exhibit several advantages over Nafion<sup>®</sup>, including cost reduction - since less polymer is used, especially if a cheaper matrix (e.g. PTFE) is used, and easy manufacture. Furthermore, CREAMFILTER<sup>®</sup> provides high water content, since they are manufactured from metal oxide. According to the literature [263,264,266-268,277,598], these types of composites can work at temperatures above 100°C.

## **4.5 RECAST NAFION<sup>®</sup> / ZrO<sub>2</sub> POWDER COMPOSITE MEMBRANES**

### **4.5.1 Introduction**

Section 2.2.2 shows that Nafion<sup>®</sup> is not suitable for high temperature fuel cells. Furthermore, Nafion<sup>®</sup> has high methanol crossover which degrades the performance of the DMFC. The addition of metal oxide to Nafion<sup>®</sup> can enhance its characteristics,

namely, mechanical stability, methanol permeability and water content at high temperature (Section 2.2.5). Recast Nafion<sup>®</sup> / ZrO<sub>2</sub> composite membrane was investigated.

#### 4.5.2 Membrane Preparation

Nafion<sup>®</sup> solution (5 wt.%, 1100 EW, purchased from Ion Power) and IPA (Sigma Aldrich) were mixed in an ultrasonic bath for 5 minutes, with a volume ratio of 1:2 (Nafion<sup>®</sup> solution to IPA).

Appropriate amounts of ZrO<sub>2</sub> (Degussa) was added to the mixture. ZrO<sub>2</sub> to Nafion<sup>®</sup> dry weight ratios from 5% to 30% were prepared in this study. The mixture was then mixed ultrasonically for 20 minutes.

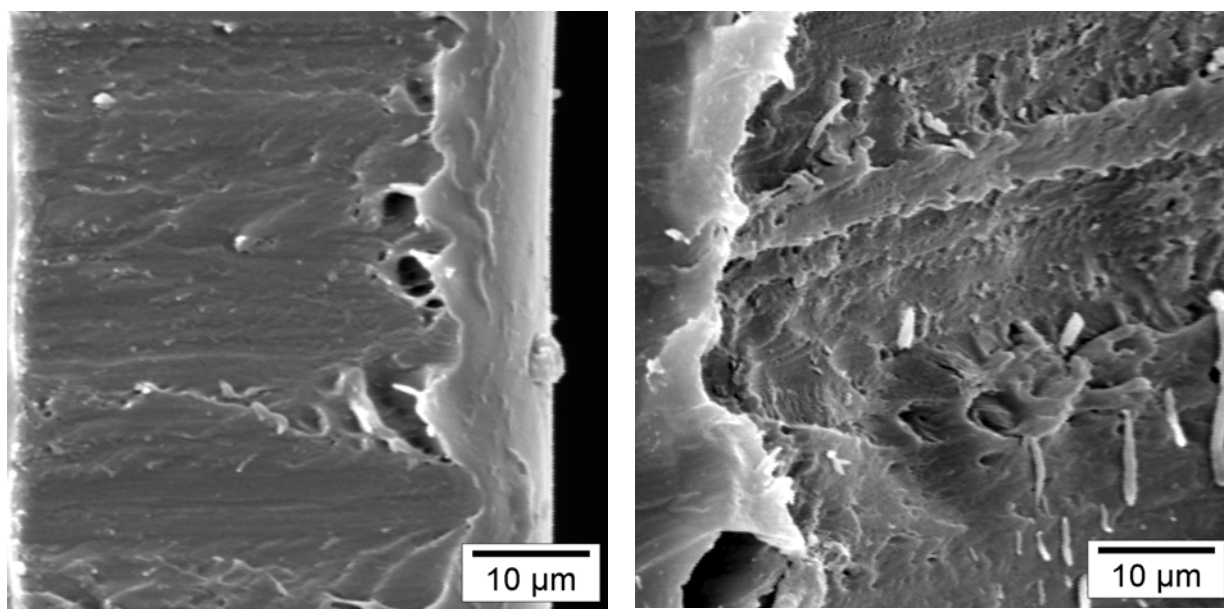
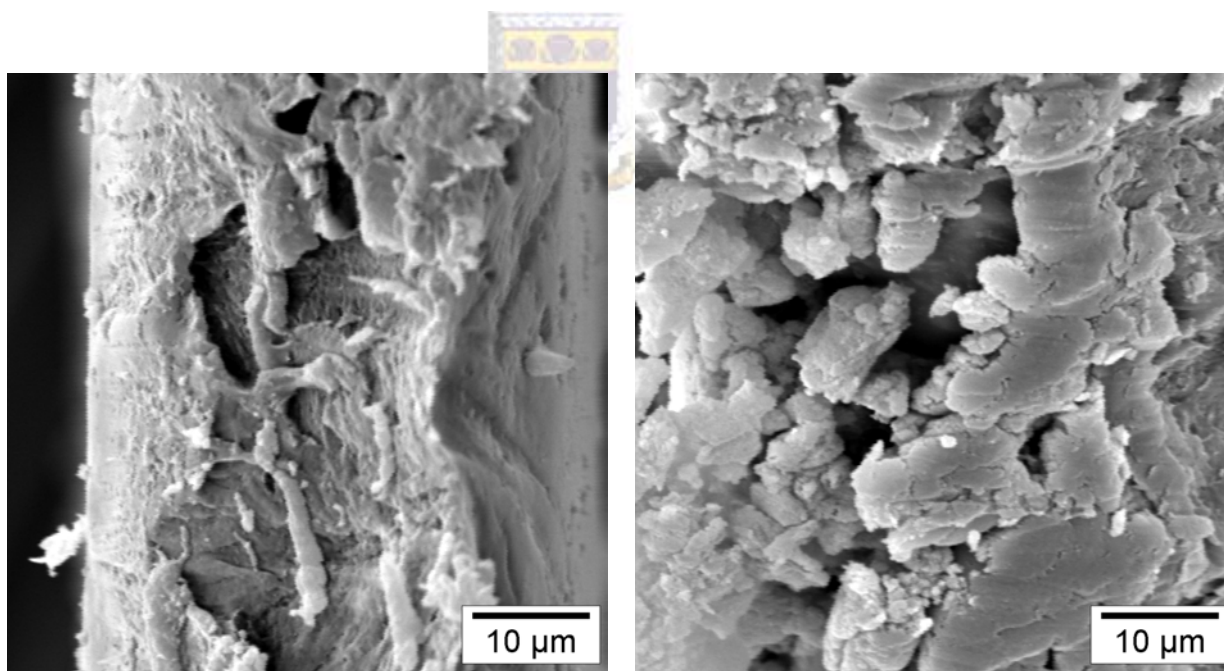
The mixture was recast in a glass Petri dish - the amount of solution will determine the thickness of recast Nafion<sup>®</sup>. The Petri dish was dried at 80°C for 24 hours in an air oven, followed by 160°C for 30 minutes in the same oven. The recast Nafion<sup>®</sup> was pulled off from the Petri dish by adding a small amount of water.

The recast Nafion<sup>®</sup> / ZrO<sub>2</sub> composite membrane was treated according to the standard procedure by boiling in 3 vol.% hydrogen peroxide (H<sub>2</sub>O<sub>2</sub>) for 1 hour to remove the organic impurities, followed by washing with boiling deionised water for 30 minutes. The composite membrane was then boiled in 1M H<sub>2</sub>SO<sub>4</sub> for 1 hour to remove the inorganic impurities and also to complete the protonation, then washed with water for 30 minutes. Washing with water was repeated several times to remove any traces of acidity. Finally the membrane was kept in water prior to measurements.

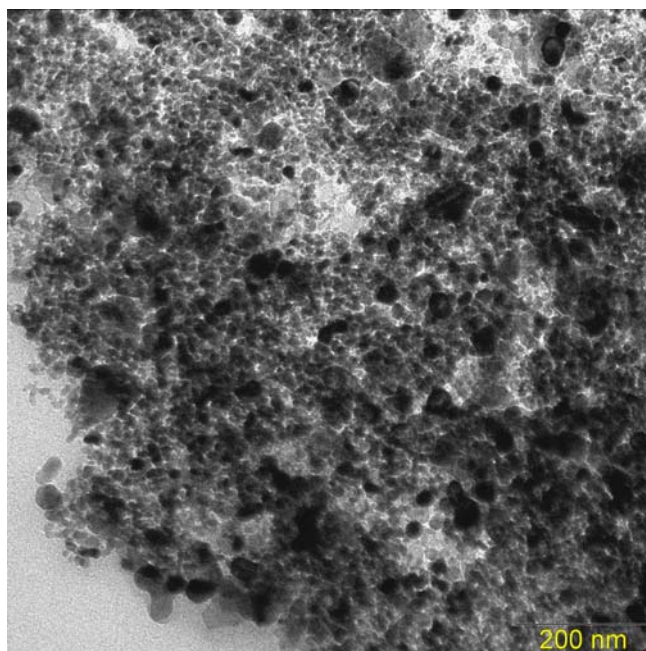
### 4.5.3 Membrane Characterization

Figure 4.41 shows cross-sectional micrographs of recast Nafion<sup>®</sup> and recast Nafion<sup>®</sup> with different amounts of ZrO<sub>2</sub>, namely 5%, 10% and 30%. The bare recast Nafion<sup>®</sup> without any additive shows a homogeneous defect-free structure and looks like Nafion<sup>®</sup> 117 polymer (Figure 4.54). The recast Nafion<sup>®</sup> and recast Nafion<sup>®</sup> with ZrO<sub>2</sub> are flexible and mechanically stable. Recast Nafion<sup>®</sup> is transparent while the recast Nafion<sup>®</sup> / ZrO<sub>2</sub> is white. The whiteness increased with ZrO<sub>2</sub> loading. Recast Nafion<sup>®</sup> / ZrO<sub>2</sub> became more rigid as ZrO<sub>2</sub> loading increases. In all the samples, ZrO<sub>2</sub> is relatively homogeneously distributed throughout recast Nafion<sup>®</sup>. In contrast recast Nafion<sup>®</sup> / ZrO<sub>2</sub> with high loading (30%) shows the presence of ZrO<sub>2</sub> on the surface and accumulates inside the membrane as confirmed by SEM cross-section. According to Nunes *et al.* [289] this phenomenon is undesired in proton conductive membranes, as the conductivity of the composite membrane will decrease dramatically.

Figure 4.42 and Figure 4.43 show the TEM cross-sections of recast Nafion<sup>®</sup> / ZrO<sub>2</sub> (5%) and bare recast Nafion<sup>®</sup>, respectively. In Figure 4.42, it can be seen that ZrO<sub>2</sub> is homogeneously distributed throughout the polymer. The sizes of ZrO<sub>2</sub> particles in the polymer are around 14 nm, which indicates that there is good compatibility between the polymer and the inorganic ZrO<sub>2</sub> fillers. It can also be seen that there is no significant agglomeration of ZrO<sub>2</sub>, since the size of ZrO<sub>2</sub> powder was found to be around 14 nm (Figure 4.8). The shapes of the ZrO<sub>2</sub> particles are approximately spherical, and are similar in shape to the ZrO<sub>2</sub> powder only.

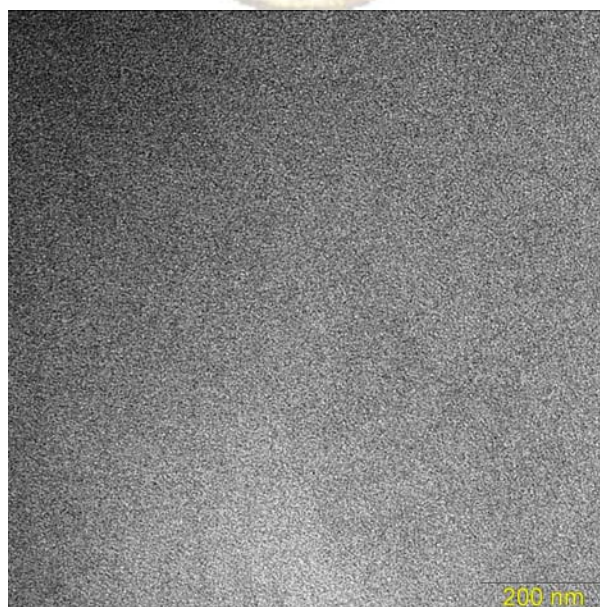
Bare recast Nafion<sup>®</sup>Recast Nafion<sup>®</sup> / ZrO<sub>2</sub> (5%)Recast Nafion<sup>®</sup> / ZrO<sub>2</sub> (10%)Recast Nafion<sup>®</sup> / ZrO<sub>2</sub> (30%)

**Figure 4.41:** SEM micrographs of cross-sections of recast Nafion<sup>®</sup> / ZrO<sub>2</sub> composite membranes.



**Figure 4.42:** TEM micrograph cross-section of recast Nafion<sup>®</sup> / ZrO<sub>2</sub> (5%).

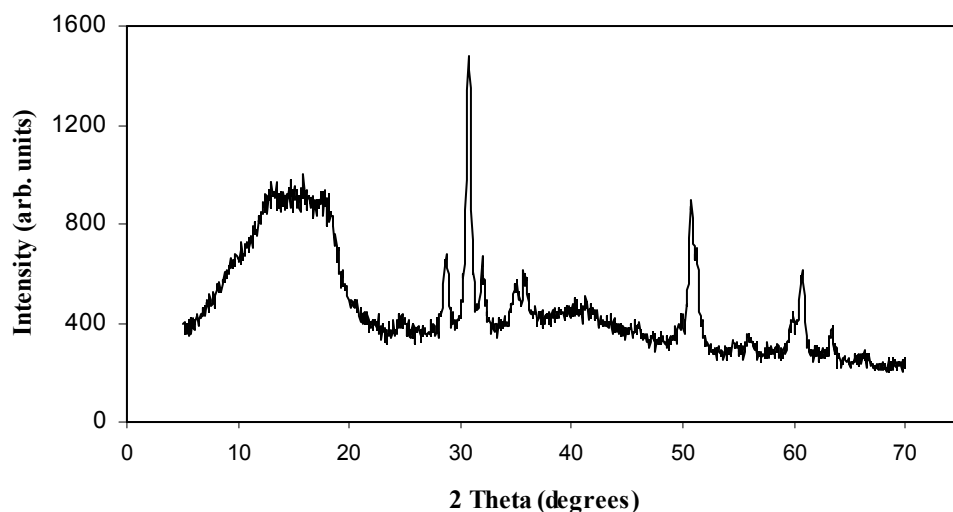
Figure 4.43 shows the TEM micrograph of a cross-section of bare recast Nafion<sup>®</sup>. Only darker and lighter regions can be seen, with no presence of inorganic materials.



**Figure 4.43:** TEM micrograph of cross-section of bare recast Nafion<sup>®</sup>.

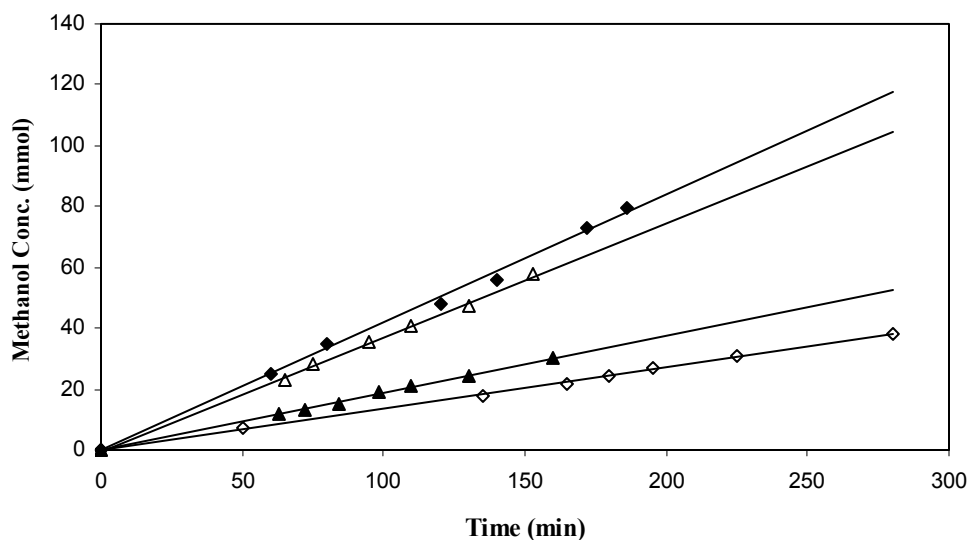


Figure 4.44 shows the X-ray diffraction pattern of recast Nafion<sup>®</sup> / ZrO<sub>2</sub> (12%). The analysis of the peaks shows reflections that are attributed to Nafion<sup>®</sup> (2 $\theta$  at 12-20° and 40°) and several others that are attributed to the presence of ZrO<sub>2</sub>. The peaks of ZrO<sub>2</sub> in the composite membrane are slightly shifted to the right compared to the peaks of ZrO<sub>2</sub> powder (Figure 4.11).



**Figure 4.44:** XRD analysis of recast Nafion<sup>®</sup> / ZrO<sub>2</sub> (12%).

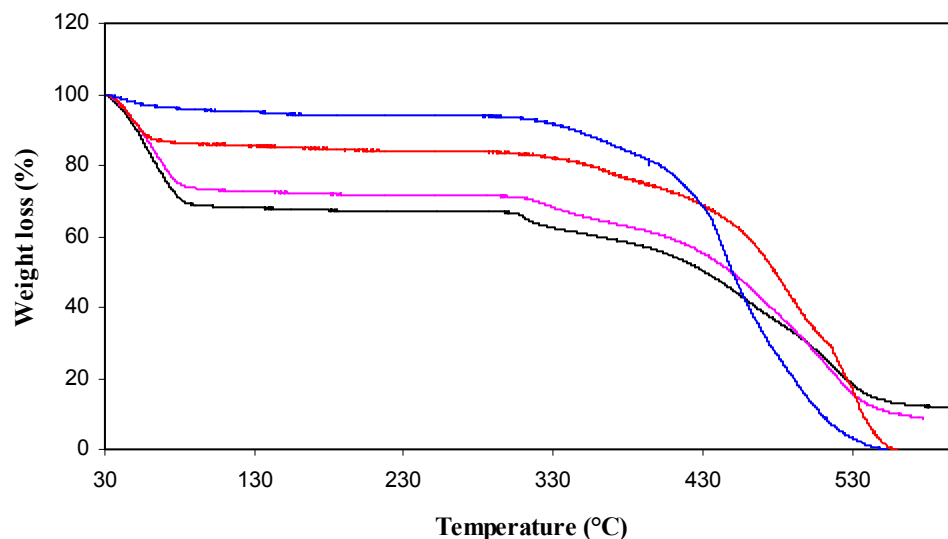
Figure 4.45 shows the measured methanol concentration in the receiving compartment (B) as a function of time for bare recast Nafion<sup>®</sup>, recast Nafion<sup>®</sup> / ZrO<sub>2</sub> (5%) and recast Nafion<sup>®</sup> / ZrO<sub>2</sub> (30%). The bare recast Nafion<sup>®</sup> has the higher methanol permeability than the recast Nafion<sup>®</sup> filled with ZrO<sub>2</sub>. Increasing the number of ZrO<sub>2</sub> particles in the polymer decreases the methanol permeability, as expected. The calculated methanol permeability ( $P$ ) was found to be  $21.5 \times 10^{-7}$ ,  $18.8 \times 10^{-7}$  and  $9.4 \times 10^{-7}$  cm<sup>2</sup>/s for recast Nafion<sup>®</sup>, recast Nafion<sup>®</sup> / ZrO<sub>2</sub> (5%) and recast Nafion<sup>®</sup> / ZrO<sub>2</sub> (30%), respectively.



**Figure 4.45:** Concentration of methanol in compartment B as a function of time:

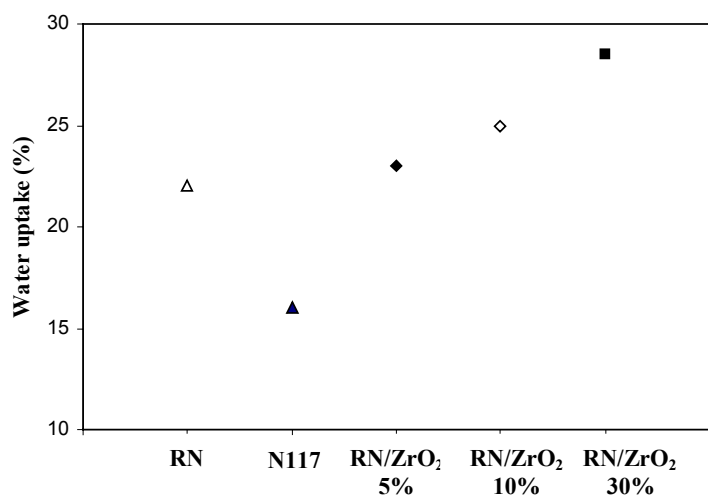
(♦) bare recast Nafion<sup>®</sup> (100µm), (Δ) recast Nafion<sup>®</sup> / ZrO<sub>2</sub> (5%) (100µm),  
 (▲) recast Nafion<sup>®</sup> / ZrO<sub>2</sub> (30%) (100µm) and (◇) Nafion<sup>®</sup> 117 (210µm).

Figure 4.46 shows the TGA analysis of Nafion<sup>®</sup> 117, bare recast Nafion<sup>®</sup>, recast Nafion<sup>®</sup> / ZrO<sub>2</sub> (8%) and recast Nafion<sup>®</sup> / ZrO<sub>2</sub> (12%). Nafion<sup>®</sup> 117 and bare recast Nafion<sup>®</sup> both evaporate completely at a temperature around 550°C, which is in agreement with the temperature reported in the literature. Tiwari *et al.* [619] found a temperature around 550°C for Nafion<sup>®</sup> 117, which is similar to the finding of Samms *et al.* [620] where a value of 600°C was found. Increasing the loading of ZrO<sub>2</sub> increased the water content of the composite membrane, as was expected.



**Figure 4.46:** Thermogravimetric analysis (TGA) of (—) bare recast Nafion<sup>®</sup>, (—) Nafion<sup>®</sup> 117, (—) recast Nafion<sup>®</sup> / ZrO<sub>2</sub> (8%) and (—) recast Nafion<sup>®</sup> / ZrO<sub>2</sub> (12%).

The water uptake was assessed by the method described in Section 3.3.2. As was expected, the water uptake of the composite membrane increases with the increase of ZrO<sub>2</sub> loading.



**Figure 4.47:** Water uptake in Nafion<sup>®</sup> 117, recast Nafion<sup>®</sup> and recast Nafion<sup>®</sup> /ZrO<sub>2</sub>.

#### 4.5.4 Discussion and Conclusions

An appropriate method to recast Nafion<sup>®</sup> was developed, where the annealing treatment at 160°C is needed to produce Nafion<sup>®</sup> film with the same characteristics as the received polymer (Nafion<sup>®</sup> 117). The recast Nafion<sup>®</sup> is transparent and has the same homogeneity as the received polymer (Nafion<sup>®</sup> 117). Adding ZrO<sub>2</sub> to Nafion<sup>®</sup> also produces a mechanically stable film. The colour of the recast Nafion<sup>®</sup> with ZrO<sub>2</sub> additive is white. No leaching of ZrO<sub>2</sub> from the film was observed. The nanometric ZrO<sub>2</sub> shows a homogeneous distribution throughout the composite membrane - however, increasing ZrO<sub>2</sub> loading leads to an accumulation of the particles. Furthermore, high loading of ZrO<sub>2</sub> resulted in the presence of particles at the surface, which is undesirable. It was proven in the literature that incorporating metal oxide in a proton conductive polymer can allow these types of composite to operate at temperatures above 100°C [263,264,266-268,277,598].

Furthermore, incorporating Nafion<sup>®</sup> with ZrO<sub>2</sub> reduces methanol permeability. Increasing ZrO<sub>2</sub> loading, leads to a further methanol permeability reduction. However, increasing ZrO<sub>2</sub> loading decreases the conductivity; on the other hand, increasing the ZrO<sub>2</sub> loading increases the water content. A balance between conductivity, methanol permeability and water content needs to be taken into consideration when preparing this type of composite. A value of 3 wt.% of metal oxide was used in the literature as an optimal value to keep a high conductivity above 100°C. Methanol permeability in the composite membrane is lower than the bare recast Nafion<sup>®</sup>.

## 4.6 RECAST NAFION<sup>®</sup> / ZrP POWDER COMPOSITE MEMBRANES

### 4.6.1 Introduction

Inorganic materials can be added to proton conductive polymers to enhance their properties. The mechanical properties of the composite are controlled by the amount of inorganic component and the degree of dispersion in the polymer. The dispersion and the particle size of the inorganic components are interdependent. Sub-micron particle sizes are preferred.

The inorganic material of choice is ZrP, since it has high water content above 100°C. Furthermore, the conductivity will not be decreased as metal oxide would cause, since ZrP itself is a proton conductor. In this study, nanometric sized ZrP was added to recast Nafion<sup>®</sup>, and the characteristics of the composite membrane were investigated.



### 4.6.2 Membrane Preparation

ZrP was prepared by mixing ZrO<sub>2</sub> (Degussa) and H<sub>3</sub>PO<sub>4</sub> and then dried at 60°C for 24 hours in an air oven.

Nafion<sup>®</sup> solution (5 wt.%, 1100 EW, purchased from Ion Power) was mixed with IPA in an ultrasonic bath for 5 minutes. IPA was added to the Nafion<sup>®</sup> solution in the ratio 2:1.

Appropriate amounts of ZrP were added to the solution and mixed ultrasonically for 20 minutes.

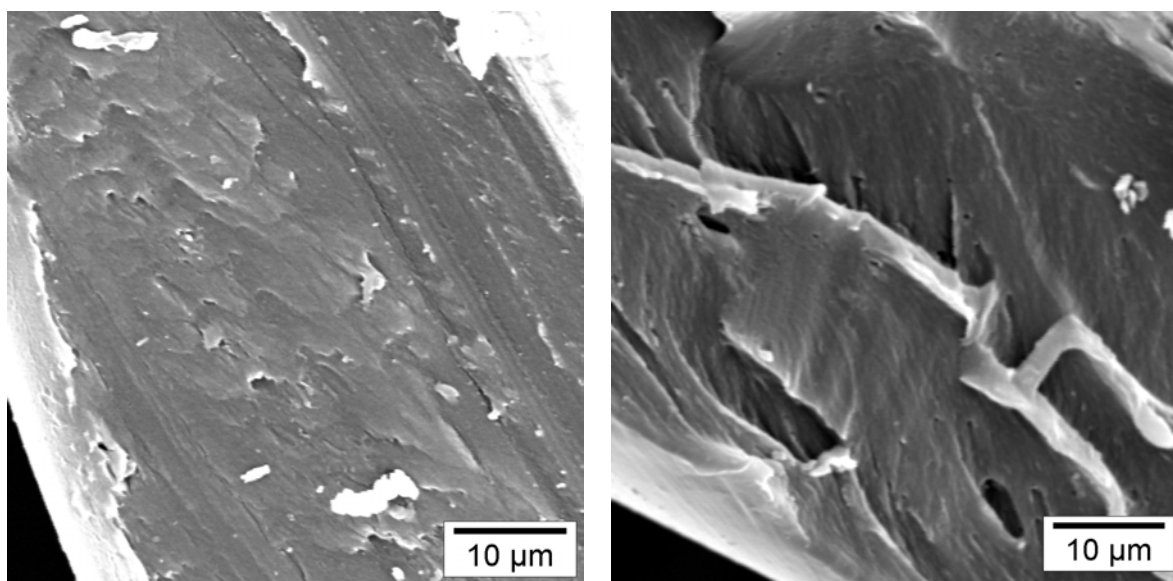
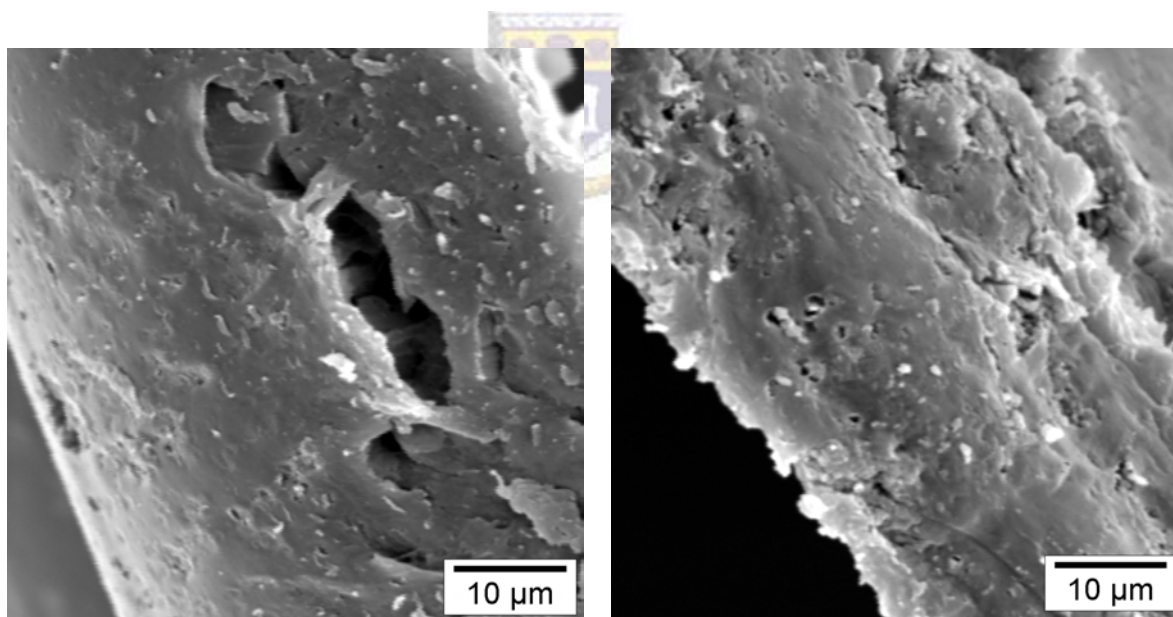
The mixture was poured into a glass Petri dish - the amount determining the thickness of the recast Nafion<sup>®</sup> - dried at 80°C for 24 hours and then at 160°C for 30 minutes in an air oven. The recast Nafion<sup>®</sup> was pulled off from the Petri dish by adding a small amount of water.

The recast Nafion<sup>®</sup> / ZrP composite membrane was treated with the standard procedure by boiling in 3 vol.% hydrogen peroxide (H<sub>2</sub>O<sub>2</sub>) for 1 hour to remove the organic impurities, followed by washing with water for 30 minutes. The composite membrane was then boiled in 1M H<sub>2</sub>SO<sub>4</sub> for 1 hour to remove the inorganic impurities and also to complete the protonation, then washed with water for 30 minutes. Washing with water was repeated several times to remove traces of acidity. Finally, the membrane was kept in water prior to measurements.



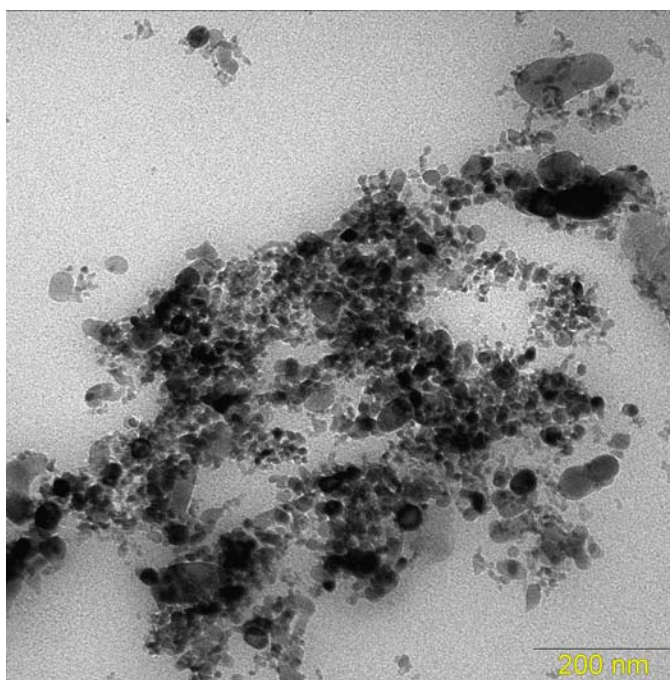
### 4.6.3 Membrane Characterization

Figure 4.48 shows SEM micrographs of a cross-section of the composite membrane. It can be seen that ZrP is homogeneously distributed throughout the polymer. The recast Nafion<sup>®</sup> without additives shows a homogeneous structure with no defects. The structure of recast Nafion<sup>®</sup> looks the same as the 'as received' polymer (Nafion<sup>®</sup> 117), as can be seen in Figure 4.54.

Bare recast Nafion<sup>®</sup>Recast Nafion<sup>®</sup> / ZrP (2.6%)Recast Nafion<sup>®</sup> / ZrP (6.4%)Recast Nafion<sup>®</sup> / ZrP (16%)

**Figure 4.48:** SEM micrographs of cross-sections of recast Nafion<sup>®</sup> / ZrP composite membranes.

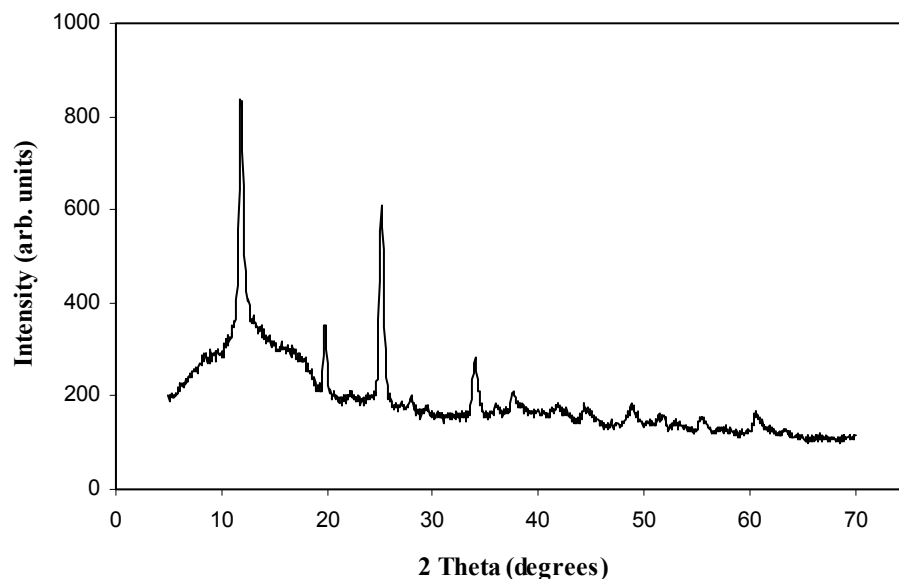
Figure 4.49 shows a TEM micrograph of recast Nafion<sup>®</sup> / ZrP. A particle size analysis shows that the sizes are in the range of 25-40 nm, with the presence of others at 12-14 nm. The latter are probably due to the unreacted ZrO<sub>2</sub>. The TEM micrographs revealed a good distribution of the inorganic materials, but less homogeneous than observed for recast Nafion<sup>®</sup> / ZrO<sub>2</sub> (Figure 4.42).



**Figure 4.49:** TEM of a cross-section of recast Nafion<sup>®</sup> / ZrP.

Figure 4.50 shows the X-ray diffraction pattern of recast Nafion<sup>®</sup> / ZrP. The analysis of the peaks of the composite membrane shows reflections that are attributed to Nafion<sup>®</sup> ( $2\theta$  at 12-20°), which is overlapped by a ZrP peak at  $2\theta=11.7^\circ$ , and others that are attributed to the presence of ZrP ( $2\theta = 20^\circ, 25^\circ$  and  $34.1^\circ$ ).

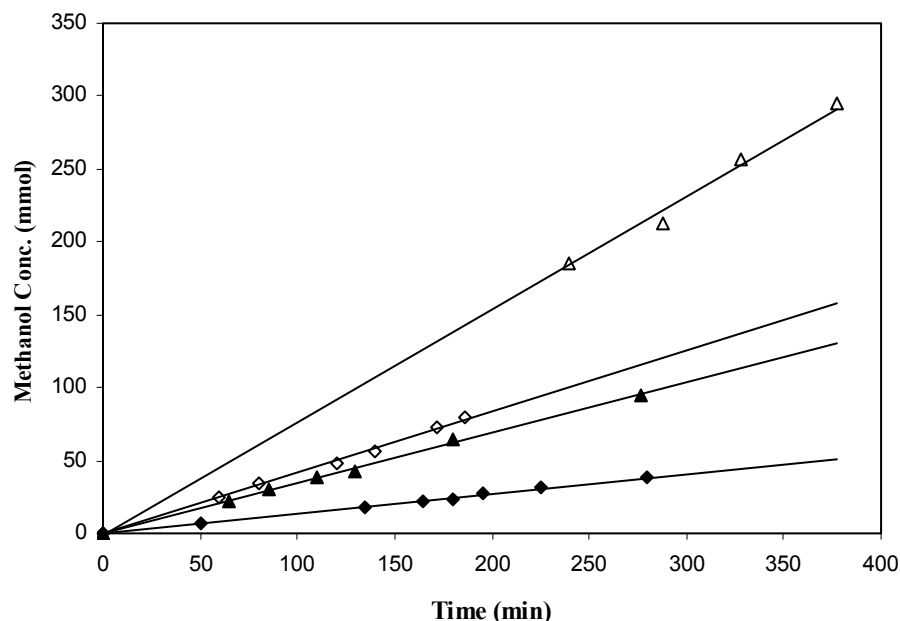




**Figure 4.50:** XRD of recast Nafion<sup>®</sup> / ZrP.



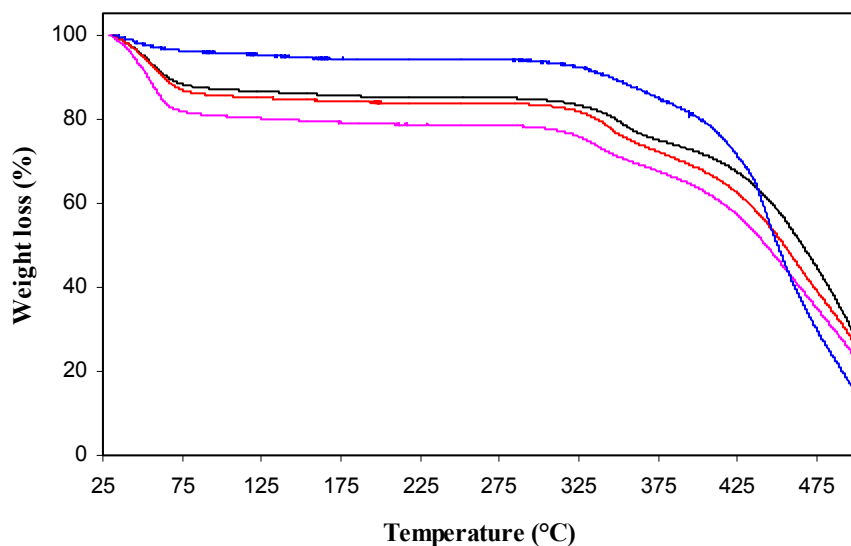
Figure 4.51 shows the measured methanol concentration in the receiving compartment (B) as a function of time for bare recast Nafion<sup>®</sup>, recast Nafion<sup>®</sup> / ZrP (6.4%) and recast Nafion<sup>®</sup> / ZrP (16%) with Nafion<sup>®</sup> 117 as reference. Recast Nafion<sup>®</sup> / ZrP (6.4%) has a higher methanol permeability (at  $44 \times 10^{-7} \text{ cm}^2/\text{s}$ ) than the bare recast Nafion<sup>®</sup>. Increasing the ZrP particle content in the polymer, decreases the methanol permeability, to a value of  $17.5 \times 10^{-7} \text{ cm}^2/\text{s}$  for recast Nafion<sup>®</sup> / ZrP (16%). The higher methanol permeability in recast Nafion<sup>®</sup> / ZrP (6.4%) compared to recast Nafion<sup>®</sup> / ZrO<sub>2</sub> (5%) is due to the difference in particle sizes - ZrP particles are bigger than ZrO<sub>2</sub> particles, as was found by TEM analysis.



**Figure 4.51:** Concentration of methanol in compartment B as a function of time: (◇) bare recast Nafion<sup>®</sup> (100μm), (Δ) recast Nafion<sup>®</sup> / ZrP (6.4%) (100μm), (▲) recast Nafion<sup>®</sup> / ZrP (16%) (100μm), and (◆) Nafion<sup>®</sup> 117 (210μm).

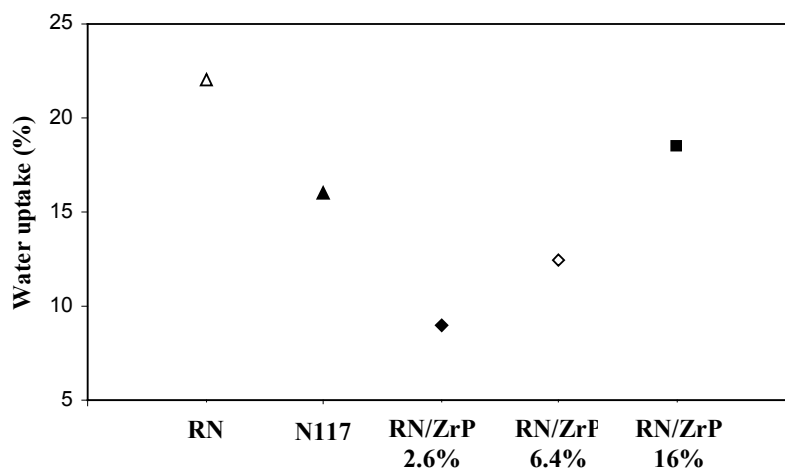
Methanol permeability in recast Nafion<sup>®</sup> is higher compared to the as received polymer (Nafion<sup>®</sup> 117). This is expected, since methanol permeability is inversely proportional to the membrane thickness – the thickness of Nafion<sup>®</sup> 117 is 210 μm, while the thickness of the recast Nafion<sup>®</sup> is around 100 μm.

Figure 4.52 shows TGA analysis of bare recast Nafion<sup>®</sup>, recast Nafion<sup>®</sup> / ZrP (2.6%), recast Nafion<sup>®</sup> / ZrP (6.4%) and recast Nafion<sup>®</sup> / ZrP (16%). As can be seen, an increasing ZrP loading leads to a higher water content, as expected.



**Figure 4.52:** TGA analysis of: (—) bare recast Nafion<sup>®</sup>, (—) recast Nafion<sup>®</sup> / ZrP powder (2.6%), (—) recast Nafion<sup>®</sup> / ZrP powder (6.4%) and (—) recast Nafion<sup>®</sup> / ZrP powder (16%).

The water uptake was assessed by the method described in Section 3.3.2. The results are reported in Figure 4.53.



**Figure 4.53:** Water uptake in Nafion<sup>®</sup> 117, recast Nafion<sup>®</sup> and recast Nafion<sup>®</sup> / ZrP.

The water uptake of the recast Nafion<sup>®</sup> is higher than the as received Nafion<sup>®</sup> 117. Similar results were reported by Dimitrova *et al.* [268,269]. However, the water uptake in recast Nafion<sup>®</sup> / ZrP is still low compared to recast Nafion<sup>®</sup>, due to the size of the prepared ZrP.

#### 4.6.4 Discussion and Conclusions

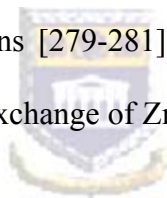
Recast Nafion<sup>®</sup> incorporated with ZrP composite membrane was prepared, where the ZrP particles are homogeneously distributed throughout the polymer. Furthermore, no leaching of ZrP was observed. Incorporating ZrP in Nafion<sup>®</sup> has several advantages: ZrP increases the mechanical stability of recast Nafion<sup>®</sup>, and increasing the ZrP loading increases the water content, thereby, allowing the composite membrane to work at high temperatures. It was reported by Bonnet *et al.* [262] that the conductivity of the composite membranes (polymer / ZrP) exceeded that of the polymer only, and increased with the amount of ZrP. The composite Nafion<sup>®</sup> / ZrP is different to the composite Nafion<sup>®</sup> / ZrO<sub>2</sub> in two ways: firstly, methanol permeability in recast Nafion<sup>®</sup> / ZrP (6.4%) was higher than the recast Nafion<sup>®</sup> / ZrO<sub>2</sub> (5%). These results show the importance of small sizes in composite organic / inorganic membranes, where ZrO<sub>2</sub> particles were found to be smaller than ZrP particles, and secondly the conductivity increases with ZrP loading, whereas the conductivity decreases with ZrO<sub>2</sub> loading. Therefore, it can be expected that ZrP has more advantages than metal oxide for composite Nafion<sup>®</sup> / inorganic composite membranes for DMFC applications.

## 4.7 NAFION<sup>®</sup> 117 / ZrP (VIA ION EXCHANGE OF Zr<sup>+4</sup>) COMPOSITE

### MEMBRANES

#### 4.7.1 Introduction

ZrP was found to be the best inorganic additive to proton conductor polymers. It was largely used by researchers to enhance the properties of the membranes. In Section 4.6, Nafion<sup>®</sup> / ZrP powder composite membranes were investigated. This section deals with the same approach of incorporating ZrP in recast Nafion<sup>®</sup> polymer, but the ZrP prepared in this section is different to Section 4.6 in that an ion exchange of Zr<sup>+4</sup> was used in membrane preparation. These membranes were first reported by Tiwari *et al.* [619] and followed by Grot and Rajendran [278] and Princeton University did several investigations [279-281]. In this section, composite Nafion<sup>®</sup> 117 impregnated with ZrP via ion exchange of Zr<sup>+4</sup>, was prepared and investigated.



#### 4.7.2 Membrane Preparation

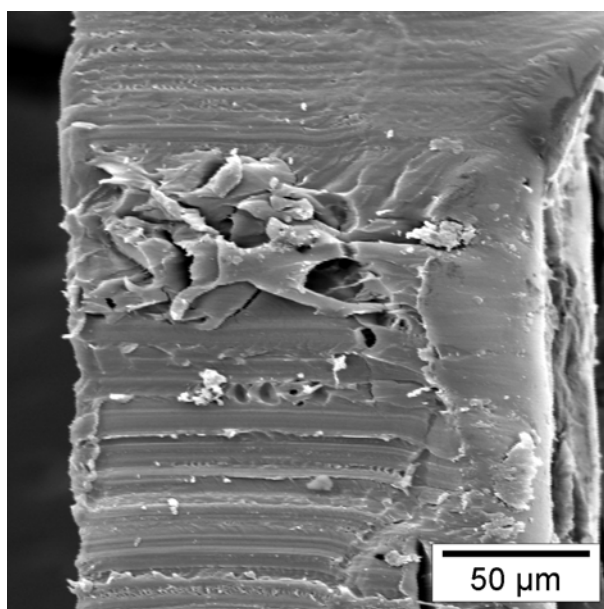
Nafion<sup>®</sup> 117 was treated with the standard procedure prior to impregnation. This included the immersion of Nafion<sup>®</sup> 117 in boiling 3 vol.% hydrogen peroxide (H<sub>2</sub>O<sub>2</sub>) for 1 hour to remove the organic impurities, followed by washing with water for 30 minutes. The membrane was then boiled in 1M H<sub>2</sub>SO<sub>4</sub> for 1 hour to remove the inorganic impurities and also to complete the protonation, then washed with water for 30 minutes. Washing with water was repeated several times to remove traces of acidity.

Nafion<sup>®</sup> 117 was subject to swelling by treatment in a 1:1 volume mixture of methanol and water at 80°C. Methanol was the solvent of choice, since maximum swelling of Nafion could be achieved [118]. ZrP was introduced by placing the swollen membrane in 1M ZrOCl<sub>2</sub> for several hours at 80°C to introduce the zirconium into the membrane. This allowed the exchange of H<sup>+</sup> ions with Zr<sup>+4</sup> ions. The membranes were then rinsed in cold water to remove excess solution and placed in 1M H<sub>3</sub>PO<sub>4</sub> overnight at 80°C. The treatment with H<sub>3</sub>PO<sub>4</sub> caused the precipitation of ZrP *in situ* in the nanopores of the Nafion<sup>®</sup> 117 membrane. The formation of ZrP was indicated when the film turned white. The amount of ZrP incorporated in the Nafion<sup>®</sup> was further increased by repeating the impregnation procedure. The membrane was then repeatedly rinsed in water to remove excess acid, and finally kept in water prior to characterization.

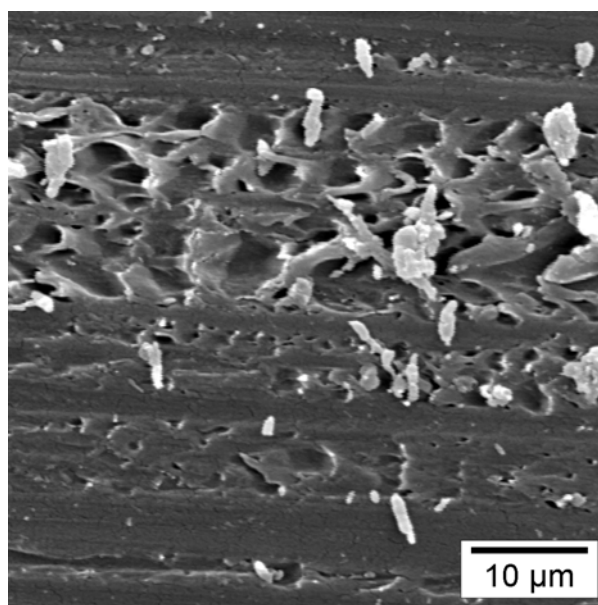
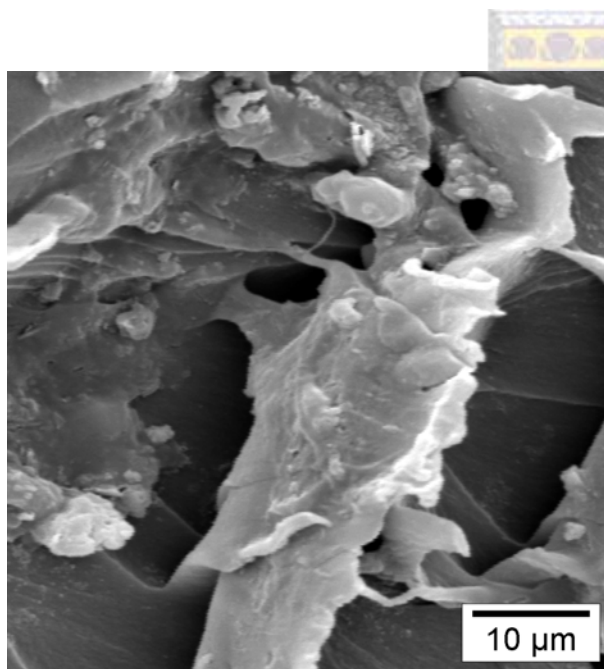
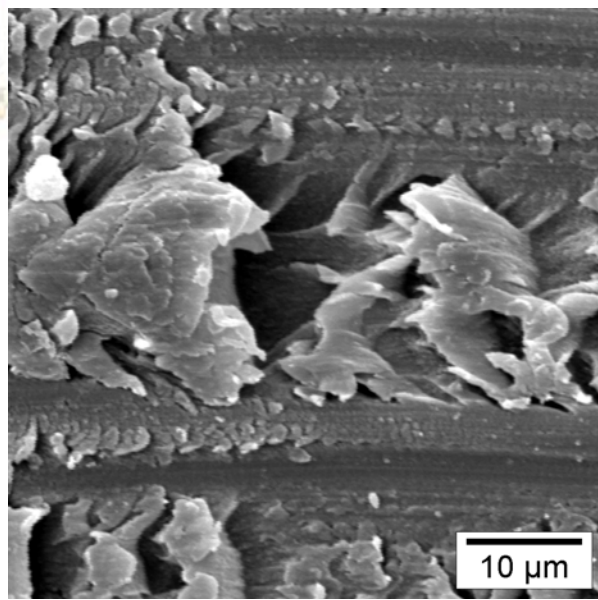


### 4.7.3 Membrane Characterization

Figure 4.54 shows SEM micrographs of cross-sections of bare Nafion<sup>®</sup> 117, Nafion<sup>®</sup> 117 / ZrP via Zr<sup>+4</sup> (9%), Nafion<sup>®</sup> 117 / ZrP via Zr<sup>+4</sup> (14%) and Nafion<sup>®</sup> 117 / ZrP via Zr<sup>+4</sup> (24%). Nafion<sup>®</sup> 117 shows a homogeneous structure, which is similar to bare recast Nafion<sup>®</sup> (see Figures 4.41 and 4.48). It can be seen that ZrP particles are homogeneously distributed throughout the Nafion<sup>®</sup> polymer.



Bare Nafion® 117

Nafion® 117 / ZrP via  $Zr^{+4}$  (9%)Nafion® 117 / ZrP via  $Zr^{+4}$  (14%)Nafion® 117 / ZrP via  $Zr^{+4}$  (24%)

**Figure 4.54:** SEM micrographs of cross-sections of Nafion® 117 / ZrP via ion exchange of  $Zr^{+4}$  composite membranes.

Figure 4.55 shows a TEM micrograph of a cross-section of Nafion<sup>®</sup> 117 / ZrP via ion exchange of Zr<sup>+4</sup>. Homogeneously distributed ZrP throughout the polymer can be clearly seen. The particle sizes calculated are around 11 nm. This is in agreement with the value reported by Princeton University [280,281], where a value of 11 nm was reported. This value was calculated from the XRD analysis. Figure 4.55 also shows that the shape of the inorganic particles is of rectangular form, whereas ZrP prepared previously was of the spherical form (see Figures 4.16, 4.17 and 4.49). It can be concluded that there is a difference between the two, and this can be attributed to the procedure used in the preparations.

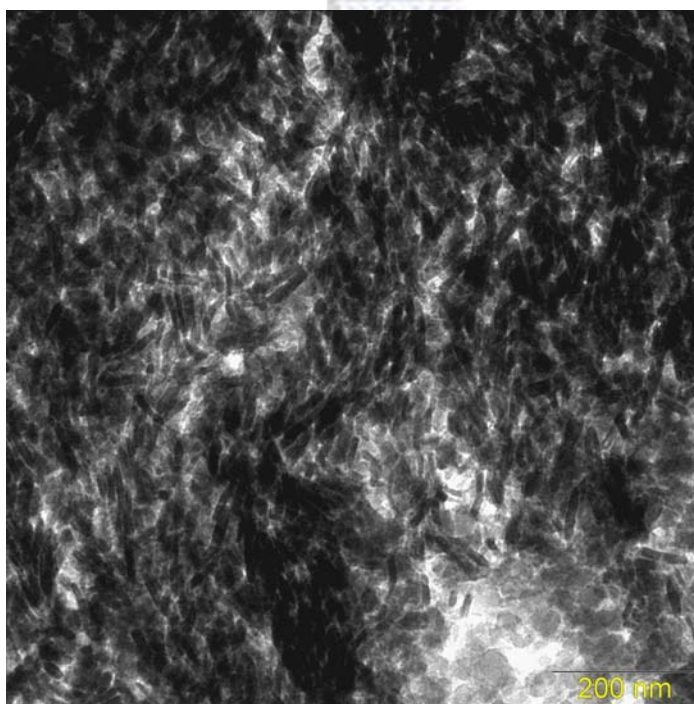


**Figure 4.55:** TEM of cross-section of Nafion<sup>®</sup> 117 / ZrP via ion exchange of Zr<sup>+4</sup> (24%).



Figure 4.56 shows the X-ray diffraction pattern of Nafion<sup>®</sup> 117/ ZrP via ion exchange of Zr<sup>+4</sup> (24%). The analysis of the peaks shows reflections that are attributed to Nafion<sup>®</sup> ( $2\theta$  at 12-20°) and others that are attributed to the presence of ZrP ( $2\theta = 20^\circ, 25^\circ$  and  $34.1^\circ$ ).

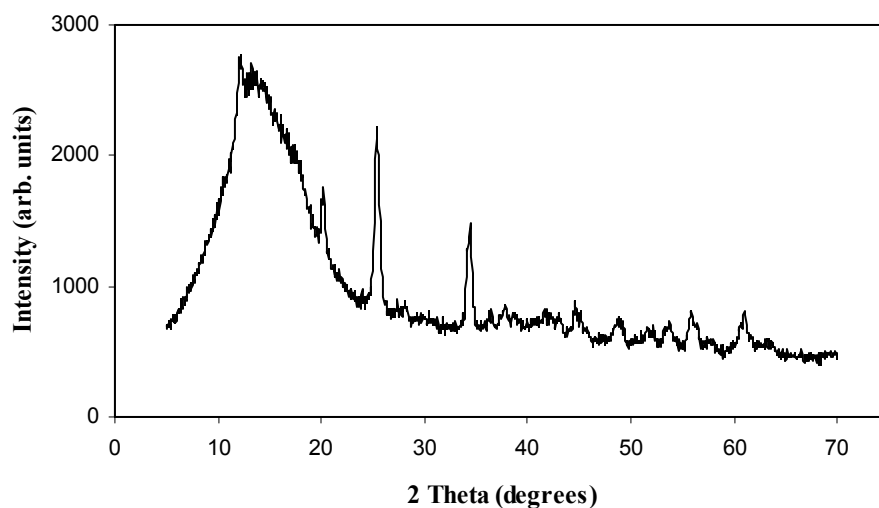


**Figure 4.56:** XRD analysis of Nafion<sup>®</sup> 117 / ZrP via Zr<sup>+4</sup> (24%).

Figure 4.57 shows a FTIR scan of Nafion<sup>®</sup> film. The bands at 982, 1057 and 1148  $\text{cm}^{-1}$  are assigned to  $-\text{COC}-$ ,  $-\text{SO}_3\text{H}-$  and  $-\text{CF}_2-$  groups, respectively [619]. The other peaks at 1636 and 3476  $\text{cm}^{-1}$  are assigned to water.

Figure 4.58 shows an FTIR scan of Nafion<sup>®</sup> film / ZrP via ion exchange of Zr<sup>+4</sup> (24%). A new peak appears at 1411  $\text{cm}^{-1}$ - apparently due to the presence of ZrP while The peak at around 1000  $\text{cm}^{-1}$  for ZrP is overlapped with the peak of Nafion<sup>®</sup>. The peak assigned to  $-\text{SO}_3\text{H}-$  at 1057  $\text{cm}^{-1}$  has disappeared. This can be explained by the type of process used to form ZrP - i.e. where an ion exchange of Zr<sup>+4</sup> with H<sup>+</sup> is used.

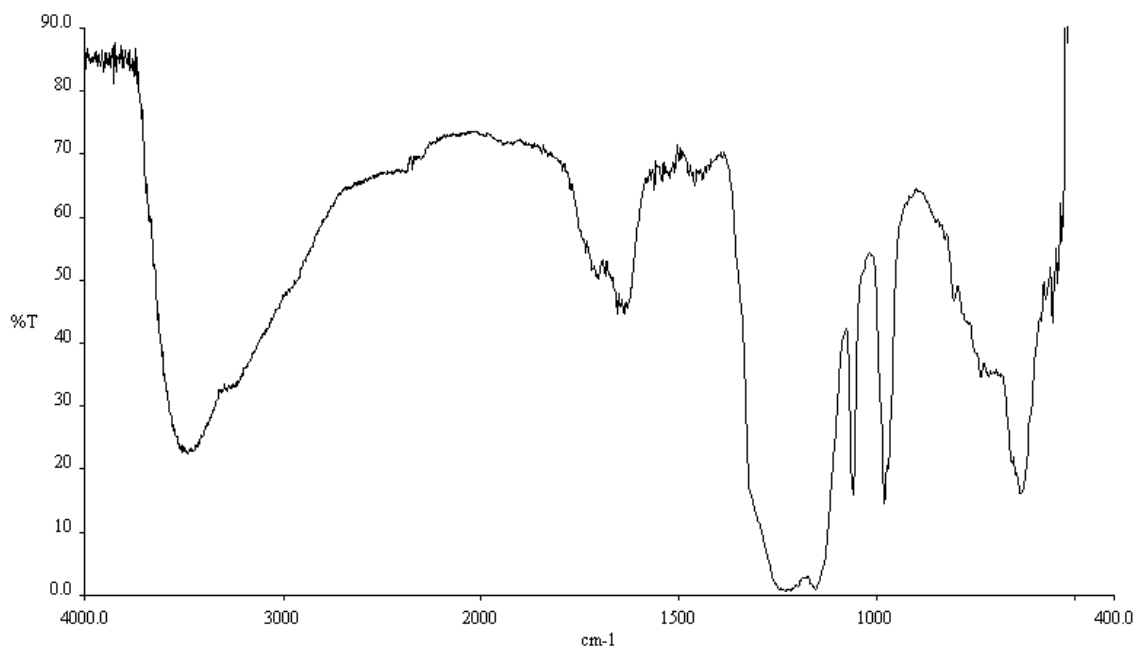


Figure 4.57: FTIR scan of bare Nafion<sup>®</sup> film.

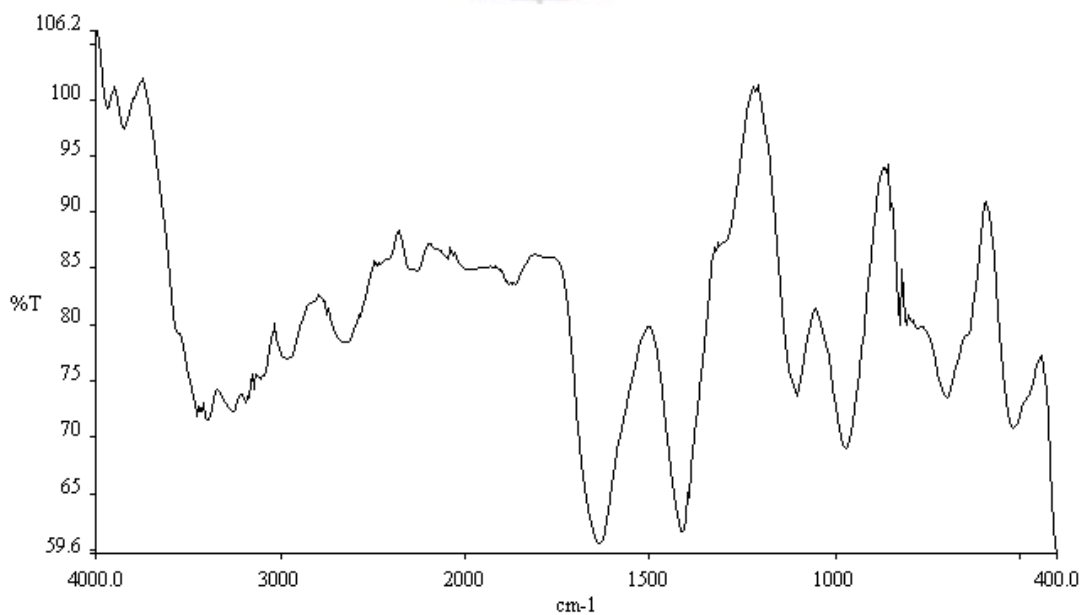
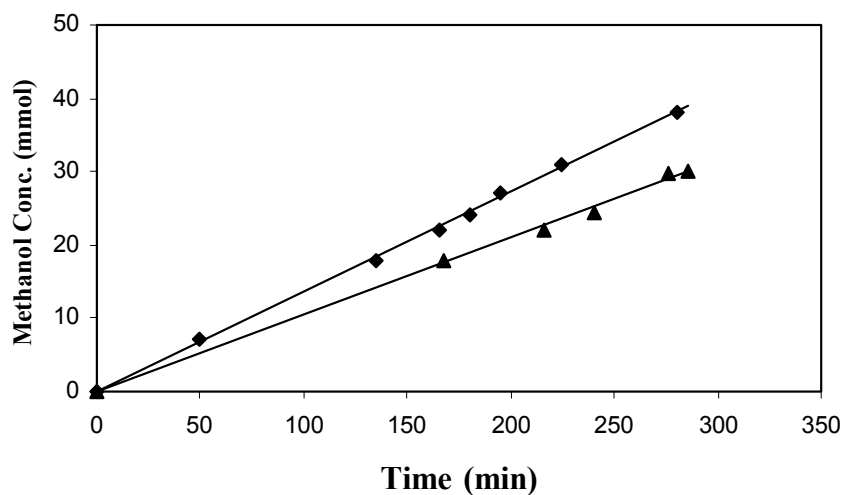


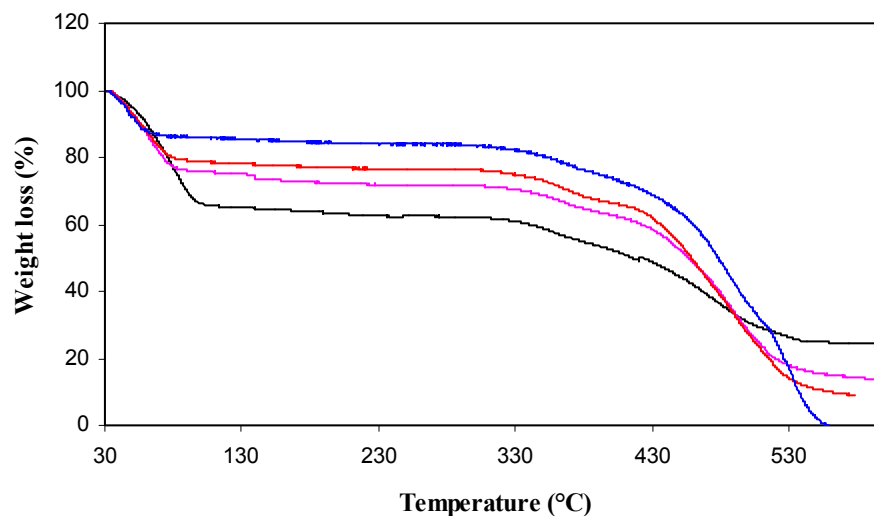
Figure 4.58: FTIR scan of Nafion<sup>®</sup> film / ZrP via ion exchange of Zr<sup>+4</sup> (24%).

Figure 4.59 shows the measured methanol concentration in the receiving compartment (B) as a function of time in Nafion<sup>®</sup> 117 and Nafion<sup>®</sup> 117 / ZrP via ion exchange of Zr<sup>+4</sup> after the third impregnation (24%). Incorporating ZrP into Nafion<sup>®</sup> polymer, reduced the methanol permeability, leading to another advantage.



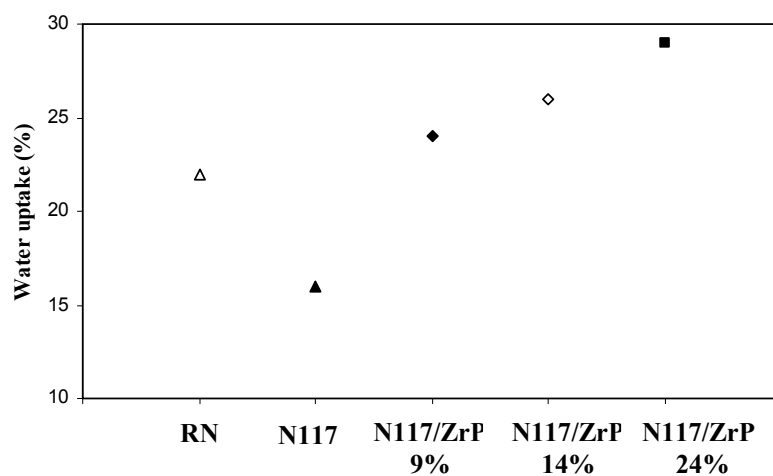
**Figure 4.59:** Methanol concentration in the receiving compartment (B) as a function of time in (◆) bare Nafion<sup>®</sup> 117 and (▲) Nafion<sup>®</sup> 117 / ZrP via ion exchange of Zr<sup>+4</sup> (24%).

Figure 4.60 shows the TGA analysis of bare Nafion<sup>®</sup> 117, Nafion<sup>®</sup> 117 / ZrP via Zr<sup>+4</sup> (9%), Nafion<sup>®</sup> 117 / ZrP via Zr<sup>+4</sup> (14%) and Nafion<sup>®</sup> 117 / ZrP via Zr<sup>+4</sup> (24%). As can be seen, increasing the loading of ZrP increased the water content of the composite membrane, as expected.



**Figure 4.60:** TGA of (—) bare Nafion® 117, (—) Nafion® 117/ ZrP via Zr<sup>+4</sup> (9%), (—) Nafion® 117/ ZrP via Zr<sup>+4</sup> (14%) and (—) Nafion® 117/ ZrP via Zr<sup>+4</sup> (24%).

The water uptake was assessed by the method described in Section 3.3.2. As was expected, the water uptake of the composite membrane increases with the increase of ZrP loading.



**Figure 4.61:** Water uptake in recast Nafion®, Nafion® 117 and Nafion® 117 / ZrP.

#### 4.7.4 Discussion and Conclusions

Nafion<sup>®</sup> modification can be done by incorporating ZrP via an ion exchange process ( $H^+$  for  $Zr^{+4}$ ). The presence of ZrP can be identified by the change of Nafion<sup>®</sup> colour from transparent to white. Increasing the loading of ZrP, by repeating the impregnation process, leads to an increase in whiteness of the film. ZrP was found to be homogeneously distributed throughout the composite membrane with particle size of 11 nm, which is slightly larger than the pore size in Nafion<sup>®</sup> under complete hydration [280,281]. Furthermore, it was found that the shapes of ZrP particles prepared by the ion exchange process are of rectangular form. These differ from the ZrP powder prepared in Section 4.6, where spherical shapes were observed. Incorporating ZrP in Nafion<sup>®</sup>, via the ion exchange of  $Zr^{+4}$ , leads to the reduction of methanol permeability. According to the literature [279-281] incorporating ZrP via the ion exchange procedure will allow these composite membranes to work at high temperature.

### 4.8 COMPOSITE INORGANIC CREAMFILTER<sup>®</sup> MATRIX / ZrP / NAFION<sup>®</sup> SOLUTION MEMBRANES

#### 4.8.1 Composite Inorganic CREAMFILTER<sup>®</sup> Matrix / ZrP / Nafion<sup>®</sup> Solution

##### Membranes

Composite membranes were prepared by impregnating inorganic CREAMFILTER<sup>®</sup> matrix with ZrP, as discussed in Section 4.3.2. It was found that these types of membranes have characteristics similar to that of Nafion<sup>®</sup>. Selectivity factors

( $\beta$ ) of 4.9 and 4.5 were found for CREAMFILTER<sup>®</sup> Z240G / ZrP and Nafion<sup>®</sup> 117, respectively. However, some ZrP leaching out of the membrane was observed. To avoid leaching, the membrane was coated with a film of Nafion<sup>®</sup> by soaking the prepared composite membrane CREAMFILTER<sup>®</sup> Z240G / ZrP in a solution of 18% Nafion<sup>®</sup> in ethanol for 4 hours at room temperature. Then the composite membrane was dried at 80°C for 24 hours. Nafion<sup>®</sup> film was formed in the pores and on the surface of the composite membrane.

To avoid the drying of ZrP, the composite membrane was not heated to 160°C, as with the previous membrane prepared in Section 4.4.2, and also no further treatment (as per the standard method to treat Nafion<sup>®</sup>) was performed. The prepared membrane was kept in water prior to characterization.



Figure 4.62 shows the measured methanol concentration in the receiving compartment (B) as a function of the exposed time in Nafion<sup>®</sup> 117, CREAMFILTER<sup>®</sup> Z240G / ZrP and CREAMFILTER<sup>®</sup> Z240G / ZrP / coated with Nafion<sup>®</sup> film. It can be seen that the Nafion<sup>®</sup> coating decreased further the methanol permeability from  $3.5 \times 10^{-7}$  to  $3 \times 10^{-7}$  cm<sup>2</sup>/s.

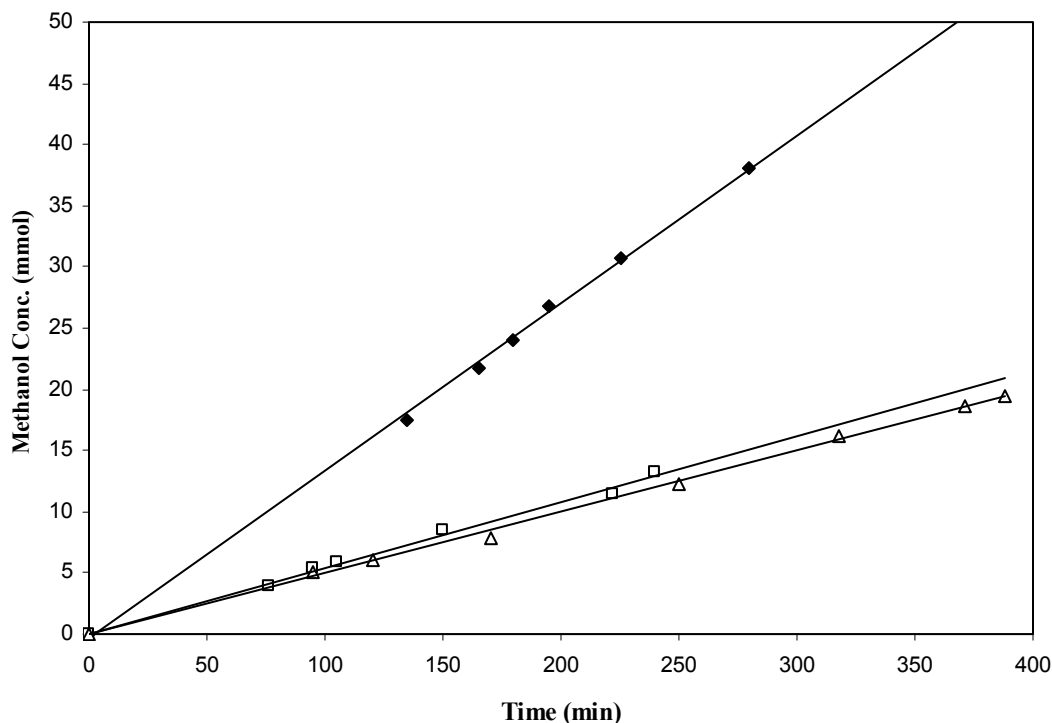


**Figure 4.62:** Concentration of methanol in compartment B as a function of time: Nafion® 117 (♦), composite Z240G/ZrP (□) and composite Z240G/ZrP / Nafion® solution (Δ).

The composite membrane prepared shows reduction in methanol permeability. However, a reduction in the conductivity by up to half was also observed. The selectivity factor ( $\beta$ ) for different membranes is presented in Table 4.7. The selectivity factor for CREAMFILTER® Z240G / ZrP ( $\beta = 4.9$ ) is higher than that for Nafion® 117 ( $\beta = 4.5$ ). Further coating of the composite membrane with Nafion® film, reduced  $\beta$  to 4.7, due to the decrease in conductivity. However,  $\beta$  is still higher than that for Nafion® 117.

Coating the composite membrane leads to no advantages *vis a vis* the selectivity factor. However, the Nafion<sup>®</sup> film will act as a barrier for ZrP leaching. Furthermore, the Nafion<sup>®</sup> film on the surface will play an important role in MEA preparation, where a good contact between the membrane and the electrode is needed.

**Table 4.7:** Composite CREAMFILTER<sup>®</sup> Z240G / ZrP / Nafion<sup>®</sup> membrane specifications

Membranes	Thickness dry ( $\mu\text{m}$ )	Conductivity ( $\sigma$ ) (S/cm)	Methanol permeability ( $P$ ) ( $\text{cm}^2/\text{s}$ )	Selectivity factor ( $\beta = \log(\sigma/P)$ )
Z240G/ZrP	120	$3 \times 10^{-2}$	$3.5 \times 10^{-7}$	4.9
Z240G/ZrP/ Nafion <sup>®</sup>	123	$1.5 \times 10^{-3}$	$3 \times 10^{-7}$	4.7
Nafion <sup>®</sup> 117	175	$5 \times 10^{-2}$	$14 \times 10^{-7}$	4.5

#### 4.8.2 Composite Inorganic CREAMFILTER<sup>®</sup> Matrix / Nafion<sup>®</sup> solution / ZrP

##### Membranes

Composite inorganic CREAMFILTER<sup>®</sup> matrix / Nafion<sup>®</sup> solution was prepared as in Section 4.4.2. Selectivity factors ( $\beta$ ) of 4.6 and 4.5 were found for CREAMFILTER<sup>®</sup> Z240G / Nafion<sup>®</sup> and Nafion<sup>®</sup> 117, respectively. The prepared membranes show similar characteristics to Nafion<sup>®</sup> 117. On the other hand, it was found that ZrP can be incorporated in Nafion<sup>®</sup> via an ion exchange process ( $\text{H}^+$  for  $\text{Zr}^{+4}$ ), as was discussed in Section 4.7. Furthermore, it was found that ZrP is the best inorganic additive to polymeric proton conductors. In this section, an attempt will be made to make a composite membrane by combining the preparation procedures of Sections 4.4 and 4.7. The composite CREAMFILTER<sup>®</sup> Z240G / Nafion<sup>®</sup> was prepared as in Section 4.4.2. The dried composite membrane was swelled in a 1:1 by volume,



methanol/water solution at 80°C. ZrP was introduced by placing the swollen composite membrane in 1M ZrOCl<sub>2</sub> for several hours at 80°C to introduce zirconium into the membrane. This allowed exchange of H<sup>+</sup> ions with Zr<sup>+4</sup> ions. The membranes were then rinsed in cold deionized water to remove excess solution and finally placed in 1M H<sub>3</sub>PO<sub>4</sub> overnight at 80°C. The treatment with H<sub>3</sub>PO<sub>4</sub> allowed the precipitation of ZrP *in situ*. Since the preparation of the composite membrane (CREAFILTER<sup>®</sup> Z240G / Nafion<sup>®</sup>) is similar to recast Nafion<sup>®</sup>, and the previous experiment (Section 4.7) was performed with Nafion<sup>®</sup> 117, recast Nafion<sup>®</sup> impregnated with ZrP via ion exchange of Zr<sup>+4</sup>, was investigated. Recast Nafion<sup>®</sup> was therefore prepared as per Section 4.5.2 followed by the procedure described in Section 4.7.

Figure 4.63 shows the X-ray diffraction pattern of recast Nafion<sup>®</sup> film impregnated with ZrP via ion exchange of Zr<sup>+4</sup>.

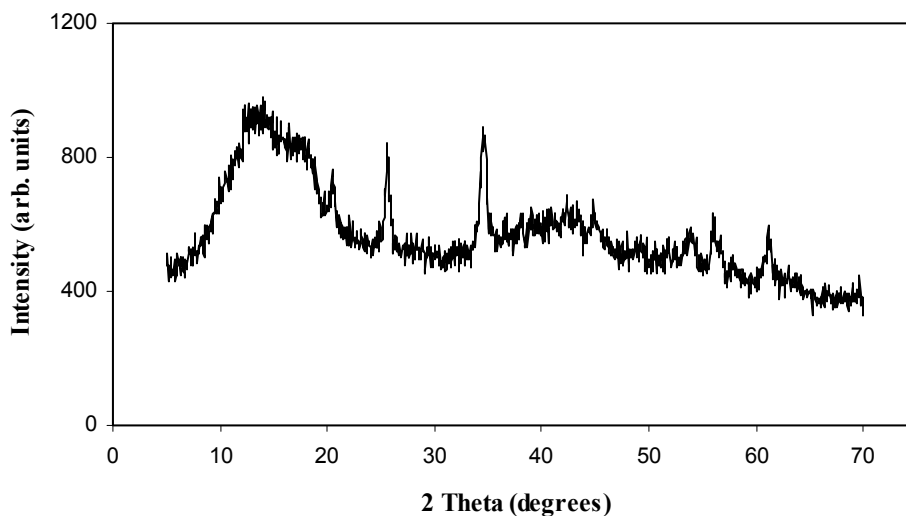


**Figure 4.63:** X-ray diffraction pattern of recast Nafion<sup>®</sup> impregnated with ZrP via ion exchange of Zr<sup>+4</sup>.

The analysis of the peaks of the composite membrane shows reflections that are attributed to Nafion<sup>®</sup> ( $2\theta$  at 12-20°) and others that are attributed to the presence of ZrP ( $2\theta = 20.6^\circ, 25.7^\circ$  and  $34.2^\circ$ ), which are similar to the X-ray diffraction pattern of the 'as received' Nafion<sup>®</sup> 117 / ZrP via  $Zr^{+4}$  (see Figure 4.56).

Note that the XRD pattern of recast Nafion<sup>®</sup> after treatment with the standard procedure is similar to that of Nafion<sup>®</sup> 117.

Figure 4.64 shows the X-ray diffraction pattern of CREAMFILTER<sup>®</sup> Z240G / Nafion<sup>®</sup>, followed by impregnation with ZrP via  $Zr^{+4}$ .

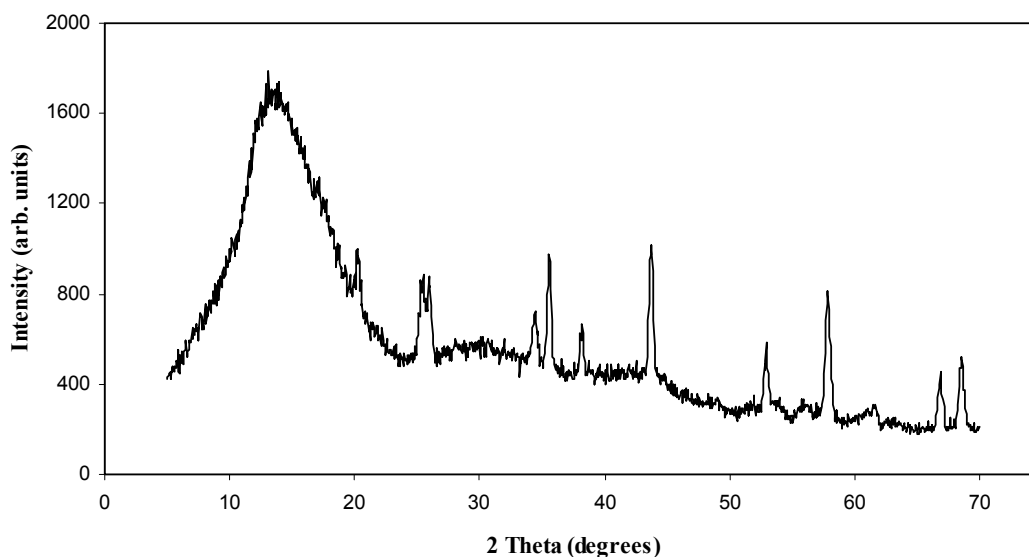


**Figure 4.64:** X-ray diffraction pattern of recast CREAMFILTER<sup>®</sup> Z240G / Nafion<sup>®</sup> / ZrP via ion exchange of  $Zr^{+4}$ .

Figure 4.64 revealed the presence of the peaks of the bare CREAMFILTER<sup>®</sup> Z240G (Figure 4.3) and the peaks of Nafion<sup>®</sup> ( $2\theta$  at 12-20°) and others that are

attributed to the presence of ZrP ( $2\theta = 20.3^\circ$ ,  $25.5^\circ$  and  $34.6^\circ$ ). Figure 4.64 shows the success of the membrane preparation protocol. These types of membranes have several advantages over the ‘as received’ polymer (e.g. Nafion<sup>®</sup> 117) and similar composite membranes (e.g. Gore Select<sup>®</sup> membrane), where PTFE support is used. These advantages include: low cost, ease of manufacture and according to the literature can operate at high temperature due to the presence of ZrP.



## CHAPTER 5

### DMFC PARAMETER OPTIMIZATION

#### 5.1 INTRODUCTION

A fuel cell is constituted of five components: anode backing layer, anode catalyst layer, proton exchange membrane, cathode catalyst layer and cathode backing layer. The heart of the fuel cell is the MEA. In this Chapter, the backing and catalyst layers and the influence of operating conditions on cell performance (temperature, pressure, gas flow rate, etc.) are investigated. Nafion<sup>®</sup> 117 was used as the proton conductive membrane. The objective of this section is to find out the optimal conditions for DMFC operation, rather than looking for a high performance cell.

#### 5.2 INK COMPOSITION

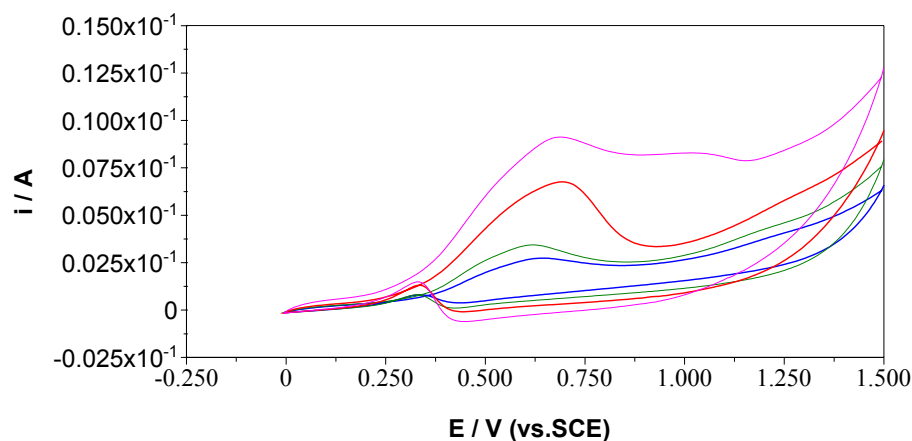
An ink was prepared to make the catalyst layer as follows: 0.21 g of the catalyst was wetted with water under magnetic stirring, followed by the addition of 0.67 g of Nafion<sup>®</sup> solution (5 wt.%, 1100 EW, Aldrich) drop by drop. Finally the solvents were added. The ink was stirred for 24 hours. Then the ink was sprayed onto the backing layer (carbon cloth or carbon paper) to the desired catalyst loading using an air brush. The solvents investigated in this study are IPA and BAc, and referred to hereafter as the solution and colloidal methods, respectively. 20%Pt-10%Ru on Carbon (Alfa Aesar) was used as the anode catalyst, whereas 40% Pt on carbon (Alfa

Aesar) was used for the cathode. The sprayed backing layer was kept at room temperature for 24 hours, and then dried at 110°C for 1 hour prior to MEA preparation.

The MEA was prepared by the hot pressing procedure as follows: Nafion<sup>®</sup> solution (5 wt.%, 1100 EW, Aldrich) was brushed on one side of the electrode, dried for 10 minutes at room temperature and 1 hour at 80°C in an air oven. The electrodes (backing layer and the catalyst layer) were placed on both sides of a treated Nafion<sup>®</sup> 117 membrane, then the MEA was sandwiched between non-stick Teflon<sup>®</sup> and placed on a hot press for 2 min at 130°C and 100 bar.

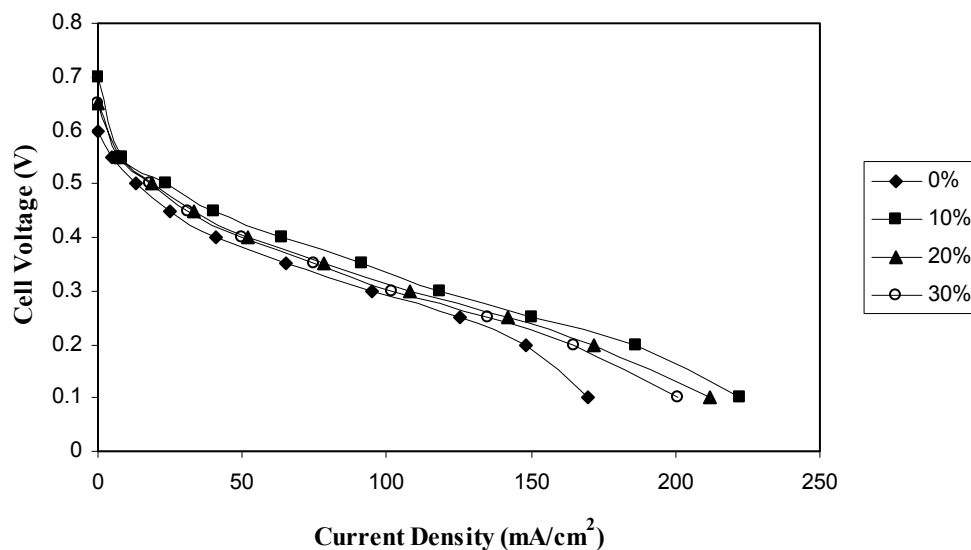
Figure 5.1 shows the influence of Nafion<sup>®</sup> content on methanol oxidation. Different Nafion<sup>®</sup> percentages (dry weight) were used in the ink preparation from 7% to 40%. The prepared ink was spread on a glassy carbon electrode and dried before use. The catalytic activity (methanol oxidation) was evaluated with cyclic voltammetry (CV) using a conventional three-electrode system - a Pt basket as counter electrode and a saturated calomel electrode (SCE) as reference electrode. The prepared electrodes were dipped in 1M H<sub>2</sub>SO<sub>4</sub> / 1M methanol and scanned in the region of 0-1.5 V at a rate of 20 mV s<sup>-1</sup>.

Figure 5.1 shows that the optimal Nafion<sup>®</sup> content in the ink is around 14% (dry weight), corresponding to a ratio of 3:1 (Nafion<sup>®</sup> to catalyst).



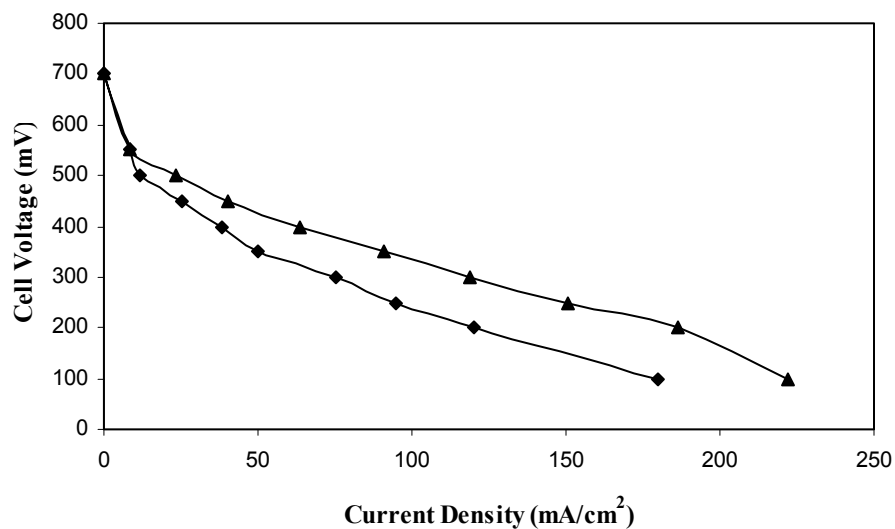
**Figure 5.1:** Cyclic voltammograms of methanol oxidation for catalytic inks with different Nafion<sup>®</sup> content: (—) 7%, (—) 14%, (—) 25% and (—) 40%.

Figure 5.2 shows the influence of Nafion<sup>®</sup> content on cell performance. As can be seen a 3:1 catalyst to Nafion<sup>®</sup> ratio represents the optimal concentration, which is roughly 14%. The presence of Nafion<sup>®</sup> in the catalyst layer enhanced the conductivity, thus extending the three-phase zone (i.e. increasing catalyst utilization). Furthermore, it was suggested by Chu *et al.* [567] that Nafion<sup>®</sup> content in the catalyst site affects the kinetics of methanol electro-oxidation by providing the protonic sites, which could promote CO oxidation. Figure 5.2 was obtained by using carbon cloth E-TEK type “A” with 20 % PTFE content, a methanol flow rate 1 ml/min, an air flow rate 1 l/min, a catalyst loading of 2 mg/cm<sup>2</sup> for both anode and cathode, a cell temperature 80°C, and atmospheric pressure for anode and cathode.



**Figure 5.2:** Cell performance with different Nafion<sup>®</sup> content in the catalyst layer, using E-TEK carbon cloth type “A” and the solution method.

When BAc was used as a solvent, the ink was thick and an ultrasonic bath was used instead of magnetic stirring. The ink formed was spread on the backing layer by using a Pasteur pipette. Figure 5.3 shows cell performance with different solvents, namely IPA and BAc. The solution method using IPA as the solvent produced the higher performance to the colloidal method using BAc. In the colloidal method the ink formed was thick, and the catalyst layer with this type of ink is thicker than the catalyst layer produced with IPA with similar catalyst loading. Therefore, the mass transfer resistance of methanol is increased in the catalyst layer, thus decreasing cell performance. Figure 5.3 was obtained by using carbon cloth E-TEK type “A” with 20 % PTFE content, a methanol flow rate 1 ml/min, an air flow rate 1 l/min, a catalyst loading of 2 mg/cm<sup>2</sup> for both anode and cathode, a cell temperature 80°C, and atmospheric pressure for anode and cathode.



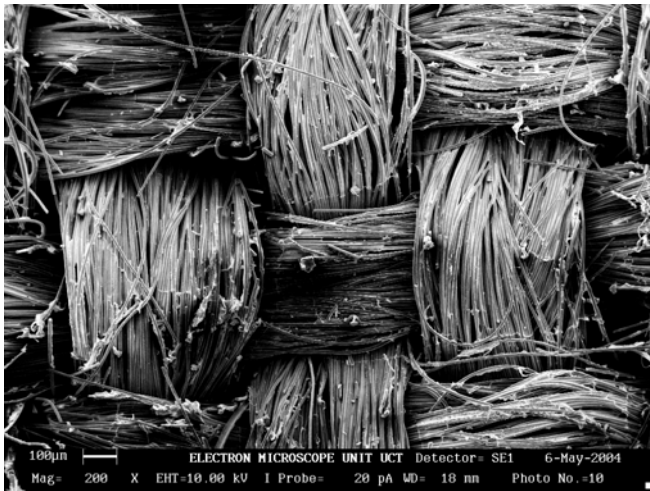
**Figure 5.3:** I-V curve at 80°C for different solvents: (▲) iso-propanol (solution method) and (◆) butyl acetate (colloidal).



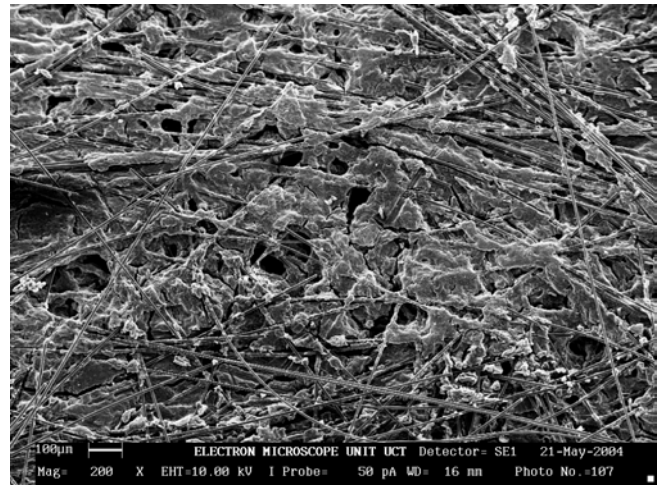
### 5.3 BACKING LAYERS

Different backing layers were investigated for the DMFC mode. All of them are commercially available materials, including E-TEK carbon cloth type “A”, Toray TGP H 120 carbon paper, Electrochem carbon paper and Lydall GDL (gas diffusion layer). The structures of these backing layers are shown in Figure 5.4, where the differences in the surface morphology are readily apparent. The cloth weaves of E-TEK produces a series of relatively large openings, approximately 50 to 100  $\mu\text{m}$  in size. Carbon paper (Toray TGP H 120 and Electrochem) have a structure with a pore size between 20-50  $\mu\text{m}$ , but a large portion of blocked passages. Lydall GDL (Lyflex C494) has very little opening area with most of the surface consisting of blocked passages.

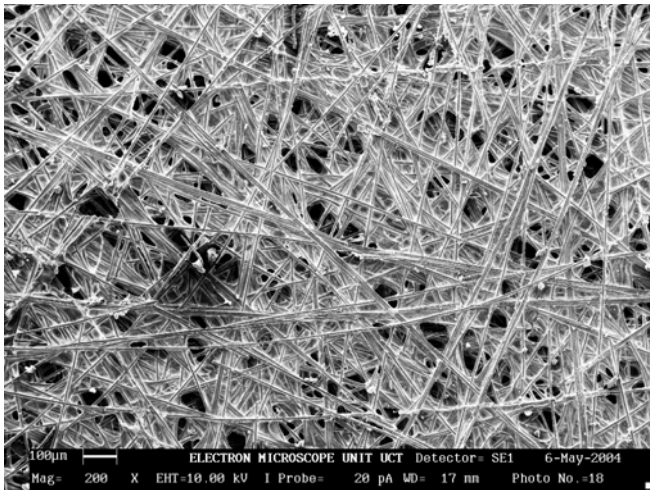




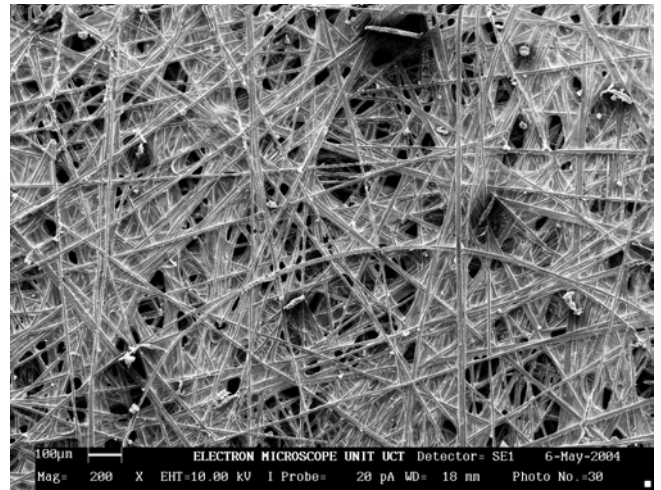
ETEK, type "A", 20 %PTFE



Lydall Lyflex C494 GDL, 10%PTFE



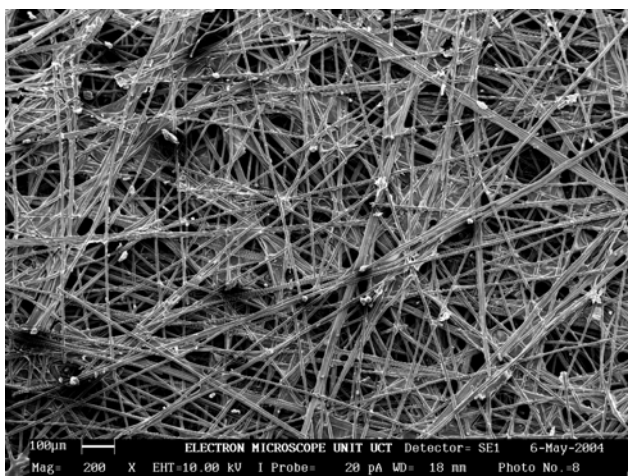
Toray TGP H 120, 20% PTFE



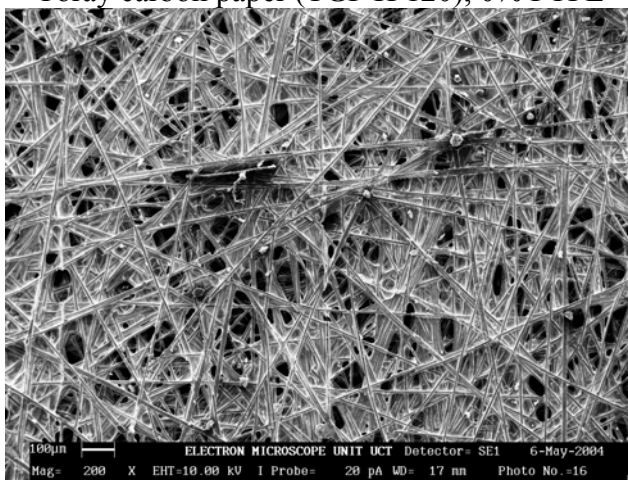
Electrochem. Carbon paper, 35% PTFE

**Figure 5.4:** Surface morphology of different backing layers.

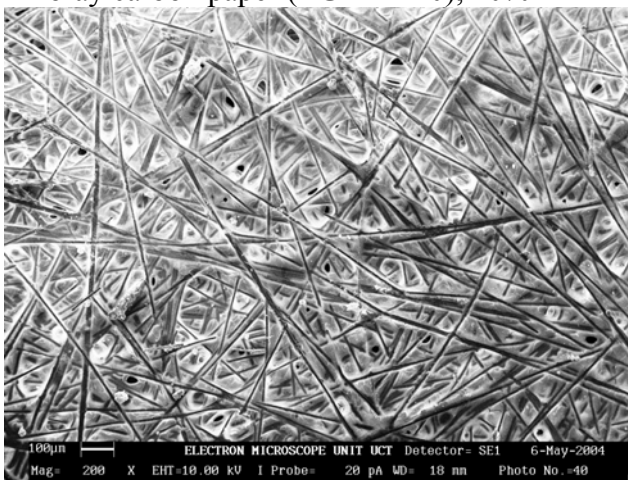
The PTFE mat area has small openings compared to the bare Toray paper, as can be seen in Figure 5.5. The open channels presumably act as liquid flow channels, while the PTFE mat acts predominantly as gas flow channels. Increasing the PTFE content, reduces the number of open channels, which negatively influences liquid flow.



Toray carbon paper (TGP H 120), 0% PTFE



Toray carbon paper (TGP H 120), 20% PTFE



Toray carbon paper (TGP H 120), 60% PTFE

**Figure 5.5:** Influence of PTFE content on Toray paper (TGP H 120) backing layers structures.

Figure 5.6 shows cell performance at 80°C with Toray paper TGP H 120, with different PTFE content. As can be seen, the optimal PTFE content is around 20%, where liquid and gas ( $\text{CO}_2$ ) flow are in separated channels. With a bare TGP H 120 paper (0% PTFE) there are no channels for  $\text{CO}_2$  evolution, whereas with high PTFE loading (60%), the liquid channels are blocked. Furthermore, at high PTFE loading there is conductivity loss within the electrode, therefore, the cell performance is affected by significant electrical losses.

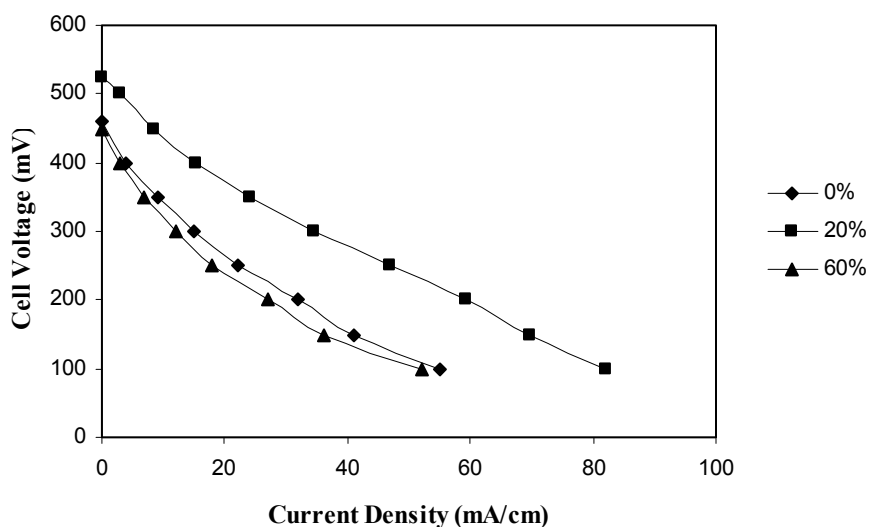


**Figure 5.6:** Influence of PTFE content on cell performance, Toray paper TGP H 120 with different loading (♦) 0%, (■) 20% and (▲) 60% PTFE content.

Figure 5.7 shows cell performance with two backing layers, namely E-TEK carbon cloth type “A”, 20% PTFE and Toray TGP H 120, 20% PTFE. The cell performances with carbon cloth are much better than with carbon paper, which is attributed to the nature of the backing layers. In the visualization studies [45], it was found that in the case of carbon paper, large  $\text{CO}_2$  slugs (groups of bubbles) are formed

with a size of 0.8-1.8 mm, and these bubbles tend to attach themselves to the surface of the paper. The CO<sub>2</sub> bubbles formed remain attached at the point of generation and accumulate. After a few minutes these bubbles completely block the channels which leads to a deterioration of cell performance. In contrast, in the case of carbon cloth, the CO<sub>2</sub> bubbles are relatively small (0.6-0.8 mm) and which have a tendency to coalesce and form bubble swarms. Since the carbon cloth has lower friction characteristics, bubbles tend to attach to the flow channels. This feature of carbon cloth is beneficial, since the surface is relatively clear and free from bubbles, thus a superior performance can be obtained due to the enhanced gas management in the cell.

This experiment shows that carbon cloth is the most suitable backing layer for DMFC application. Furthermore, the results obtained with carbon paper show that this material is not suited for DMFC under the conditions used in this study, where a dual electrode was prepared (backing layer and a catalyst layer).

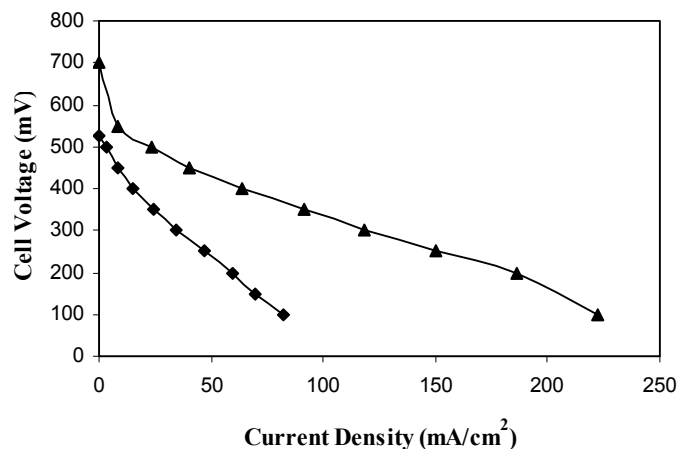


**Figure 5.7:** Cell performance using two different backing layers, (▲) E-TEK carbon cloth type “A”, 20% PTFE and (◆) Toray carbon paper TGP H 120, 20% PTFE.

## 5.4 INFLUENCE OF OPERATING PARAMETERS ON CELL

### PERFORMANCE

The operating parameters, namely, cell temperature, cathode pressure, air flow rate, etc. affect cell performance. In this section, experiments were conducted in an attempt to find the optimal conditions for DMFC operation and the influence of each one on cell performance.

Since a temperature of 130°C was used in MEA preparation, which is the glass transition temperature of Nafion<sup>®</sup>, where it will lose water, thereby significantly reducing conductivity, the MEA must be conditioned to restore the water in Nafion<sup>®</sup>, prior to evaluating cell performance. The conditioning of the MEA was investigated by circulating methanol in the anode side at 80°C at open circuit potential for several days. Figure 5.8 shows cell performance after the second and third days. As can be seen three days are necessary to restore water (fully hydrated) to the membrane. After three days, the cell performances were constant. The experiment in Figure 5.8 was conducted with E-TEK type “A” carbon cloth, 20 % PTFE as a backing layer, a 1 ml/min methanol flow rate, a 1 l/min air cathode flow rate, cell temperature 80°C and with anode and cathode at atmospheric pressure. This moisturizing procedure is time consuming, but it is necessary to generate optimal performance. Another way to moisturize the MEA, is to heat the MEA in water for 30 min at 80°C before connection in the cell. Figure 5.9 shows the results between the two methods.

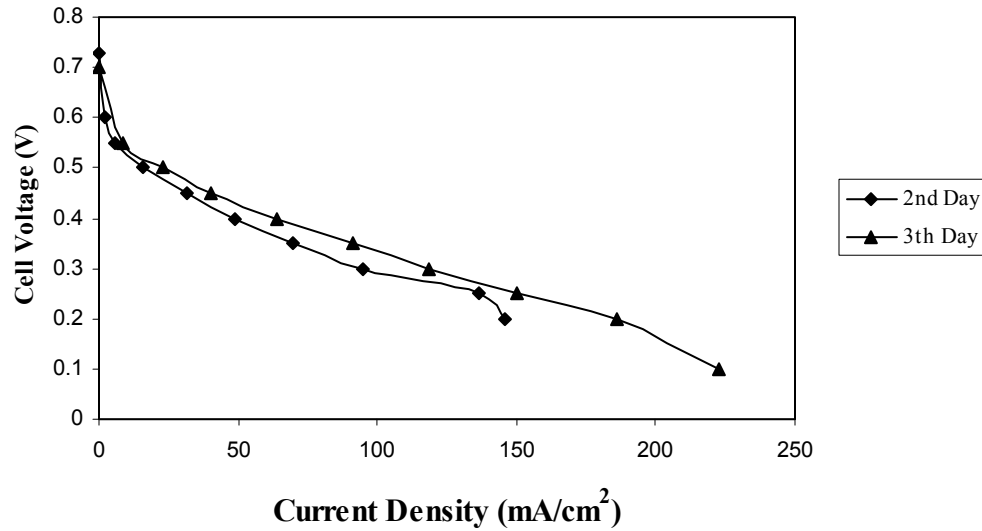


**Figure 5.8:** DMFC polarization curve: influence of moisturizing on cell performance.

As can be seen from Figure 5.9, the MEA moisturized at 80°C before connection to the cell gave better results than moisturizing in the cell for 8 hours. However, heating the MEA in water, is not a good way of moisturizing, since Nafion<sup>®</sup> polymer (Nafion<sup>®</sup> 117) when soaked in water will bend. This deformation of the polymer is not predicted, and will delaminate the electrodes from the membrane, which leads to a decrease in cell efficiency. This method can be used efficiently if an appropriate holder is used during moisturizing. Figure 5.9 was obtained with similar operating conditions to those in Figure 5.8.

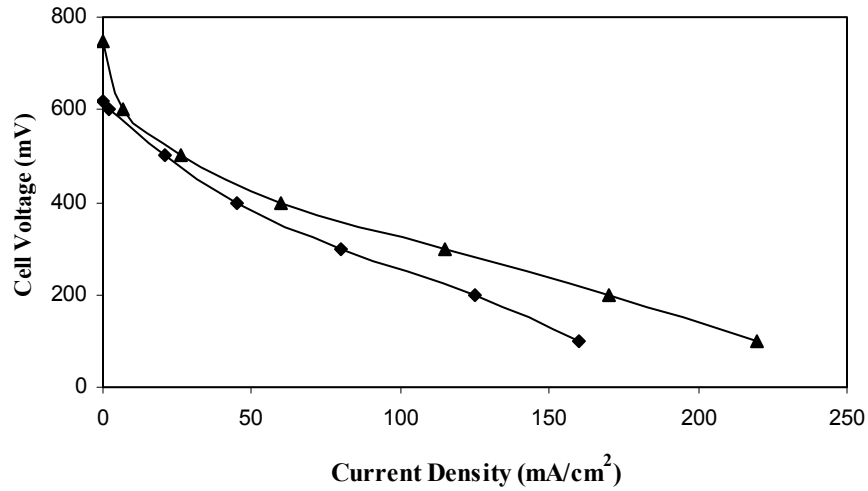


**Figure 5.9:** Polarization curve of a DMFC with different moisturizing methods: (▲) moisturizing by heating the MEA at 80°C, (◆) moisturizing in the cell at 80°C.

Figure 5.10 shows the effect of catalyst loading on cell performance. While Figures 5.11 and 5.12 are SEM micrographs of the anode electrode with different catalyst loading.

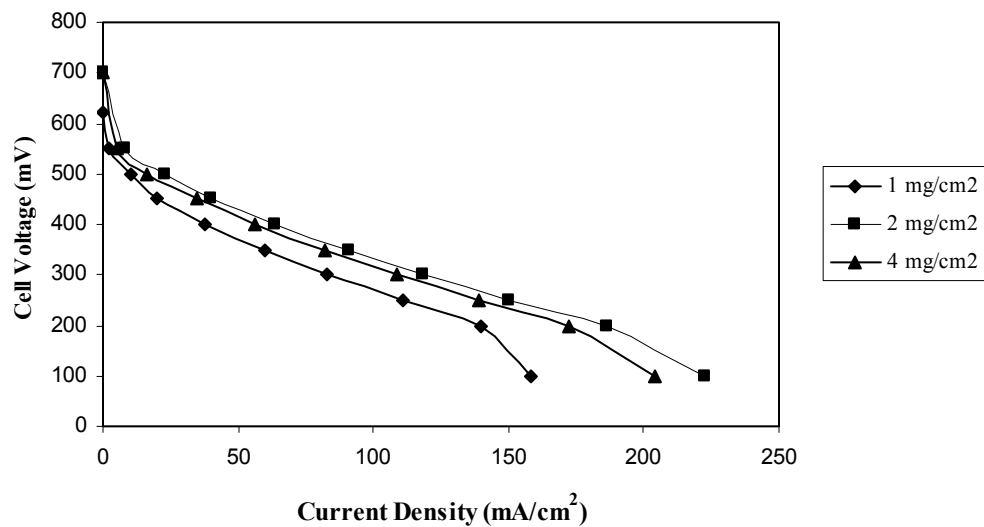


**Figure 5.10:** Effect of anode catalyst loading on cell performance at 80°C.

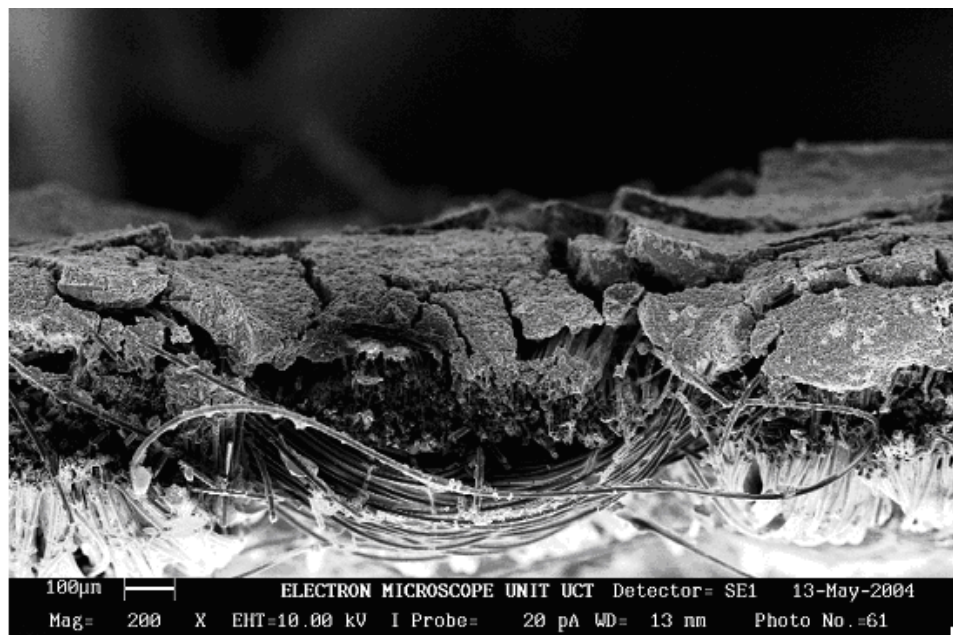


**Figure 5.11:** SEM micrograph of anode electrode, 1 mg/cm<sup>2</sup> catalyst loading.

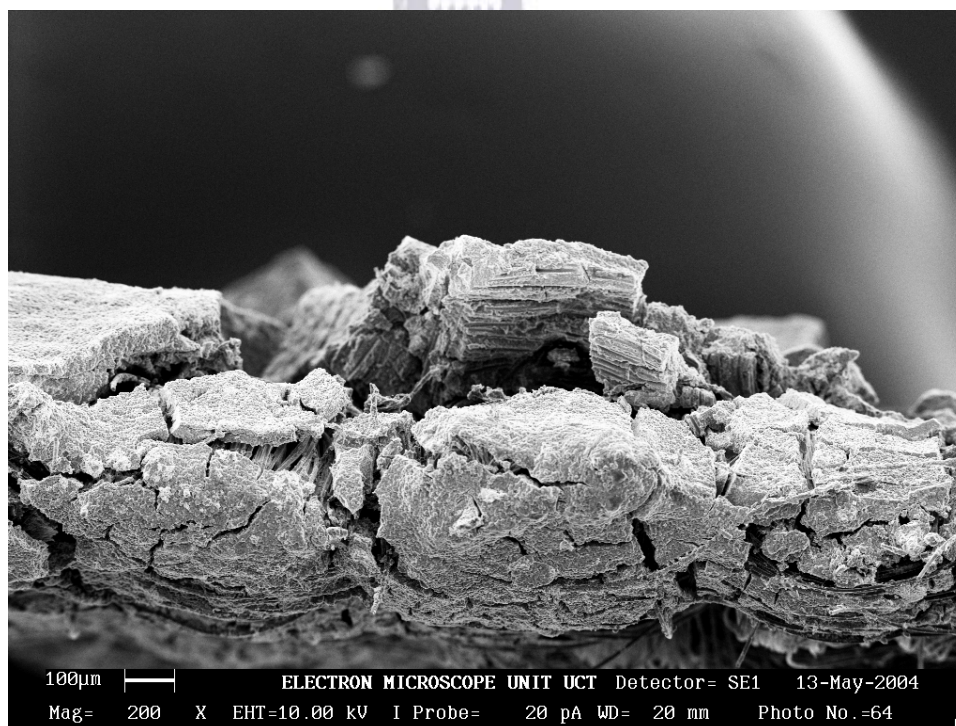


**Figure 5.12:** SEM micrograph of anode electrode, 2.3 mg/cm<sup>2</sup> catalyst loading.



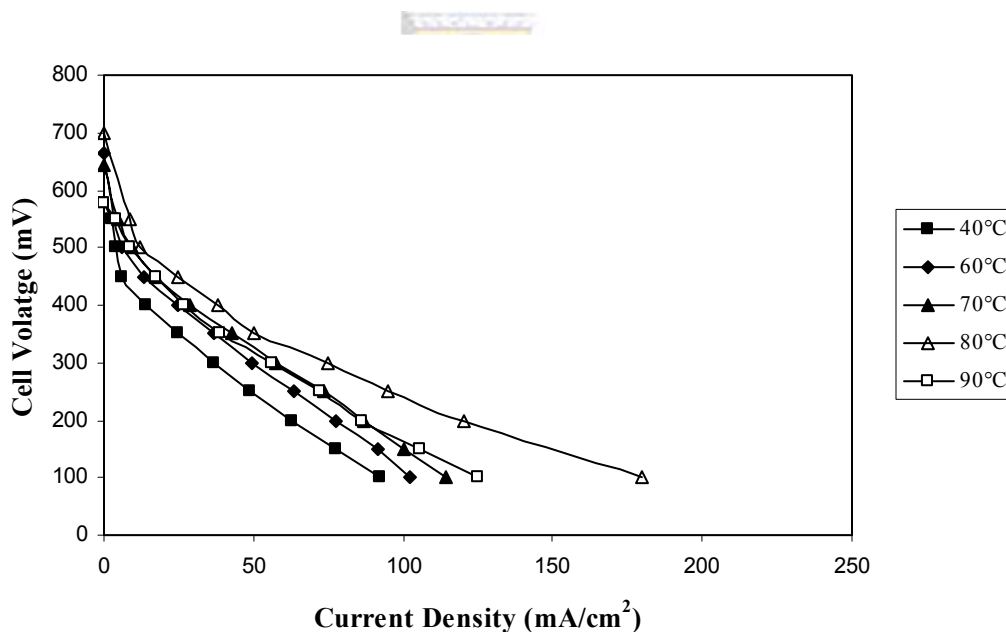
Figure 5.10 was obtained by using 20% Pt-10% Ru supported on carbon (HiSPEC 5000) purchased from Alfa Aesar for the anode electrode, while the cathode was prepared using 40% Pt supported on carbon (HiSPEC 4000) purchased from Alfa Aesar with a catalyst loading of  $2 \text{ mg/cm}^2$ . The cell operating conditions were as above. From figure 5.10 it can be seen clearly that increasing the catalyst loading will increase cell performance. After reaching an optimum, cell performance will start to decrease, due to the increase in electrode resistance. The optimal catalyst loading found with HiSPEC 5000 is around  $2 \text{ mg/cm}^2$ .

Figure 5.11 and 5.12 show clearly the influence of catalyst loading on cell performance. Increasing the catalyst loading will increase the thickness of the electrode. Therefore, the cell performance will suffer from mass transport limitations. With a thick electrode, methanol cannot enter the entire electrode structure, whereas  $\text{CO}_2$  cannot escape from the electrode.

The influence of temperature on cell performance was investigated. The results obtained are reported in Figure 5.13. Increasing the temperature from  $40^\circ\text{C}$  to  $80^\circ\text{C}$  leads to a significant increase in cell performance. This is due to two reasons: firstly, an increasing temperature will increase membrane conductivity, thus reducing ohmic losses, and secondly enhance methanol oxidation. The best performances were obtained with a temperature of  $80^\circ\text{C}$ . This temperature is optimal for Nafion<sup>®</sup> 117. However, at  $90^\circ\text{C}$ , the cell performance starts to deteriorate, due to membrane dehydration, where the membrane starts to lose water, thereby increasing resistance,

which leads to cell performance decreases. Figure 5.13 was obtained by using E-TEK carbon cloth and BAc as ink solvent. The methanol flow rate was 1 ml/min, air flow rate 1 l/min, catalyst loading 2 mg/cm<sup>2</sup> and atmospheric pressure for both anode and cathode.

Figure 5.14 was obtained using Toray paper TGP H 120 with 20% PTFE content and the ink was prepared with IPA. The same trend as Figure 5.13 was observed - for temperatures above 80°C, the membrane was subject to dehydration, which decreased cell performance.



**Figure 5.13:** Influence of temperature on cell performance, E-TEK carbon cloth (20% PTFE) and colloidal method.

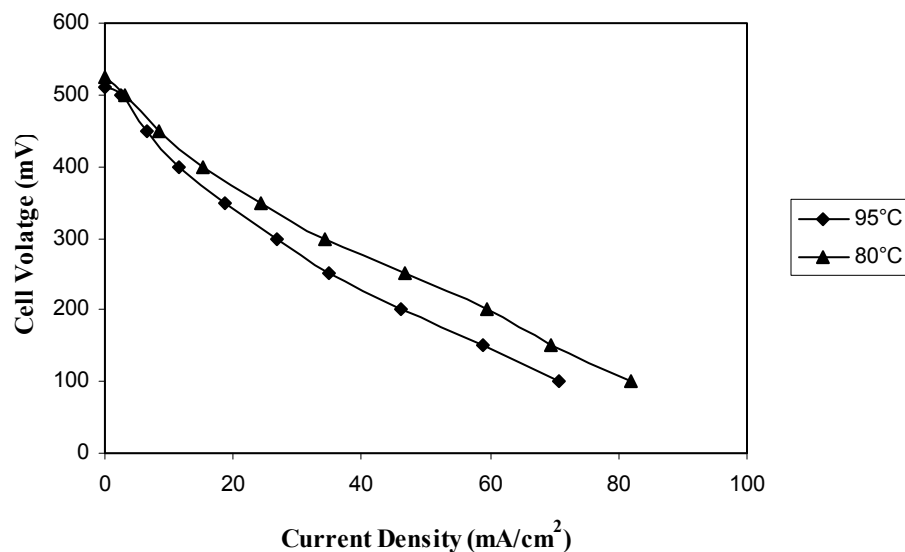


**Figure 5.14:** Influence of temperature on cell performance, Toray carbon paper (TGP H 120) with 20% PTFE and solution method.

The influence of cathode air flow rate was investigated with a cell constituted of E-TEK carbon cloth type “A” with 20% PTFE, IPA as the ink solvent, and the following cell operating parameters: methanol flow rate 1 ml/min, cell temperature 80°C, catalyst loading around 2 mg/cm<sup>2</sup> for anode and cathode, and atmospheric pressure for the anode and cathode. The results obtained are reported in Figure 5.15. Increasing the cathode air flow rate from 0.5 l/min to 1 l/min, increased the cell performance significantly. This increase in cell performance can be attributed to the better methanol and water removal at the cathode side. Above 1 l/min cathode air flow rate, the cell performance starts to decrease. This can be explained by the MEA dehydration.

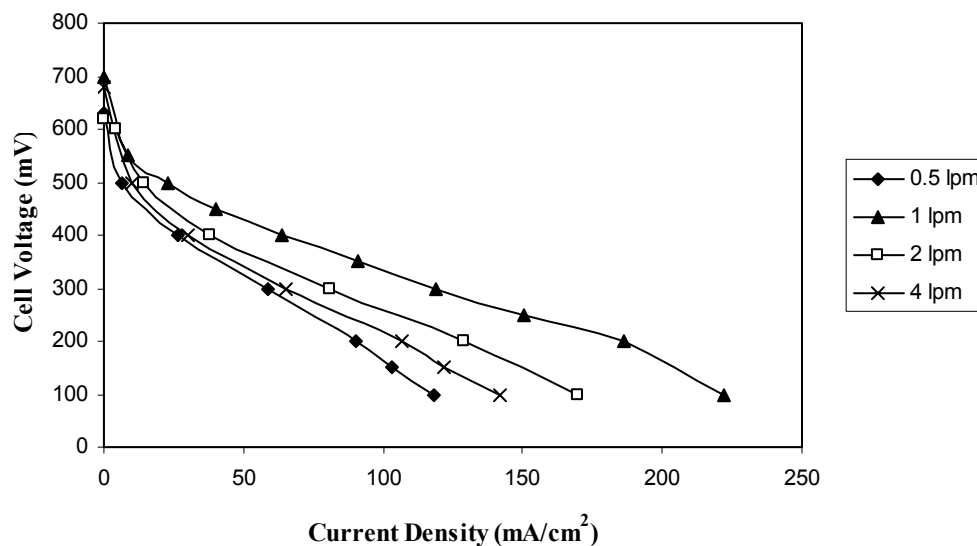


**Figure 5.15:** DMFC cell performance with different air cathode flow rates, E-TEK carbon cloth type “A”, 20% PTFE and using iso-propanol as the ink solvent.



Figure 5.16 shows the influence of cathode pressure on cell performance. As can be seen, increasing the cathode pressure increased cell performance. Usually high performance cells are obtained with a cathode pressure of 2 bar. Increasing cathode cell pressure will increase the cell performance as was demonstrated by Ren *et al.* [621] where an air pressure of 3 bar and an oxygen pressure of 5 bar were used. Figure 5.16 was obtained using a cell constituted of Toray TGP H 120 paper with 20% PTFE, IPA as the ink solvent, and the following cell operating parameters: methanol flow rate 1 ml/min, cell temperature 80°C, catalyst loading around 2 mg/cm<sup>2</sup> for anode and cathode, and atmospheric pressure for the anode and cathode was changed using a needle valve at the exhaust..

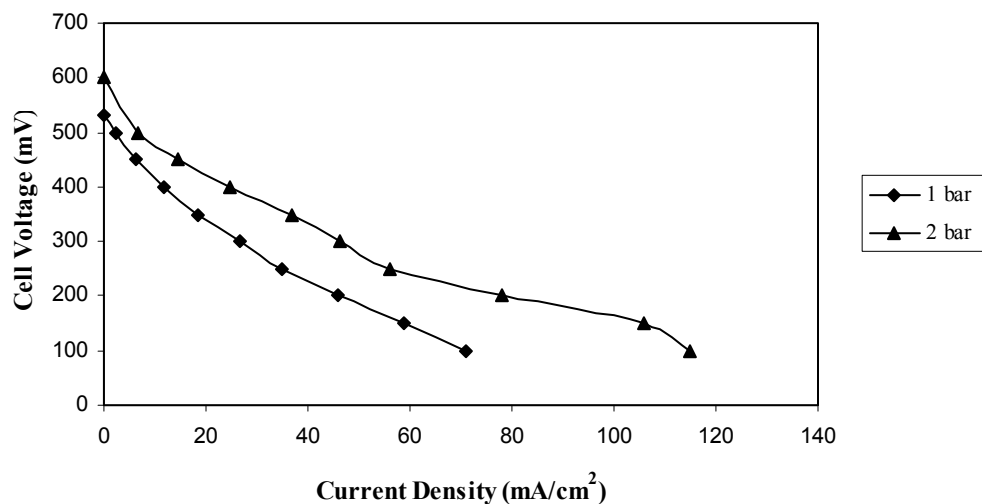


**Figure 5.16:** Influence of air cathode pressure on cell performance at 80°C, Toray TGP H 120 paper with 20% PTFE, (◆) 1 bar, (▲) 2 bar.

Figure 5.17 shows cell performance with air and oxygen. The cell operating parameters were as follows: E-TEK carbon cloth type “A” with 20% PTFE, IPA as the ink solvent, a methanol flow rate 1 ml/min, cathode gas flow rate 1 l/min, cell temperature 80°C, catalyst loading around 2 mg/cm<sup>2</sup> for anode and cathode, and atmospheric pressure for the anode and cathode.

As can be seen, using oxygen is an attractive way to maximize the power output due to the minimizing of ORR losses. Furthermore, the mass transfer resistance at the cathode is increased when using air, due to the presence of a blanket of nitrogen. However, from an operational point of view, using neat oxygen is not practical and air fed cathodes is the most realistic option for terrestrial applications.

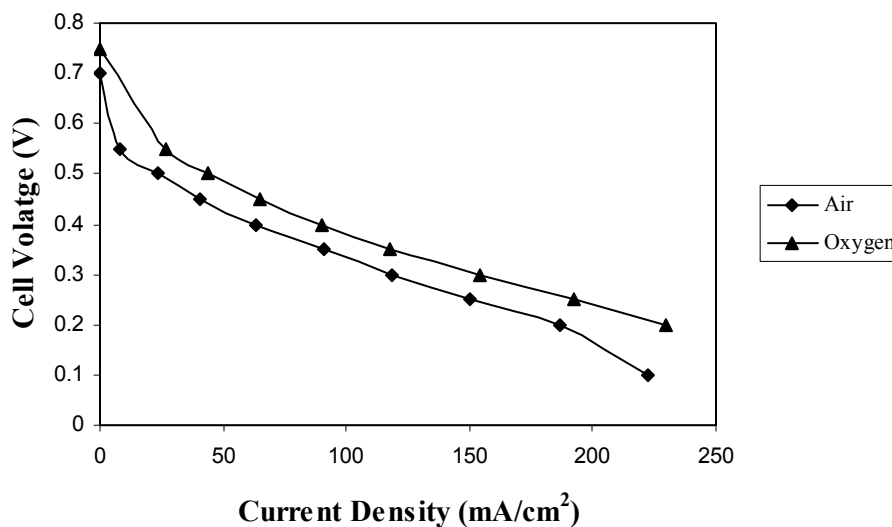


**Figure 5.17:** DMFC performance using air and oxygen at the cathode.

## 5.5 DISCUSSION AND CONCLUSIONS

Nafion<sup>®</sup> provides the necessary conductivity to the electrodes, thus enhancing catalyst utilization by extending the three-phase zone. However, too much Nafion<sup>®</sup> will decrease the electrode performance. A 14 wt.% Nafion<sup>®</sup> content in the electrode, which corresponds to a ratio of 3:1 (catalyst to Nafion<sup>®</sup>) was found to be optimal.

In electrode fabrication an ink was prepared. The state of the ink depends on the type of solvent used. IPA ( $\epsilon = 18.30$ ) forms a solution, while BAc ( $\epsilon = 5.01$ ) forms colloids. Cell performance was found to be better with solution ink than with colloidal ink, due to the high electrode resistance.

From the commercially available backing layers tested in this study, E-TEK type “A” was found to be the most suited for DMFC application. The CO<sub>2</sub> bubbles tend to attach to the Toray TGP H 120 carbon paper, forming slugs of bubbles which

block the electrode. Electrochem and Lydall Lyflex were the least suited for DMFC application due to the high PTFE loading and the high friction in the former and cathode flooding in the latter.

To avoid a two-phase flow, CO<sub>2</sub> bubbles moving counter-currently to liquid methanol, PTFE needs to be added to the electrode. A concentration of 20% was found to be optimal to create discrete paths for CO<sub>2</sub> to move out from the electrode.

In MEA preparation the membrane is subject to drying. Therefore, prior to cell testing, water must be restored to the membrane. Circulating water through the anode cell for three days was found to be the most adequate way to restore water, thus high performance can be achieved. Increasing the temperature up to 80°C, enhanced cell performance due to the increased membrane conductivity and methanol oxidation. However, above 80°C cell performance starts to deteriorate due to membrane dehydration.

Increasing the cathode pressure enhanced cell performance. However, from a DMFC application point of view, high pressure is not a realistic option. Pure oxygen at the cathode produces better results than air, but for DMFC commercialization, air at the cathode is the most desirable.

The optimal operating conditions were found to be: 1 ml/min methanol flow rate, 1 l/min cathode flow rate and it is preferable to preheat the methanol before entering the cell.


## CHAPTER 6

# DEVELOPED MEMBRANE PERFORMANCE

### 6.1 INTRODUCTION

The MEA is the heart of the DMFC. Therefore, the challenge facing the development of a new proton conductor membrane is to find the optimal conditions to make a good MEA. In general, MEAs are made by the hot pressing procedure using a catalyst layer spread onto a backing layer. This Section discuss the newly developed membranes that were tested in DMFC mode and their performances evaluated.

### 6.2. MEA FABRICATION



The MEA fabrication protocol is similar to the procedure reported in Section 6.1. A catalytic ink was prepared according to Section 5.2. Thus, 0.21 g of the catalyst was wetted with water. 0.67 g of 5 wt.% Nafion<sup>®</sup> solution (Aldrich) was added to the catalyst drop by drop under stirring. IAP was added to the ink and kept under stirring for 24 hours. The ink was then sprayed with an air brush onto E-TEK type “A” carbon cloth (20% PTFE). The electrode was dried at room temperature for 24 hours, then at 110°C for 1 hour. Prior to MEA fabrication the electrodes were coated with a film of Nafion<sup>®</sup> solution. The MEA was prepared with the hot pressing procedure, where a temperature of 130°C was used for 2 minutes. For Nafion<sup>®</sup> 117 a pressure of 100 bar was used whereas for CREAMFILTER<sup>®</sup>s membranes a pressure of 50 bar was used. Figures 6.1 and 6.2 show SEM cross-sections of MEAs.



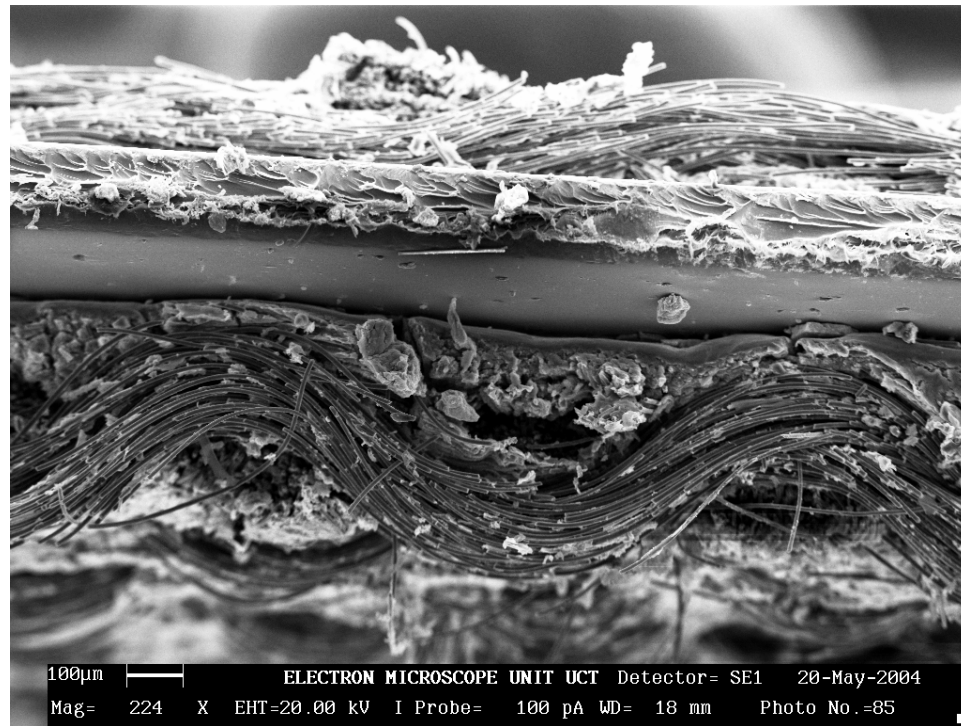


**Figure 6.1:** SEM cross-section of an MEA with Nafion® 117 as the membrane.

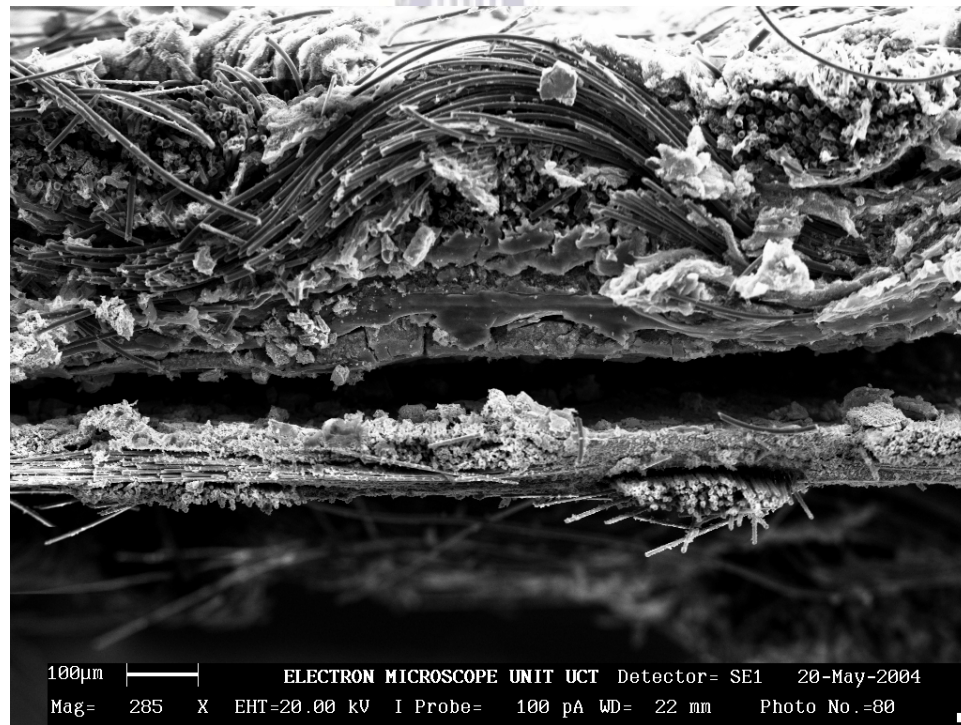


**Figure 6.2:** SEM cross-section of MEA with Z240G/ZrP/Nafion® as the membrane.

The MEAs reported in Figure 6.1 and 6.2 were obtained as described above with a catalyst loading of 2 mg/cm<sup>2</sup> for both anode and cathode. For anode catalyst (at the bottom of the micrograph) a 20% Pt – 10% Ru supported on carbon (HiSPEC 5000, Alfa Aesar) was used, whereas for cathode catalyst (at the top of the micrograph) a 40% Pt supported on carbon (HiSPEC 4000, Alfa Aesar) was used. The MEA cross-section was cut under liquid nitrogen and the micrographs were taken with a Leo instrument.

From Figure 6.1, it can be clearly seen that there is a good contact between the Nafion<sup>®</sup> membrane and the electrode, thus small electrical loss was obtained in the fuel cell test. In contrast, Figure 6.2 shows clearly there is the delamination of the electrode, especially the anode. It can be concluded that the performance of the MEA with CREAMFILTER<sup>®</sup> Z240G impregnated with ZrP and followed by Nafion<sup>®</sup> film coating will be less than that of Nafion<sup>®</sup> 117 membrane. To increase the performance of the newly developed membrane an appropriate MEA fabrication procedure needs to be developed.

### 6.3 SINGLE CELL PERFORMANCE

Prior to single cell testing, the CREAMFILTER<sup>®</sup> Z240G impregnated with ZrP and followed with Nafion<sup>®</sup> film coating was tested in a Nafion<sup>®</sup> stack, similar to the procedure used in conductivity measurement to avoid the electrode contact problems. For that, three Nafion<sup>®</sup> stack were first tested in a fuel cell. After that the middle Nafion<sup>®</sup> polymer was replaced with CREAMFILTER<sup>®</sup> Z240G/ZrP/ Nafion<sup>®</sup> membrane.

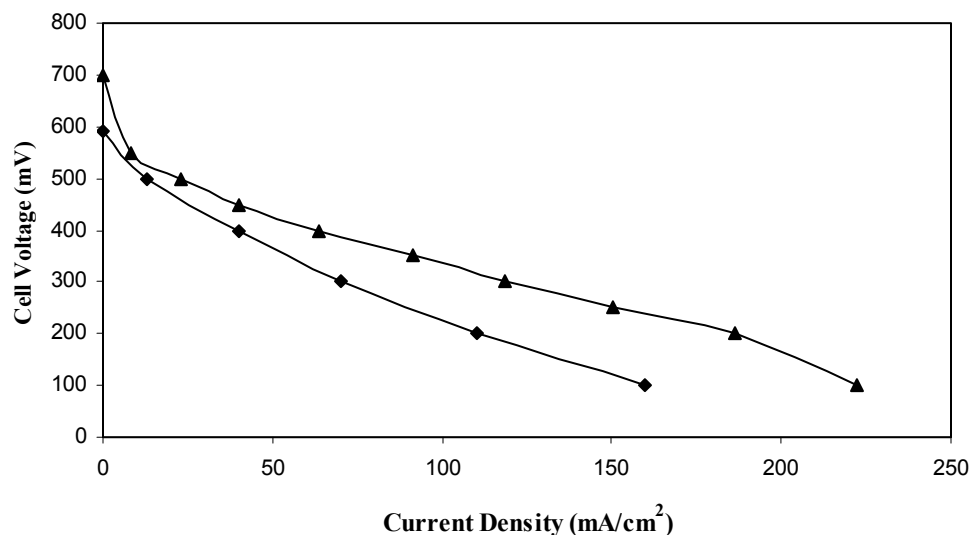
This procedure was adopted in order to eliminate the delamination problem, since only Nafion<sup>®</sup> membranes are in contact with the electrodes. The results obtained are summarized in Table 6.1.

**Table 6.1:** DMFC performance in 5 cm<sup>2</sup> three layers stack

<b>Voltage</b>	<b>Middle Membrane</b>	<b>Cell Current</b>
At 0 V	Nafion <sup>®</sup> 117	400 mV
At 0 V	CREAFILTER <sup>®</sup> Z240G/ZrP/ Nafion <sup>®</sup>	320 mV

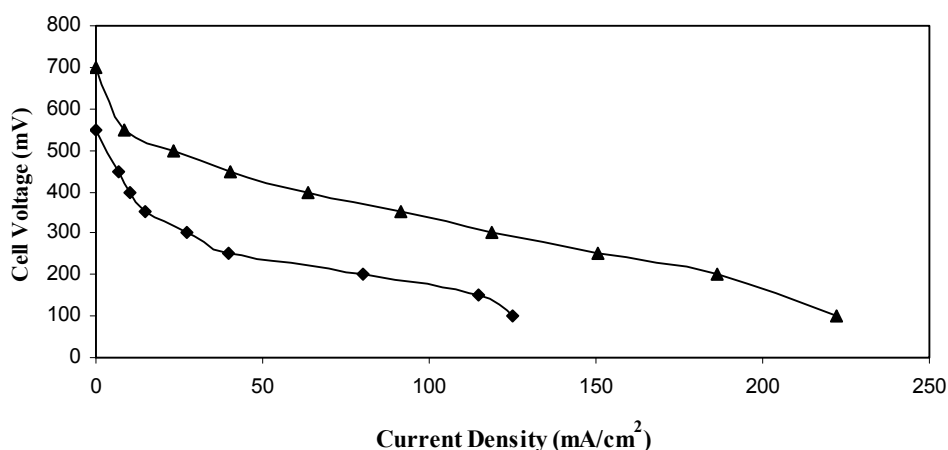
Table 6.1 shows the potential of CREAMFILTER<sup>®</sup> Z240G/ZrP/ Nafion<sup>®</sup> for DMFC applications. However, an appropriate MEA fabrication procedure needs to be developed. It can also be seen that the contact between the membrane and the electrode play an important role to enable high currents to be drawn from the cell.

Figure 6.3 show cell performances with Nafion<sup>®</sup> 117 and CREAMFILTER<sup>®</sup> Z240G/ZrP/ Nafion<sup>®</sup>. The cell performances were obtained with identical MEA, the only difference being the pressure used in MEA fabrication, where 100 bar was used with Nafion<sup>®</sup> 117, whereas a 50 bar was used with CREAMFILTER<sup>®</sup> Z240G/ZrP/ Nafion<sup>®</sup>. The results show that the composite membrane can achieve high performance.



**Figure 6.3:** DMFC performance of CREAMFILTER<sup>®</sup> Z240G impregnated with ZrP (◆) and Nafion<sup>®</sup> 117 (▲).

Figure 6.4 show cell performance results with Nafion<sup>®</sup> 117 and CREAMFILTER<sup>®</sup> S450P impregnated with Nafion<sup>®</sup> solution. Here also, the prepared composite membrane shows a good potential for DMFC application.



**Figure 6.4:** DMFC performance of CREAMFILTER<sup>®</sup> S450P impregnated with Nafion<sup>®</sup> solution (◆) and Nafion<sup>®</sup> 117 (▲).

#### 6.4 DISCUSSION AND CONCLUSIONS

CREAFILTER<sup>®</sup>s were found to be good potential membranes to replace Nafion<sup>®</sup>. The selectivity factor was found to be very close to that of Nafion<sup>®</sup> 117. However, as with all newly developed membranes, an appropriate method to prepare the MEA needs to be developed. In this Section, preliminary attempts to draw current from the prepared membrane were studied by using Nafion<sup>®</sup> technology to prepare the MEAs. Relatively good performance was obtained. In CREAMFILTER<sup>®</sup> composite membrane delamination was observed, thus much efficiency was lost due to the bad contact between the membrane and the electrodes.



## CHAPTER 7

# OVERALL CONCLUSION AND RECOMMENDATIONS FOR FUTURE WORK

### 7.1 OVERALL CONCLUSION

Flexible inorganic ceramics were used as a matrix for proton conductor materials. The inorganic matrixes used were development materials from Creavis Technology and Innovation under the trade name CREAMFILTER<sup>®</sup>. These materials show good chemical and thermal stability. Furthermore, these materials are fabricated from metal oxides (e.g. ZrO<sub>2</sub>, SiO<sub>2</sub> and Al<sub>2</sub>O<sub>3</sub>), which have high water content.

Two novel composite proton conductor membranes were prepared by using an impregnation technique. These include the impregnation of CREAMFILTER<sup>®</sup> with zirconium phosphate and Nafion<sup>®</sup> solution.

Different ZrO<sub>2</sub> sources were investigated to find out the optimal source for zirconium phosphate preparation and the most compatible with the inorganic matrix. ZrO<sub>2</sub> powder purchased from Degussa was found to be the ideal starting material to prepare zirconium phosphate, since it has a high surface area and high water content.

CREAMFILTER<sup>®</sup> impregnated with zirconium phosphate shows a selectivity factor better than or similar to Nafion<sup>®</sup> 117. The selectivity factor, which is the ratio of the proton conductivity ( $\sigma$ ) and methanol permeability ( $P$ ), was adopted as a way of

membrane characterization. Nafion<sup>®</sup> 117 was studied as a reference, since it is the membrane of choice for DMFC applications.

Selectivity factors ( $\beta$ ) of 4.9 and 4.5 were found for CREAMFILTER<sup>®</sup> Z240G/zirconium phosphate and Nafion<sup>®</sup> 117, respectively. These results show the potential of these composite membranes to replace Nafion<sup>®</sup> 117.

CREAFILTER<sup>®</sup> impregnated with Nafion<sup>®</sup> solution also shows good characteristics - where selectivity factors of 4.6 and 4.5 were found for CREAMFILTER<sup>®</sup> Z240G/ Nafion<sup>®</sup> solution and CREAMFILTER<sup>®</sup> S450P/ Nafion<sup>®</sup> solution , respectively.

The impregnation technique was found to be useful to reduce methanol permeability in both composite CREAMFILTER<sup>®</sup> impregnated with zirconium phosphate and CREAMFILTER<sup>®</sup> impregnated with Nafion<sup>®</sup> solution. Methanol permeability was found to be  $3.5 \times 10^{-7} \text{ cm}^2/\text{s}$  in CREAMFILTER<sup>®</sup> Z240G impregnated with zirconium phosphate and a value of  $5.5 \times 10^{-7} \text{ cm}^2/\text{s}$  was obtained with CREAMFILTER<sup>®</sup> Z240G impregnated with Nafion<sup>®</sup> solution, whereas, a value of  $14 \times 10^{-7} \text{ cm}^2/\text{s}$  was found for Nafion<sup>®</sup> 117.

It was found that the solvent has an important influence on the characteristics of recast Nafion<sup>®</sup>. Furthermore, the thermal treatment at high temperature, typically around 160°C, proved to be necessary to produce a mechanically stable film. Thus, the thermal treatment at 160°C was used in composite membrane preparation (CREAFILTER<sup>®</sup> impregnated with Nafion<sup>®</sup> solution).

The water content was found to be higher in CREAMFILTER<sup>®</sup> S type than Z type. This is due to the type of metal oxide used in the CREAMFILTER<sup>®</sup> fabrication. S type is constituted of SiO<sub>2</sub> and Al<sub>2</sub>O<sub>3</sub>, whereas Z type is constituted of ZrO<sub>2</sub> and Al<sub>2</sub>O<sub>3</sub>. SiO<sub>2</sub> has higher water content than ZrO<sub>2</sub>, followed by Al<sub>2</sub>O<sub>3</sub>. Furthermore, it was found that CREAMFILTER<sup>®</sup> impregnated with zirconium phosphate has a higher water content than the same CREAMFILTER<sup>®</sup> type impregnated with Nafion<sup>®</sup> solution.

CREAMFILTER<sup>®</sup> impregnated with zirconium phosphate was further coated with Nafion<sup>®</sup> film. The coating serves as a barrier to zirconium phosphate to avoid leaching and also as a barrier to methanol. A reduced methanol permeability was found, where a value of  $3 \times 10^{-7}$  cm<sup>2</sup>/s was obtained with CREAMFILTER<sup>®</sup> Z240G. Furthermore, the Nafion<sup>®</sup> coating will play an important role as a binder in MEA fabrication.



Recast Nafion<sup>®</sup> incorporated with ZrO<sub>2</sub> composite membranes was prepared with different loadings. It was found that incorporating ZrO<sub>2</sub> in the film reduced methanol permeability and increased water content. Increasing the loading, decreases methanol permeability and increases the water content. On the other hand, the conductivity decreases with increasing loading. Small amounts of ZrO<sub>2</sub>, typically less than 5%, are needed to optimize methanol permeability and conductivity.

Recast Nafion<sup>®</sup> with zirconium phosphate powder as an additive, was also prepared. The addition of zirconium phosphate to recast Nafion<sup>®</sup> enhanced the



characteristics of the film, by reducing methanol permeability and increasing water content. Zirconium phosphate has an advantage over  $ZrO_2$  in that the conductivity increases with increasing loading, since zirconium phosphate is itself a proton conductor. However, it was found that recast Nafion<sup>®</sup> incorporated with zirconium phosphate (6.4%) has higher methanol permeability than recast Nafion<sup>®</sup> incorporated with  $ZrO_2$  (5%). This is due to particle size effects, where  $ZrO_2$  particles were found to be in the range of 12-14 nm, while zirconium phosphate particles were found to be in the range of 30-40 nm. The results show the importance of the small size in dispersing an inorganic material in a polymer.

Nafion<sup>®</sup> 117 incorporated with zirconium phosphate via an ion exchange of  $Zr^{+4}$  was also prepared. The presence of zirconium phosphate was confirmed by the change in the film colour from transparent to white, and also by XRD and FTIR analysis. The size of the zirconium phosphate particles produced by the ion exchange method is around 11 nm, and the shape is rectangular as revealed by TEM analysis, in contrast to zirconium phosphate powder particles, where spherical shapes were observed.

In all the composite Nafion<sup>®</sup> / inorganic membranes, the inorganic materials are homogeneously distributed throughout the polymer, and this is due to the nanometric size of the inorganic materials used in this study. Furthermore, no leaching

of the inorganic additives from the polymer was observed, showing the good compatibility between the polymer (Nafion<sup>®</sup>) and the inorganic materials.

CREAFILTER<sup>®</sup>s impregnated with Nafion<sup>®</sup> were prepared with high conductivity and reduced methanol permeability. On the other hand, zirconium phosphate was found to be the best inorganic additive to proton conductive polymers, since zirconium phosphate it is itself a proton conductor and has a high water content. A composite membrane was successfully prepared by impregnating CREAMFILTER<sup>®</sup> with Nafion<sup>®</sup> solution, followed by the introduction of zirconium phosphate via an ion exchange of H<sup>+</sup> in the Nafion<sup>®</sup> with Zr<sup>+4</sup>, followed by precipitation of zirconium phosphate. This type of composite membrane has higher water content over similar commercially available membranes (e.g. Gore Select<sup>®</sup> from Gore and Associates).



DMFC operating parameters were investigated in a 5 cm<sup>2</sup> single cell and using Nafion<sup>®</sup> 117 as proton conductor membrane. The following are the findings:

A catalytic ink was prepared by mixing the catalyst, Nafion<sup>®</sup> solution, water and a solvent. The state of the ink depends of the type of solvent. IPA forms a solution whereas BAc forms a colloidal paste. The cell performance with IPA was found to be higher than BAc. This is due to the increased mass transfer resistance in the catalyst layer.

Adding Nafion<sup>®</sup> to the catalyst layer can play to some extent an important role in catalyst utilization by extending the three-phase zone. A 14 wt.% Nafion<sup>®</sup> content was found to be optimal.

E-TEK type “A” carbon cloth was found to be the best backing layer for DMFC. Carbon paper is not a suitable backing layer for methanol fuel cell, since CO<sub>2</sub> bubbles, a byproduct of methanol oxidation, tend to attach to the surface of the paper, whereas CO<sub>2</sub> bubbles do not attach themselves to carbon cloth.

Adding PTFE to the backing layer, enhanced CO<sub>2</sub> removal from the catalyst layer and backing layer. 20 wt.% PTFE content was found to be an optimal loading. With no PTFE, CO<sub>2</sub> is moving counter-currently against liquid methanol (two-phase flow) and with high PTFE loading, the liquid methanol does not penetrate deeply in the backing layer to reach the catalyst layer, thus decreasing cell performance.

Moisturizing the membrane was found to be necessary to restore water. The best way for moisturizing is by circulating water through the cell anode for 48 hours at 80°C.

Increasing the cathode pressure enhanced cell performance. On the other hand, using oxygen at the cathode produces better results than using air. For DMFC applications, air is favored than oxygen.

Preliminary results with CREAMFILTER<sup>®</sup>s membranes show the potential of these membranes to perform similarly as Nafion<sup>®</sup> in DMFC mode. However, it was found that the MEAs prepared in this study are not yet optimized where the delamination problem occurs with a bad contact between the membrane and the electrode.

## 7.2 RECOMMENDATIONS FOR FUTURE WORK

The prepared membranes show good characteristics. However, long term stability tests need to be performed.

The mechanical properties of the CREAMFILTER<sup>®</sup> composite membranes need to be investigated including tensile strengths and shrinkage.

In this study, the proton conductivity and methanol permeability were measured at room temperature. For advanced membrane characterization, the conductivity as a function of temperature and relative humidity needs to be measured. The cell used does not allow measurement of conductivity at high temperatures where the membrane will be exposed to dehydration. Therefore, an appropriate cell needs to be designed. Furthermore, methanol vapor permeability needs to be investigated.

Nafion<sup>®</sup> coating on CREAMFILTER<sup>®</sup> impregnated with zirconium phosphate was found to be an adequate way to avoid zirconium phosphate leaching. The coating was done by soaking the membrane in Nafion<sup>®</sup> solution. An appropriate method to achieve high conductivity and low methanol permeability need to be developed.

To achieve high performance with the prepared membranes, a good MEA preparation procedure needs to be developed. A good contact between the membrane and the electrodes can be obtained in two ways: firstly, by optimizing the backing layers and secondly by coating the catalyst layer directly onto the membrane instead of the backing layer

The inorganic additives used in this study proved to enhance the characteristics of Nafion<sup>®</sup>. Similarly, these inorganic materials can be added to other polymeric proton conductor (e.g. S-PEEK or S-PSU).

H<sub>2</sub>-PEMFC is outside the scope of this study. However, the prepared membranes can be tested in a hydrogen fuel cell. Prior to cell testing, gas permeability needs to be investigated since hydrogen fuel cells require a gas tight membrane.



## REFERENCES

- [1] E.S. Goodstein, *Economics and Environment*, Upper Saddle River, NJ, Prentice Hall, 1999
- [2] M.G.L. Santarelli, M. Cali, A. Bertonasco, *Energy Conversion and Management* **44** (2003) 2353-2370
- [3] L. Carrette, K.A. Friedrich, U. Stimming, *Fuel Cells* **1** (2001) 5-39
- [4] K.V. Kordesch and G.R. Simader, *Chem. Rev.* **95** (1995) 191-207
- [5] J.W. Raadschelders and T. Jansen, *J. Power Sources* **96** (2001) 160-166
- [6] D.M. Bernardi, M.W. Verbrugge, *AIChE Journal* **37** (8) (1991) 1151-1163
- [7] S.-J. Shin, J.-K. Lee, H.-Y. Ha, S.-A. Hong, H.-S. Chun, I.-H. Oh, *J. Power Sources* **106** (2002) 146-152
- [8] M. Uchida, Y. Aoyama, N. Eda, A. Ohta, *J. Electrochem. Soc.* **142** (1995) 463-468
- [9] J.S. Yi and T.V. Nguyen, *J. Electrochem. Soc.* **146** (1999) 38-45
- [10] D. Chu and R. Jiang, *J. Power Sources* **80** (1999) 226-234
- [11] R.W. Glazebrook, *J. Power Sources* **7** (1982) 215-256
- [12] M.J. Schatter, in *Fuel Cells*, G.J. Young (Ed.), Vol. 2, Reinhold, New York, 1983, p. 290
- [13] K. Tamura, T. Tsukui, T. Kamo, T. Kudo, *Hitachi Hyoron* **66** (1984) 135-138
- [14] K.R. Williams, *An Introduction to Fuel Cells*, Elsevier, 1966, p. 152
- [15] C. Lamy, E.M. Belgsir, J.-M. Léger, *J. Appl. Electrochem.* **31** (2001) 799-809
- [16] K. Kordesch and G. Simader, *Fuel cells and their Applications*, VCH, Weinheim, 1996
- [17] J.N. Murray and P.G. Grimes, in *Fuel Cells*, American Institute of Chemical Engineers, New York, 1963, p. 57
- [18] L.K. Verma, *J. Power Sources* **86** (2000) 464-468
- [19] M. Mench, S. Boslet, S. Thynell, J. Scott, C.Y. Wang, in *Direct Methanol Fuel Cells*, S. Narayanan, T. Zawodzinski, S. Gottesfeld (Eds.), PV 2001-4, *The Electrochemical Society Proceeding Series*, Pennington, NJ, 2001, p. 241

- [20] A.J. Appleby, G. Bronoel, M. Chemla, H. Kita, in *Encyclopedia of Electrochemistry of the Elements*, A.J. Bard (Ed.), Vol. IX, Part A, Dekker, New York, 1983, p. 383
- [21] S. Gottesfeld and T.A. Zawodzinski, in *Advances in Electrochemical Science and Engineering*, R.C. Alkire, H. Gerischer, D.M. Kolb, C.W. Tobias (Eds.), Vol. 5, Chapter 4, Wiley-VCH, Weinheim, 1997
- [22] T.R. Ralph, *Platinum Metals Rev.* **41** (1997) 102-113
- [23] A. Parthasarathy, C.R. Martin, S. Srinivasan, *J. Electrochem. Soc.* **138** (1991) 916-920
- [24] S. Srinivasan, E.A. Ticianelli, C.R. Derouin, A. Redondo, *J. Power Sources* **22** (1988) 359-375
- [25] M.S. Wilson and S. Gottesfeld, *J. Electrochem. Soc.* **139** (1992) L28-L30
- [26] M.S. Wilson, *US Patent*, **5,211,984** (1993)
- [27] M.S. Wilson, J.A. Valerio, S. Gottesfeld, *Electrochim. Acta* **40** (1995) 355-363
- [28] A.J. Appleby, E.B. Yeager, in *Assessment of Research Needs for Advanced Fuel Cells*, S.S. Penner (Ed.), Chapter 4, Pergamon, New York, 1986
- [29] A.J. Appleby and E.B. Yeager, *Energy* **11** (1986) 137-151
- [30] H. Dohle, J. Divisek, J. Mergel, H.F. Oetjen, C. Zingler, D. Stolten, *J. Power Sources* **105** (2002) 274-282
- [31] A.V. Anantaraman and C.L. Gardner, *J. Electroanal. Chem.* **414** (1996) 115-120
- [32] C. Gavach, G. Pamboutzoglou, M. Nedyalkov, G. Pourcelly, *J. Membr. Sci.* **45** (1989) 37-53
- [33] T.A. Zawodzinski, Jr., M. Neeman, L.O. Sillerud, S. Gottesfeld, *J. Phys. Chem.* **95** (1991) 6040-6044
- [34] T.A. Zawodzinski, Jr., T.E. Springer, J. Davey, R. Jestel, C. Lopez, J. Valerio, S. Gottesfeld, *J. Electrochem. Soc.* **140** (1993) 1981-1985
- [35] J.J. Fontanella, M.C. Wintersgill, R.S. Chen, Y. Wu, S.G. Greenbaum, *Electrochim. Acta* **40** (1995) 2321-2326
- [36] F. Finsterwalder and G. Hambitzer, *J. Membr. Sci.* **185** (2001) 105-124
- [37] T.R. Ralph and M.P. Hogarth, *Platinum Metals Rev.* **46** (2002) 117-135

- [38] U.A. Paulus, T.J. Schmidt, H.A. Gasteiger, R.J. Behm, *J. Electroanal. Chem.* **495** (2001) 134-145
- [39] F. Gloaguen, P. Convert, S. Gamburgzev, O.A. Velez, S. Srinivasan, *Electrochim. Acta* **43** (1998) 3767-3772
- [40] J. Larminie and A. Dicks, *Fuel Cell Systems Explained*, Wiley, Chichester, 2000
- [41] J.-M. Léger, *J. Appl. Electrochem.* **31** (2001) 767-771
- [42] Z. Qi and A. Kaufman, *J. Power Sources* **110** (2002) 177-185
- [43] K. Scott, W.M. Taama, P. Argyropoulos, *J. Appl. Electrochem.* **28** (1998) 1389-1397
- [44] D. Chu and S. Gilman, *J. Electrochem. Soc.* **141** (1994) 1770-1773
- [45] A. Argyropoulos, K. Scott, W.M. Taama, *J. Appl. Electrochem.* **29** (1999) 661-669
- [46] S. Surampudi, S.R. Narayanan, E. Vamos, H. Frank, G. Halpert, A. LaConti, J. Kosek, G.K. Surya Prakash, G.A. Olah, *J. Power Sources* **47** (1994) 377- 385
- [47] M. Hogarth, P. Christensen, A. Hamnett, A. Shukla, *J. Power Sources* **69** (1997) 113-124
- [48] C. Lim and C.Y. Wang, *J. Power Sources* **113** (2003) 145-150
- [49] M.P. Hogarth and T.R. Ralph, *Platinum Metals Rev.* **46** (4) (2002) 146-164
- [50] P. Argyropoulos, K. Scott, W.M. Taama, *Electrochim. Acta* **44** (1999) 3575-3584
- [51] J. Nordlund, A. Roessler, G. Lindbergh, *J. Appl. Electrochem.* **32** (2002) 259-265
- [52] X. Ren and S. Gottesfeld, *J. Electrochem. Soc.* **148** (2001) A87-A93
- [53] J.C. Amphlett, B.A. Peppley, E. Halliop, A. Sadiq, *J. Power Sources* **96** (2001) 204-213
- [54] Z.H. Wang, C.Y. Wang, K.S. Chen, *J. Power Sources* **94** (2001) 40-50
- [55] S.R. Narayanan, A. Kindler, B. Jeffries-Nakamura, W. Chun, H. Frank, M. Smart, T.I. Valdez, S. Surampudi, G. Halpert, J. Kosek, C. Cropley, in *Proceedings of 11<sup>th</sup> Annual Battery Conference on Applications and Advances*, Long Beach, Calif., Jan. 9-12, 1996, p. 113-122



- [56] M.W. Mench and C.Y. Wang, *J. Electrochem. Soc.* **150** (2003) A79-A85
- [57] V.C.Y. Kong, F.R. Foulkes, D.W. Kirk, J.T. Hinatsu, *Int. J. Hydrogen Energy* **24** (1999) 665-675
- [58] V. Raman, in *fuel cell power for transportation*, J. Seaba, R. Stobart (Eds.), Society of Automotive Engineers, Vol. 4, Warrendale, PA, 1999, p. 2
- [59] R.G. Ding, G.Q. Lu, Z.F. Yan, M.A. Wilson, *J. Nano. Nanotechno.* **1** (2001) 7-19
- [60] F.L. Darkrim and D. Levesque, *J. Phys. Chem. B* **104** (2000) 6773-6776
- [61] F.L. Darkrim, P. Malbrunot, G.P. Tartaglia, *Int. J. Hydrogen Energy* **27** (2002) 193-202
- [62] A.C. Dillon, K.M. Jones, T.A. Bekkedahl, C.H. Kiang, D.S. Bethune, M.J. Heben, *Nature* **386** (1997) 377-379
- [63] A. Züttel, P. Sudan, Ph. Mauron, T. Kiyobayashi, Ch. Emmenegger, L. Schlapbach, *Int. J. Hydrogen Energy* **27** (2002) 203-212
- [64] S.M. Lee, J.H. Kim, H.H. Lee, P.S. Lee, J.Y. Lee, *J. Electrochem. Soc.* **149** (2002) A603-A606
- [65] V. Guthier and A. Otto, *J. Alloys and Compounds* **293-295** (1999) 889-892
- [66] G. Sandrock and R.B. Bowman Jr., *J. Alloys and Compounds* **356-357** (2003) 794-799
- [67] J.M. Ogden, M.M. Steinbugler, T.G. Kreutz, *J. Power Sources* **79** (1999) 143-168
- [68] K. Ledjeff-Hey, V. Formanski, Th. Kalk, J. Roes, *J. Power Sources* **71** (1998) 199-207
- [69] C.E. Borroni-Bird, *J. Power Sources* **61** (1996) 33-48
- [70] EA Engineering, Science, and Technology, Inc. Report: "Methanol Refueling Station Costs", Prepared for the American Methanol Institute, February 1, 1999
- [71] K.-A. Adamson and P. Pearson, *J. Power Sources* **86** (2000) 548-555
- [72] K. Takahashi, N. Takezawa, H. Kobayashi, *Appl. Cat.* **2** (1982) 363-366
- [73] N. Takezawa, H. Kobayashi, Y. Kamegai, M. Shimokawabe, *Appl. Cat.* **3** (1982) 381-388
- [74] J.C. Amphlett, M.J. Evans, R.F. Mann, R.D. Weir, *Can. J. Chem. Eng.* **63** (1985) 605-611

- [75] C.J. Jiang, D.L. Trimm, M.S. Wainwright, N.W. Cant, *Appl. Catal. A* **93** (1993) 245-255
- [76] K. Kochloefl, L.H. Lunsford, J.B. Hansen, J.H. Sinfelt: in *Handbook of Heterogeneous Catalysis, Energy-Related Reactions*, G. Ertl, H. Knozinger, J. Weitkamp (Eds.), Volume 4, Wiley-VCH, Weinheim, 1997
- [77] B. Emonts, J.B. Hansen, S.L. Jørgensen, B. Höhle, R. Peters, *J. Power Sources* **71** (1998) 288-293
- [78] H.G. Duesterwald, B. Höhle, H. Kraut, J. Meusinger, R. Peters, U. Stimming, *Chem. Eng. Technol.* **20** (1997) 617-623
- [79] J.P. Breen and J.R.H. Ross, *Catalysis Today* **51** (1999) 521-533
- [80] M.L. Cubiero and J.L.G. Fierro, *J. Catalysis* **179** (1998) 150-162
- [81] S. Velu, K. Suzuki, T. Osaki, *Catal. Lett.* **62** (1999) 159-167
- [82] J. Agrell, K. Hesselbo, K. Jansson, S.G. Jaras, M. Boutonnet, *Appl. Catal. A* **211** (2001) 239-250
- [83] L. Ma, C. Jiang, A.A. Adesina, D.L. Trimm, M.S. Wainwright, *Chem. Eng. J.* **62** (1996) 103-111
- [84] N. Edwards, S.R. Ellis, J.C. Frost, S.E. Golunski, A.N.J. van Keulen, N.G. Lindewald, J.G. Reinkingh, *J. Power Sources* **71** (1998) 123-128
- [85] B. Höhle, M. Boe, J. Bøgild-Hansen, P. Bröckerhoff, G. Colman, B. Emonts, R. Menzer, E. Riedel, *J. Power Sources* **61** (1996) 143-147
- [86] P. Mizsey, E. Newson, T.-B. Truong, P. Hottinger, *Appl. Catal. A* **213** (2001) 233-237
- [87] F. Panik, *J. Power Sources* **71** (1998) 36-38
- [88] T. Ioannides and S. Neophytides, *J. Power Sources* **91** (2000) 150-156
- [89] J.C. Amphlett, R.F. Mann, B.A. Peppley, P.R. Roberge, A. Rodrigues, J.P. Salvador, *J. Power Sources* **71** (1998) 179-184
- [90] N. Fujiwara, K.A. Friedrich, U. Stimming, *J. Electroanal. Chem.* **472** (1999) 120-125

- [91] X. Gong, A. Bandis, A. Tao, G. Meresi, Y. Wang, P.T. Inglefield, A.A. Jones, W.-Y. Wen, *Polymer* **42** (2001) 6485-6492
- [92] W.J. Zhou, B. Zhou, W.Z. Li, Z.H. Zhou, S.Q. Song, G.Q. Sun, Q. Xin, S. Douvartzides, M. Goula, P. Tsiakaras, *J. Power Sources* **126** (2004) 16-22
- [93] A.S. Aricò, P. Cretì, P.L. Antonucci, V. Antonucci, *Electrochem. Solid State Lett.* **1** (1998) 66-68
- [94] J. Wang, S. Wasmus, R.F. Savinell, *J. Electrochem. Soc.* **142** (1995) 4218-4224
- [95] H. Cnoblach, D. Gröppel, H. Kohlmüller, D. Kuhl, H. Poppa, G. Siemsen, *Progr. Batteries & Solar Cells* **4** (1982) 225-229
- [96] C. Lamy, *Electrochim. Acta* **29** (1984) 1581-1588
- [97] E. Peled, V. Livshits, T. Duvdevani, *J. Power Sources* **106** (2002) 245-248
- [98] H. Cnoblach, H. Kohlmüller, *27<sup>th</sup> I.S.E. Meeting*, Extended Abstract, Zurich, Sept., 1976, p. 282
- [99] Z. Qi and A. Kaufman, *J. Power Sources* **110** (2002) 65-72
- [100] Z. Qi and A. Kaufman, *J. Power Sources* **112** (2002) 121-129
- [101] Z. Qi and A. Kaufman, *J. Power Sources* **118** (2003) 54-60
- [102] Z.G. Qi, M. Hollett, A. Attia, A. Kaufman, *Electrochem. Solid State Lett.* **5** (2002) A129-A130
- [103] D. Cao and S.H. Bergens, *J. Power Sources* **124** (2003) 12-17
- [104] O. Savadogo and B. Xing, *J. New Mater. Electrochem. Systems* **3** (2000) 343-347
- [105] O. Savadogo and F.J. Rodriguez Varela, *J. New Mater. Electrochem. Systems* **4** (2001) 93-97
- [106] J.T. Wang, W.F. Lin, M. Weber, S. Wasmus, R.F. Savinell, *Electrochim. Acta* **43** (1998) 3821-3828
- [107] J.T. Müller, P.M. Urban, W.F. Hölderich, K.M. Colbow, J. Zhang, D.P. Wilkinson, *J. Electrochem. Soc.* **147** (11) (2000) 4058-4060
- [108] B.A. Adams and E.L. Holmes, Synthetic resins and their use, *Fr. Patent* **796,796** (1936)

- [109] B.A. Adams and E.L. Holmes, *Brit. Patent* **450,308** (1936)
- [110] G. D'Alelio, Ion exchanger, *US Patent* **2,366,007** (1944)
- [111] G. D'Alelio, *US Patent* **2,340,110** (1944)
- [112] G. D'Alelio, *US Patent* **2,340,111** (1944)
- [113] G.G. Scherer, *Ber. Bunsenges. Phys. Chem.* **94** (1990)1008-1014
- [114] J.A. Kerres, *J. Membr. Sci.* **185** (2001) 3-27
- [115] N. Yoshida, T. Ishisaki, A. Watakabe, M. Yoshitake, *Electrochim. Acta* **43** (1998) 3749-3754
- [116] W. Grot, *Chem. Ing. Tech.* **50** (1978) 299-301; *Chem. Ing. Tech.* **47** (1975) 617; *Chem. Ing. Tech.* **44** (1972) 167-169
- [117] O. Savadogo, *J. New Mater. Electrochem. Systems* **1** (1998) 47-66
- [118] A. Eisenberg, H.L. Yeager, Perfluorinated ionomer membranes, *ACS Symposium Series* 180, American Chemical Society, Washington, DC, 1982
- [119] A.E. Steck, Membrane materials in fuel cells, in *Proceedings of the First International Symposium on New Materials for Fuel Cell Systems* 1, O. Savadogo, P.R. Roberge, T.N. Veziroglu (Eds.), Montréal, Quebec, Canada, July 9-13, 1995, p.74
- [120] M. Eikerling, A.A. Kornyshev, U. Stimming, *J. Phys. Chem. B* **101** (1997) 10807-10820
- [121] M. Eikerling, A.A. Kornyshev, *J. Electroanal. Chem.* **502** (2001) 1-14
- [122] S.J. Paddison, *J. New Mater. Electrochem. Systems* **4** (2001) 197-207
- [123] K.A. Mauritz, C.J. Hora, A.J. Hopfinger, in *Ions in Polymers*, A. Eisenberg (Ed.), *ACS Advances in Chemistry Series 187*, American Chemical Society, Washington DC, 1980, p.124-154
- [124] H.L. Yeager and A. Steck, *J. Electrochem. Soc.* **128** (1981) 1880-1884
- [125] A. Eisenberg, B. Hird, R.B. Moore, *Macromolecules* **23** (1990) 4098-4107
- [126] T.D. Gierke, G.E. Munn, F.C. Wilson, *J. Polym. Sci. Polym. Phys. Ed.* **19** (1981) 1687-1704
- [127] K.D. Kreuer, W. Weppner, A. Rabenau, *Angew. Chem. Int. Ed. Engl.* **21** (1982) 208-209

- [128] A.T. Howe, M.G. Shilton, *J. Solid. State Chem.* **28** (1979) 345-361; A.T. Howe, M.G. Shilton *J. Solid. State Chem.* **34** (1980) 149-155 ; L. Bernard, A. Fitch, A.F. Wright, B.E.F. Fender, A.T. Howe, *Solid State Ionics* **5** (1981) 459-462
- [129] K.D. Kreuer, *Solid State Ionics* **97** (1997) 1-15
- [130] K.D. Kreuer, *Solid State Ionics* **136-137** (2000) 149-160
- [131] T.A. Zawodzinski, Jr., C. Derouin, S. Radzinski, R.J. Sherman, V.T. Smith, T.E. Springer, S. Gottesfeld, *J. Electrochem. Soc.* **140** (1993) 1041-1047
- [132] T.A. Zawodzinski, Jr., T.E. Springer, F. Urribe, S. Gottesfeld, *Solid State Ionics* **60** (1993) 199-211
- [133] J.A. Kolde, B. Bahar, M.S. Wilson, T.A. Zawodzinski, S. Gottesfeld, in *Proceeding of the First International Symposium on Proton Conducting Membrane Fuel Cells I*, S. Gottesfeld, G. Halpert, A. Landgrebe (Eds.), *The Electrochemical Society Proceedings Series*, PV 95-23, 1995, p. 193-201
- [134] J. Halim, F.N. Büchi, O. Haas, M. Stamm, G.G. Scherer, *Electrochim. Acta* **39** (1994) 1303-1307
- [135] K.M. Nouel and P.S. Fedkiw, *Electrochim. Acta* **43** (1998) 2381-2387
- [136] Y. Sone, P. Ekdunge, D. Simonsson, *J. Electrochem. Soc.* **143** (1996) 1254-1259
- [137] J.J. Sumner, S.E. Creager, J.J. Ma, D.D. DesMarteau, *J. Electrochem. Soc.* **145** (1998) 107-110
- [138] C.A. Edmondson, P.E. Stallworth, M.C. Wintersgill, J.J. Fontanella, Y. Dai, S.G. Greenbaum, *Electrochim. Acta* **43** (1998) 1295- 1299
- [139] M. Wakizoe, O.A. Velev, S. Srinivasan, *Electrochim. Acta* **40** (1995) 335-344
- [140] K.A. Mauritz and R.-M. Fu, *Macromolecules* **21** (1988) 1324-1333
- [141] B.D. Cahan and J.S. Wainright, *J. Electrochem. Soc.* **140** (1993) L185-L186
- [142] J.J. Fontanella, M.G. McLin, M.C. Wintersgill, J.P. Calame, S.G. Greenbaum, *Solid State Ionics* **66** (1993) 1-4
- [143] P.D. Beattie, F.P. Orfino, V.I. Basura, K. Zychowska, J. Ding, C. Chuy, J. Schmeisser, S. Holdcroft, *J. Electroanal. Chem.* **503** (2001) 45-56
- [144] M.W. Verbrugge and R.F. Hill, *J. Electrochem. Soc.* **137** (1990) 3770-3777

- [145] M.W. Verbrugge, E.W. Schneider, R.S. Conell, R. Hill, F. Robert, *J. Electrochem. Soc.* **139** (1992) 3421-3428
- [146] J.R. Perez, M. Lopez-Atalaya, G. Codina, J.L. Vazquez, A. Aldaz, *Bull. Electrochem.* **7** (1991) 555-558
- [147] S. Slade, S.A. Campbell, T.R. Ralph, F.C. Walsh, *J. Electrochem. Soc.* **149** (2002) A1556-A1564
- [148] F.N. Büchi and G.G. Scherer, *J. Electroanal. Chem.* **404** (1996) 37-43
- [149] P.C. Rieke and N.E. Vanderborgh, *J. Membr. Sci.* **32** (1987) 313-323
- [150] T. Lehtinen, G. Sundholm, S. Holmberg, F. Sundholm, P. Björnbom, M. Bursell, *Electrochim. Acta* **43** (12-13) (1998) 1881-1890
- [151] B. Baradie, J.P. Dodelet, D. Guay, *J. Electroanal. Chem.* **489** (2000) 101-105
- [152] C. Pu, W. Huang, K.L. Ley, E.S. Smotkin, *J. Electrochem. Soc.* **142** (1995) L119-L120
- [153] W.C. Choi, J.D. Kim, S.I. Woo, *J. Power Sources* **96** (2001) 411-414
- [154] Z.Q. Ma, P. Cheng, T.S. Zhao, *J. Membr. Sci.* **215** (2003) 327-336
- [155] J. Feichtinger, R. Galm, M. Walker, K.-M. Baumgärtner, A. Schulz, E. Räu­chle, U. Schumacher, *Surf. Coat. Technol.* **142-144** (2001) 181-186
- [156] M. Walker, K.-M. Baumgärtner, J. Feichtinger, M. Kaiser, E. Räu­chle, J. Kerres, *Surf. Coat. Technol.* **116-119** (1999) 996-1000
- [157] L.J. Hobson, H. Ozu, M. Yamaguchi, S. Hayase, *J. Electrochem. Soc.* **148** (2001) A1185-A1190
- [158] R. Zeng, Z. Pang, H. Zhu, *J. Electroanal. Chem.* **490** (2000) 102-106
- [159] R. Savinell, E. Yeager, D. Tryk, U. Landau, J. Wainright, D. Weng, K. Lux, M. Litt, C. Rogers, *J. Electrochem. Soc.* **141** (1994) L46-L48
- [160] D. Weng, J.S. Wainright, U. Landau, R.F. Savinell, *Proceeding of the First International Symposium on Proton Conducting Membrane Fuel Cells I*, S. Gottesfeld, G. Halpert, A. Landgrebe (Eds.), *Electrochemical Society Proceedings Series*, PV 95-23, 1995, p. 214-225

- [161] S. Wasmus, A. Valeriu, G.D. Mateescu, D.A. Tryk, R.F. Savinell, *Solid State Ionics* **80** (1995) 87-92
- [162] K.W. Lux, J.S. Wainright, R.F. Savinell, U. Landau, in *Proceeding of Symposium on Electrode Materials and Processes for Energy Conversion and Storage*, S. Srinivasan, D.D. Macdonald, A.C. Khandkar (Eds.), *Electrochemical Society Proceedings Series*, PV 94-23, 1994, p. 302-315
- [163] K.W. Lux, J.S. Wainright, R.F. Savinell, U. Landau, in *Proceeding of Symposium on Electrode Materials and Processes for Energy Conversion and Storage*, S. Srinivasan, D.D. Macdonald, A.C. Khandkar (Eds.), *Electrochemical Society Proceedings Series*, PV 94-23, 1994, p. 201-219
- [164] C.R. Martin, T.A. Rhoades, J.A. Ferguson, *Anal. Chem.* **54** (1982) 1639-1641
- [165] R.B. Moore, III and C.R. Martin, *Anal. Chem.* **58** (1986) 2569-2570
- [166] R.B. Moore, III and C.R. Martin, *Macromolecules* **21** (1988) 1334-1339
- [167] G. Gebel, P. Aldebert, M. Pineri, *Macromolecules* **20** (1987) 1425-1428
- [168] R.M. Penner and C.R. Martin, *J. Electrochem. Soc.* **132** (1985) 514-515
- [169] C. Liu and C.R. Martin, *J. Electrochem. Soc.* **137** (1990) 510-515
- [170] C. Liu and C.R. Martin, *J. Electrochem. Soc.* **137** (1990) 3114-3120
- [171] M.W. Verbrugge, R.F. Hill, E.W. Schneider, *AIChE J.* **38** (1992) 93-100
- [172] B. Bahar, A.R. Hobson, J.A. Kolde, D. Zuckerbrod, *U.S. Patent* **5,547,551** (1996)
- [173] S.H. Kwak, D.H. Peck, Y.G. Chun, C.S. Kim, K.H. Yoon, *J. New Mater. Electrochem. Systems* **4** (2001) 25-29
- [174] J. Shim, H.Y. Ha, S.-A. Hong, I.-H. Oh, *J. Power Sources* **109** (2002) 412-417
- [175] B. Bae, B.-H. Chun, H.-Y. Ha, I.-H. Oh, D. Kim, *J. Membr. Sci.* **202** (2002) 245-252
- [176] F. Liu, B. Yi, D. Xing, J. Yu, H. Zhang, *J. Membr. Sci.* **212** (2003) 213-223
- [177] S. Haufe and U. Stimming, *J. Membr. Sci.* **185** (2001) 95-103
- [178] S. Hommura, Y. Kunisa, I. Terada, M. Yoshitake, *J. Fluorine Chemistry* **120** (2003) 151-155
- [179] V. Tricoli, *J. Electrochem. Soc.* **145** (1998) 3798-3801

- [180] M. Watanabi, H. Uchida, M. Emori, *J. Phys. Chem. B* **102** (1998) 3129-3137
- [181] A. Steck, C. Stone, in *Proceedings of the Second International Symposium on New Materials for Fuel Cell and Modern Battery Systems*, O. Savadogo, P.R. Roberge (Eds.), Montréal, Canada, July 6-10, 1997, p.792-807
- [182] J. Wei, C. Stone, A.E. Steck, *US Patent* **5,422,411** (1995)
- [183] J. Wei, C. Stone, A.E. Steck, Trifluorostyrene and substituted trifluorostyrene copolymeric compositions and ion-exchange membranes formed therefrom, Ballard Power Systems, **WO 95/08581**, 30 March 1995
- [184] D.I. Livingston, P.M. Kamath, R.S. Corley, *J. Polym. Sci.* **20** (1956) 485-490
- [185] G.G. Scherer, F.N. Büchi, B. Gupta, *Polym. Mater. Sci. Eng.* **68** (1993) 114
- [186] B. Gupta, F.N. Büchi, G.G. Scherer, A. Chapiro, *Solid State Ionics* **61** (1993) 213-218
- [187] F.N. Büchi, B. Gupta, O. Haas, G.G. Scherer, *Electrochim. Acta* **40** (3) (1995) 345-353
- [188] F.N. Büchi, B. Gupta, O. Haas, G.G. Scherer, *J. Electrochem. Soc.* **142** (1995) 3044-3048
- [189] H.P. Brack, F.N. Büchi, J. Huslage, G.G. Scherer, *Proton Conducting Membrane Fuel Cells II*, S. Gottesfeld, T.F. Fuller (Eds.), *The Electrochemical Society Proceedings*, PV 98-27, 1999, p. 52-65
- [190] H.P. Brack, F.N. Büchi, J. Huslage, M. Rota, G.G. Scherer, *ACS Symposium Series No 744*, Washington DC, 2000, p. 174-188
- [191] P. Gode, J. Itonen, A. Strandroth, H. Ericson, G. Lindbergh, M. Paronen, F. Sundholm, G. Sundholm, N. Walsby, *Fuel Cells* **3** (1-2) (2003) 21-27
- [192] H.P. Brack, M. Wyler, G. Peter, G.G. Scherer, *J. Membr. Sci.* **214** (2003) 1-19
- [193] W. Lee, A. Shibasaki, K. Saito, K. Sugita, K. Okuyama, T. Sugo, *J. Electrochem. Soc.* **143** (1996) 2795-2798
- [194] T. Hatanaka, N. Hasegawa, A. Kamiya, M. Kawasumi, Y. Morimoto, K. Kawahara, *Fuel* **81** (2002) 2173-2176



- [195] B. Gupta, F.N. Büchi, G.G. Scherer, *J. Polym. Sci. A: Polym. Chem.* **32** (1994) 1931-1938
- [196] B. Gupta and G.G. Scherer, *Chimia* **48** (1994) 127-137
- [197] F. Sundholm, New Polymer Electrolytes for Low Temperature Fuel Cells, in *Proceedings of the 9<sup>th</sup> International Conference on Solid State Protonic Conductors SSPC'98*, Extended Abstract Book, Bled, Slovenia, 17-21 August, 1998, p. 155-158
- [198] D.J. Jones and J. Rozière, *J. Membr. Sci.* **185** (2001) 41-58
- [199] D. Hoel and E. Grunwald, *J. Phys. Chem.* **81** (1977) 2135-2136
- [200] X. Glipta, M. El Haddad, D.J. Jones, J. Rozière, *Solid State Ionics* **97** (1997) 323-331
- [201] E.D. Powers and G.A. Serad, in *High Performance Polymers: Their Origin and Development*, R.B. Seymour, G.S. Kirschenbaum (Eds.), Elsevier, Amsterdam, 1986, p. 355
- [202] S.M. Aharoni and M.H. Litt, *J. Polym. Sci., Polym. Chem. Ed.* **12** (1974) 639-650
- [203] J.S. Wainright, R.F. Savinell, M.H. Litt, in *Proceedings of the Second International Symposium on New Materials for Fuel Cell and Modern Battery Systems*, O. Savadogo, P.R. Roberge (Eds.), Montréal, Canada, July 6-10, 1997, p. 808-817
- [204] J.S. Wainright, J.-T. Wang, D. Weng, R.F. Savinell, M. Litt, *J. Electrochem. Soc.* **142** (1995) L121-L123
- [205] J.-T. Wang, R.F. Savinell, J. Wainright, M. Litt, H. Yu, *Electrochim. Acta* **41** (1996) 193-197
- [206] S.R. Samms, S. Wasmus, R.F. Savinell, *J. Electrochem. Soc.* **143** (1996) 1225-1232
- [207] J.-T. Wang, J.S. Wainright, R.F. Savinell, M. Litt, *J. Appl. Electrochem.* **26** (7) (1996) 751-756
- [208] B. Xing and O. Savadogo, *J. New Mater. Electrochem. Systems* **2** (1999) 95-101
- [209] Y.-L. Ma, J.S. Wainright, M.H. Litt, R.F. Savinell, *J. Electrochem. Soc.* **151** (2004) A8-A16

- [210] S. Faure, N. Cornet, G. Gebel, R. Mercier, M. Pineri, B. Sillion, in *Proceeding of the Second International Symposium on New Materials for Fuel Cell and Modern Battery Systems*, O. Savadogo, P.R. Roberge (Eds.), Montréal, Canada, July 6-10, 1997, p. 818
- [211] S. Faure, R. Mercier, P. Aldebert, M. Pineri, B. Sillion, *Fr. Patent* **96 05707** (1996)
- [212] G. Gebel, P. Aldebert, M. Pineri, *Polymer* **34** (1993) 333-339
- [213] N. Cornet, O. Diat, G. Gebel, F. Jousse, D. Marsaq, R. Mercier, M. Pineri, *J. New Mater. Electrochem. Systems* **3** (2000) 33-42
- [214] Y. Woo, S.Y. Oh, Y.S. Kang, B. Jung, *J. Membr. Sci.* **220** (2003) 31-45
- [215] Y. Zhang, M. Litt, R.F. Savinell, J.S. Wainright, J. Vendramini, *Polym. Prepr.* **41** (2000) 1561-1562
- [216] N. Gunduz and J.E. McGrath, *Polym. Prepr.* **41** (2000) 182-183
- [217] C. Genies, R. Mercier, B. Sillion, N. Cornet, G. Gebel, M. Pineri, *Polymer* **42** (2001) 359-373
- [218] X. Guo, J. Fan, T. Watari, K. Tanaka, H. Kita, K. Okamoto, *Macromolecules* **35** (2002) 6707-6713
- [219] J. Fan, X. Guo, S. Harada, T. Watari, K. Tanaka, H. Kita, K. Okamoto, *Macromolecules* **35** (2002) 9022-9028
- [220] R. Wycisk and P.N. Pintauro, *J. Membr. Sci.* **119** (1996) 155-160
- [221] Q. Guo, P.N. Pintauro, H. Tang, S. O'Connor, *J. Membr. Sci.* **154** (1999) 175-181
- [222] H. Tang, P.N. Pintauro, Q. Guo, S. O'Connor, *J. Appl. Polym. Sci.* **71** (1999) 387-399
- [223] H.R. Allcock, M.A. Hofmann, C.M. Ambler, R.V. Morford, *Macromolecules* **35** (2002) 3484-3489
- [224] H.R. Allcock, M.A. Hofmann, C.M. Ambler, S.N. Lvov, X.Y. Zhou, E. Chalkova, J. Weston, *J. Membr. Sci.* **201** (2002) 47-54
- [225] X.Y. Zhou, M.A. Hofmann, J.A. Weston, E. Chalkova, H.R. Allcock, S.N. Lvov, in *Direct Methanol Fuel Cells*, S. Narayanan, T. Zawodzinski, S.

- Gottesfeld (Eds.), *The Electrochemical Society Proceedings Series*, Pennington, NJ, 2002, p. 34-41
- [226] X. Zhou, J. Weston, E. Chalkova, M.A. Hofmann, C.M. Ambler, H.R. Allcock, S.N. Lvov, *Electrochim. Acta* **48** (2003) 2173-2180
- [227] B.C. Johnson, I. Yilgor, C. Tran, M. Iqbal, J.P. Wightman, D.R. Llyod, J.E. McGrath, *J. Polym. Sci.* **22** (1984) 721-737
- [228] R. Nolte, K. Ledjeff, M. Bauer, R. Mulhaupt, *J. Membr. Sci.* **83** (1993) 211-220
- [229] J. Kerres, A. Ullrich, F. Meier, T. Häring, *Solid State Ionics* **125** (1999) 243-249
- [230] J. Kerres, W. Cui, S. Reichle, *J. Polym. Sci.: Part A: Polym. Chem.* **34** (1996) 2421-2438
- [231] J. Kerres, W. Cui, R. Disson, W. Neubrand, *J. Membr. Sci.* **139** (1998) 211-225
- [232] B. Baradie, C. Poinignon, J.Y. Sanchez, Y. Piffard, G. Vitter, N. Bestaoui, D. Foscallo, A. Denoyelle, D. Delabouglise, M. Vaujany, *J. Power Sources* **74** (1998) 8-16
- [233] F. Lufrano, G. Squadrito, A. Patti, E. Passalacqua, *J. Appl. Polym. Sci.* **77** (2000) 1250-1257
- [234] F. Lufrano, I. Gatto, P. Staiti, V. Antonucci, E. Passalacqua, *Solid State Ionics* **145** (2001) 47-51
- [235] Y.S. Kim, L. Dong, M.A. Hickner, B.S. Pivovar, J.E. McGrath, *Polymer* **44** (2003) 5729-5736
- [236] W. Cui, J. Kerres, G. Eigenberger, *Sep. Purif. Technol.* **14** (1998) 145-154
- [237] M. Walker, K.-M. Baurngdrtnr, M. Kaiser, *et al.*, *J. Appl. Polym. Sci.* **74** (1999) 67-73
- [238] W. Preidel, M. Baldauf, U. Gebhardt, J. Kerres, A. Ullrich, G. Eigenberger, in *Extended Abstract of the 3<sup>rd</sup> International Symposium on New Materials for Electrochemical Systems*, Montréal, Canada, 4-8 July, 1999, p. 233-234
- [239] J. Kerres, A. Ullrich, T. Häring, M. Baldauf, U. Gebhardt, W. Preidel, *J. New Mater. Electrochem. Systems* **3** (2000) 229-239

- [240] L. Jörissen, V. Gogel, J. Kerres, J. Garche, *J. Power Sources* **105** (2002) 267-273
- [241] W. Zhang, C.-M. Tang, J. Kerres, *Sep. Purif. Technol.* **22-23** (2001) 209-221
- [242] J. Kerres, W. Cui, W. Schnurnberger, *D. Patent* **19622337.7** (1997); *Fr. Patent F. 9706706* (1997); *US Patent 08/868943* (1997)
- [243] J. Kerres, W. Zhang, W. Cui, *J. Polym. Sci.: Part A: Polym. Chem.* **36** (1998) 1441-1448
- [244] J. Kerres, W. Cui, M. Junginger, *J. Membr. Sci.* **139** (1998) 227-241
- [245] L. Jörissen, J. Kerres, V. Gogel, A. Ullrich, Th. Häring, in *Proceedings of the 11<sup>th</sup> Annual Conference of the North American Membrane Society, NAMS2000*, Boulder, CO, USA, 23-27 May, 2000
- [246] A. Schneller, H. Ritter, K. Ledjeff, R. Nolte, R. Thorwirth, *EP* **0574791 A2** (1993)
- [247] C. Bailly, D.J. Williams, F.E. Karasz, W.J. MacKnight, *Polymer* **28** (1987) 1009-1016
- [248] F. Helmer-Metzmann *et al.*, *EP* **0 574 791 A2**, Hoechst AG, 1993
- [249] B. Bauer, Th. Menzel, P. Kehl, *EP* **0 645 175 A1** (1994)
- [250] B. Bauer, G. Rafler, H.-H. Ulrich, *Ger. Patent* **DE 195 38 025** (1995)
- [251] K.D Kreuer, *J. Membr. Sci.* **185** (2001) 29-39
- [252] J.C. Lasségues, *Mixed inorganic-organic systems: the acid/polymer blends*, in *Proton Conductors: Solids, Membranes and Gels – Materials and Devices*, Ph. Colomban (Ed.), Chapter 20, Cambridge University Press, Cambridge, 1992, p. 311-328
- [253] C.A. Linkous, H.R. Anderson, R.W. Kopitzke, G.L Nelson, *Int. J. Hydrogen Energy* **23** (1998) 525-529
- [254] S.M.J. Zaidi, S.D. Mikhailenko, G.P. Robertson, M.D. Guiver, S. Kaliaguine, *J. Membr. Sci.* **173** (2000) 17-34
- [255] G. Alberti, M. Casciola, L. Massinelli, B. Bauer, *J. Membr. Sci.* **185** (2001) 73-81

- [256] B. Bauer, D.J. Jones, J. Rozière, L. Tchicaya, G. Alberti, M. Casciola, L. Massinelli, A. Peraio, S. Besse, E. Ramunni, *J. New Mater. Electrochem. Systems* **3** (2000) 93-98
- [257] T. Kobayashi, M. Rikukawa, K. Sanui, N. Ogata, *Solid State Ionics* **106** (1998) 219-225
- [258] P. Xing, G.P. Robertson, M.D. Guiver, S.D. Mikhailenko, K. Wang, S. Kaliaguine, *J. Membr. Sci.* **229** (2004) 95-106
- [259] T. Soczka-Guth, J. Baurmeister, G. Frank, R. Knauf, *International Patent WO 99/29763* (1999)
- [260] G. Hubner and E. Roduner, *J. Mater. Chem.* **9** (1999) 409-418
- [261] S.-P.S. Yen, S.R. Narayanan, G. Halpert, E. Graham, A. Yavrouian, *US Patent 5,795,496* (1998)
- [262] B. Bonnet, D.J. Jones, J. Rozière, L. Tchicaya, G. Alberti, M. Casciola, L. Massinelli, D. Bauer, A. Peraio, E. Ramunni, *J. New Mater. Electrochem. Systems* **3** (2000) 87-92
- [263] M. Watanabe, H. Uchida, Y. Seki, M. Emori, P. Stonehart, *J. Electrochem. Soc.* **143** (1996) 3847-3852
- [264] P.L. Antonucci, A.S. Aricò, P. Cretì, E. Ramunni, V. Antonucci, *Solid State Ionics* **125** (1999) 431-437
- [265] V. Antonuccia and A. Aricò, *European Patent EP 0 926 754 A1*, 1999
- [266] T. Arimura, D. Ostrovskii, T. Okada, G. Xie, *Solid State Ionics* **118** (1999) 1-10
- [267] K.T. Adjemian, S. Srinivasan, J. Benziger, A.B. Bocarsly, *J. Power Sources* **109** (2002) 356-364
- [268] P. Dimitrova, K.A. Friedrich, B. Vogt, U. Stimming, *J. Electroanal. Chem.* **532** (2002) 75-83
- [269] P. Dimitrova, K.A. Friedrich, U. Stimming, B. Vogt, *Solid State Ionics* **150** (2002) 115-122
- [270] D.H. Jung, S.Y. Cho, D.H. Peck, D.R. Shin, J.S. Kim, *J. Power Sources* **106** (2002) 173-177

- [271] Q. Deng, R.B. Moore, K.A. Mauritz, *J. Appl. Polym. Sci.* **68** (1998) 747-763
- [272] K.A. Mauritz, I.D. Stefanithis, S.V. Davis, R.W. Scheetz, R.K. Pope, G.L. Wilkes, H.-H. Huang, *J. Appl. Polym. Sci.* **55** (1995) 181-190
- [273] K.A. Mauritz, *Mater. Sci. Eng. C* **6** (1998) 121-133
- [274] P. Staiti, A.S. Aricò, V. Baglio, F. Lufrano, E. Passalacqua, V. Antonucci, *Solid State Ionics* **145** (2001) 101-107
- [275] Z.-G. Shao, P. Joghee, I.-M. Hsing, *J. Membr. Sci.* **229** (2004) 43-51
- [276] A.S. Aricò, V. Baglio, A. Di Blasi, V. Antonucci, *Electrochem. Communications* **5** (2003) 882-866
- [277] A.S. Aricò, V. Baglio, A. Di Blasi, P. Cretì, P.L. Antonucci, V. Antonucci, *Solid State Ionics* **161** (2003) 251-265
- [278] W.G. Grot and G. Rajendran, *US Patent* **5,919,583** (1999)
- [279] C. Yang, P. Costamagna, S. Srinivasan, J. Benziger, A.B. Bocarsly, *J. Power Sources* **103** (2001) 1-9
- [280] C. Yang, S. Srinivasan, A.S. Aricò, P. Cretì, V. Baglio, V. Antonucci, *Electrochem. Solid State Lett.* **4** (2001) A31-A34
- [281] P. Costamagna, C. Yang, A.B. Bocarsly, S. Srinivasan, *Electrochim. Acta* **47** (2002) 1023-1033
- [282] B. Tazi and O. Savadogo, in *Proceedings of the Second International Symposium on New Materials for Fuel Cell and Modern Battery Systems*, O. Savadogo, P.R. Roberge (Eds.), Montréal, Canada, July 6-10, 1997, p. 864
- [283] B. Tazi and O. Savadogo, *Electrochim. Acta* **45** (2000) 4329-4339
- [284] W. Apichatachutapan, R.B. Moore, K.A. Mauritz, *J. Appl. Polym. Sci.* **62** (1996) 417-426
- [285] N. Jia, M.C. Lefebvre, J. Halfyard, Z. Qi, P.G. Pickup, *Electrochem. Solid-State Lett.* **3** (12) (2000) 529-531
- [286] K.D. Kreuer, A. Fuchs, M. Ise, M. Spaeth, J. Maier, *Electrochim. Acta* **43** (1998) 1281-1288

- [287] K.D. Kreuer, *New Proton conducting polymers for fuel cell applications*, in *Solid State Ionics: Science and Technology*, B.V.R. Chowdari *et al.* (Eds.), Singapore, World Science Publishing Co., 1998, p. 263-274
- [288] P. Genova-Dimitrova, B. Baradie, D. Foscallo, C. Poinignon, J.Y. Sanchez, *J. Membr. Sci.* **185** (2001) 59-71
- [289] S.P. Nunes, B. Ruffmann, E. Rikowski, S. Vetter, K. Richau, *J. Membr. Sci.* **203** (2002) 215-225
- [290] M.L. Ponce, L. Prado, B. Ruffmann, K. Richau, R. Mohr, S.P. Nunes, *J. Membr. Sci.* **217** (2003) 5-15
- [291] B. Ruffmann, H. Silva, B. Schulte, S.P. Nunes, *Solid State Ionics* **162-163** (2003) 269-275
- [292] V.N. Belyakov and V.M. Linkov, *US Patent 5,932,361* (1999)
- [293] G. Alberti, M. Casciola, L. Boccali, L. Massinelli, E. Montoneri, *Solid State Ionics* **84** (1996) 97-104
- [294] P. Staiti, M. Minutoli, S. Hocevar, *J. Power Sources* **90** (2000) 231-235
- [295] P. Staiti and M. Minutoli, *J. Power Sources* **94** (2001) 9-13
- [296] Y.-I. Park and M. Nagai, *Solid State Ionics* **145** (2001) 149-160
- [297] I. Honma, S. Hirakawa, K. Yamada, J.M. Bae, *Solid State Ionics* **118** (1999) 29-36
- [298] I. Honma, Y. Takeda, J.M. Bae, *Solid State Ionics* **120** (1999) 255-264
- [299] I. Honma, S. Nomura, H. Nakajima, *J. Membr. Sci.* **185** (2001) 83-94
- [300] H. Schmidt, M. Popall, F. Rousseau, C. Poinignon, M. Armand, J.Y. Sanchez, in *Second Intern. Symp. on Polymer Electrolyte*, B. Scrosati (Ed.), Elsevier, London, 1990, p.325
- [301] I. Gautier-Luneau, A. Denoyelle, J.Y. Sanchez, C. Poinignon, *Electrochim. Acta* **37** (1992) 1615-1618
- [302] M. Popall and X.-M. Du, *Electrochim. Acta* **40** (1995) 2305-2308
- [303] L. Depre, J. Kappel, M. Popall, *Electrochim. Acta* **43** (1998) 1301-1306
- [304] L. Depre, M. Ingram, C. Poinignon, M. Popall, *Electrochim. Acta* **45** (2000) 1377-1383

- [305] S. Jacob, S. Cochet, C. Poinsignon, M. Popall, *Electrochim. Acta* **48** (2003) 2181-2186
- [306] S.G. Ehrenberg, J.M. Serpico, G.E. Wnek, J.N. Rider, *US Patent* **5,468,574** (1995)
- [307] G.E. Wnek, J.N. Rider, J.M. Serpico, A.G. Einset, S.G. Ehrenberg, L. Raboin, in *Proceeding of the First International Symposium on Proton Conducting Membrane Fuel Cells*, S. Gottesfeld, G. Halpert, A. Landgrebe (Eds.), *The Electrochemical Society Proceedings*, PV 95-23, 1995, p.247
- [308] S.G. Ehrenberg, J.M. Serpico, B.M. Sheikh-Ali, T.N. Tangredi, E. Zador, G.E. Wnek, in *Proceedings of the Second International Symposium on New Materials for Fuel Cell and Modern Battery Systems*, O. Savadogo, P.R. Roberge (Eds.), Montréal, Canada, July 6-10, 1997, p.828
- [309] N. Carretta, V. Tricoli, F. Picchioni, *J. Membr. Sci.* **166** (2000) 189-197
- [310] T. Yamaguchi, F. Miyata, S.-I. Nakao, *J. Membr. Sci.* **214** (2003) 283-292
- [311] S. Petty-Weeks, J.J. Zupancic, J.R. Swedo, *Solid State Ionics* **31** (1988) 117-125
- [312] J. Przyluski, W. Wieczorek, S. Glowinkowski, *Electrochim. Acta* **37** (1992) 1733-1735
- [313] W. Wieczorek, K. Such, Z. Florjanczyk, J.R. Stevens, *J. Phys. Chem.* **98** (1994) 6840-6850
- [314] G. Alberti and M. Casciola, *Solid State Ionics* **145** (2001) 3-16
- [315] M. Casciola, U. Costantino, *Solid State Ionics* **20** (1986) 69-73
- [316] G. Alberti, M. Casciola, U. Costantino, A. Peraio, T. Rega, *J. Mater. Chem.* **5** (1995) 1809-1812
- [317] G. Alberti, M. Casciola, L. Massinelli, R. Palombari, *Ionics* **2** (1996) 179-183
- [318] G. Alberti, M. Casciola, *Solid State Ionics* **97** (1997) 177-186
- [319] G. Alberti, M. Casciola, U. Costantino, A. Peraio, E. Montoneri, *Solid State Ionics* **50** (1992) 315-322
- [320] G. Alberti, M. Casciola, R. Palombari, A. Peraio, *Solid State Ionics* **58** (1992) 339-344
- [321] G. Alberti, M. Casciola, R. Palombari, *J. Membr. Sci.* **172** (2000) 233-239



- [322] O. Nakamura, I. Ogino, T. Kodama, *Solid State Ionics* **3-4** (1981) 347-351
- [323] K.-D. Kreuer, *J. Mol. Struct.* **177** (1988) 265-276
- [324] A.I. Baranov, L.A. Shuvalov, N.M. Shchagina, *JETP Lett.* **36** (1982) 459
- [325] N. Knudsen, E. Krogh Andersen, I.G. Krogh Andersen, E. Skou, *Solid State Ionics* **35** (1989) 51-55
- [326] D.J. Jones, J. Rozière, *Solid State Ionics* **61** (1993) 13-22
- [327] Z. Poltarzewski, W. Wiczorek, J. Przyłuski, V. Antonucci, *Solid State Ionics* **119** (1999) 301-304
- [328] T. Kenjo and Y. Ogawa, *Solid State Ionics* **76** (1995) 29-34
- [329] M. Cappadonia, O. Niemzig, U. Stimming, *Solid State Ionics* **125** (1999) 333-337
- [330] D.A. Boysen, C.R.I. Chisholm, S.M. Haile, S.R. Narayanan, *J. Electrochem. Soc.* **147** (2000) 3610-3613
- [331] K.A. Kraus, H.O. Phillips, *J. Am. Chem. Soc.* **78** (1956) 694
- [332] K.A. Kraus, *Chem. Eng. News* **34** (1956) 4760
- [333] C.B. Amphlett, L.A. McDonald, M.J. Redman, *J. Inorg. Nucl. Chem.* **6** (1958) 220-235
- [334] C.B. Amphlett, L.A. McDonald, J.S. Burgess, J.C. Maynard, *J. Inorg. Nucl. Chem.* **10** (1959) 69-73
- [335] C.B. Amphlett, P. Eaton, L.A. McDonald, A.J. Miller, *J. Inorg. Nucl. Chem.* **26** (1964) 297-304
- [336] E.M. Larsen and D.R. Vessers, *J. Phys. Chem.* **64** (1960) 1732-1734
- [337] A. Clearfield and J.A. Stynes, *J. Inorg. Nucl. Chem.* **26** (1964) 117-129
- [338] A. Clearfield, W.L. Duax, A.S. Medina, G.D. Smith, J.R. Thomas, *J. Phys. Chem.* **73** (1969) 3424-3430
- [339] A. Clearfield and G.D. Smith, *Inorg. Chem.* **8** (1969) 431-436
- [340] A. Clearfield and J.M. Troup, *J. Phys. Chem.* **77** (1973) 243-247
- [341] A. Clearfield, L. Kullberg, A. Oskarsson, *J. Phys. Chem.* **78** (1974) 1150-1153
- [342] J.M. Troup and A. Clearfield, *Inorg. Chem.* **16** (1977) 3311-3314
- [343] A. Clearfield and Z. Wang, *J. Chem. Soc. Dalton Trans.* (2002) 2937-2947

- [344] G. Alberti and E. Torracca, *J. Inorg. Nucl. Chem.* **30** (1968) 317-318
- [345] G. Alberti, U. Costantino, *J. Chromatography* **102** (1974) 5-29
- [346] G. Alberti, M. Casiola, U. Costantino, G. Levi, G. Ricciardi, *J. Inorg. Nucl. Chem.* **40** (1978) 533-537
- [347] G. Alberti, *Atti. Accad. Naz. Lincei. Cl. Fis. Mat. Nat. Rend.* **31** (1961) 427-428
- [348] R.P. Hamlen, *J. Electrochem. Soc.* **109** (1962) 746-749
- [349] A. Dravnieks and J.I. Bregman, *Fuel Cell Symposium of the Electrochemical Society*, Detroit, Oct. 1-5, 1961, as Abstract 27
- [350] A. Dravnieks, D.B. Bois, J.I. Bregman, *16<sup>th</sup> Annual Power Sources Conference, Session of Fuel Cell Materials and Mechanism*, May 22-24, 1962, pp. 4-6
- [351] A. Dravnieks and J.I. Bregman, *Chem. Eng. News*, Oct. 16, 1961, p. 40
- [352] R.P. Hamlen and E.J. Szymalak, *Electrochem. Technol.* **4** (1966) 172
- [353] C. Berger and M.P. Strier, *J. Electrochem. Soc.* **115** (1968) 230-233
- [354] Y. Abe, G. Li, M. Nogami, T. Kasuga, L.L. Hench, *J. Electrochem. Soc.* **143** (1996) 144-147
- [355] Y.-I. Park, J.-D. Kim, M. Nagai, *J. Material Science Letters* **19** (2000) 1735-1738
- [356] J. Tamura, Y. Katayama, T. Miura, *Electrochemistry (Tokyo, Japan)* **70** (12) (2002) 956-957
- [357] G. Alberti *et al.* *J. Inorg. Nucl. Chem.* **37** (1975) 1779-1786
- [358] S. Ahrland, J. Albertsson, A. Oskarsson, A. Niklasson, *J. Inorg. Nucl. Chem.* **32** (1970) 2069-2078
- [359] E. Krogh Andersen, I.G. Krogh Andersen, C. Knakkegård Møller, K.E. Simonsen, E. Skou, *Solid State Ionics* **7** (1982) 301-306
- [360] A. Hamnett, *Catalysis Today* **38** (1997) 445-457
- [361] R. Parsons and T.J. VanderNoot, *J. Electroanal. Chem.* **257** (1988) 9-45
- [362] R. Inada, K. Shimazu, H. Kita, *J. Electroanal. Chem.* **277** (1990) 315-326
- [363] T. Frelink, W. Visscher, J.A.R. van Veen, *Surf. Sci.* **335** (1995) 353-360
- [364] W. Vielstich and T. Iwasita, in *Handbook of Heterogeneous Catalysis*, G. Ertl,

- H. Knözinger, J. Weitkamp (Eds.), Vol. 4, Wiley, Chichester, 1997
- [365] S. Wasmus and A. Küver, *J. Electroanal. Chem.* **461** (1999) 14-31
- [366] B. Beden, J.-M. Léger, C. Lamy, in *Modern Aspects of Electrochemistry*, J. O'M. Bockris, B.E. Conway, R.E. White (Eds.), Vol. 22, Plenum Press, New York, 1992, p. 97-247
- [367] J.-M. Léger and C. Lamy, *Ber. Bunsenges. Phys. Chem.* **94** (1990) 1021-1025
- [368] A. Papoutsis, J.-M. Léger, C. Lamy, *J. Electroanal. Chem.* **359** (1993) 141-160
- [369] E. Herrero, K. Franaszczuk, A. Wieckowski, *J. Phys. Chem.* **98** (1994) 5074-5083
- [370] P.C. Biswas, Y. Nodasaka, M. Enyo, *J. Appl. Electrochem.* **26** (1996) 30-35
- [371] G.T. Burstein, C.J. Barnett, A.R. Kucernak, K.R. Williams, *Catalysis Today* **38** (1997) 425-437
- [372] W.-F. Lin, J.-T. Wang, R.F. Savinell, *J. Electrochem. Soc.* **144** (1997) 1917-1922
- [373] Y. Zhu, H. Uchida, T. Yajima, M. Watanabe, *Langmuir* **17** (2001) 146-154
- [374] P.A. Christensen, A. Hamnett, G.L. Troughton, *J. Electroanal. Chem.* **362** (1993) 207-218
- [375] D. Pletcher and V. Solis, *Electrochim. Acta* **27** (1982) 775-782
- [376] J. Sobkowski and A. Wieckowski, *J. Electroanal. Chem.* **41** (1973) 373-379
- [377] D.N. Upadhyay, V. Yegnaraman, G. Prabhakara Rao, *J. Power Sources* **36** (1991) 11-16
- [378] K. Yahikozawa, Y. Fujii, Y. Matsuda, K. Nishimura, Y. Takasu, *Electrochim. Acta* **36** (1991) 973-978
- [379] K. Kinoshita, *J. Electrochem. Soc.* **137** (1990) 845-848
- [380] Y. Takasu, Y. Fujii, Y. Matsuda, *Bull. Chem. Soc. Jpn.* **59** (1986) 3973-3974
- [381] P.A. Attwood, B.D. McNicol, R.T. Short, J.A van Amstel, *J. Chem. Soc. Farad. Trans. I* **76** (1980) 2310-2321
- [382] B.D. McNicol, P.A. Attwood, R.T. Short, *J. Chem. Soc. Farad. Trans. I* **77** (1981) 2017-2028

- [383] B.J. Kennedy and A. Hamnett, *J. Electroanal. Chem.* **283** (1990) 271-285
- [384] J.B. Goodenough, A. Hamnett, B.J. Kennedy, S.A. Weeks, *Electrochim. Acta* **32** (1987) 1233-1238
- [385] L.D. Burke and J.K. Casey, *Ber. Bunsenges. Phys. Chem.* **94** (1990) 931-937
- [386] M. Watanabe, S. Saegusa, P. Stonehart, *J. Electroanal. Chem.* **271** (1989) 213-220
- [387] T. Frelink, W. Visscher, J.A.R. van Veen, *J. Electroanal. Chem.* **382** (1995) 65-72
- [388] R.A. Lampitt, L.P.L. Carrette, M.P. Hogarth, A.E. Russell, *J. Electroanal. Chem.* **460** (1999) 80-87
- [389] B. Beden, C. Lamy, A. Bewick, K. Kunimatsu, *J. Electroanal. Chem.* **121** (1981) 343-347
- [390] W. Vielstich, P.A. Christensen, S.A. Weeks, A. Hamnett, *J. Electroanal. Chem.* **242** (1988) 327-333
- [391] P.A. Christensen, A. Hamnett, S.A. Weeks, *J. Electroanal. Chem.* **250** (1988) 127-142
- [392] T. Iwasita and W. Vielstich, *J. Electroanal. Chem.* **250** (1988) 451-456
- [393] K.J. Kunimatsu, *J. Electroanal. Chem.* **145** (1985) 219-224
- [394] B. Bedan, F. Hahn, S. Juanto, C. Lamy, J.-M. Léger, *J. Electroanal. Chem.* **225** (1987) 215-225
- [395] R.J. Nichols and A. Bewick, *Electrochim. Acta* **33** (1988) 1691-1694
- [396] T.D. Jarvi and E.M. Stuve, in *Electrocatalysis*, J. Lipkowski, P.N. Ross (Eds.), Wiley/VCH, New York, 1988, p.75
- [397] L.-W.H. Leung and M.J. Weaver, *Langmuir* **6** (1990) 323-333
- [398] N.M. Marković, H.A. Gasteiger, P.N. Ross Jr., X. Jiang, I. Villegas, M.J. Weaver, *Electrochim. Acta* **40** (1995) 91-98
- [399] T. Iwasita-Vielstich, in *Advances in Electrochemical Science and Engineering*, H. Gerischer, C.W. Tobias (Eds.), 1<sup>st</sup> edn., VCH, Weinheim, 1990, p. 127-170
- [400] M. Watanabe and S. Motoo, *J. Electroanal. Chem.* **60** (1975) 259-266
- [401] M.M.P. Janssen and J. Moolhuysen, *Electrochim. Acta* **21** (1976) 861-868

- [402] M. Watanabe, Y. Furuuchi, S. Motoo, *J. Electroanal. Chem.* **191** (1985) 367-375
- [403] S.A. Campbell and R. Parsons, *J. Chem. Soc. Farad. Trans.* **88** (1992) 833-841
- [404] Y.B. Vassiliev, V.S. Bagotzky, N.V. Osetrova, A.A. Mikhailova, *J. Electroanal. Chem.* **97** (1979) 63-76
- [405] B. Beden, F. Kadirgan, C. Lamy, J.-M. Léger, *J. Electroanal. Chem.* **127** (1981) 75-85
- [406] C.E. Lee, P.B. Tiege, Y. Xing, J. Nagendran, S.H. Bergens, *J. Am. Chem. Soc.* **119** (1997) 3543-3549
- [407] C.E. Lee and S.H. Bergens, *J. Phys. Chem. B* **102** (1998) 193-199
- [408] B. Beltowska-Brzezinska, J. Heitbaum, W. Vielstich, *Electrochim. Acta* **30** (1985) 1465-1471
- [409] M. Shibata and S. Motoo, *J. Electroanal. Chem.* **229** (1987) 385-394
- [410] A.B. Anderson, E. Grantscharova, S. Seong, *J. Electrochem. Soc.* **143** (1996) 2075-2082
- [411] A.S. Aricò, V. Antonucci, N. Giordano, A.K. Shukla, M.K. Ravikumar, A. Roy, S.R. Barman, D.D. Sarma, *J. Power Sources* **50** (1994) 295-309
- [412] A.K. Shukla, A.S. Aricò, K.M. El-Khatib, H. Kim, P.L. Antonucci, V. Antonucci, *Applied Surface Science* **137** (1999) 20-29
- [413] M.R. Andrew, J.S. Drury, B.D. McNicol, C. Pinnington, R.T. Short, *J. Appl. Electrochem.* **6** (1976) 99-106
- [414] A. Hamnett and B.J. Kennedy, *Electrochim. Acta* **33** (1988) 1613-1618
- [415] F. Kadirgan, B. Beden, J.-M. Léger, C. Lamy, *J. Electroanal. Chem.* **125** (1982) 89-103
- [416] V.B. Hughes and R. Miles, *J. Electroanal. Chem.* **145** (1983) 87-107
- [417] J.B. Goodenough, A. Hamnett, B.J. Kennedy, R. Manoharan, S.A. Weeks, *J. Electroanal. Chem.* **240** (1988) 133-145
- [418] M. Watanabe, M. Uchida, S. Motoo, *J. Electroanal. Chem.* **229** (1987) 395-406

- [419] M.A. Quiroz, I. Gonzalez, Y. Meas, E. Lamy-Pitara, J. Barbier, *Electrochim. Acta* **32** (1987) 289-291
- [420] H.A. Gasteiger, N. Marković, P.N. Ross, Jr., E. J. Cairns, *J. Phys. Chem.* **98** (1994) 617-625
- [421] A.B. Anderson and E. Grantscharova, *J. Phys. Chem.* **99** (1995) 9149-9154
- [422] G.A. Camara, M.J. Giz, V.A. Paganin, E.A. Ticianelli, *J. Electroanal. Chem.* **537** (2002) 21-29
- [423] H.N. Dinh, X. Ren, F.H. Garzon, P. Zelenay, S. Gottesfeld, *J. Electroanal. Chem.* **491** (2000) 222-233
- [424] A.S. Aricò, G. Monforte, E. Modica, P.L. Antonucci, V. Antonucci, *Electrochem. Commun.* **2** (2000) 466-470
- [425] A.S. Aricò, P. Cretì, E. Modica, G. Monforte, V. Baglio, V. Antonucci, *Electrochim. Acta* **45** (2000) 4319-4328
- [426] C.H. Lee, C.W. Lee, D.I. Kim, D.H. Jung, C.S. Kim, D.R. Shin, *J. Power Sources* **86** (2000) 478-481
- [427] H.M. Saffarian, R. Srinivasan, D. Chu, S. Gilman, *Electrochim. Acta* **44** (1998) 1447-1454
- [428] A. Hamnett, B.J. Kennedy, S.A. Weeks, *J. Electroanal. Chem.* **240** (1988) 349-353
- [429] A.K. Shukla, M.K. Ravikumar, A.S. Aricò, G. Candiano, V. Antonucci, N. Giordano, A. Hamnett, *J. Appl. Electrochem.* **25** (1995) 528-532
- [430] K. Lasch, L. Jörissen, J. Garche, *J. Power Sources* **84** (1999) 225-230
- [431] P.K. Shen, K.Y. Chen, A.C.C. Tseung, *J. Electrochem. Soc.* **141** (1994) 1758-1762
- [432] P.K. Shen and A.C.C. Tseung, *J. Electrochem. Soc.* **141** (1994) 3082-3090
- [433] K.Y. Chen, P.K. Shen, A.C.C. Tseung, *J. Electrochem. Soc.* **142** (1995) L54-L56
- [434] E.A. Meulenkaamp, *J. Electrochem. Soc.* **144** (1997) 1664-1671

- [435] C.-H. Lee, C.-W. Lee, D.-H. Jung, C.-S. Kim, D.-R. Shin, *J. New Mater. Electrochem. Systems* **2** (1999) 125-129
- [436] B. Rajesh, V. Karthik, S. Karthikeyan, K.R. Thampi, J.-M. Bonard, B. Viswanathan, *Fuel* **81** (2002) 2177-2190
- [437] J. Wang, H. Nakajima, H. Kita, *J. Electroanal. Chem.* **250** (1988) 213-217
- [438] H. Kita, H. Nakajima, K. Shimazu, *J. Electroanal. Chem.* **248** (1988) 181-191
- [439] M. Uchida, Y. Aoyama, M. Tanabe, N. Yanagihara, N. Eda, A. Ohta, *J. Electrochem. Soc.* **142** (1995) 2572-2576
- [440] B.R. Rauche, F.R. McLarnon, E.J. Cairns, *J. Electrochem. Soc.* **142** (1995) 1073-1084
- [441] A.K. Shukla, P.A. Christensen, A. Hamnett, M.P. Hogarth, *J. Power Sources* **55** (1995) 87-91
- [442] L. Dubau, F. Hahn, C. Coutanceau, J.-M. Léger, C. Lamy, *J. Electroanal. Chem.* **554-555** (2003) 407-415
- [443] E. Ticianelli, J.G. Beery, M.T. Paffett, S. Gottesfeld, *J. Electroanal. Chem.* **258** (1989) 61-77
- [444] H.A. Gasteiger, N. Marković, P.N. Ross Jr., E.J. Cairns, *J. Phys. Chem.* **97** (1993) 12020-12029
- [445] H.A. Gasteiger, N. Marković, P.N. Ross, E.J. Cairns, *J. Electrochem. Soc.* **141** (1994) 1795-1803
- [446] K. Wang, H.A. Gasteiger, N.M. Marković, P.N. Ross Jr., *Electrochim. Acta* **41** (1996) 2587-2593
- [447] G.L. Troughton and A. Hamnett, *Bull. Electrochem.* **7** (1991) 488-492
- [448] A. Aramata and M. Masuda, *J. Electrochem. Soc.* **138** (1991) 1949-1957
- [449] K.L. Ley, B. Liu, C. Pu, Q. Fan, N. Leyarowska, C. Segre, E.S. Smotkin, *J. Electrochem. Soc.* **144** (1997) 1543-1548
- [450] B. Gurau, R. Viswanathan, R. Liu, T.J. Lafrenz, K.L. Ley, E.S. Smotkin, E. Reddington, A. Sapienza, B.C. Chan, T.E. Mallouk, S. Sarangapani, *J. Phys. Chem. B* **102** (1998) 9997-10003

- [451] E. Reddington, A. Sapienza, B. Gurrau, R. Viswanathan, S. Sarangapani, E.S. Smotkin, T.E. Mallouk, *Science* **280** (1998) 1735-1737
- [452] C. He, H.R. Kunz, J.M. Fenton, *J. Electrochem. Soc.* **144** (1997) 970-979
- [453] M. Götz and H. Wendt, *Electrochim. Acta* **43** (1998) 3637-3644
- [454] W.C. Choi, J.D. Kim, S.I. Woo, *Catalysis Today* **74** (2002) 235-240
- [455] A.S. Aricò, Z. Poltarzewski, H. Kim, A. Morana, G. Giordano, V. Antonucci, *J. Power Sources* **55** (1995) 159-166
- [456] A.S. Aricò, P. Cretì, N. Giordano, V. Antonucci, P.L. Antonocci, A. Chuvilin, *J. Appl. Electrochem.* **26** (1996) 959-967
- [457] A.S. Aricò, P. Cretì, Z. Poltarzewski, R. Mantegna, H. Kim, N. Giordano, V. Antonocci, *Mater. Chem. Phys.* **47** (1997) 257-262
- [458] L. Liu, C. Pu, R. Viswanathan, Q. Fan, R. Liu, E.S. Smotkin, *Electrochim. Acta* **43** (1998) 3657-3663
- [459] H. Bönnemann, R. Brinkmann, W. Brijoux, E. Dinjus, T. Jousen, B. Korall, *Angew. Chem.* **103** (1991) 1344-1346
- [460] T.J. Schmidt, M. Noeske, H.A. Gasteiger, R.J. Behm, P. Britz, W. Brijoux, H. Bönnemann, *Langmuir* **14** (1997) 2591-2595
- [461] T.J. Schmidt, M. Noeske, H.A. Gasteiger, R.J. Behm, P. Britz, W. Brijoux, H. Bönnemann, *J. Electrochem. Soc.* **145** (1998) 925-931
- [462] T.J. Schmidt, H.A. Gasteiger, R.J. Behm, *Electrochem. Commun.* **1** (1998) 1-4
- [463] H. Bönnemann, R. Brinkmann, P. Britz, U. Endruschat, R. Mörtel, U. Paulus, G. Feldmeyer, T.J. Schmidt, H.A. Gasteiger, R.J. Behm, *J. New Mater. Electrochem. Systems* **3** (2000) 199-206
- [464] C. Roth, M. Götz, H. Fuess, in *Proceedings of the Workshop on Electrocatalysis in Indirect and Direct Methanol PEM Fuel Cell*, C. Lamy, H. Wendt (Eds.), 12-14 September, Portoroz, Slovenia, 1999, p.30
- [465] K. Lasch, L. Jörissen, J. Garche, in *Proceedings of the Workshop on Electrocatalysis in Indirect and Direct Methanol PEM Fuel Cell*, C. Lamy, H.



- Wendt (Eds.), 12-14 September, Portoroz, Slovenia, 1999, p.104
- [466] A.J. Dickinson, L.P.L. Carrette, J.A. Collins, K.A. Friedrich, U. Stimming, *Electrochim. Acta* **47** (2002) 3733-3739
- [467] W.E. O'Grady, E.J. Taylor, S. Srinivasan, *J. Electroanal. Chem.* **132** (1982) 137-150
- [468] K.-L. Hsueh, D.-T. Chin, S. Srinivasan, *J. Electroanal. Chem.* **153** (1983) 79-95
- [469] K.L. Hsueh, E.R. Gonzales, S. Srinivasan, *Electrochim. Acta* **28** (1983) 691-697
- [470] M.R. Tarasevich, A. Sadkovski, E. Yeager, in *Comprehensive Treatise of Electrochemistry*, B.E. Conway, J.O'M. Bockris, S.V.M. Khan, R.E. White (Eds.), Vol. 7, Plenum Press, New York (1983)
- [471] G. Kokkinidis and D. Jannakoudakis, *J. Electroanal. Chem.* **162** (1984) 163-173
- [472] N.A. Anastasijević, V. Vesović, R.R. Adžić, *J. Electroanal. Chem.* **229** (1987) 305-316
- [473] N.A. Anastasijević, V. Vesović, R.R. Adžić, *J. Electroanal. Chem.* **229** (1987) 317-325
- [474] E.A. Ticianelli, C.R. Derouin, S. Srinivasan, *J. Electroanal. Chem.* **251** (1988) 275-295
- [475] F. El Kadiri, R. Faure, R. Durand, *J. Electroanal. Chem.* **301** (1991) 177-188
- [476] K. Kinoshita, *Electrochemical oxygen technology*, John Wiley & Sons, Inc. New York, 1992
- [477] D.M. Bernardi and M. Verbrugge, *J. Electrochem. Soc.* **139** (1992) 2477-2491
- [478] T.E. Springer, M.S. Wilson, S. Gottesfeld, *J. Electrochem. Soc.* **140** (1993) 3513-3526
- [479] J. Perez, A.A. Tanaka, E.R. Gonzales, E.A. Ticianelli, *J. Electrochem. Soc.* **141** (1994) 431-436
- [480] C.F. Zinola, A.M. Castro Luna, W.E. Triaca, A.J. Arvia, *J. Appl. Electrochem.* **24** (1994) 119-125
- [481] C.F. Zinola, A.M. Castro Luna, W.E. Triaca, A.J. Arvia, *J. Appl. Electrochem.* **24** (1994) 531-541

- [482] F. Gloaguen, F. Andolfatto, R. Durand, P. Ozil, *J. Appl. Electrochem.* **24** (1994) 863-869
- [483] F. Gloaguen and R. Durand, *J. Appl. Electrochem.* **27** (1997) 1029-1035
- [484] N.M. Marković, R.R. Adžić, B.D. Cahan, E.B. Yeager, *J. Electroanal. Chem.* **377** (1994) 249-259
- [485] N.M. Marković, H.A. Gasteiger, P.N. Ross, *J. Phys. Chem.* **100** (1996) 6715-6721
- [486] N.M. Marković, H.A. Gasteiger, B.N. Grgur, P.N. Ross, *J. Electroanal. Chem.* **467** (1999) 157-163
- [487] N.M. Marković and P.N. Ross, in *Interfacial Electrochemistry: Theory, Experiment and Applications*, A. Wieckowski (Ed.), Marcel Dekker, New York, 1999, p. 521-841
- [488] L. Qingfeng, H.A. Hjuler, N.J. Bje, *Electrochim. Acta* **45** (2000) 4219-4226
- [489] O. Antoine and R. Durand, *J. Appl. Electrochem.* **30** (2000) 839-844
- [490] S. Lj. Gojković, S.K. Zečević, R.F. Savinell, *J. Electrochem. Soc.* **145** (1998) 3713-3720
- [491] A. Damjanovic, D.B. Sepa, M.V. Vojnovic, *Electrochim. Acta* **24** (1979) 887-889
- [492] D.B. Sepa, M.V. Vojnovic, A. Damjanovic, *Electrochim. Acta* **25** (1980) 1491-1496
- [493] D.B. Sepa, M.V. Vojnovic, A. Damjanovic, *Electrochim. Acta* **26** (1981) 781-793
- [494] D.B. Sepa, M.V. Vojnovic, Lj.M. Vracar, A. Damjanovic, *Electrochim. Acta* **32** (1987) 129-134
- [495] A. Damjanovic, in *Electrochemistry in Transition*, O.J. Murphy, S. Srinivasan, E. Conway (Eds.), Plenum Press, New York, 1992
- [496] J.T. Hwang and I.S. Chung, *Electrochim. Acta* **38** (1993) 2715-2723
- [497] A. Kabbabi, F. Gloaguen, F. Andolfatto, R. Durand, *J. Electroanal. Chem.* **373** (1994) 251-254

- [498] A. Gamez, D. Richard, P. Gallezot, F. Gloaguen, R. Faure, R. Durand, *Electrochim. Acta* **41** (1996) 307-314
- [499] Y. Takasu, N. Ohashi, X.-G. Zhang, Y. Murakami, H. Minagawa, S. Sato, K. Yahikozawa, *Electrochim. Acta* **41** (1996) 2595-2600
- [500] T. Schultz, S. Zhou, K. Sundmacher, *Chem. Eng. Technol.* **24** (2001) 1223-1233
- [501] T.E. Springer, T.A. Zawodzinski, M.S. Wilson, S. Gottesfeld, *J. Electrochem. Soc.* **143** (1996) 587-600
- [502] B. Mueller, T. Zawodzinski, J. Bauman, F. Uribe, S. Gottesfeld, E. De Costa, M. De Marinis, *Proceedings of the Electrochemical Society*, S. Gottesfeld, T.F. Fuller (Eds.), PV 98-27, 1998, p. 1-9
- [503] C. Lim and C.Y. Wang, *Proc. Electrochemical Society Meeting*, Philadelphia, PA, May 2002
- [504] M.V. Williams, E. Begg, L.J. Bonville, H.R. Kunz, J.M. Fenton, *Proc. Electrochemical Society Meeting*, Philadelphia, PA, May 2002
- [505] D.L. Wood, P.M. Wilde, M. Maendle, M. Murata, *2002 Fuel Cell Seminar*, Palm Spring, California, November 18 – November 21, 2002, p. 41-44
- [506] A. Heinzl, C. Hebling, M. Müller, M. Zedda, C. Müller, *J. Power Sources* **105** (2002) 250-255
- [507] H. Gharibi and R.H. Mirzaie, *J. Power Sources* **115** (2003) 194-202
- [508] S. Gamburgzev and A.J. Appleby, *J. Power Sources* **107** (2002) 5-12
- [509] R.W. Reeve, G.T. Burstein, K.R. Williams, *J. Power Sources* **128** (2004) 1-12
- [510] A. Oedegaard, C. Hebling, A. Schmitz, S. Møller-Holst, R. Tunold, *J. Power Sources* **127** (2004) 187-196
- [511] L.R. Jordan, A.K. Shukla, T. Behrsing, N.R. Avery, B.C. Muddle, M. Forsyth, *J. Appl. Electrochem.* **30** (2000) 641-646
- [512] E. Passalacqua, F. Lufrano, G. Squadrito, A. Patti, L. Giorgi, *Electrochim. Acta* **43** (1998) 3665-3673
- [513] E. Antolini, L. Giorgi, A. Pozio, E. Passalacqua, *J. Power Sources* **77** (1999) 136-142

- [514] E. Antolini, L. Giorgi, A. Pozio, E. Passalacqua, *J. Mater. Sci.* **33** (1998) 1837-1843
- [515] L. Giorgi, E. Antolini, A. Pozio, E. Passalacqua, *Electrochim. Acta* **43** (1998) 3675-3680
- [516] F. Lufrano, E. Passalacqua, G. Squadrito, A. Patti, L. Giorgi, *J. Appl. Electrochem.* **29** (1999) 445-448
- [517] E. Passalacqua, G. Squadrito, F. Lufrano, A. Patti, L. Giorgi, *J. Appl. Electrochem.* **31** (2001) 449-454
- [518] J. Moreira, A.L. Ocampo, P.J. Sebastian, M.A. Smit, M.D. Salazar, P. Del Angel, J.A. Montoya, R. Pérez, L. Martínez, *Int. J. Hydrogen Energy* **28** (2003) 625-627
- [519] K. Scott, W.M. Taama, P. Argyropoulos, *J. Power Sources* **79** (1999) 43-59
- [520] K. Scott, W.M. Taama, S. Kramer, P. Argyropoulos, K. Sundmacher, *Electrochim. Acta* **45** (1999) 945-957
- [521] K. Scott, W.M. Taama, P. Argyropoulos, *J. Power Sources* **87** (2000) 153-161
- [522] T. Shultz, S. Zhou, K. Sundmacher, *Chem. Eng. Technol.* **24** (2001) 1223-1233
- [523] J. Eigeldinger and H. Vogt, *Electrochim. Acta* **45** (2000) 4449-4456
- [524] E. Barendrecht, Electrochemistry of Fuel Cells, in *Fuel Cell Systems*, L.J.M.J. Blomen, M.N. Mugerwa (Eds.), Plenum Press, New York, 1993, p. 73-119
- [525] V.A. Paganin, E.A. Ticianelli, E.R. Gonzalez, *J. Appl. Electrochem.* **26** (1996) 297-304
- [526] M. Wöhr, K. Bolwin, W. Schnurnberger, M. Fischer, W. Neubrand, G. Eigenberger, *Int. J. Hydrogen Energy* **23** (3) (1998) 213-218
- [527] G.S. Kumar, M. Raja, S. Parthasarathy, *Electrochim. Acta* **40** (1995) 285-290
- [528] E. Passalacqua, F. Lufrano, G. Squadrito, A. Patti, L. Giorgi, *Electrochim. Acta* **46** (2001) 799-805
- [529] S.J. Lee, S. Mukerjee, J. McBreen, Y.W. Rho, Y.T. Kho, T.H. Lee, *Electrochim. Acta* **43** (1998) 3693-3701
- [530] I.D. Raistrick, in *Proceedings of the Symposium on Diaphragms, Separators and Ion Exchange Membranes*, J.W. Van Zee, R.E. White, K. Kinoshita, and

- H.S. Burney (Eds.), The Electrochemical Society, Pennington, New Jersey, 1986, p. 172
- [531] I.D. Raistrick, *US Patent* **4,876,115** (1989)
- [532] E.A. Ticianelli, C.R. Derouin, A. Redondo, S. Srinivasan, *J. Electrochem. Soc.* **135** (1988) 2209-2214
- [533] E.A. Ticianelli, J.G. Beery, S. Srinivasan, *J. Appl. Electrochem.* **21** (1991) 597-605
- [534] M.S. Wilson and S. Gottesfeld, *J. Appl. Electrochem.* **22** (1992) 1-7
- [535] S. Srinivasan, D.J. Manko, H. Koch, M.A. Enayetullah, A.J. Appleby, *J. Power Sources* **29** (1990) 367-387
- [536] S. Mukerjee, S. Srinivasan, A.J. Appleby, *The Electrochemical Society Extended Abstracts*, St. Louis Meeting, Vol. 92-1, 1992, p.13
- [537] J. Zhang, K.M. Colbow, D.P. Wilkinson, *US Patent* **6,187,467** (2001)
- [538] N. Jia, R.B. Martin, Z. Qi, M.C. Lefebvre, P.G. Pickup, *Electrochim. Acta* **46** (2001) 2863-2869
- [539] A.K. Shukla, P.A. Christensen, A.J. Dickinson, A. Hamnett, *J. Power Sources* **76** (1998) 54-59
- [540] M. Neergat and A.K. Shukla, *J. Power Sources* **104** (2002) 289-294
- [541] Z. Wei, S. Wang, B. Yi, J. Liu, L. Chen, W. Zhou, W. Li, Q. Xin, *J. Power Sources* **106** (2002) 364-369
- [542] M. Uchida, Y. Fukuoka, Y. Sugawara, H. Ohara, A. Ohta, *J. Electrochem. Soc.* **145** (1998) 3708-3713
- [543] Y.-G. Chun, C.-S. Kim, D.-H. Peck, D.-R. Shin, *J. Power Sources* **71** (1998) 174-178
- [544] A. Fischer, J. Jindra, H. Wendt, *J. Appl. Electrochem.* **28** (1998) 277-282
- [545] N. Nakagawa and Y. Xiu, *J. Power Sources* **118** (2003) 248-255
- [546] L.R. Jordan, A.K. Shukla, T. Behrsing, N.R. Avery, B.C. Muddle, M. Forsyth, *J. Power Sources* **86** (2000) 250-254
- [547] E. Antolini, R.R. Passos, E.A. Ticianelli, *J. Appl. Electrochem.* **32** (2002) 383-388

- [548] D.R. Sena, E.A. Ticianelli, V.A. Paganin, E.R. Gonzalez, *J. Electroanal. Chem.* **477** (1999) 164-170
- [549] A.S. Aricò, P. Cretì, H. Kim, R. Mantegna, N. Giordano, V. Antonucci, *J. Electrochem. Soc.* **143** (1996) 3950-3959
- [550] E. Passalacqua, I. Gatto, F. Lufrano, A. Patti, G. Squadrito, *2000 Fuel Cell Seminar Abstracts*, Portland, Oregon, October 30-November 2, 2000, p. 118-121
- [551] J. Soler, R. Benitez, S. Jimenez, L. Daza, *2002 Fuel Cell Seminar Abstracts*, Palm Springs, California, 18-21 November, 2002, p. 141-144
- [552] E. Gülzow, T. Kaz, R. Reissner, H. Sander, L. Schilling, M.V. Bradke, *J. Power Sources* **115** (2003) 194-202
- [553] E. Gülzow, M. Schulze, N. Wagner, T. Kaz, R. Reissner, G. Steinhilber, A. Schneider, *J. Power Sources* **86** (2000) 352-362
- [554] T.R. Ralph and M.P. Hogarth, *Platinum Metals Rev.* **46** (2002) 3-14
- [555] J. Denton, J.M. Gascoyne, D. Thompsett, *European Patent* **731,520** (1996)
- [556] G.G. Scherer, *Solid State Ionics* **94** (1997) 249-257
- [557] M. Inaba, M. Uno, J. Maruyama, A. Tasaka, K. Katakura, Z. Ogumi, *J. Electroanal. Chem.* **417** (1996) 105-111
- [558] S.C. Thomas, X. Ren, S. Gottesfeld, *J. Electrochem. Soc.* **146** (1999) 4354-4359
- [559] M.C. Lefebvre, R.B. Martin, P.G. Pickup, *Electrochem. Solid-State Lett.* **2** (1999) 259-261
- [560] C. Boyer, S. Gamburgzev, O. Velev, S. Srinivasan, A.J. Appleby, *Electrochim. Acta* **43** (1998) 3703-3709
- [561] Z. Poltarzewski, P. Staiti, V. Alderucci, W. Wieczorek, N. Giordano, *J. Electrochem. Soc.* **139** (1992) 761-765
- [562] P. Staiti, Z. Poltarzewski, V. Alderucci, G. Maggio, N. Giordano, *Int. J. Hydrogen Energy* **19** (1994) 523-527
- [563] Z. Siroma, T. Ioroi, N. Fujiwara, K. Yasuda, *Electrochem. Commun.* **4** (2002) 143-145

- [564] Z. Siroma, T. Sasakura, K. Yasuda, M. Azuma, Y. Miyazaki, *J. Electroanal. Chem.* **546** (2003) 73-78
- [565] Z. Siroma, N. Fujiwara, T. Ioroi, S. Yamazaki, K. Yasuda, Y. Miyazaki, *J. Power Sources* **126** (2004) 41-45
- [566] A.S. Aricò, P. Cretì, P.L. Antonucci, J. Cho, H. Kim, V. Antonucci, *Electrochim. Acta* **43** (1998) 3719-3729
- [567] Y.-H. Chu, Y. G. Shul, W.C. Choi, S. I. Woo, H.-S. Han, *J. Power Sources* **118** (2003) 334-341
- [568] M. Watanabe, H. Igarashi, K. Yosioka, *Electrochim. Acta* **40** (1995) 329-334
- [569] L.A. Zook, M.D. Dejohn, J. Leddy, in the *Electrochemical Society Proceedings Series*, S. Gottesfeld, T.F. Fuller (Eds.), PV 98-27, 1998, 10-22
- [570] K.E. Swider, C.I. Merzbacher, P.L. Hagans, D.R. Rolison, *Chem. Mater.* **9** (1997) 1248-1255
- [571] D.R. Rolison, P.L. Hagans, K.E. Swider, J.W. Long, *Langmuir* **15** (1999) 774-779
- [572] S. Gamburgzev, C. Boyer, A.J. Appleby, in *Proceedings of the Electrochemical Society*, S. Gottesfeld, T.F. Fuller (Eds.), PV 98-27, 1998, p. 23-29
- [573] M.W. Verbrugge, *J. Electrochem. Soc.* **136** (1989) 417-423
- [574] P.S. Kauramen and E. Skou, *J. Appl. Electrochem.* **26** (1996) 909-917
- [575] T.I. Valdez, S.R. Narayanan, Recent Studies on Methanol Crossover in Liquid-Feed Direct Methanol Fuel Cells, *194<sup>th</sup> Meeting of the Electrochemical Society*, Boston, Nov. 1998, 1998
- [576] K. Sundmacher and K. Scott, *Chem. Eng. Sci.* **54** (1999) 2927-2936
- [577] A. Küver and W. Vielstich, *J. Power Sources* **74** (1998) 211-218
- [578] M.K. Ravikumar and A.K. Shukla, *J. Electrochem. Soc.* **143** (1996) 2601-2606
- [579] K. Scott, W.M. Taama, P. Argyropoulos, K. Sundmacher, *J. Power Sources* **83** (1999) 204-216
- [580] J. Cruickshank and K. Scott, *J. Power Sources* **70** (1998) 40-47
- [581] V.M. Barragán and A. Heinzl, *J. Power Sources* **104** (2002) 66-72

- [582] X. Ren, T.A. Zawodzinski, F. Uribe, H. Dai, S. Gottesfeld, in *Proton Conducting Membrane Fuel Cells 1*, S. Gottesfeld, G. Halpert, A. Landgrebe (Eds.), *The Electrochemical Society Proceedings Series*, Pennington, NJ, PV 95-23, 1995, p. 284
- [583] S.R. Narayanan, H. Frank, B. Jeffries-Nakamura, M. Smart, W. Chun, G. Halpert, in *Proton Conducting Membrane Fuel Cells 1*, S. Gottesfeld, G. Halpert, A. Landgrebe (Eds.), *The Electrochemical Society Proceedings Series*, Pennington, New Jersey, PV 95-23, 1995, p. 278
- [584] D.L. Maricle, B.L. Murach, L.L. Van Dine, *The Electrochemical Society Extended Abstracts*, Abstract 35, San Francisco, CA, May 22-27, Vol. 94-1, 1994, p. 58
- [585] T.I. Valdez and S.R. Narayanan, in *Proceedings of the 2<sup>nd</sup> International Symposium on Proton Conducting Membrane Fuel Cells II*, *The Electrochemical Society Proceedings Series*, Pennington, New Jersey, PV 98-27, 1998, p. 380-387
- [586] R. Jiang and D. Chu, *Electrochem. Solid State Lett.* **5** (2002) A156-A159
- [587] S. Hikita, K. Yamane, Y. Nakajima, *JSAE Review* **22** (2001) 151-156
- [588] R. Liu and P.S. Fedkiw, *J. Electrochem. Soc.* **139** (1992) 3514-3523
- [589] A.S. Aricò, P. Cretì, V. Baglio, E. Modica, V. Antonucci, *J. Power Sources* **91** (2000) 202-209
- [590] D.H. Jung, C.H. Lee, C.S. Kim, D.R. Shin, *J. Power Sources* **71** (1998) 169-173
- [591] J.-T. Wang, S. Wasmus, R.F. Savinell, *J. Electrochem. Soc.* **143** (1996) 1233-1239
- [592] S. Wasmus, J.-T. Wang, R.F. Savinell, *J. Electrochem. Soc.* **142** (1995) 3825-3833
- [593] S.R. Narayanan, E. Vamos, S. Surampudi, H. Frank, G. Halpert, in *Extended Abstracts of the Battery Division of Electrochemical Society Meeting*, The Electrochemical Society, October 1993, p. 126
- [594] Q. Fan, C. Pu, K.L. Ley, E.S. Smotkin, *J. Electrochem. Soc.* **143** (2) (1996) L21-L23



- [595] Q. Fan, C. Pu, E.S. Smotkin, *J. Electrochem. Soc.* **143** (10) (1996) 3053-3057
- [596] X. Ren, T.S. Springer, T.A. Zawodzinski, S. Gottesfeld, *J. Electrochem. Soc.* **147** (2) (2000) 466-474
- [597] X. Ren, T.E. Springer, S. Gottesfeld, *J. Electrochem. Soc.* **147** (1) (2000) 92-98
- [598] N. Miyake, J.S. Wainright, R.F. Savinell, *J. Electrochem. Soc.* **148** (8) (2001) A905-A909
- [599] Z. Qi and A. Kaufman, *J. Power Sources* **110** (2002) 177-185
- [600] A. Küver, K. Potje-Kamloth, *Electrochim. Acta* **43** (1998) 2527-2535
- [601] D. Weng, J.S. Wainright, U. Landau, R.F. Savinell, in *Electrode Materials and Processes for Energy Conversion and Storage*, S. Srinivasan, D.D. Macdonald, A.C. Khandhar (Eds.), *The Electrochemical Society Proceedings Series*, PV 94-23, Pennington, New Jersey, 1994, p. 201
- [602] J. Crank and G.S. Park, *Diffusion in Polymers*, Academic Press, London, 1968, p. 176
- [603] E.L. Cussler, *Diffusion*, 2<sup>nd</sup> Ed., Cambridge University Press, Cambridge, 1997
- [604] V. Tricoli, N. Carretta, M. Bartolozzi, *J. Electrochem. Soc.* **147** (2000) 1286-1290
- [605] B. Pivovar, Y. Wang, E.L. Cussler, *J. Membr. Sci.* **154** (1999) 155-162
- [606] G. Deluga and B.S. Pivovar, in *Proceedings of the 3<sup>rd</sup> International Symposium on New Materials for Electrochemical Systems*, O. Savadogo (Ed.), Montreal, July 4-8, 1999, p. 132
- [607] K. Ramya and K.S. Dhathathreyan, *J. Electroanal. Chem.* **542** (2003) 109-115
- [608] H. Wu, Y. Wang, S. Wang, *J. New Mater. Electrochem. Systems* **5** (2002) 251-254
- [609] M.V. Fedkin, X. Zhou, M.A. Hofmann, E. Chalkova, J.A. Weston, H.R. Allcock, S.N. Lvov, *Mater. Lett.* **52** (2002) 192
- [610] F. Sarfert, *Membrane Characterization*, Advanced Course on Electro-Membrane Processes, University of Stuttgart, September 4-6, 2000
- [611] S. Augustin, V. Hennige, G. Hörpel, C. Hying, *Desalination* **146** (2002) 23-28

- [612] B. Penth, C. Hying, G. Hörpel, F.-G. Schmidt, **WO99/15262** (1999)
- [613] B. Bondars, G. Heidemane, J. Grabis, K. Laschke, H. Boyesen, J. Schneider, F. Frey, *J. Mater. Sci.* **30** (1995) 1621-1625.
- [614] J. Haines, J.M. Leger, A. Atouf, *J. Am. Ceram. Soc.* **78** (1995) 445-448
- [615] A.F. Bedilo, K.J. Klabunde, *Nanostructured Materials* **8** (2) (1997) 119-135
- [616] P. Colomban and A. Novak, *J. Molecular Structure* **198** (1989) 277-295
- [617] S.E. Horsley, D.V. Nowell, D.T. Stewart, *Spectrochimica Acta* **30A** (1974) 535-541
- [618] J. Albertson, *Acta Chem. Scand.* **20** (1966) 1689-1702
- [619] S.K. Tiwari, S.K. Nema, Y.K. Agarwal, *Thermochimica Acta* 317 (1998) 175-182
- [620] S.R. Samms, S. Wasmus, R.F. Savinell, *J. Electrochem. Soc.* **143** (1996) 1498-1504
- [621] X. Ren, M.S. Wilson, S. Gottesfeld, *J. Electrochem. Soc.* **143** (1996) L12-L15



## APPENDIX A

### METHANOL PERMEABILITY

#### Introduction

The diffusion cell was adopted in this study to measure methanol permeability in membranes. Section 3.3.3 discussed the principle of the method and the measurements. This Section reports on the derivation of methanol permeability equation (equation 3.1) and the detailed calculation for methanol permeability in different membranes.

#### Derivation of Methanol Permeability Equation

The flux across the membrane at any instant is given by equation (A.1):

$$J = \left( \frac{DH}{l} \right) [C_{1,B} - C_{1,A}] \quad (\text{A.1})$$

- $J$  the flux [ $\text{cm}^3 \cdot \text{cm}^{-2} \cdot \text{s}^{-1}$ ]  
 $D$  diffusion coefficient [ $\text{m}^2 / \text{s}$ ]  
 $H$  repartition coefficient  
 $l$  effective thickness of the membrane [ $\text{m}$ ]  
 $C_{1,B}$  concentration of methanol in compartment B [ $\text{mol} / \text{l}$ ] at any time ,  $t$   
 $C_{1,A}$  concentration of methanol in compartment A [ $\text{mol} / \text{l}$ ] at any time ,  $t$

The mass balance in compartment B can be written as:

$$V_B \frac{dC_{1,B}}{dt} = AJ \quad (\text{A.2})$$

- $A$  membrane area available for diffusion [ $\text{m}^2$ ]  
 $V_B$  volume of compartment B [ $\text{m}^3$ ]  
 $V_A$  volume of compartment A [ $\text{m}^3$ ]

$$\frac{dC_{1,B}}{dt} = \frac{A}{V_B} J \quad (\text{A.3})$$

Replacing  $J$  in equation (A.3):

$$\frac{dC_{1,B}}{dt} = \frac{A}{V_B} \frac{DH}{l} [C_{1,B} - C_{1,A}] \quad (\text{A.4})$$

Rearranging equation (A.3) as:

$$\frac{dC_{1,B}}{C_{1,B} - C_{1,A}} = \frac{A}{V_B} \frac{DH}{l} dt \quad (\text{A.5})$$

The differential equation is subject to the initial condition:

$$t = 0 \quad C_{1,B} - C_{1,A} = C_{1,B}^0 - C_{1,A}^0$$

$C_{1,B}^0$  initial concentration in compartment B [ mol / l ]

$C_{1,A}^0$  initial concentration in compartment A [ mol / l ]

The integration of equation (A.5) with this condition gives:

$$\ln[C_{1,B}^0 - C_{1,A}^0] - \ln[C_{1,B} - C_{1,A}] = \frac{A}{V_B} \frac{DH}{l} t \quad (\text{A.6})$$

$$\ln \frac{C_{1,B}^0 - C_{1,A}^0}{C_{1,B} - C_{1,A}} = \frac{A}{V_B} \frac{DH}{l} t \quad (\text{A.7})$$

$$DH = \frac{l V_B}{A t} \ln \frac{C_{1,B}^0 - C_{1,A}^0}{C_{1,B} - C_{1,A}} \quad (\text{A.8})$$

methanol concentration changes in compartment A are negligible, thus:

$$C_{1,A}^0 \approx C_{1,A}$$

$$DH = \frac{W_B}{At} \ln \frac{C_{1,B}^0 - C_{1,A}}{C_{1,B} - C_{1,A}} \quad (\text{A.9})$$

The product  $DH$  is equal to methanol permeability ( $P$ ). Therefore, equation (A.9) was used to calculate methanol permeability in membranes.

The following are the results:

**Table A.1:** Calculated methanol permeability in bare CREAMFILTER<sup>®</sup> s and Nafion<sup>®</sup> 117

	$l$	$A$	$V_B$	$t_{\text{exp}}$	$C_{1,B}^0$	$C_{1,B}$	$C_{1,A}$	$P$
	(cm)	(cm <sup>2</sup> )	(cm <sup>3</sup> )	(s)	(M)	(M)	(M)	(cm <sup>2</sup> /s)
Z100G	$1.0 \times 10^{-2}$	12.13	365	6660	0	$20.1 \times 10^{-3}$	1	$9.14 \times 10^{-7}$
	$1.0 \times 10^{-2}$	12.13	365	9600	0	$28.7 \times 10^{-3}$	1	$9.09 \times 10^{-7}$
	$1.0 \times 10^{-2}$	12.13	365	13320	0	$39.7 \times 10^{-3}$	1	$9.13 \times 10^{-7}$
Z240G	$0.9 \times 10^{-2}$	12.13	365	2400	0	$9.7 \times 10^{-3}$	1	$10.96 \times 10^{-7}$
	$0.9 \times 10^{-2}$	12.13	365	3000	0	$12.6 \times 10^{-3}$	1	$11.41 \times 10^{-7}$
	$0.9 \times 10^{-2}$	12.13	365	4800	0	$19.3 \times 10^{-3}$	1	$10.96 \times 10^{-7}$
S450P	$0.3 \times 10^{-2}$	12.13	365	6300	0	$128 \times 10^{-3}$	1	$19.56 \times 10^{-7}$
	$0.3 \times 10^{-2}$	12.13	365	8100	0	$172.9 \times 10^{-3}$	1	$21.09 \times 10^{-7}$
	$0.3 \times 10^{-2}$	12.13	365	9900	0	$210.9 \times 10^{-3}$	1	$21.5 \times 10^{-7}$
Z450P	$2.0 \times 10^{-2}$	12.13	365	7440	0	$22.0 \times 10^{-3}$	1	$17.94 \times 10^{-7}$
	$2.0 \times 10^{-2}$	12.13	365	9600	0	$28.0 \times 10^{-3}$	1	$17.74 \times 10^{-7}$
	$2.0 \times 10^{-2}$	12.13	365	14400	0	$42.0 \times 10^{-3}$	1	$17.87 \times 10^{-7}$
Nafion <sup>®</sup> 117	$2.1 \times 10^{-2}$	12.13	365	8100	0	$18.0 \times 10^{-3}$	1	$14.12 \times 10^{-7}$
	$2.1 \times 10^{-2}$	12.13	365	9900	0	$22.0 \times 10^{-3}$	1	$14.15 \times 10^{-7}$
	$2.1 \times 10^{-2}$	12.13	365	10800	0	$24.0 \times 10^{-3}$	1	$14.17 \times 10^{-7}$

**Table A.2:** Calculated methanol permeability in CREAMFILTER<sup>®</sup>s impregnated with zirconium phosphate

Membrane	$l$	$A$	$V_B$	$t_{\text{exp}}$	$C_{1,B}^0$	$C_{1,B}$	$C_{1,A}$	$P$	
	(cm)	(cm <sup>2</sup> )	(cm <sup>3</sup> )	(s)	(M)	(M)	(M)	(cm <sup>2</sup> /s)	
Z100G/ZrP	$1.2 \times 10^{-2}$	12.13	365	5700	0	$11.5 \times 10^{-3}$	1	$7.3 \times 10^{-7}$	$7 \times 10^{-7}$
	$1.2 \times 10^{-2}$	12.13	365	6540	0	$13 \times 10^{-3}$	1	$7.2 \times 10^{-7}$	
	$1.2 \times 10^{-2}$	12.13	365	7440	0	$14 \times 10^{-3}$	1	$6.8 \times 10^{-7}$	
Z240G/ZrP	$1.2 \times 10^{-2}$	12.13	365	5700	0	$5.3 \times 10^{-3}$	1	$3.4 \times 10^{-7}$	$3.5 \times 10^{-7}$
	$1.2 \times 10^{-2}$	12.13	365	9000	0	$9.3 \times 10^{-3}$	1	$3.7 \times 10^{-7}$	
	$1.2 \times 10^{-2}$	12.13	365	14400	0	$13.2 \times 10^{-3}$	1	$3.3 \times 10^{-7}$	
Z450P/ZrP	$2.2 \times 10^{-2}$	12.13	365	9660	0	$24.7 \times 10^{-3}$	1	$17.1 \times 10^{-7}$	$17 \times 10^{-7}$
	$2.2 \times 10^{-2}$	12.13	365	10740	0	$27.2 \times 10^{-3}$	1	$16.9 \times 10^{-7}$	
	$2.2 \times 10^{-2}$	12.13	365	11160	0	$27.8 \times 10^{-3}$	1	$16.7 \times 10^{-7}$	



**Table A.3:** Calculated methanol permeability in CREAMFILTER<sup>®</sup>s impregnated with Nafion<sup>®</sup> solution

Membrane	$l$	$A$	$V_B$	$t_{\text{exp}}$	$C_{1,B}^0$	$C_{1,B}$	$C_{1,A}$	$P$	
	(cm)	(cm <sup>2</sup> )	(cm <sup>3</sup> )	(s)	(M)	(M)	(M)	(cm <sup>2</sup> /s)	
Z100G/Nafion <sup>®</sup>	$1.3 \times 10^{-2}$	12.13	365	11880	0	$19.6 \times 10^{-3}$	1	$6 \times 10^{-7}$	$6 \times 10^{-7}$
	$1.3 \times 10^{-2}$	12.13	365	12720	0	$21.1 \times 10^{-3}$	1	$6 \times 10^{-7}$	
	$1.3 \times 10^{-2}$	12.13	365	13680	0	$23.2 \times 10^{-3}$	1	$6.1 \times 10^{-7}$	
Z240G/Nafion <sup>®</sup>	$1.2 \times 10^{-2}$	12.13	365	7200	0	$9.6 \times 10^{-3}$	1	$5.2 \times 10^{-7}$	$5.5 \times 10^{-7}$
	$1.2 \times 10^{-2}$	12.13	365	7800	0	$11.6 \times 10^{-3}$	1	$5.8 \times 10^{-7}$	
	$1.2 \times 10^{-2}$	12.13	365	12600	0	$18.1 \times 10^{-3}$	1	$5.6 \times 10^{-7}$	
Z450P/Nafion <sup>®</sup>	$0.6 \times 10^{-2}$	12.13	365	4500	0	$33.4 \times 10^{-3}$	1	$13.5 \times 10^{-7}$	$13 \times 10^{-7}$
	$0.6 \times 10^{-2}$	12.13	365	11460	0	$77.8 \times 10^{-3}$	1	$12.7 \times 10^{-7}$	
	$0.6 \times 10^{-2}$	12.13	365	13800	0	$91.8 \times 10^{-3}$	1	$12.5 \times 10^{-7}$	

**Table A.4:** Calculated methanol permeability in bare recast Nafion<sup>®</sup> (RN), recast Nafion<sup>®</sup>/ZrO<sub>2</sub> and recast Nafion<sup>®</sup>/ZrP powders

Membrane	$l$	$A$	$V_B$	$t_{\text{exp}}$	$C_{1,B}^0$	$C_{1,B}$	$C_{1,A}$	$P$	
	(cm)	(cm <sup>2</sup> )	(cm <sup>3</sup> )	(s)	(M)	(M)	(M)	(cm <sup>2</sup> /s)	
RN	$1.0 \times 10^{-2}$	12.13	365	3600	0	$25 \times 10^{-3}$	1	$21 \times 10^{-7}$	$21.5 \times 10^{-7}$
	$1.0 \times 10^{-2}$	12.13	365	4800	0	$35 \times 10^{-3}$	1	$22 \times 10^{-7}$	
	$1.0 \times 10^{-2}$	12.13	365	10320	0	$73.2 \times 10^{-3}$	1	$22 \times 10^{-7}$	
RN/ZrO <sub>2</sub> (5%)	$1.0 \times 10^{-2}$	12.13	365	4500	0	$28 \times 10^{-3}$	1	$18.9 \times 10^{-7}$	$18.8 \times 10^{-7}$
	$1.0 \times 10^{-2}$	12.13	365	6600	0	$41 \times 10^{-3}$	1	$19 \times 10^{-7}$	
	$1.0 \times 10^{-2}$	12.13	365	7800	0	$47 \times 10^{-3}$	1	$18.5 \times 10^{-7}$	
RN/ZrO <sub>2</sub> (30%)	$1.1 \times 10^{-2}$	12.13	365	3780	0	$11.9 \times 10^{-3}$	1	$9.5 \times 10^{-7}$	$9.4 \times 10^{-7}$
	$1.1 \times 10^{-2}$	12.13	365	7800	0	$24 \times 10^{-3}$	1	$9.3 \times 10^{-7}$	
	$1.1 \times 10^{-2}$	12.13	365	9600	0	$30 \times 10^{-3}$	1	$9.5 \times 10^{-7}$	
RN/ZrP (6.4%)	$1.0 \times 10^{-2}$	12.13	365	14400	0	$185.6 \times 10^{-3}$	1	$42 \times 10^{-7}$	$44 \times 10^{-7}$
	$1.0 \times 10^{-2}$	12.13	365	19680	0	$256.3 \times 10^{-3}$	1	$45 \times 10^{-7}$	
	$1.0 \times 10^{-2}$	12.13	365	22620	0	$295.4 \times 10^{-3}$	1	$46 \times 10^{-7}$	
RN/ZrP (16%)	$1.1 \times 10^{-2}$	12.13	365	3900	0	$22 \times 10^{-3}$	1	$17.1 \times 10^{-7}$	$17.5 \times 10^{-7}$
	$1.1 \times 10^{-2}$	12.13	365	5100	0	$30 \times 10^{-3}$	1	$17.9 \times 10^{-7}$	
	$1.1 \times 10^{-2}$	12.13	365	6600	0	$38 \times 10^{-3}$	1	$17.6 \times 10^{-7}$	